INTERCORRELATED SATELLITE AND GROUND OBSERVATIONS AND MODEL CALCULATIONS OF MAGNETIC STORMS

A

DISSERTATION

Presented to the Faculty of the

University of Alaska in Partial Fulfillment

of the Requirements

for the Degree of

DOCTOR OF PHILOSOPHY

by

Koji Kawasaki, B.A., M.S.

College, Alaska

May 1971

INTERCORRELATED SATELLITE AND GROUND OBSERVATIONS AND

MODEL CALCULATIONS OF MAGNETIC STORMS

APPROVED:

Chairman

Department Head

APPROVED: _____ DATE: May 10, 1971

Dean of the College of Mathematics, Physical Sciences, and Engineering

Vice President for Research and Advanced Study

PLEASE NOTE:

Some pages have indistinct print. Filmed as received.

UNIVERSITY MICROFILMS.

ABSTRACT

As a background for the study of the relationship between ground and satellite observations of magnetic disturbances, studies of the quiet day geomagnetic variations are reviewed. A model for the polar quiet day variation, S_q^p, which is thought to be related to the formation of the magnetospheric tail, is then presented. The model consists of Chapman-Ferraro boundary charges mapped onto the dayside auroral oval and the Hall currents expected of this distribution of charge. The model is consistent with the observed S_q^p below the auroral oval, but not consistent in the polar cap.

The auroral oval is the region in which intense electric currents flow, causing polar magnetic substorms. Polar magnetic substorms can occur throughout a magnetic storm, but of particular interest are those which occur nearly simultaneously to storm sudden commencements (ssc's). One hundred seventy-seven ssc's which occurred during the IGY (1957-58) and IQSY (1964-1965) are examined for the occurrence of simultaneous events. Of 105 IGY ssc's investigated, 49% were associated with simultaneous polar substorms. For 72 IQSY ssc's, this figure is less than 3%. For the IGY data, it was also found that the occurrence of these events depends on the amplitude of the ssc, but not on the existence of a previously disturbed magnetosphere.

Typically, magnetic storms at low latitudes are accompanied by numerous polar magnetic substorms. In this dissertation, several magnetic storms are investigated to determine the relationship between the low latitude longitudinally-asymmetric development of a magnetic

storm and the occurrence of polar magnetic substorms. It is found that low latitude changes often do not correlate well with high latitude changes, and thus, it is inferred that the non-symmetric component of a magnetic storm at low latitudes cannot be chiefly due to return currents of the polar electrojets. In addition, from the similarity of the synchronous satellite, ATS-I, and Honolulu magnetic storm records, it is concluded that a large part of the low latitude storm-time field must arise from the magnetotail current. However, correlations between the asymmetric component of the low-latitude storm-time field and the polar electrojets also exist. Thus, these require an explanation for the low latitude component in terms of ionospheric return currents and/or the direct effects of the distant auroral electrojets.

It has been observed by the ATS-I that the recovery phase of a geomagnetic storm proceeds much more rapidly at synchronous altitudes than at the ground. On the basis of a simple model consistent with particle data, it is shown that the 'early recovery' may be due to the combined effects of the magnetotail and ring currents. That is, during the recovery phase the ATS-I satellite may be located in the region between the ring current and the magnetotail current.

The magnetic field equations for two, three-dimensional models of the known currents are listed and the results of some calculations are presented. A relatively simple model of ring, auroral electrojet and field-aligned currents is shown to be consistent with the major part of observed disturbance field. The second of the models consists of a distributed ring current, boundary currents and magnetotail

current. This can reproduce the 'early recovery' of a magnetic storm observed by the ATS-I satellite.

ACKNOWLEDGEMENTS

The research in this dissertation was supported in part by the National Science Foundation, Atmospheric Sciences Section, through grants GA-17663, GA-1703, GA-1506, GA-1661, and GA-28101 and in part by the National Aeronautics and Space Administration through Grant No. NGR -02-001-001. It was also supported in part by the United States Atomic Energy Commission Grant AT(45-1)-2096 and by the United States Air Force Contract No. F-19628-C-0182.

The people who have contributed to the successful completion of this dissertation are too many to fully enumerate. However, some require special recognition.

My deepest and sincerest gratitude is reserved for Dr. Syun-Ichi Asasofu. It was his guidance and encouragement which made this dissertation possible.

During the formulative period of this dissertation, many useful discussions were held with Dr. Ching-I. Meng; these discussions are herein acknowledged with deep appreciation.

I also wish to express my gratitude to Professor Daniel W. Swift for the careful and diligent manner in which he read the manuscript and for pointing out and discussing some of the more obscure passages.

I wish to thank Dr. Paul J. Coleman, Jr., for supplying the ATS-1 magnetometer data, and Dr. Harold E. Taylor for supplying further information on the IMP-3 solar wind discontinuity measurements.

Discussions on various facets of the dissertation with my fellow students, Fumihiko Yasuhara and Paul D. Perreault, are gratefully acknowledged.

I am indebted to Robert A. Porter and Mrs. Anita Harry of the Data Processing Group, under whose direction the tedious task of scaling the data was carried out, and to Mrs. Sharon Dean and Steve Geller and especially Miss Shirley Liss who did the computer programming. I am also indebted to Mrs. Shirley Wilson of the Drafting Office and to Photographic Services, particularly Frank Daniels, for expediting the work on the illustrations used in this dissertation.

I am grateful to the Steno Pool, under the direction of Mrs. Meg McCoy, for the efficient typing of this dissertation despite the numerous other deadlines which had to be met.

The preliminary typing was done by Mrs. Jean Lipscomb, whose cheerfulness, efficiency, and general helpfulness made the difficult task of completing this dissertation far easier than it might have been.

Last but not least, I wish to thank my wife, Virginia, for her help and especially for her patience in sharing the often difficult life of a graduate student in Alaska.

TABLE OF CONTENTS

LIST OF ILLUSTRATIONS

LIST OF TABLES

CHAPTER I

INTRODUCTION

I.I A BRIEF HISTORY OF GROUND-BASED STUDIES OF GEOMAGNETIC DISTURBANCES

Historical documents and artifacts indicate that the Chinese first discovered the directive properties of the earth's magnetic field on lodestone (Needham, 1962). Although the earliest use of the magnetic compass by the Chinese was in the metaphysical art of geomancy, the more practical applications of the instrument to marine navigation and to surveying probably antedate Western European and Arabic counterpart by at least a few centuries. The declination of the earth's magnetic field and polarity of a magnet were also discovered by the Chinese sometime well before the 10th Century, A.D.

There is no documented evidence that the Chinese invention of the navigational magnetic compass was ever transmitted to Western Europe; the European-Arabic compass may merely have been a parallel development. However, it is known that some contact existed between China and pre-Rennaissance Europe, but any precise date of the supposed transmission of the knowledge of the magnetic compass has been lost to antiquity.

The navigational magnetic compass and the study of magnetism developed sporadically in Europe in the Middle Ages. It was during this period that secular variation was found, and magnetic declination and inclination began to be studied in great detail. In conjunction with the need for accurate navigational data, land-based observations became commonplace. Thus, just as chemistry evolved from alchemy, so too, evolved the study of geomagnetism from the Chinese geomancer's art.

The existence of transient variations (disturbances) of the earth's magnetic field were first noted in 1722 by Graham, a London clock-maker. By comparing observations through lengthy correspondences, Graham and Celsius of Sweden in 1741, discovered that magnetic disturbances often occurred simultaneously at the two locations. Thus, although crude, this was the first instance of a synoptic study of geomagnetic storms. Celsius was also the first to note the association of magnetic disturbances with aurora.

By the latter part of the 19th Century, a network of geomagnetic observatories sufficiently dense to reveal the major features of geomagnetic storms had evolved. It was determined that geomagnetic storms were world-wide phenomena, which began nearly simultaneously all over the earth. Its development was found to be similar at stations widely separated in longitude, and its magnitude much more intense in the auroral region.

An Indian scientist, Moos (1910), from the Bombay records of many magnetic storms, conducted the first study of the average features of a magnetic storm at low latitudes. Chapman (1918) further elucidated the average features of magnetic storms at different latitudes from a study of many storms. Thus, by the end of the first half of the 20th Century a considerable amount of observational data on magnetic storms had been gathered.

On the theoretical side, Birkeland (1901) attempted to explain what we now call polar magnetic substorms in terms of intense overhead currents, i.e. polar electrojets. Birkeland (1908, 1911) further suggested that the ultimate source of the horizontal currents and auroras

was solar corpuscular radiation flowing along field lines, i.e., field-aligned currents, and attempted experimental verification of the hypothesis. Störmer (1911) also suggested solar corpuscular radiation was the source of auroras. Schmidt (1917) ascribed the decrease of the earth's magnetic field during a geomagnetic storm to a westward electric current which encircles the earth, i.e., a ring current. Later, Chapman and Ferraro (1930, 1931, 1932) examined the effect of a neutral ionized stream of solar particles advancing on the earth's magnetic field. Thus, they determined on theoretical grounds that the solar wind carves out a hollow which shields the earth from the direct effects of solar particles. This cavity is now termed the magnetosphere.

By the late 1950's much was known about the morphological features of the disturbance field of a magnetic storm. Relatively rudimentary theories had been advanced to account for the major features of geomagnetic storms. Among these were a ring current for the main phase decrease of a storm, field-aligned currents and auroral electrojets for auroral zone magnetic disturbances, and boundary currents arising from the interaction of the solar wind and the earth's magnetic field to account for the sudden commencement phase of a storm. Direct verification of the existence of these currents had to await the post-Sputnik era.

1.2 A REVIEW OF SATELLITE STUDIES OF GEOMAGNETIC DISTURBANCES

1.2.1. Introduction

Magnetic measurements above the earth's ionosphere began with Sputnik 3 (1958) and Vanguard 3 (1959), which were relatively low

orbiting satellites. The primary purpose of these satellites was to map precisely and comprehensively the main field of the earth. It was determined from the measurements that the field in the near earth region (∿0.1 to ∿0.5 earth radii) very closely approximates the reference field obtained upon extending the field measured on earth by means of spherical harmonic expansion (see the review article by Cahill, 1964).

Low-altitude measurements by Vanguard 3 also showed that part of the ground level activity during magnetic storms could be attributed to distant currents beyond the satellite orbit.

In this section, satellite and space probe observations of the geomagnetic field during magnetic storms will be briefly reviewed. The magnetic observations have been divided arbitrarily into those made in four regions: the Van Allen belt region containing the low energy protons and electrons which presumably form the ring current belt; the transition region between the ring current belt and the tail region; the tail region; and the magnetospheric boundary region.

1.2.2. The Van Allen region

Vanguard 3 magnetometer data (Cain et al., 1962) indicated that the postulated ring current must be located at least above 500 km and probably beyond 2400 km in altitude. On courses to the moon, both Lunik 1 and Lunik 2 detected depressions of the field below the reference field near 2 R_e (earth radii) during moderate magnetic storms (Dolginov et al., 1960). The interpretation of the depression as due to a ring current was disputed, however, since

the field did not rise above the reference field beyond 2 R_e as would be expected of a ring current. On the other hand, Explorer 6 did not detect any evidence of a ring current in the same region traversed by the Lunik probes (Sonett et al., 1960).

During the early 1960's, several satellites carrying magnetometers were launched which traversed the region in which a ring current was thought to flow. None of the results were conclusive enough to clearly indicate the location of the ring current, and hence, whether a ring current did indeed exist. Thus, the measurements chiefly indicated where the ring current was not to be found.

The first conclusive observations on the existence of a ring current during a magnetic storm and its location were supplied by the Explorer 26 satellite (Cahill, 1966). Explorer 26 traversed the inner magnetosphere between the geocentric equatorial radii $r_e = 2\ R_e$ and $r_e = 6\ R_e$ many times during the great magnetic storm, which commenced at 1312 UT on April 17, 1965. It was observed that both the declination and inclination were distorted from the reference field directions in the late afternoon and evening quadrants during the main phase decrease of the storm. Measurements in other quadrants did not show such large distortions. This asymmetrical inflation of the geomagnetic field was interpreted to be due to the rapid growth of charged particle energy in the evening-afternoon quadrant, deep in the magnetosphere.

During the recovery phase of the storm, the geomagnetic field inflation became more symmetrical, that is, the inclination deviation from the reference field remained large, but the declination deviation became relatively small. Cahill (1966) suggested this observation was consistent with the existence of an axially symmetric ring of current with a peak particle energy density near $r_e = 3.5\ R_e$.

Further evidence for the existence of the ring current and its initially asymmetric development was presented by Cahill (1970), who studied four other storms observed by Explorer 36 in 1965.

OGO 3 measurements of the differential energy spectrums of low energy protons and electrons in the ring current region presented by Frank (1967) were the first complete and coherent observations of the actual particles which constitute the ring current belt. Frank found that the energy density of protons in the energy range ∿3 to 50 Kev was sufficient to account for the major part of magnetic disturbances observed at the ground during a period in June and July, 1966. Electrons in the range 200 ev to 50 Kev were found to provide 25% of the storm-time ring current. Observations of the asymmetric increases of ring current proton energy densities are presented by Frank (1970).

1.2.3. Inner tail region

Long-term magnetic observations of the inner tail region of the magnetosphere have been provided by the synchronous orbit satellite ATS-1, which was launched on December 6, 1966. The satellite is located at a geocentric range of 6.6 R_e, latitude 0°

and longitude 150.3°W. The magnetic measurement of Cahill (1966, 1970) and the particle measurements of Frank (1967, 1970) indicate that ring current particles are rapidly introduced deep within the magnetosphere during the main phase decrease of a storm, and that there is a subsequent recession of the peak of the ring current during the recovery phase. The location of the peak of the ring current particles during quiet periods is in the vicinity of the synchronous orbit. Thus, a synchronous orbit satellite is often located between the region of the ring current and the tail of the magnetosphere during the course of a geomagnetic storm.

Cummings and Coleman (1968a), Coleman and Cummings (1968), Cummings et al., (1968), Coleman (1970), and Coleman and Cummings (1971) have reported the results of the ATS-I magnetic measurements. The major observations directly relevant to magnetic storms in the inner tail region are as follows:

(a) The magnitude of the main phase of a storm tends to be smaller at synchronous altitudes than at ground stations.

(b) There are instances when an almost one-to-one correspondence exists between the H-component field changes in the midnight sector at ATS-I and at the ground station, Honolulu.

(c) During the main phase decrease, substantial V-component changes (radially outward changes, corresponding to the negative Z-component of the usual H, D, Z system used at ground stations) occur which is indicative of a tail-like configuration at these times.

(d) Substantial D-component changes also occur during main phase decreases. Coleman (1970) suggests that these changes are possibly due to field-aligned currents.

Transverse magnetic changes detected above the auroral zone ionosphere by a polar orbiting satellite and a rocket probe have been interpreted as due to field-aligned currents (Armstrong and Zmuda, 1970; Cloutier et al., 1970).

1.2.4. Outer tail region

The first comprehensive mapping of the topology of the magnetic field in the tail region of the magnetosphere was made by the IMP-I (Explorer 18) satellite (Ness, 1965; Speiser and Ness, 1967). The measurements showed that the tail of the magnetosphere was elongated to at least 32 R_e in the anti-solar direction. A few earth radii, above the ecliptic plane, the field was found to point generally toward the sun, while below the plane, the field pointed in an anti-solar direction. The transition region between the two field directions is now called the 'neutral sheet'. Its thickness is in the order $\sim$.1 to $\sim$1.0 R_e. Significant particle flux exists in a limited region below and above the neutral sheet (Bame et al., 1966); this has been termed the 'plasma sheet'.

From numerous observations, the topology of the tail that has emerged is one of roughly cylindrical cross-section in the plane perpendicular to the solar wind direction with fields anti-parallel and parallel to the sun-earth line, respectively, above and below the ecliptic plane. The tail is quite elongated; observations of

the magnetic field and particles by Pioneer 7 in the geomagnetic wake of the earth suggest that the tail may extend to 1000 R_e (Wolfe et al., 1967; Ness et al., 1967), but that it is highly disordered at that distance. Ness (1965) found that the magnitude of the tail field was from 10 to 20 gammas at 30 R_e where the dipole field is expected to be only 1 gamma. IMP-1 data (Speiser and Ness, 1967) and Explorer 14 data (Laird, 1969) indicated that there was a small field (of a few gammas or less) vertical to the neutral sheet.

The magnetotail field during magnetic storms has also been studied (Behannon and Ness, 1966). Positive correlations of the tail field disturbances with low latitude ground changes were interpreted as due to large-scale compressional effects of the solar wind such as that which occurs during an ssc. Anti-correlations between low latitude ground records and magnitude of the tail field disturbances were also observed. Thus, during the decreasing phase of a storm, the magnitude of the tail field increases. IMP 4 data supplied more detailed observations of the sequence of magnetic changes in the tail during magnetic substorms (Fairfield and Ness, 1970). It was found that during quiet and post-substorm periods the field tends to be relaxed into a more dipolar state with some northward directed field lines passing through the neutral sheet. Prior to and during the early stages of a substorm, the tail field increases while the northward field perpendicular to the neutral sheet decreases. Simultaneously, the plasma sheet thins. Thus, the tail field, its associated particles and geometry undergo rather

dynamic changes during the course of a substorm.

1.2.5. Boundary region

The existence of a boundary region between solar corpuscular radiation and the earth's geomagnetic field was first suggested by Chapman and Ferraro (1930, 1931, 1932). Such a boundary was thought to be transient in nature, occurring only at the time of solar flares; however, Biermann (1951), from comet tail observations, concluded that corpuscular radiation must be continuously emitted from the sun. Thus, the boundary should be a permanent feature.

The first clear identification of the magnetospheric boundary (or magnetopause) was made by Cahill and Amazeen (1963) with a magnetometer on the Explorer 12 satellite. Magnetic measurements during radial passes of the satellite near the subsolar point showed that an abrupt change in field occurred near 8 R_e. The field was about what one would expect of a dipole in the solar wind up to the crossing, but beyond that the field became highly irregular in magnitude and direction.

Numerous observations of the magnetopause have since been made. Notable observations of the effect of an enhanced solar wind were provided by the ATS-I satellite during the storm of January 14, 1967 (Cummings and Coleman, 1968b). The satellite encountered and passed through the boundary several times between 1400 to 1500 LT (0000 to 0001 UT, January 14). Since the satellite had already passed its local noon, the boundary was actually moving in and out, past the satellite, in response to the dynamical pressure of the solar wind.

The field measured just inside the boundary was nearly 50% higher than expected at that location during quiet times. Thus, these measurements indicate that some solar wind parameters are highly variable.

1.3 AN OUTLINE OF SUBJECTS COVERED

It is certain that magnetic disturbances on the earth and in the magnetosphere occur in response to variations of the parameters of the interplanetary medium. However, although a considerable number of observations have been made of the solar wind and interplanetary magnetic field by space probes and astronomical means, as yet, no one-to-one correspondence between specific parameters and the occurrence of magnetic disturbances on the earth has been definitely established.

Magnetic disturbances observed on the earth and in space are structurally more complex than the average morphology implies. For example, observed at the ground, magnetic storms are often not preceded by an identifiable storm sudden commencement (ssc) and also can have a lengthy initial phase or a very brief one. Such variable responses and response rates to changes of the parameters of the inter planetary medium must also be related to conditions within the magnetosphere.

This dissertation is primarily a correlative study of available satellite and ground magnetic field observations. Relevant particle observations are also included in the study.

Chapter II deals with ionospheric and non-ionospheric sources of quiet day variations of the geomagnetic field. Such variations form the basis for the study of disturbed conditions presented in subsequent chapters.

Chapter III contains a study of the low latitude asymmetric component of the storm-time disturbance field observed at the ground. As the name implies, the asymmetric component is that component of the storm-time field which remains after subtraction of the part symmetrical with respect to the dipole axis. Thus, it is essentially the DS part of the storm-time field; in Chapter III, this component is studied in terms of the asymmetry (or ASY) index, which retains the higher harmonics of the DS component.

Geomagnetic storm fields observed at synchronous orbits are discussed in Chapter IV. In particular, this chapter deals with the rapid recovery of storm-time fields as observed by the synchronous satellite ATS-I.

Some statistical results concerning the occurrence of polar magnetic substorms coincident with the onset of storm sudden commencements is presented in Chapter V. A few available satellite observations of discontinuities in the solar wind are also studied with relation to sudden commencements and polar magnetic substorms.

Chapter VI discusses two, three-dimensional current models of the magnetospheric configuration during quiet and disturbed times. Equations for the various currents and fields involved are given.

Discussions and conclusions concerning the studies presented in this dissertation may be found in Chapter VII.

CHAPTER II

THE QUIET MAGNETOSPHERE - BACKGROUND FOR THE STUDY OF GEOMAGNETIC DISTURBANCES

2.1 INTRODUCTION

The earth is not an isolated body in space, but is subjected to gravitational forces and to extensive electromagnetic and particle radiations both from the sun and galactic sources. The balance of magnetic and particle pressures between the steady solar wind (plasma particles from the sun) and the earth's magnetic field determines the primary configuration of the magnetosphere. Electro-magnetic radiations, principally of solar origin, continually ionize the neutral constituents of the upper atmosphere, thereby producing an extensive conducting region above the earth's atmosphere, called the ionosphere. In a frame of reference rotating with the earth, these sources, which are quasi-stationary with respect to the sun, give rise to near-cyclic variations of the geomagnetic field. These 'quiet day variations' of the geomagnetic field, which form a background for the investigation of the disturbed magnetosphere presented in the ensuing chapters, will be reviewed in this chapter.

It is generally well agreed that the interaction of tide-induced horizontal winds in the ionospheric region and the vertical (Z) component of the geomagnetic field produces currents, which in turn produce variations of the geomagnetic field. These ionospheric contributions to the quiet day geomagnetic variations can be further sub-divided into solar and lunar contributions. The lunar quiet day geomagnetic variations are simpler than the solar variations, since

the former is related only to the lunar gravitational tides, while the latter depends both on the solar gravitational tides and on the thermally-induced tides. The lunar variations are reviewed in Section 2.2, and the solar variations in Section 2.3.

On the other hand, there are non-ionospheric currents such as the magnetospheric boundary current, whose field distributions are non-symmetric with respect to the rotational axis, which can give rise to significant contributions to the quiet day variations. These are reviewed in Section 2.4.

A recently discovered high latitude quiet day variation, S_q^p, is also reviewed and studied. This geomagnetic variation is not explainable in terms of the conventional ionospheric and non-ionospheric mechanisms; a model of a possible mechanism which can give rise to a part of S_q^p is described and presented in Section 2.5.

2.2 THE LUNAR QUIET DAY GEOMAGNETIC VARIATIONS

Ground-based vertical incidence ionosondes have shown there are several distinct layers of electron densities in the ionosphere. The main layers are the F2, F1, E, and the sporadic E layer, E_s, which is only occasionally observed. From continuous ionosonde measurements, the tidal effects of both the sun and the moon have been observed in the various ionospheric layers. It is the horizontal component of these tides interacting with the main geomagnetic field of the earth which produces steady currents observed on the surface of the earth as the solar and lunar geomagnetic variations.

The dynamo theory of quiet day geomagnetic variations has been fairly well established. Both solar and lunar variations can be

reasonably explained by this theory. With the tides producing the necessary horizontal velocities of the ionized component of the ionosphere, the primary dynamo field ($\underline{v} \times \underline{B}_o$) sets up a charge distribution with potential (S) which, together with the initial dynamo field, produces a steady distribution of current. The morphology and strengths of the resulting currents also depend on the distribution of the conductivity of the ionosphere.

The relevant equations which describe the dynamo theory are as follows. The beginning point is Maxwell's equations:

$$\text{curl } \underline{E} = -\frac{\partial \underline{B}}{\partial t} ,$$

$$\text{curl } \underline{H} = \underline{j} + \frac{\partial \underline{D}}{\partial t}$$

and the generalized Ohm's law

$$\underline{j} = [\sigma] \cdot (\underline{E} + \underline{v} \times \underline{B}_o),$$

where $[\sigma]$ is the conductivity tensor, $\underline{B}_o$ is the earth's field and the other quantities have their usual meaning. With the assumption of the steady state conditions, $\partial \underline{B}/\partial t = \partial \underline{E}/\partial t = 0$, it follows that

$$\underline{E} = -\text{ grad } S \text{ and } \text{div } \underline{j} = 0,$$

where S is an electrostatic potential.

The preceding equations along with Ohm's law lead to the dynamo equations:

$$\text{div } \underline{j} = 0 = -\text{ div } ([\sigma] \cdot \text{grad } S) + \text{div } ([\sigma] \cdot \{\underline{v} \times \underline{B}_o\})$$

and $$\text{curl } \{[\sigma]^{-1} \cdot \underline{j}\} = \text{curl } \{\underline{v} \times \underline{B}_o\}$$

Once the conductivity tensor $[\sigma]$, the vector velocity field $\underline{v}$ for the ionized particles of the ionosphere and $\underline{B}_o$ are known, the current $\underline{j}$ can be determined.

The lunar influence on geomagnetic variations was discovered over a century ago. Later, Chapman and Bartels (1940) obtained external equivalent current systems of the lunar or L-current component of the quiet day variation. Recently, Matsushita and Maeda (1965b), Matsushita (1966) and Matsushita (1969) from extensive data have obtained more accurate representations of the external L-current system. The basic method used is spherical harmonic analysis applied to the lunar quiet day variation after the solar quiet day variation has been removed.

The actual strength of the L-geomagnetic variation is quite small; the maximum range of the L-field occurs in the H-component during the northern winter months and is about 8 gammas at the equator and about 2 gammas at 60° dipole latitude. The larger value of the L-field at the equator is a reflection of the enhanced lunar tidal effect on the equatorial electrojet. Unlike the solar variations discussed in the following section, the semi-diurnal component of the lunar variation is much larger than the other components, which is to be expected since the phenomenon should be due solely to lunar tidal forces.

Matsushita (1966) finds that the semi-diurnal component of the L-variation field can be represented by an average external equivalent current system consisting of four pairs of current vortices in the northern and southern hemispheres, whose foci are located on about the 02, 08, 14, and 20 hour local lunar time meridians and at approximately the $\pm$ 20° dipole latitudes. The current flows eastward at the equator at the 08 and 20 hour local lunar time meridians and westward at the 02 and 14 hour meridians.

2.3 THE SOLAR QUIET DAY GEOMAGNETIC VARIATIONS

The solar quiet day geomagnetic variation has been extensively studied (cf. Schuster, 1889; Chapman, 1919; Maeda, 1953, and more recently, by Matsushita and Maeda, 1965a and Matsushita, 1967), since it was first discovered in 1722 by Graham.

The dynamo equations which govern the morphology of both the solar and lunar variations have been outlined in Section 2.2. It has been relatively well established that lunar variations can be explained by the dynamo theory, since the tidal effects of the moon are well known. However, although it is believed by most investigators that the dynamo equations are also valid for the solar quiet day variations, there remains a major difficulty. This is that no adequate theory has been presented to account for a large diurnal component of the wind system and/or conductivity distribution which is required to produce the extremely large diurnal geomagnetic variation observed. The semi-diurnal and third harmonic components of the variations obtained from Fourier analyzing the record of a station along a particular latitude can be adequately explained by atmospheric tides excited by the gravitational attraction of the sun and by thermal insolation by ozone, water vapor, carbon dioxide and other atmospheric constituents (Siebert, 1961; Butler and Small, 1963).

Regardless of the difficulties with the dynamo theory of Sq, an equivalent current system can be obtained independently of the distribution of conductivities from the distribution of the variation field by spherical harmonic analysis. Our present state of knowledge of the ionosphere and the dynamo theory suggests that this current

system is primarily located in the ionosphere.

The solar quiet day variation Sq is very large in a narrow band containing the dip equator, where it can reach a range of 180 gammas in the H-component; at typical low latitude stations (about 20° dp lat) the range may be as large as 50 gammas. (These values include the part of Sq internal to the earth, and therefore should be reduced by a factor of approximately 0.6 to account for the induced currents. Induction currents in the earth have been discussed by Chapman and Bartels (1940), Ashour and Price (1965) and Ashour (1971).) There is a seasonal and solar cycle variation of the intensity of the Sq variations which is a reflection of the solar control of the conductivity of the ionosphere.

The diurnal component of Sq obtained from Fourier analysis is about twice the magnitude of the semi-diurnal component at all latitudes, which suggests a large thermal tide consisting of a single high pressure node exists.

Since the diurnal term is dominant, the equivalent overhead current system of Sq consists of a pair of intense current vortices, one in each hemisphere, centered at about the 11 to 12 hour local time meridian and a much less intense pair near the local midnight meridian; the current vortices are located at about the $\pm$ 30° dipole latitude. At the 11 hour local time meridian the currents adjacent to the equator flow eastward. However, it should be noted that the current pattern can vary greatly from day to day as well as from season to season.

2.4 NON-IONOSPHERIC QUIET DAY GEOMAGNETIC VARIATIONS

In the previous section, the solar quiet day variations have been ascribed to the ionospheric dynamo. It should be noted that there

also exist other current systems which can produce very similar variations. One can separate the lunar effects from the other variations since the variations progress around the earth with lunar age. However, no such separation can be made of the non-ionospheric sources of quiet day variations, namely the magnetospheric boundary current, the quiet-time ring current and the tail or neutral sheet current, since their contributions have the same phase and diurnal character as the variations from the solar ionospheric dynamo.

Mead (1964) and Olson (1970) studied the effects of the various non-ionospheric contributions to Sq. These contributions arise because the earth rotates within inhomogeneous field lines approximately fixed with respect to the sun-earth line.

Mead (1964) and Olson (1970) find that a daily range of 2 to 4 gammas is to be expected of the quiet-time magnetopause boundary current contribution to the Sq variation. The direction of the solar wind is slightly inclined from the sun-earth direction (about 8° to the x-axis and from the negative y-direction of the geocentric-solar-ecliptic coordinates), and thus, this part of Sq and those of the tail and ring, as well, should peak at about 1130 hours local time.

The quiet-time magnetotail current, which flows from dawn to dusk in the neutral sheet of the tail and which is thought to be completed by currents flowing on the surface of the tail, produces a range of about 2 gammas in the model of Olson (1970).

A uniform ring current belt concentric with the earth can produce only a change in level of the main field of the earth; however, if the quiet-time ring current is not concentric with the earth or has an

asymmetric distribution of current, a daily variation should result. On the basis of a simple ring of current whose center is displaced toward the sun, as suggested by the work of Siscoe (1966), Olson (1970) has obtained a range of 1 to 2 gammas for the variation at the surface of the earth. The estimate of the strength of the ring current was based on an extrapolation from ground records of storm-time periods and on the ATS-1 magnetometer measurements during quiet periods.

Plausible models of the three non-ionospheric current.systems give a value of about 10 gammas for the total contributions to the Sq variation. If induction currents in the earth are included, a maximum range of about 15 gammas is to be expected. This value is approximately one-tenth of the observed range of Sq, so that non-ionospheric sources are probably not significant. However, as was noted by Olson (1970), it is possible that these currents can account for the day-to-day variability of Sq, since even the quiet solar wind parameters can change considerably.

2.5 THE POLAR QUIET DAY GEOMAGNETIC VARIATIONS

2.5.1 Introduction

Geomagnetic quiet day variations in the polar regions have not been explicitly discussed in the preceding sections. Since the tidal forces have nodes in the polar regions and the daily variations of inhomogeneities of the fields due to the recognized non-ionospheric currents there are believed to be small, the only significant contribution to the quiet day variations near the poles must arise from the thermally-induced solar tide. However, extrapolation of the lower latitude quiet day geomagnetic variation field to the higher latitudes

shows that there is an anomalously high, quiet day variation in polar regions.

Hasegawa (1939) was the first to make an extensive study of quiet day geomagnetic variations at high latitudes, but failed to take note of the anomalous daily variation in this region. Nagata and Kokubun (1962), from more extensive and accurate IGY data, extrapolated the low latitude Sq field into the polar regions and showed that an additional variation existed there. The Sq expected at high latitudes ($\geq$ 60° dip lat) was denoted S_q^o and the additional quiet daily variation was denoted S_q^p; thus, $Sq = S_q^o + S_q^p$. Unfortunately, these investigators used the five International Quiet Days of each month for a few months around the solstices during the IGY, which are only relatively more 'quiet' than the other days of a month. It is inevitable that the records of such days are 'contaminated' by the polar electrojet. For this reason, Feldstein and Zaytsev (1967) and Kawasaki and Akasofu (1967) have recently re-examined the pattern of S_q^p on very quiet days during the IGY and the IQSY. The latter investigators obtained the high latitude Sq field by using two of the quietest days during the IQSY (December 10, 1963: Kp = $0_o 0_o 0_+ 0_o$ $0_o 0_o 0_o 0_o$ and May 8, 1964: Kp = $0_o 0_o 0_+ 0_o$ $0_o 0_+ 0_+ 0_+$).

However, the methods of analysis differed. For example, the analysis by Kawasaki and Akasofu (1967) was based on the conventional Sq analysis; that is, Fourier analysis and expansion in spherical harmonics. Figure 2.1a and 2.1b show $Sq = S_q^o + S_q^p$ for May 8, 1964 and December 10, 1963, respectively. The extended Sq variation from lower latitudes is most clearly seen in the 6-12 hour local time sector below

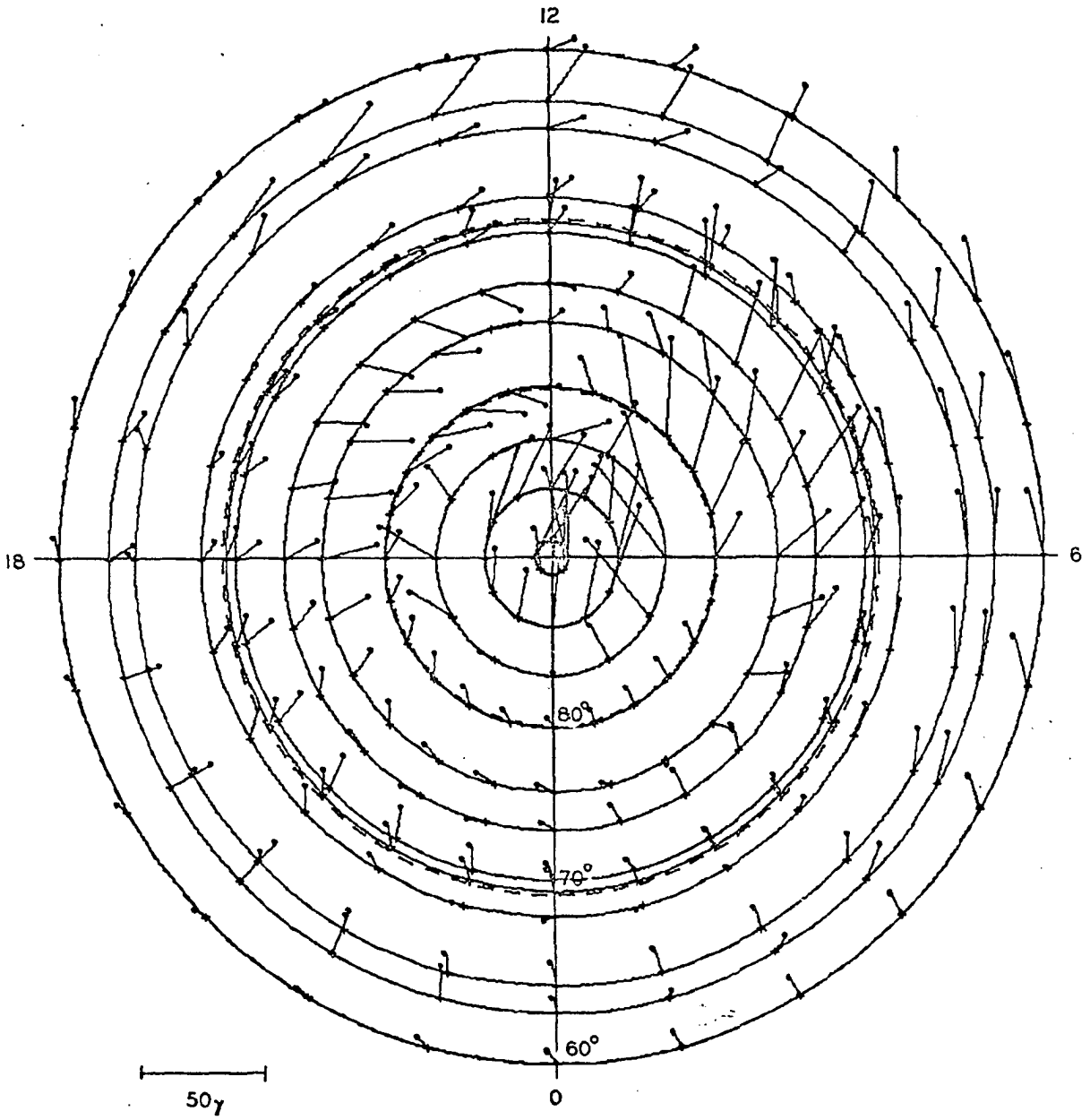

Fig. 2.1a Polar plot of the four term Fourier expansion of the horizontal geomagnetic component ($Sq = S_q^o + S_q^p$) at high latitudes on the extremely quiet day May 8, 1964, (Kawasaki and Akasofu 1967).

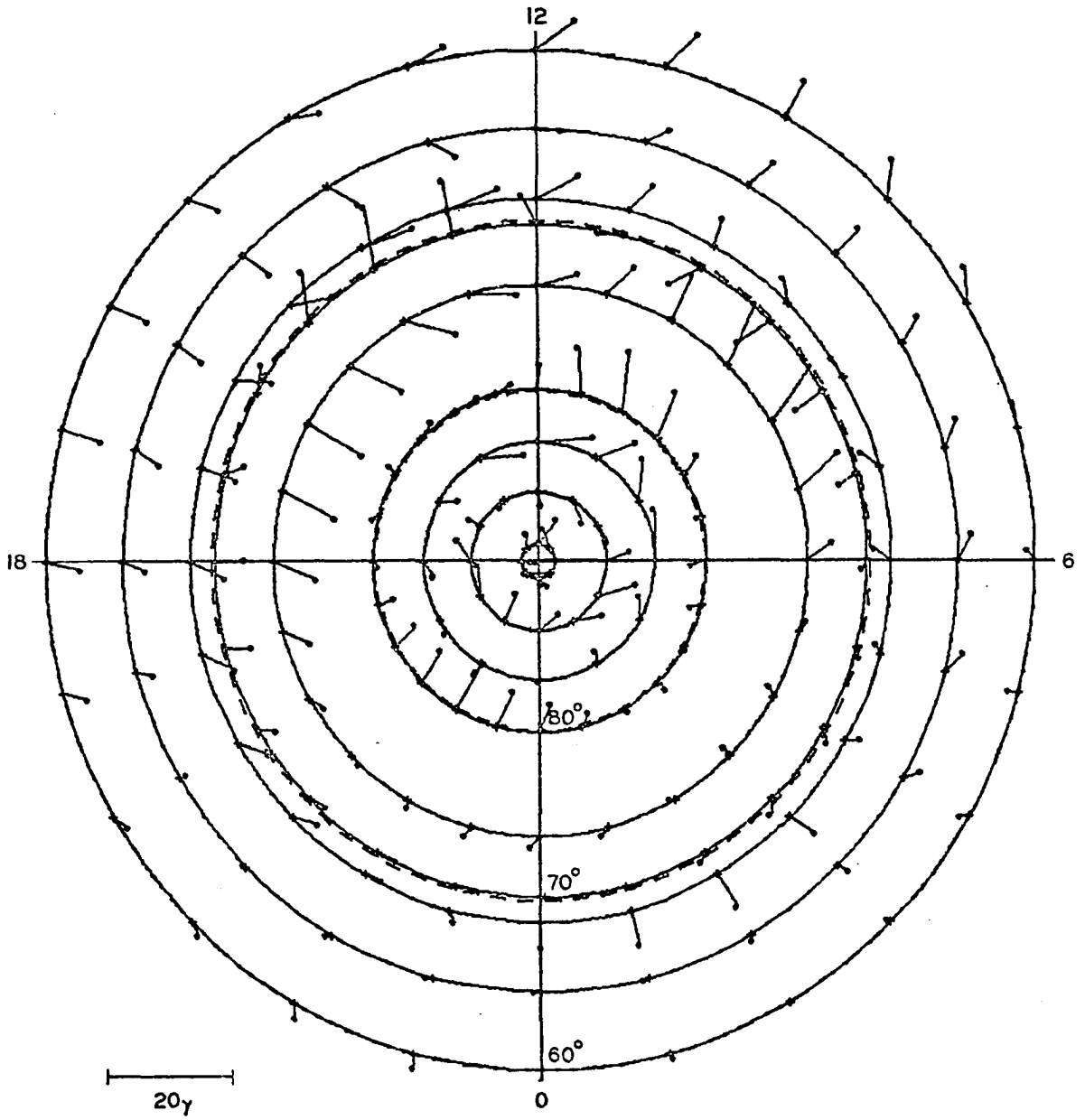

Fig. 2.1b Polar plot of the four term Fourier expansion of the horizontal geomagnetic component ($Sq = S_q^0 + S_q^p$) at high latitudes on the extremely quiet day December 10, 1963, (Kawasaki and Akasofu, 1967).

dipole latitude 65°. On the other hand, Feldstein and Zaytsev (1967) obtained $Sq = S_q^o + S_q^p + DP$ from a few very quiet days during the IGY; here, DP denotes the field of the polar electrojet which was thought to exist even during quiet days of the IGY. Figure 2.2 shows the diagram for $S_q^p + DP$; a certain pattern of S_q^o was assumed and subtracted from Sq.

In spite of the differences in the methods and also the data employed, the agreement between the two studies is reasonable. The main results, together with some comments, may be summarized as follows:

1) There exists a particular solar daily variation (S_q^p), other than S_q^o, even during extremely quiet days (Nagata and Kokubun (1962)).
2) The major part of the S_q^p variation is confined to the day sector of the polar cap.
3) In the latitude belt 70° - 80°, the vectors have an equatorward component in the 06-12 hour sector, and a poleward component in the 12-18 hour sector. Feldstein and Zaytsev (1967) imply that a part of the component in the 06-12 hour sector is caused by the polar electrojet. However, it was persistently seen on all quiet days during the IQSY when the absence of the jet could hardly be doubted.
4) Above 80°, the vectors have a sunward component.
5) There is a large seasonal dependence of the distribution and strength of the quiet day variations in the polar regions. Compare Figures 2.1a and 2.1b.

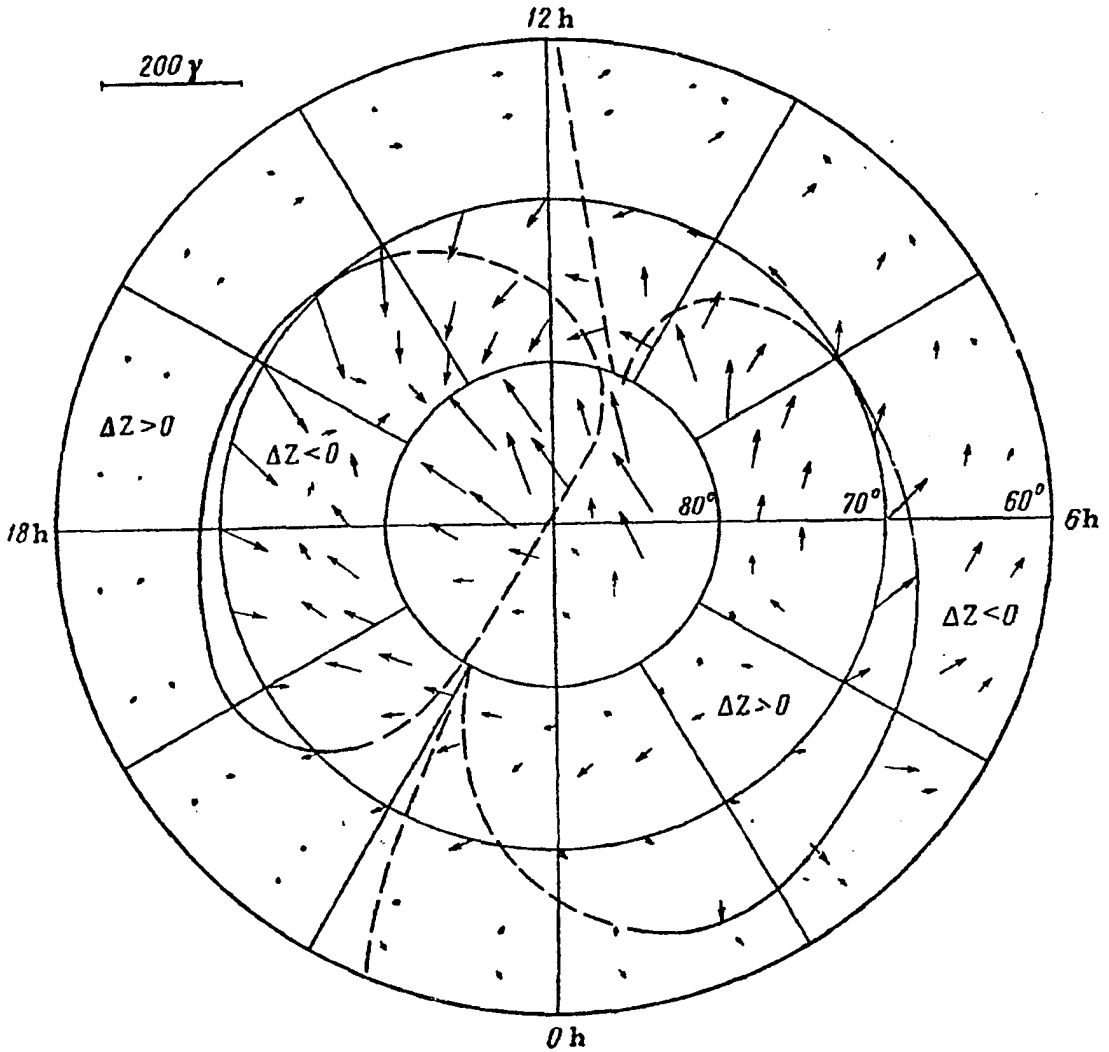

Fig. 2.2. S_q^p plus residual DP, (S_q^p + DP) for five quiet days during the summer of IGY, (Feldstein and Zaytsev 1967).

6) In addition to these findings, both Feldstein and Zaytsev (1967) and Kawasaki and Akasofu (1967) conclude that the S_q^p pattern differs significantly from that of the polar electrojet. This indicates that the polar electrojet cannot be due to a simple enhancement of the S_q^p current intensity, without requiring drastic changes of the pattern. The polar electrojet must thus be associated either with changes of the charge distribution, additional electric fields, changes of ionospheric conductivity or a combination of these.

2.5.2 The neutral line and quiet-time convection in the magnetosphere

The relatively large polar quiet day variation suggests the existence of mechanisms other than those described in Sections 2.2 through 2.4. Here, a background for the model presented in the next subsections is presented.

Chapman and Ferraro (1931 a, b) and Ferraro (1952) discussed the space charge distribution on the surface of the magnetospheric cavity carved out by the solar wind. A positive space charge appears on the inner edge of the dayside boundary because the massive positive ions penetrate more deeply than the electrons (Ferraro, 1952; p. 44). Space charges also develop in the morning and evening sides of the boundary because of the $e\underline{v} \times \underline{B}$ force which is experienced by the solar wind particles when they flow in the transition region of the boundary. The space charge is negative on the evening-side boundary and positive on the morning side.

Piddington (1960, 1962), Axford and Hines (1961) and Axford (1964) discussed a convective motion of the magnetospheric plasma associated

with these space charges and drew convective patterns (stream lines) at the ionospheric level (cf. Axford,1964; his Fig. 2). However, such a convective pattern depends greatly on the geometry of geomagnetic field lines inside the boundary. The Chapman-Ferraro model (or any subsequently developed ones, such as that of Mead, 1964) predicts two singular neutral points, one in each hemisphere, on the noon-time meridian plane where two 'adjacent' field lines diverge from each other, one toward the sun and the other to the nightside of the earth. All the field lines which lie near the magnetospheric boundary converge to the neutral points (cf. Axford,1962; his Fig. 2), so that the area from which they originate will be a small circular area, with radius of order 200 km, centered at the 'foot' of the field line from the neutral point (cf. Akasofu,1966 ;p. 119). In this case, the major part of the convective pattern will be limited to a small area surrounding the circular area, and thus,the large-scale convective pattern drawn by Axford (1964) would not occur.

During recent years, there have been suggestions that instead of a point, the singularity or neutral region should be a line or part of an arc (Piddington, 1965 and Frank, 1970). The projection of a neutral line onto the polar ionosphere along the geomagnetic field lines will also be a line. Imagine two geomagnetic field lines which originate just poleward and equatorward of the projected neutral line, respectively. They lie closely together in space between the solid earth and the neutral line in the polar ionosphere; from there they deviate greatly, the polar one toward the tail region and the equatorial one toward the front side of the magnetosphere. In this case, the space

charges near the boundary may be distributed along the projected neutral line on the polar cap ionosphere. The precise geometry of the expected convective pattern depends also on the distribution of the geomagnetic field lines inside the magnetosphere.

The convection of the magnetospheric plasma should cause an electric current at the ionospheric level. The current arises because of the interactions between the magnetospheric plasma and the neutral atmosphere underneath. At the ionospheric E level, positive ions cannot participate in the convective motion because the frequency of their collisions with neutral particles becomes comparable with or greater than their gyration frequency; on the other hand, the electron gyro-frequency greatly exceeds the electron collision frequency, and thus, electrons can participate in the motion. These electrons constitute the Hall current (which is oppositely directed to the stream line of the convective motion). Piddington (1960, 1962) and Axford and Hines (1961) originally proposed that it is this electric current that causes a polar magnetic substorm. However, the convective pattern of a particularly simple situation should be examined before such an inference is made.

The magnetospheric cavity formation is a permanent feature as long as the solar wind flows, and thus, the convective motion must also be a permanent feature. The convective pattern during extremely quiet conditions may provide information on fundamental features of the magnetosphere; for example, the geometry of the singularity (point or line) may be indicated by the pattern. The pattern of the polar electrojet is not necessarily a good foundation for inferring the

basic pattern of convection. This is because the growth of the polar electrojet is closely associated with the auroral substorm, so that the ionospheric conductivity is extremely variable in both space and time. Secondary space charges can also develop in the ionosphere during such disturbed conditions, which makes it difficult to infer the distribution of the primary ones. Furthermore, the polar electrojet probably results from an entirely different space charge system than the quiet-time situation being discussed here.

Although the mechanism of charge transfer is not fully understood, it is assumed here that the S_q^p variation below dp lat 80° is caused by the convection of the magnetopause plasma and thus by an ionospheric current system associated with the space charges on the boundary. If this assumption is correct, it must be concluded that the singularity on the cavity boundary cannot be a point. This is because the current is well distributed over an extensive area on the dayside of the polar cap and is not confined to a small area around the expected location of the foot of the field line from the hypothetical neutral point.

2.5.3 Model calculations

2.5.3.1 S_q^p below dp lat 80°

It is assumed that there is a fixed distribution of charges on a semi-circular arc in the polar cap ionosphere. The distribution of the associated current and the resulting magnetic vectors is examined. The arc is suggestive of the dayside of the auroral oval where auroras are permanently located, even during an extremely quiet day (Akasofu, 1968). The dipole latitude of the dayside part of the oval

is of the order 80° on very quiet days, so that for simplicity, the semi-circle is taken to be the dayside half of the 80° dp lat circle.

Actually, the charges should be distributed along a sector of an annulus, rather than along an arc. However, the transition region of the magnetospheric boundary is known to be rather thin and its projection onto the earth makes it thinner by a factor of about 100. Therefore, if the thickness of the boundary transition region is of order 1,000 km, the projected annulus will have a width of the order of 10 km, which is small compared with the length of the arc.

In the model calculation, two cases, A and B, are considered. In model A, the portion of the semi-circle $0 \leq \phi \leq 3\pi/4$ is positively charged and the portion $3\pi/4 \leq \phi \leq \pi$ is negatively charged ($\phi = 0$ on the 06 hr time meridian). The net charge on the semi-circle is zero and it is assumed that the charge density is uniform. In model B, the portion of the semi-circle $0 \leq \phi \leq \pi/4$ is positively charged and the portion $3\pi/4 \leq \phi \leq \pi$ is negatively charged. The latter model has a resemblance to Axford's Fig. 2 (Axford, 1964), but the distribution of the charges in the present model is limited to the day sector (since it is unlikely that the neutral line extends greatly to the night side). To further simplify the calculations, it is assumed that the charge distribution and the associated currents all lie in a plane; this is not too unrealistic since only the limited area of the polar cap is being considered.

The Cartesian components of the electric field due to a line charge in the form of an arc of a circle of radius unity are given by

$$E_{\pm x}(R,\alpha) = k_{\pm} \int_{\phi_{\pm 1}}^{\phi_{\pm 2}} \frac{(R\cos\alpha - \cos\phi)\, d\phi}{[R^2 + 1 - 2R\cos(\phi-\alpha)]^{3/2}}$$

$$E_{\pm y}(R,\alpha) = k_{\pm} \int_{\phi_{\pm 1}}^{\phi_{\pm 2}} \frac{(R\sin\alpha - \sin\phi)\, d\phi}{[R^2 + 1 - 2R\cos(\phi-\alpha)]^{3/2}} \quad ,$$

where the upper sign of $\pm$ is to be taken for the positively charged segment and the lower, the negatively charged segment; $k_{\pm}$ is the linear charge density. The observation point (R,α) is located at a distance R from the center of curvature (coincident with the origin (the north geomagnetic pole) of the coordinate system) of the arc segments, and at an angle α, positive eastward from the 06 local time meridian.

The electric field, the resulting ionospheric current intensity and the magnetic vectors have been numerically computed. Only the relative magnitude of the vectors and their distribution have been obtained, but it will be shown below that the mechanism provides a reasonable intensity for the convective electric field. Figures 2.3a and 2.3b show the distribution of the magnetic vectors for the two models for the height-integrated conductivity ratio $\sigma_H/\sigma_P = 5.0$. The actual northern polar ionosphere has been simplified to one of plane geometry with only a vertically downward magnetic field. The conductivities, σ_H and σ_P, are height-integrated Hall and Pedersen

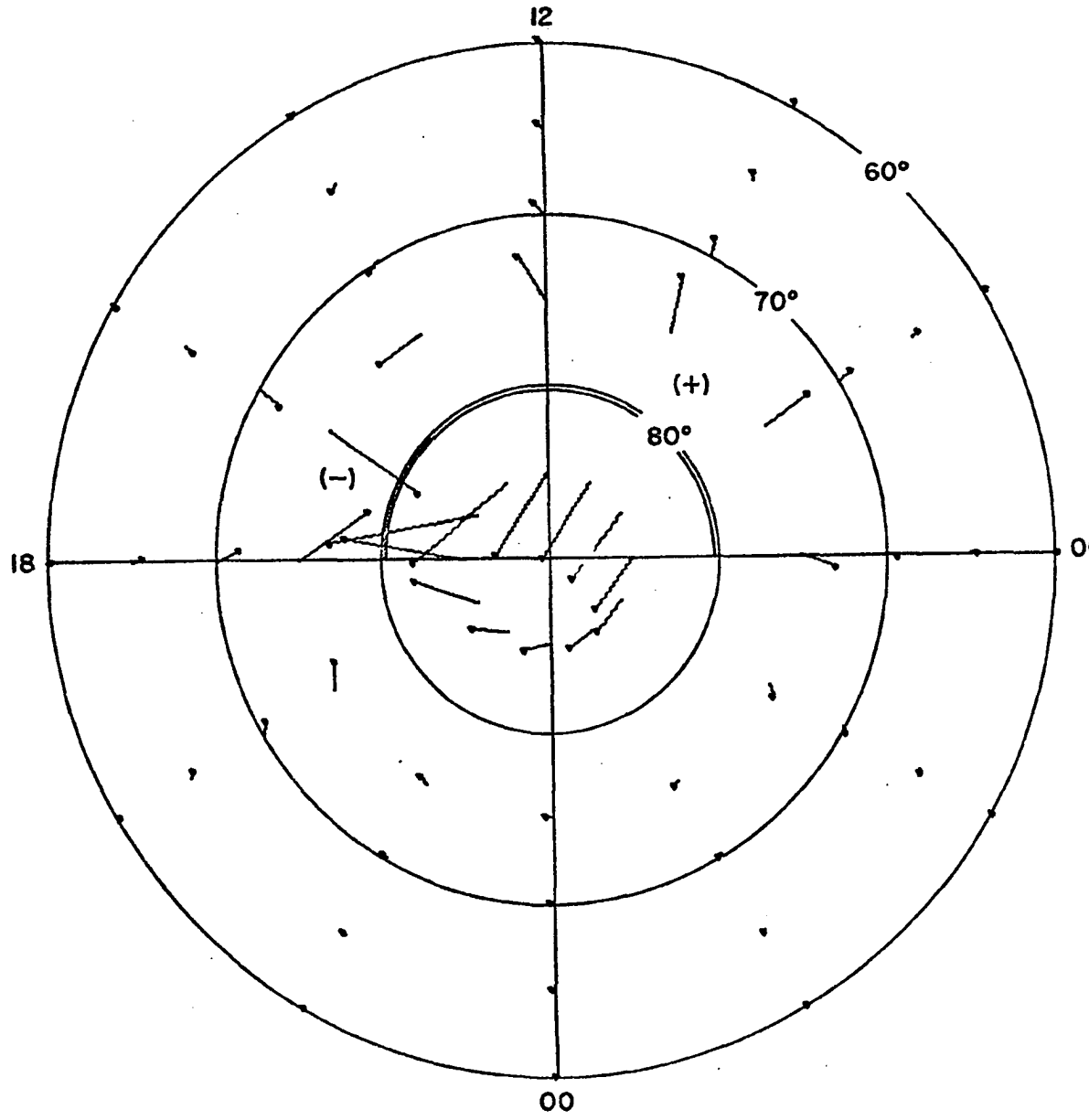

Fig. 2.3a. Polar plot of distribution of magnetic vectors produced by magnetopause charges on polar ionosphere. The segment of the 80° dp lat circle $0 \leq \phi \leq 3\pi/4$ is positively charged and the segment $3\pi/4 \leq \phi \leq \pi$ is negatively charged ($\phi = 0$ on the 06 hr time meridian). The magnitudes of the total positive and negative charges are equal.

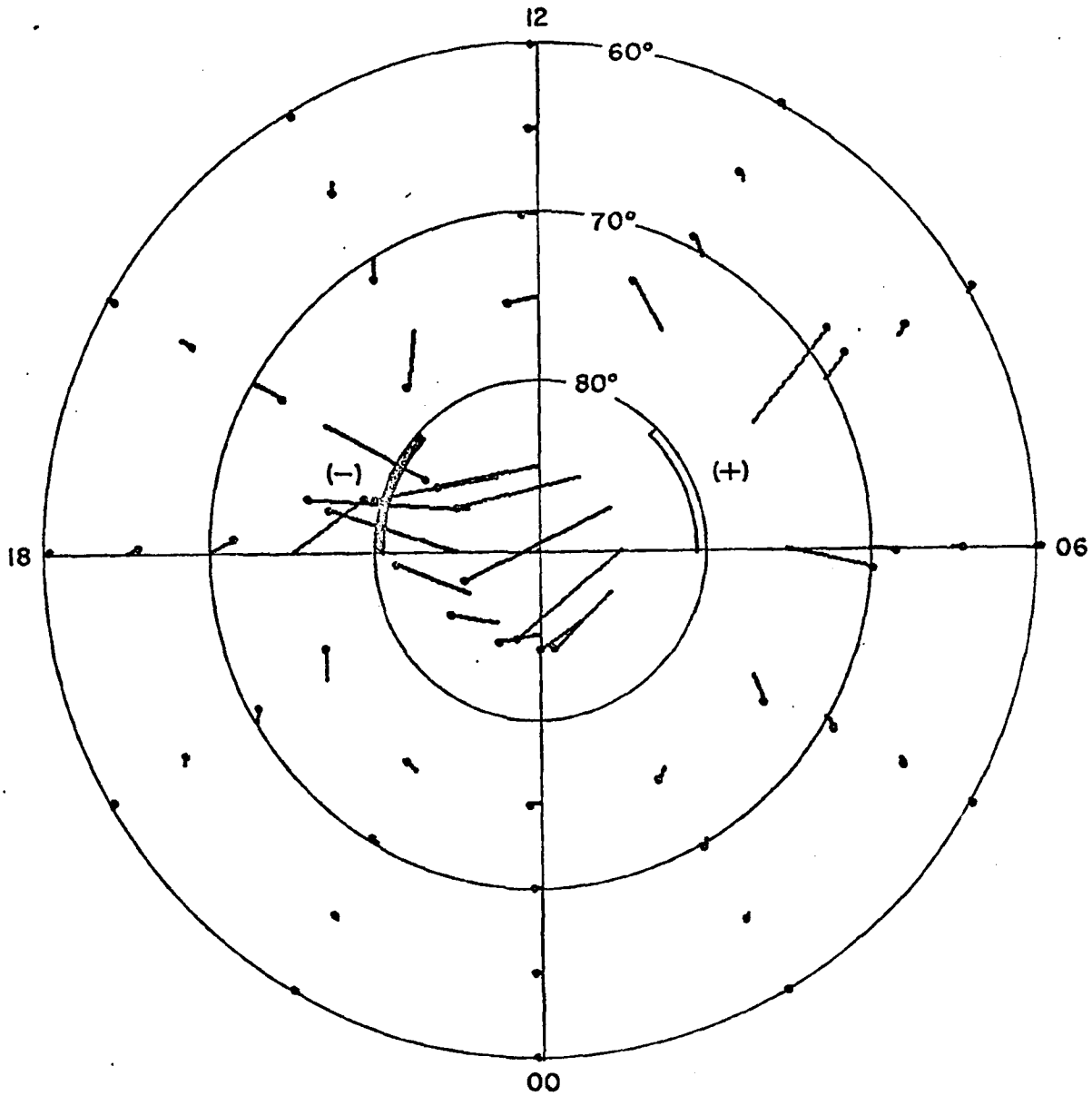

Fig. 2.3b. Polar plot of distribution of magnetic vectors produced by magnetopause charges on polar ionosphere. The segment of the 80° dp lat circle $0 \leq \phi \leq \pi/4$ is positively charged and the segment $3\pi/4 \leq \phi \leq \pi$ is negatively charged. The magnitudes of the total charges are equal.

conductivities, respectively (cf. Baker and Martyn, 1953).

It can be seen that both models reproduce fairly well the gross features of the distribution of the magnetic vectors below dp lat 80°, in spite of the simple assumptions made for the charge distribution. However, since high latitude stations are equipped with rather insensitive magnetometers, the accuracy of the scalings is insufficient to decide which of the two models is the most appropriate.

Several values of the ratio σ_H/σ_P, ranging from 0.5 to 5.0, have been examined, but it appears that a larger ratio best reproduces the observations. These ratios are in agreement with the estimates made by Baker and Martyn (1953) and Fejer (1953, 1964) for the sunlit hemisphere. This range is also in agreement with the values recently inferred from electron concentration measurements near the auroral ionosphere during twilight hours by Föppl, et al. (1968). The ratio is expected to be considerably smaller (the Pedersen dominates the Hall height-integrated conductivity) during nighttime conditions in the absence of ionizing sources. Estimates of each of these conductivities indicate that nighttime values are at least one order of magnitude smaller than daytime values (Boström, 1964).

Taking the magnitude of the S_q^p magnetic variation vector to be 50γ, the current density in the ionosphere is approximately given (Chapman and Bartels, 1940, p. 233) by $i_o = 10f\Delta X_o/2\pi = 10 \times 0.6 \times 5 \times 10^{-4}$ gauss$/2\pi = 4.8 \times 10^{-5}$ emu/cm $= 4.8 \times 10^{-4}$ amps/cm. Taking the height-integrated conductivity $\sigma_H = 8 \times 10^{-9}$ emu = 8 mho (Fejer, 1953; Föppl et al., 1968), the electric field (E) is of order 6.0×10^{3} emu $= 6 \times 10^{-5}$ volts/cm, so that the required speed of the

convective motion (v) in the transition region of the magnetospheric boundary will be of order $v = E/B \simeq 6.0 \times 10^{3}$ emu/ 2×10^{-4} gauss = 3.0×10^{7} cm/sec. Here, B in the transition region has been taken to be 20γ. This value for the speed of the convective motion is comparable to the speed of the solar wind, so that it is not an unreasonable one.

2.5.3.2 S_q^p above dp lat 80°

The computed distribution of the magnetic vectors above dp lat 80° (Figures 2.3a and 2.3b) differs greatly from the observed S_q^p pattern near the summer solstice (Figure 2.1a). For example, comparing the distribution along the dp lat circle 85° with that of Resolute Bay (third circle from the pole), there is a difference of order 60° ∿ 100° in the direction of the vectors.

Before continuing, it is worthwhile to comment on the assumption of constant conductivity throughout the polar region used to obtain Figures 2.3a and 2.3b. Heppner, et al. (1970) have recently inferred the electric field in the polar cap ionosphere from the motion of barium clouds. According to this study, these measurements suggest that the Hall and Pedersen conductivities in the polar cap regions are small relative to those along the auroral oval. This conclusion was based on the fact that the observed ground magnetic disturbance vectors were not compatible with either the Hall or the Pedersen current directions deduced from the direction of the electric field. These experiments were conducted during the late winter in twilight conditions and during periods of moderate magnetic disturbances which are known to be associated with enhancement of the auroral zone ionospheric conductivities. Absolute conductivities which would have proven useful in the

present work were not estimated in the paper by Heppner, et al. (1970). However, the strong seasonal dependence of S_q^p found by Kawasaki and Akasofu (1967) and Nagata and Kokubun (1962) strongly suggests a solar control of the polar quiet day magnetic variations. The most obvious solar effect is in the ionizing radiation, and hence in an increase in the conductivities (Hall more than Pedersen). Therefore, the assumption that the Hall conductivity dominates, and that its value is of order 10 mhos does not seem too unreasonable for the 'quiet' sunlit polar cap ionosphere.

It should be noted that the field lines originating inside the auroral oval are drawn away from the earth, downstream of the solar wind. The auroral oval delineates approximately the intersection line between the ionosphere and the outer boundary of the trapping region. For the quiet conditions which S_q^p represents, the oval is located at about dipole latitude 80° (cf. Akasofu, 1968).

It is instructive to estimate the lower limit of the boundary current contribution to S_q^p. Piddington (1964) has suggested that the full force of the solar wind is transferred as a Lorentz force ($\underline{i}_E \times \underline{B}$) on the earth, to which the magnetosphere is firmly anchored. For the portion of the geomagnetic field above 80° exposed to the solar wind, the earth current ($\underline{i}_E$) flows from dawn to dusk across the polar cap. This formulation is equivalent to determining the boundary current effects directly.

Another way of looking at this situation is to consider that the polar field lines, which are anchored nearly perpendicularly to the solid earth, are drawn away from the earth along the direction of the

solar wind, so that they tend to incline away from the sun. In the northern hemisphere, this is equivalent to adding to $\underline{B}$, a field $\Delta\underline{B}$, which is directed toward the sun. Such an additional field can be produced by an earth current flowing in the solid earth. A large seasonal variation of the magnitude of $\Delta\underline{B}$ may be due to the fact that the field lines originating in the summer polar cap are more greatly distorted along the sun-earth line than those originating in the winter polar cap (Nishida, Kokubun and Iwasaki, 1966).

Suppose that the field lines of the tail which are exposed to the full force of the solar wind and which originate in the area bounded by the 80° dp lat circle, lie in the cylindrical shell of inner and outer radii of 10 and 15 earth radii, respectively (i.e., it is assumed that the magnetospheric tail has a circular cross-section). The area of the cross-section of the shell is 1.60×10^{20} cm^2, and the force exerted by solar wind particles (speed $v = 3 \times 10^7$ cm/sec; number density = 5/cm^3) on the area is $2 \times 1.6 \times 10^{-24}$ g $\times$ 5/cm^3 $\times$ $(3 \times 10^7$ cm/sec$)^2$ $\times$ 1.60×10^{20} cm^2 = 2.30×10^{12} dyne.

The northern polar cap region (the area bounded by the 80° dp lat circle, A = 3.80×10^{16} cm^2) experiences one-half of the above force, F = 1.15×10^{12} dyne. The pressure there is then 1.15×10^{12} dyne $\div$ 3.80×10^{16} cm^2 = 3.03×10^{-5} dyne/cm^2. If the force is balanced by the Lorentz force resulting from the earth current i_E, then i_E = $(3.03 \times 10^{-5}$ dyne/cm$^2) \div (6 \times 10^{-1}$ gauss $\times$ 10) = 5.05×10^{-6} amp/cm. Here, the following relationship has been used: $F/A = (I/\ell) \times B$, where I denotes the total current, ℓ may be considered to be the diameter of the polar cap and $\underline{B}$ the average geomagnetic field in the polar cap.

Thus, the resulting magnetic field is of order $2\pi i_E/10 = 3.2 \times 10^{-6}$ gauss $= .32\gamma$.

Clearly, the effect at high latitudes of the boundary currents is negligible. It, along with the ring and tail contributions, is insufficient to direct the charge distribution field discussed in 2.5.3.1 toward the sun.

2.6 SUMMARY

This chapter describes the quiet time state of the magnetosphere and is presented as background for the studies of the disturbed conditions presented in the following chapters.

The main features of the lunar and solar (at low and middle latitudes) quiet day magnetic variations are both adequately explained by the action of the ionospheric dynamo. However, with regard to the latter variation, mechanism(s) have yet to be found which can give the necessary vector velocity field and/or conductivities required in the dynamo theory to explain the larger diurnal variation.

Non-ionospheric sources also produce diurnal variations; however, theoretical predictions and some satellite observations (cf. Cummings et al., 1971) indicate these contributions at low and middle latitudes are approximately a magnitude smaller than the observed surface variations.

The anomalously large polar quiet day variations S_q^p below 80° dp lat in the daylit polar cap can be explained by space charges distributed along the projection of the 'neutral line' on the polar ionosphere. This charge distribution is assumed to exist. Evidence for the existence of a neutral line (or neutral 'band', Frank, 1970) on the

magnetopause surface suggests that boundary space charges are the sources of the ionospheric space charges. These are continuously maintained by the solar wind and a convective S_q^p pattern in the polar ionosphere is the result.

The S_q^p pattern above 80° dp lat cannot be explained by the commonly recognized non-ionospheric sources discussed in Section 2.4, since these contributions are about two orders of magnitude too small. Moreover, the conventional dynamo theory of quiet day variations does not predict the existence of the polar cap S_q^p. The neutral line space distribution model presented in Section 2.5.3.1 for uniform polar region conductivities requires that a substantial sunward directed field exists during quiet times in the sunlit hemisphere in order to rotate the polar cap component sunward. The seasonal dependence of S_q^p suggests that ionospheric conductivities must play an important part in a full explanation of S_q^p. Also, since the polar cap field lines extend into the tail region, the theory should be related to the magnetospheric tail and, indeed, to its very existence during quiet times.

CHAPTER III

THE LOW LATITUDE ASYMMETRIC COMPONENT OF THE GEOMAGNETIC STORM FIELD

3.1 INTRODUCTION

The purpose of this chapter is to study the relationship between the low latitude DS component of the geomagnetic storm field and polar magnetic substorms in terms of an asymmetry index (defined in Section 3.3) and the auroral electrojet index. The field of the DS component is apparently related to the changes of the field and particles recently measured by the synchronous ATS-1 and ATS-5 satellites.

Geomagnetic disturbances recorded on the surface of the earth are observed to have a variety of forms. A class of disturbances, geomagnetic storms, has certain regular and distinguishing features.

At low and middle latitudes, the major characteristic which distinguishes a geomagnetic storm from other periods of disturbance is the growth and decay, in a relatively regular fashion, of a period of depression of the H-component field below that during undisturbed periods. Usually, the onset of a geomagnetic storm is signalled by a sudden positive change in the H-component field. Following this onset (ssc), there is an initial phase, during which the H-component may remain positive for several hours before the main phase decrease begins. A main phase decrease may last from a few hours to several hours before the maximum main phase decrease is reached; the field then slowly recovers (recovery phase) to its undisturbed value.

Polar magnetic substorms, which are large positive and negative changes with a duration of about 1 to 3 hours in the horizontal

component of the geomagnetic field at auroral latitudes, are the polar manifestations of the geomagnetic storm. In general, polar magnetic substorms are associated with the growth of the main phase decrease observed at lower latitudes. Negative bays (polar magnetic substorms) are also observed at the time of onset of ssc's and sometimes during the early part of the recovery phase. Geomagnetic storms may differ considerably in form from the typical but somewhat idealized description given above. In some examples there are no clearly identifiable onsets (ssc's), while in other cases the occurrence of more than a single sudden impulse (si) leaves in doubt which is to be associated with the subsequent main phase decrease. The duration of the initial phase, the main phase decrease and the recovery phase can also vary considerably from storm to storm.

In the preceding description, the average or typical variation of a geomagnetic storm after onset has been given; however, the beginning, duration and amplitude of all the phases except the recovery phase of a geomagnetic storm are strongly local time dependent.

The longitudinal dependence and latitudinal dependence of the geomagnetic storm and the concomitant polar magnetic substorms provide a basis, along with satellite measurements, for determining the structure of the magnetosphere.

The morphological features of the geomagnetic storm observed at the surface of the earth at any epoch can be represented in terms of a spherical harmonic expansion provided no radial currents pass through the surface of the earth. The spherical harmonic expansion coefficients can be obtained by first Fourier analyzing the disturbance magnetic

field (denoted by D) along a particular dipole (dp) latitude circle, $\theta = \theta_1$, and at a particular time, t, of a storm.

The disturbance field D can be separated into a part constant in longitude, Dst, and harmonic terms, DS. Thus, at a particular time and latitude,

$$DS = \Sigma\, DS_n = \Sigma\, C_n(t, \theta = \theta_1)\sin(n\lambda + \varepsilon_n).$$

where ε_n is a phase angle which depends on t and θ.

It is technically possible to obtain all the spherical harmonic coefficients of expansion from the Fourier coefficients C_n and phase angles ε_n of at least two of the three geomagnetic components (H, D and Z or X, Y and Z). However, practically all previous studies of geomagnetic storms have been based on only the first Fourier term DS_1, because of limited data and accuracy of measurements.

Once the distribution of the field is known over the entire surface of the earth, it is possible to obtain a current system which can synthesize the observed distribution of field. However, such current systems are not unique and to distinguish them from the actual current system which must exist, they have been termed 'equivalent' current systems.

Chapman (1918, 1935) obtained equivalent current systems for the Dst, DS_1, and $(Dst + DS_1)$ components from the analyses of geomagnetic storms at different latitude circles. For many years after Chapman's pioneering works, it was thought that the Dst component resulted from a ring or zonal current symmetric with respect to the dipole axis and that the DS component was produced by an ionospheric current system.

In constructing the DS current system, only the first harmonic component [$DS_1 = C_1 \sin(\lambda + \varepsilon_1)$] has generally been considered. However, in order to construct an accurate equivalent current system at high latitudes by this method, great care is necessary; at the very minimum the data of several stations are needed between dp lat 60° and 75° where the geomagnetic storm field fluctuates rapidly and where, therefore, higher harmonic terms must be taken into account. Indeed, this method failed to reveal some essential features of the westward auroral electrojet which has on occasion been observed to flow all along the auroral oval. For example, it has been shown by other methods that magnetic disturbance activity peaks twice a day at stations between dp lat 65° to 75° (Nikolsky, 1947). Furthermore, when only the first harmonic term is used in the analysis, one is certain to obtain a pair of electrojets along the auroral zone ($\theta \simeq 65°$), the so-called "eastward electrojet" and the "westward electrojet". This is because the first harmonic component of DS(H), $DS_1(H)$, is positive in the noon-evening sector and negative in the midnight-morning sector in the auroral zone.

The DS component in middle and low latitudes is, however, relatively simple and the first harmonic term is a good first approximation.

As has been mentioned, it had long been thought that DS_1 was due to the return currents from the eastward and westward auroral electrojets. Specifically, it was thought that the H component of DS_1, $DS_1(H) > 0$ was due to the return current from the westward electrojet and that $DS_1(H) < 0$ was due to the return current of the eastward electrojet. Clearly, this suggests that the amplitude of the $DS_1(H)$ component, $C_1(t)$,

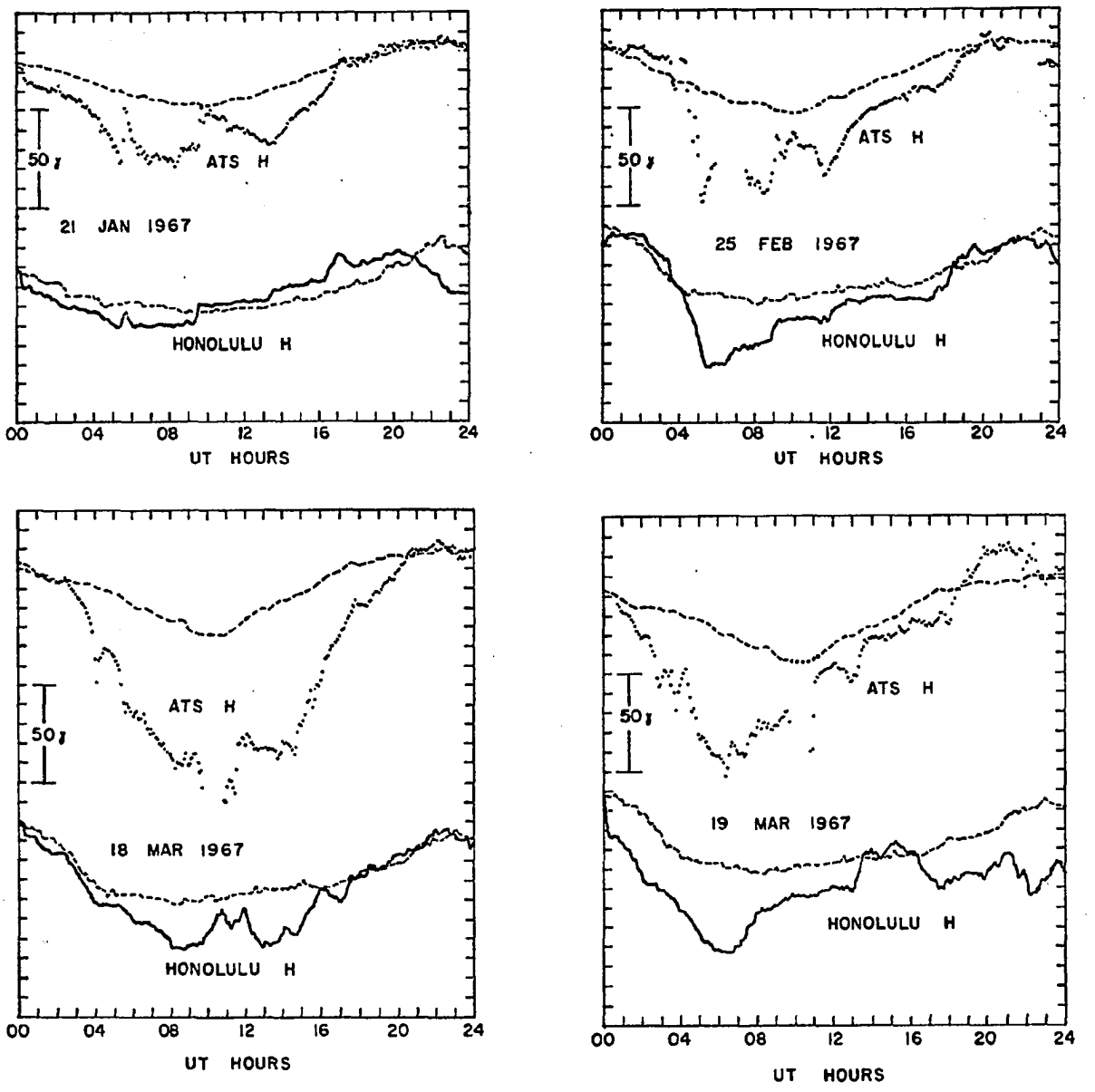

Fig. 3.1. Comparison of ATS-1 and Honolulu H-component records for four days in early 1967.

in middle and low latitudes should be proportional to that along the auroral zone. However, Akasofu and Chapman (1964) showed that this was not always the case and proposed, as a first approximation, that the low and middle latitude DS_I component is due to the asymmetry of the ring current.

Although the asymmetry of the ring current field was later directly observed by satellite-borne magnetometers (Cahill, 1966), the interpretation of the low and middle latitude magnetic disturbance fields in terms of the asymmetry of the ring current is not straightforward. Moreover, electric currents in the tail, field-aligned currents and currents flowing on the magnetospheric boundary can also contribute to the asymmetry and to the morphological distribution of the disturbance field in general.

3.2 A COMPARISON OF MAGNETIC RECORDS AT SYNCHRONOUS ALTITUDES AND GROUND STATIONS

An important and opportune moment in the investigation of geomagnetic storm fields arrived when the synchronous orbit ATS-I was placed nearly directly above Honolulu in late 1966. It was found by Cummings and Coleman (1968) and Cummings, Barfield and Coleman (1968) that the ATS-I and Honolulu magnetic records of short-lived magnetic substorm phenomena were qualitatively similar. However, a comparison of the records shows that there is also a qualitativee similarity of the daily variation of the storm fields at the two locations. Figure 3.1 shows four such examples. Daily variation, here, means the variation of the storm field observed at a station during the course of a day. There were also many other days when the ATS-I and Honolulu records were remarkably similar.

The similarity of magnetic records at the two locations leads to the conclusion that the fields observed must primarily arise from a current distant from either location (since no other single source of current external to the earth can give the proper amplitude and phase similarity that is observed). As a first approximation, then, one can conclude that the primary current which produces the observed Honolulu and ATS-I disturbance field is largely outside the orbit of ATS-I.

In the following sections, the low latitude storm fields will be examined to determine whether the morphology of such changes is compatible with this conclusion.

3.3 THE AURORAL ELECTROJET AND THE ASYMMETRY INDICES

In studying the time dependence of the occurrence of polar magnetic substorms, Davis and Sugiura (1966) introduced a new index, AE (for auroral electrojet). Their method of producing the AE index is essentially equivalent to superposing the H-component records of several auroral zone stations and obtaining the range between the upper and lower envelopes as a function of Universal Time. By reducing the H-component traces to the same sensitivity and time scale and choosing a quiet-time baseline for each of the traces, it is possible to obtain the AE index as a function of UT on a continuous basis. Such a continuous index is needed in studying rapidly varying phenomena as magnetospheric substorms.

The lower and the upper envelopes of the superposed auroral zone records, measured from the quiet-time baseline, were denoted by Davis and Sugiura (1966) as AI and AU, respectively. The AL index is a

measure of the westward auroral electrojet while the AU index gives a measure of eastward flowing currents in the auroral zone. In the present work, the continuous lower envelope which gives the AL index will be used instead of the AE index unless otherwise specified, since it has more definite meaning in that it provides a measure of the intensity of the auroral electrojet in the midnight-early-morning sector as a function of UT.

One can similarly obtain a measure of the longitudinally asymmetric development of a geomagnetic storm by superposing the records of several low or middle latitude stations after extraction of the quiet day variations. The range of the envelope of the superposed records is here denoted the ASY index. This is the same quantity defined by Davis and Sugiura (1966) as the range of DS, R(DS). The average value of the storm field at any instant over a set of low latitude stations widely spaced in longitude is denoted the Dst index and provides a measure of the intensity of the storm. It is clear that if the values of the fields at any pair of stations at any particular instant differs considerably above and below the Dst value, a substantial value is obtained for the ASY index.

The two indices ASY and AE (or AL) form the basis for studying the geomagnetic storm in a way other than has been conventional, namely harmonic expansions and iso-intensity contours of the geomagnetic disturbance field components (cf. Akasofu and Chapman (1964)). The growth and decay of the asymmetry index, ASY, and the westward auroral electrojet, AL, together with satellite data will have direct bearing

on the question of whether the observed polar substorms and low latitude DS type changes are related.

3.4 A STUDY OF SEVERAL GREAT GEOMAGNETIC STORMS

3.4.1 The geomagnetic storm of September 13, 1957

This storm has been extensively studied since it was one of the largest to occur during the IGY period. Akasofu and Chapman (1964) made a detailed analysis of the event and proposed from this work that the ring current is asymmetric. Their study was primarily based on maps of the iso-intensity contours of the H-component at various epochs of the storm.

Figure 3.2a shows the superposition of the H-component records of five auroral zone stations (College, Cape Chelyuskin, Kiruna, Leirvogur and Byrd Station in Antarctica). Figure 3.2b is a superposition of the H-component records of five low latitude stations (Honolulu, Memambetsu, Quetta, Tamanrasset and San Juan) after removal of the quiet day variation at each of the stations. The mean dipole latitude of the latter set of stations is about 25°.

In Figure 3.2c, the lower envelope from the superposed auroral zone records in Figure 3.2a (designated as the intensity), the range between the upper and lower envelopes in Figure 3.2b (designated as the asymmetry) and values of the corresponding hourly Dst index are plotted as a function of Universal Time. It is immediately clear that although the jet intensity and the asymmetry show some degree of correlation, their UT dependence differs considerably from that of the Dst index. On the other hand, it may be noted, in this

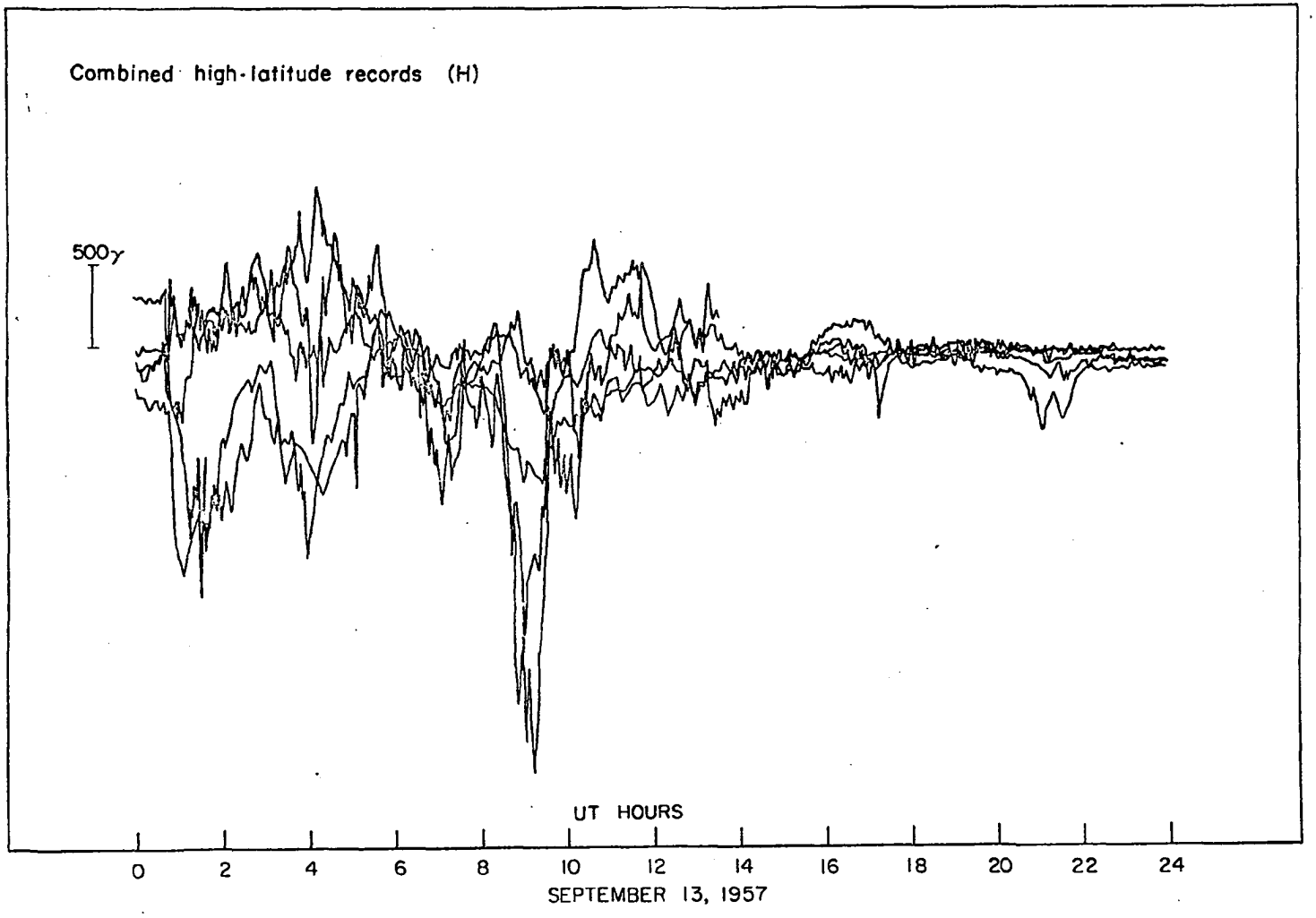

Fig. 3.2.a Superposition of H-component records of several high latitude stations during the September 13, 1957, storm. The AE index is defined as the range of the upper and lower envelopes. The AL and AU indices are defined as the ranges from the baseline of the lower and upper envelopes, respectively.

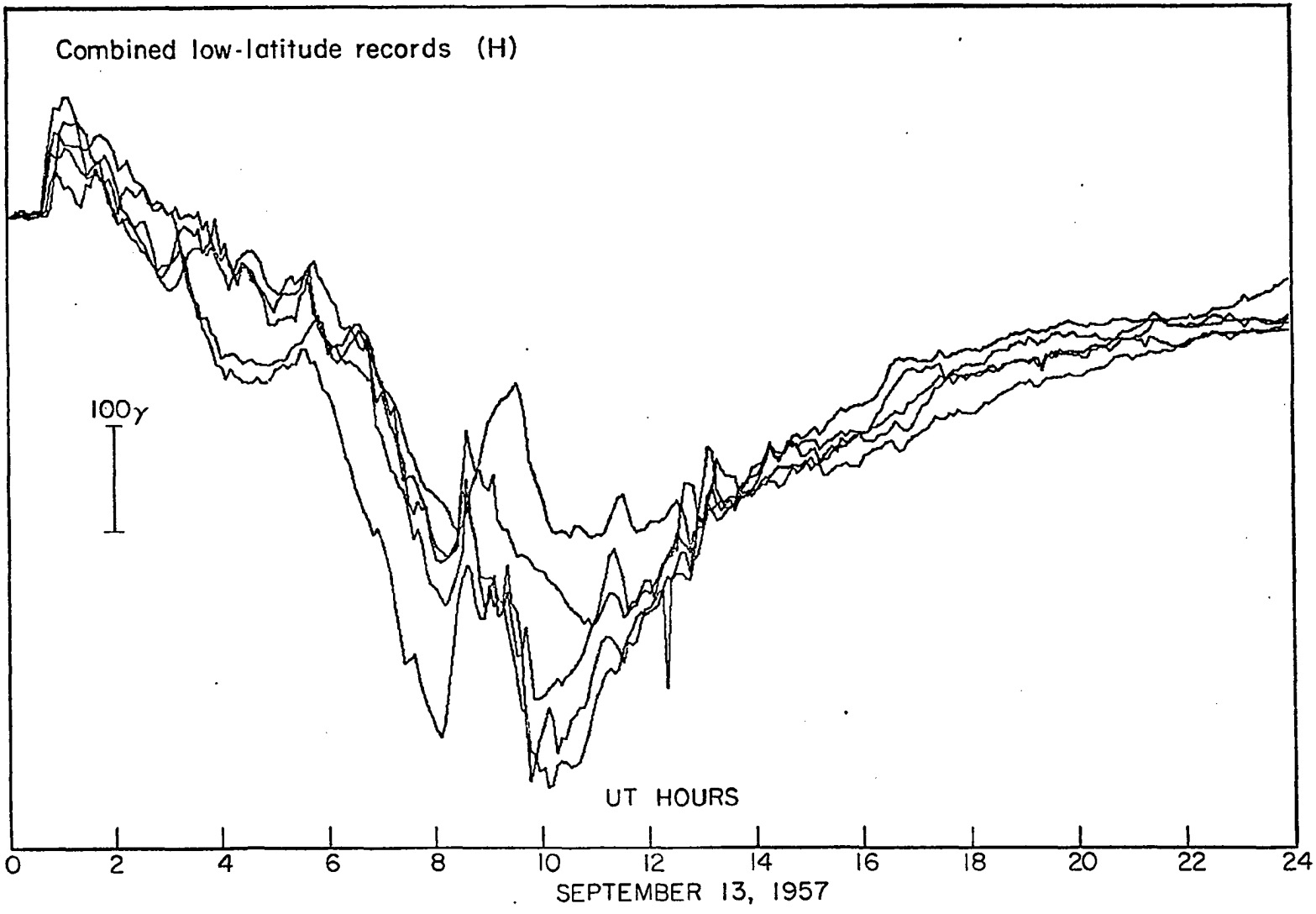

Fig. 3.2.b Superposition of H-component records of several low-latitude stations during the September 13, 1957, storm. The ASY index is defined as the range of the upper and lower envelopes. The Dst index is the mean value of these records.

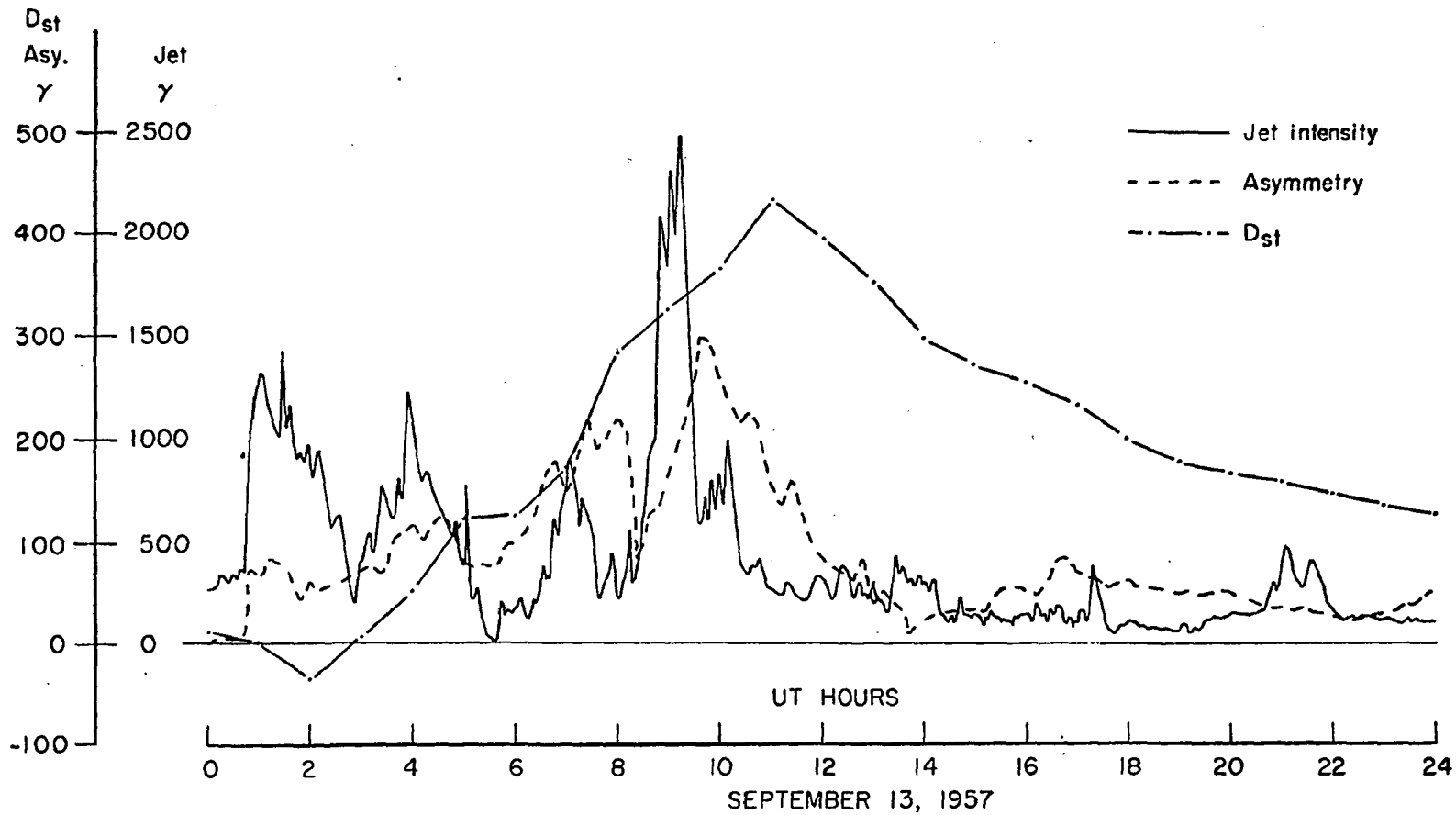

Fig. 3.2.c Westward electrojet intensity (AL), asymmetry (ASY) and Dst indices for September 13, 1957, storm.

particular example, that the correlation between the ASY and AL indices is far from what one might expect if the DS changes at low latitudes were of ionospheric origin, that is, due to return currents of the auroral electrojet in the ionosphere. Three major points which argue against such an interpretation are:

(i) The presence of a large asymmetry when the intensity of the jet was low, particularly at about 0800 UT.

(ii) The peak value of the jet intensity occurred 30 minutes prior to that of the asymmetry.

(iii) Between 0800 and 0900 UT the jet intensity varied by an order of magnitude whereas the magnitude of the asymmetry varied by a factor of two.

3.4.2 The geomagnetic storm of September 21-23, 1963

The combined records for the September 21-23, 1963, storm of several high latitude stations are shown in Figure 3.3a. Figure 3.3b shows the corresponding combined low latitude records. The ASY, AL, and Dst indices for this storm are presented in Figure 3.3c.

This period of activity appears to contain two distinct main phase decreases. There certainly occurred an ssc at approximately 1400 UT on September 21, with a corresponding moderate maximum main phase decrease occurring at about 0545 UT, September 23. However, thereafter, the field became nearly symmetric; a second, very deep main phase decrease began about 1900 UT, September 22. Both main phase decreases were accompanied by large, rapid positive and negative fluctuations. Although the storm was extremely complex, there was a remarkable correlation between the ASY and AL indices for the occurrence times of the major peaks. However, the magnitudes of the changes in the ASY

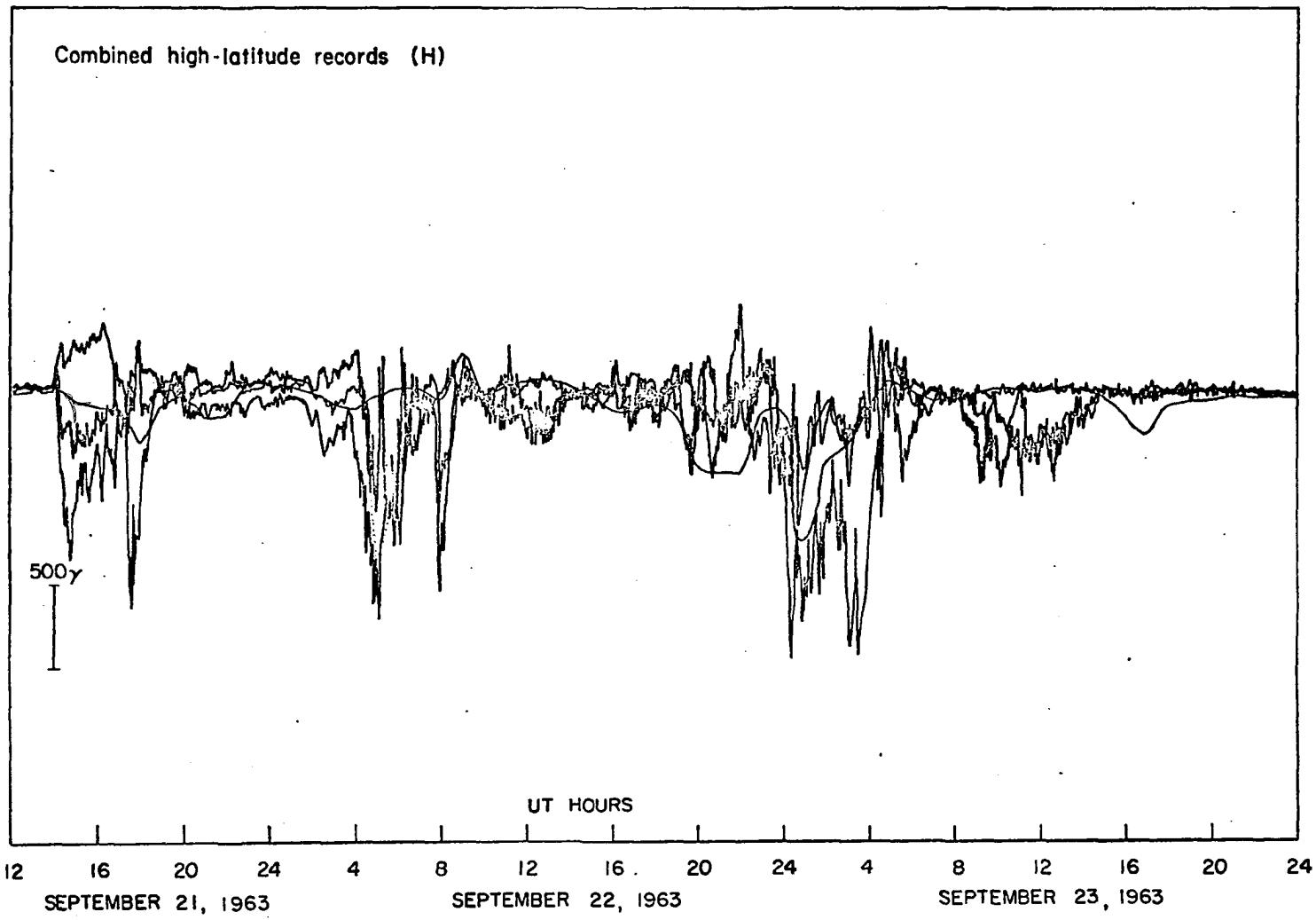

Fig. 3.3.a Superposition of H-component records of several high latitude stations during the September 21-23, 1963, storm.

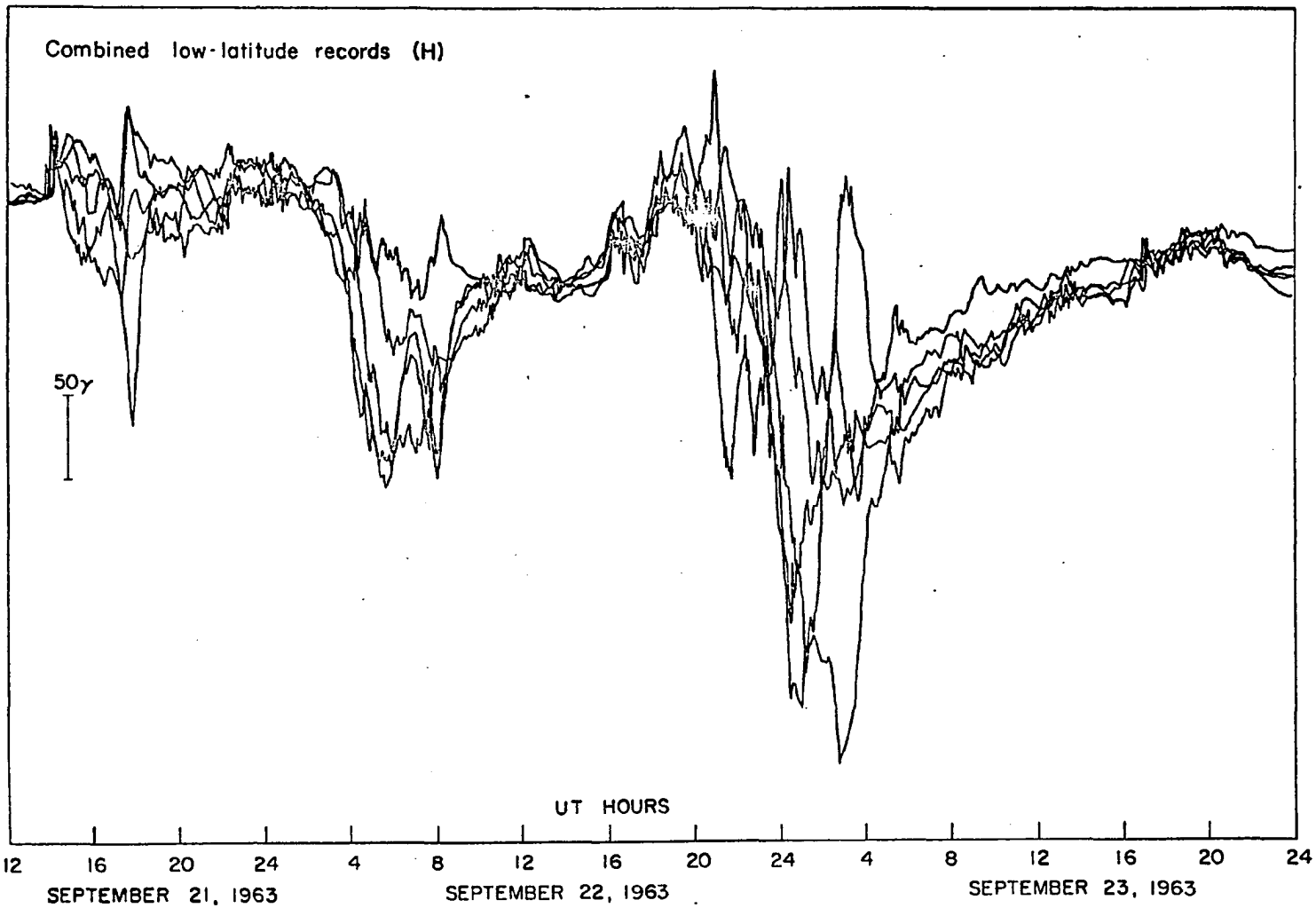

Fig. 3.3.b Superposition of H-component records of several low latitude stations during the September 21-23, 1963, storm.

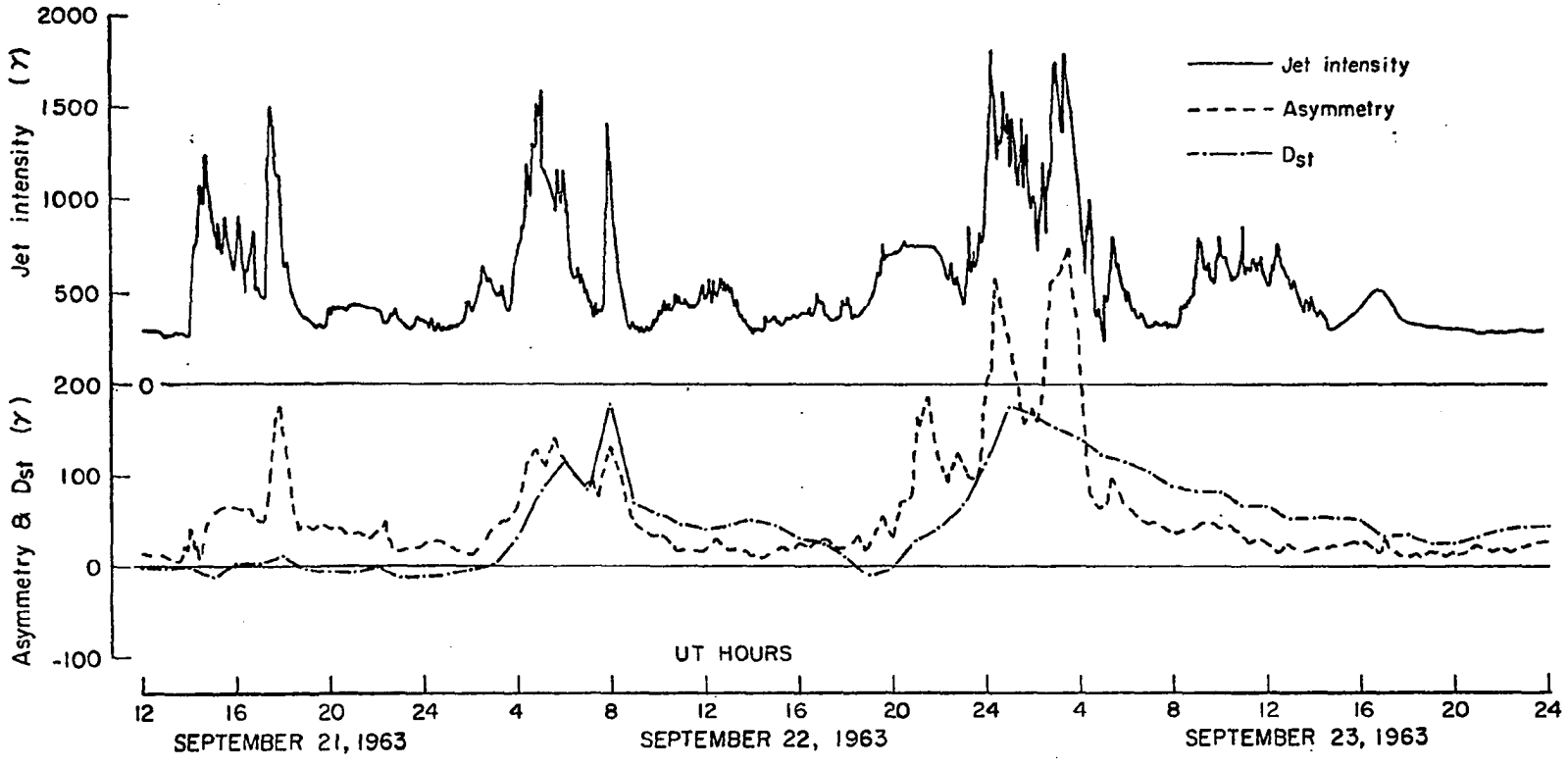

Fig. 3.3.c AL, ASY and Dst indices for September 21-23, 1963, storm.

index are not as well correlated with the AL index as one might expect if the source of the ASY type changes were due chiefly to return currents.

3.4.3 The geomagnetic storm of April 17/18, 1965

This storm was studied earlier by Meng and Akasofu (1967) and Akasofu and Meng (1969). Figures 3.4a and 3.4b are superpositions of the high and low latitude records of the H-component, respectively, for this period. The AL index (denoted as the jet intensity), the ASY index (denoted as the asymmetry) and the Dst index for this storm are shown in Figure 3.4c, in which it has been assumed that no disturbance field D(H) existed at 1200 UT on April 18, 1965.

It can be seen in Figures 3.4b and 3.4c that there is a remarkable decrease at 0610 to 0650 UT, April 18, 1965, in the asymmetry index during the time when the most intense polar substorm was in progress. Just before the onset of this particular substorm, that is, at about 0600 UT, the largest main phase decrease was observed in the evening sector at such stations as Honolulu and Apia; the lower envelope between 0400 and 0600 UT in Figure 3.4b. is the Honolulu trace. However, during the substorm, there occurred a very intense positive change at low latitude stations located in the evening sector; it is this change which was the cause of the temporary reduction in the ASY index. This is the same type of positive change discussed by Cummings, Barfield and Coleman (1968) and Coleman (1970) who noted it in satellite data.

This phenomenon can also be recognized in the September 13, 1957, storm at about 0800 UT. In Figure 3.2b the lower envelope between 0600 and 0800 happens to be the Honolulu record. Because of the large positive change which began soon after 0800 UT, the magnitude of the

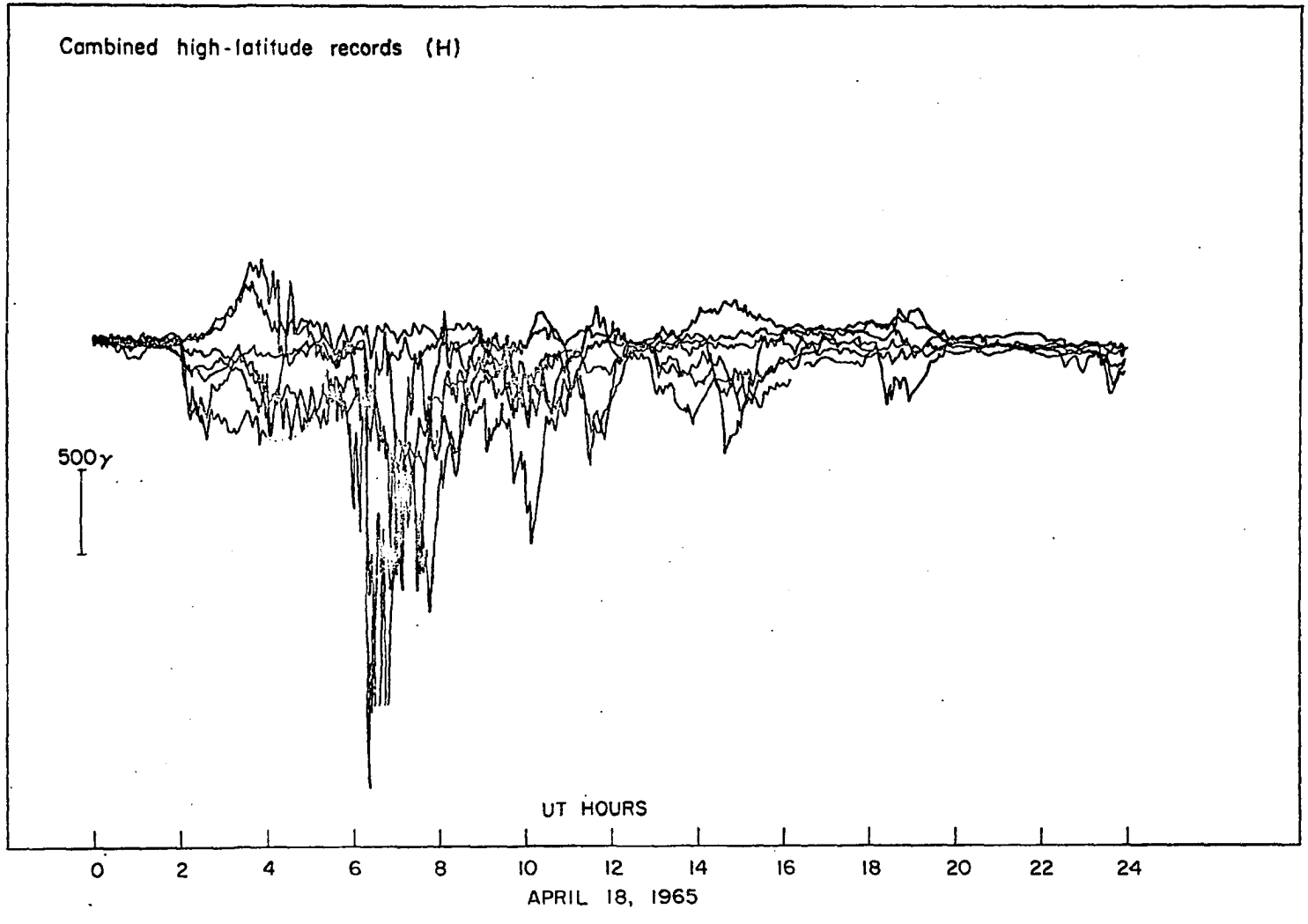

Fig. 3.4.a Superposition of H-component records of several high latitude stations during the April 17-18, 1965, storm.

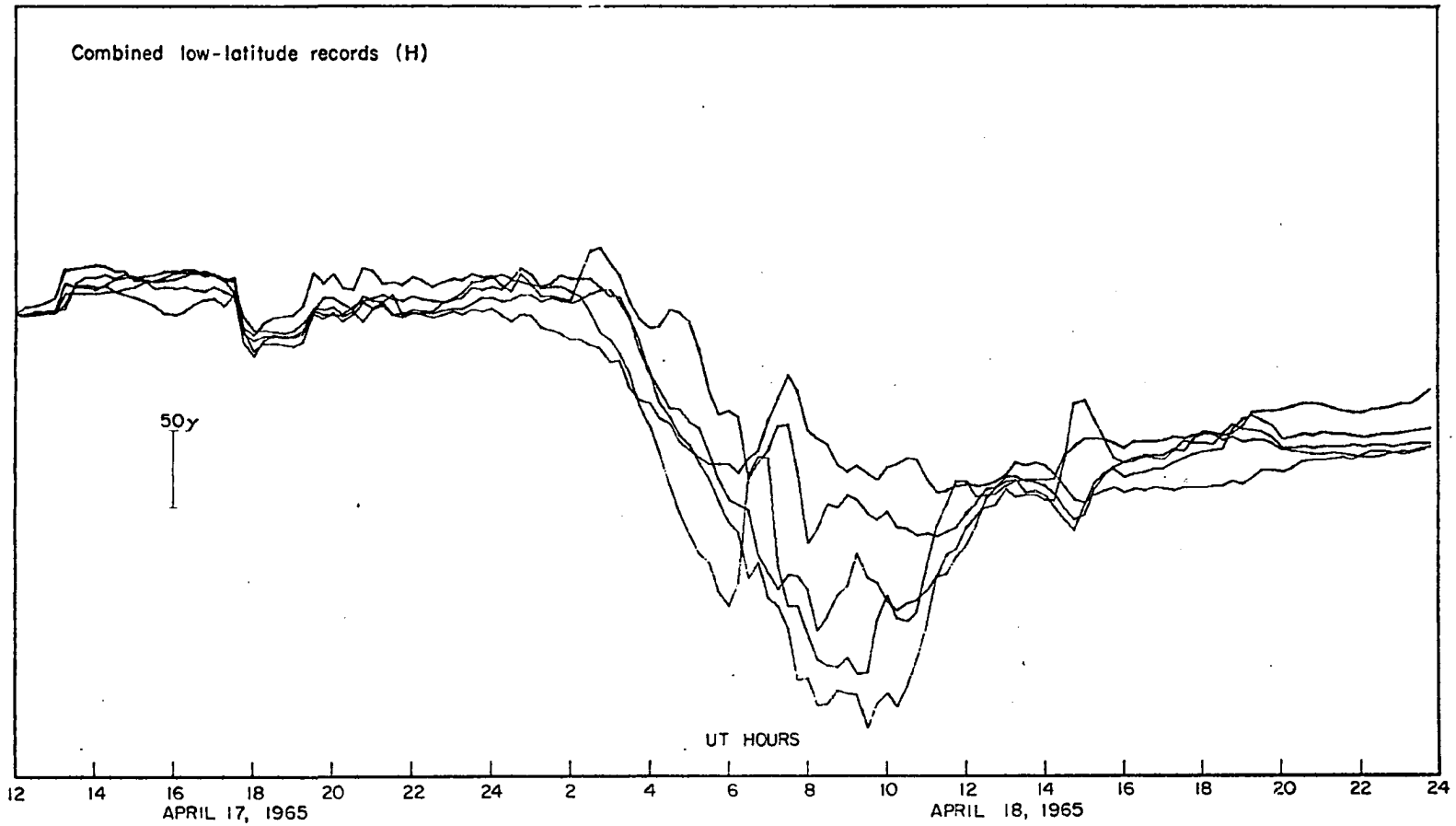

Fig. 3.4.b Superposition of H-component records of several low latitude stations during the April 17-18, 1965, storm.

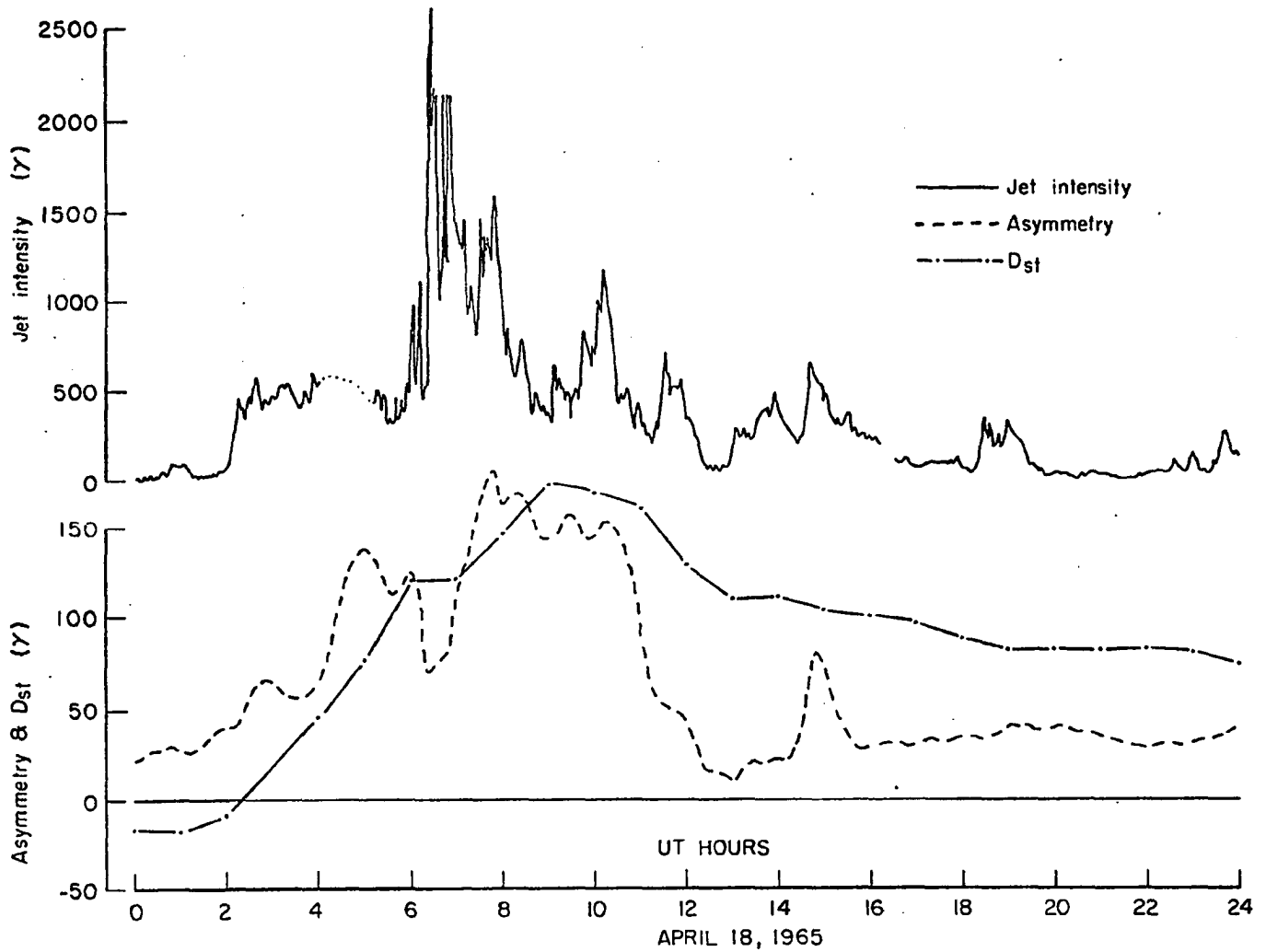

Fig. 3.4.c AL, ASY and Dst indices for April 17-18, 1965, storm.

ASY index became small relative to the previous period. However, by the end of the substorm (~0950 UT) the asymmetry had grown considerably.

Another feature of interest of the April 18, 1965, storm (see Figures 3.4b and 3.4c) is the rapid decrease of the asymmetry index after 1000 UT. In particular, it is the rapid convergence of the lower envelope to the more slowly recovering upper envelope between 1000 and 1300 UT which produced the rapid decay of the ASY index. This was also the case for the September 13, 1957, storm.

3.4.4 The geomagnetic storm of January 13/14, 1967

Figures 3.5a and 3.5b show the superposition of the high and low latitude magnetic records, respectively, for the January 13/14, 1967, storm and Figure 3.5c the jet intensity, magnitude of asymmetry and the Dst index. Although there occurred a small positive change at about 0015 UT on January 14, it was not large enough to substantially reduce the asymmetry index. At about the same time the AL index decreased. Except for the period between 0100 and 0300 UT, it may be noted that the AL and ASY indices were well correlated. Around 1100 UT on January 14, the traces began to converge and, thereafter, both the asymmetry and electrojet indices became quite small.

3.4.5 The geomagnetic storm of May 25/26, 1967

This storm was one of the most intense to occur during the last decade; the Dst index reached -400 gammas (Akasofu, Perreault and Yoshida, 1969). An intense main phase began to develop after 1930 UT on May 25 (see Figures 3.6b and 3.6c). Intense substorm activity between 2000 UT and 2300 UT (see Figure 3.6a) was associated with an increase in the asymmetry index. the correlation between the two indices AL

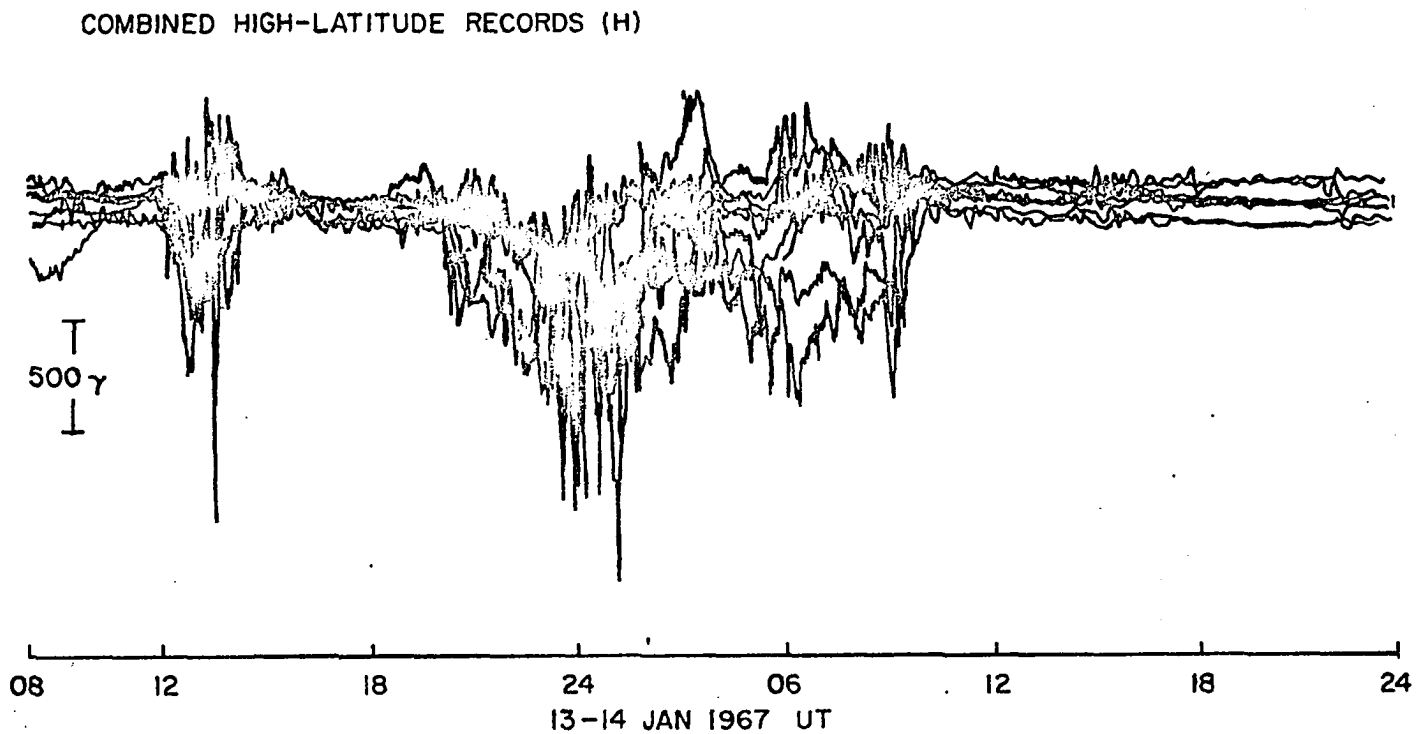

Fig. 3.5.a Superposition of H-component records of several high latitude stations during the January 13-14, 1967, storm.

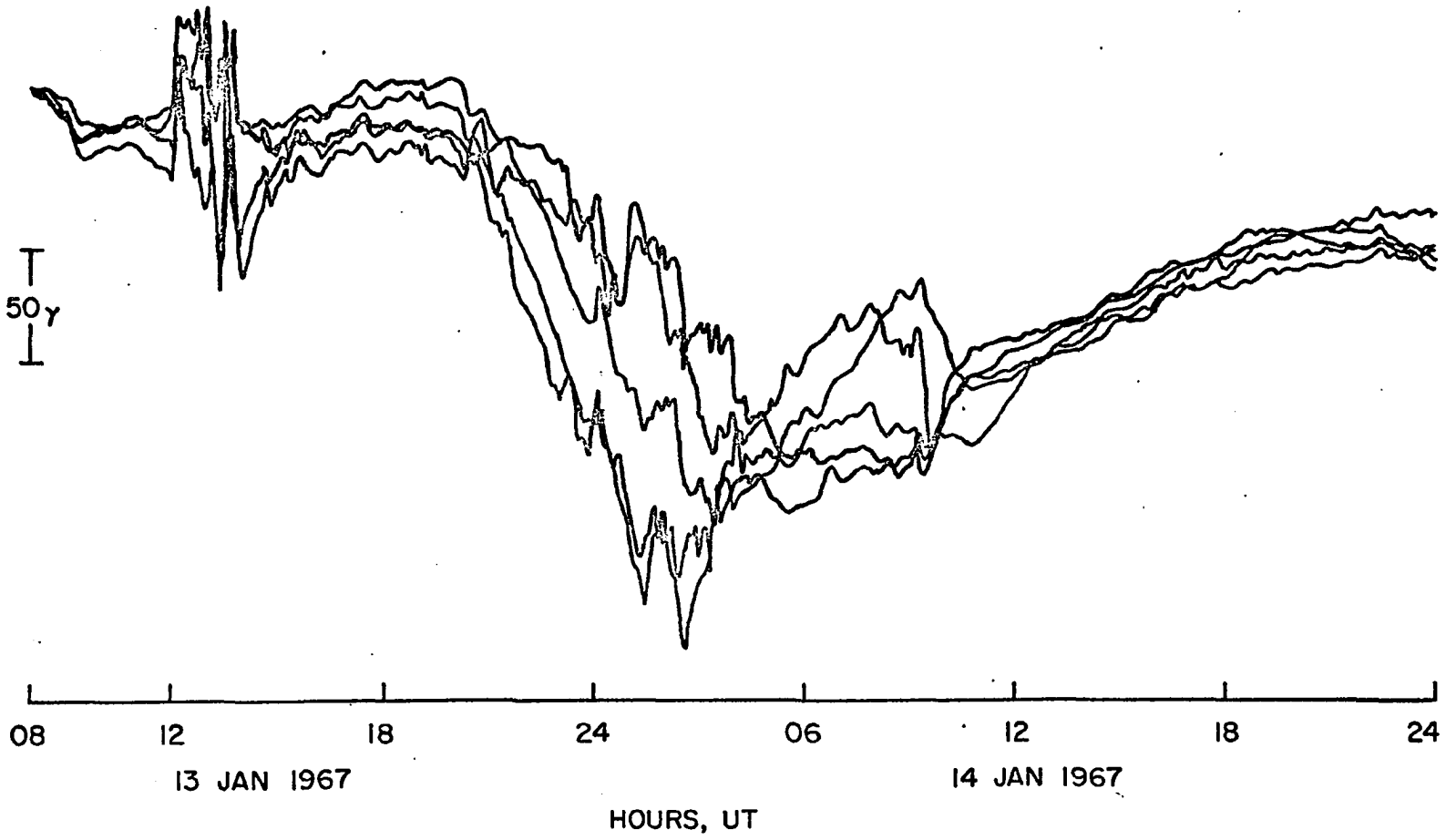

Fig. 3.5.b Superposition of H-component records of several low latitude stations during the January 13-14, 1967, storm.

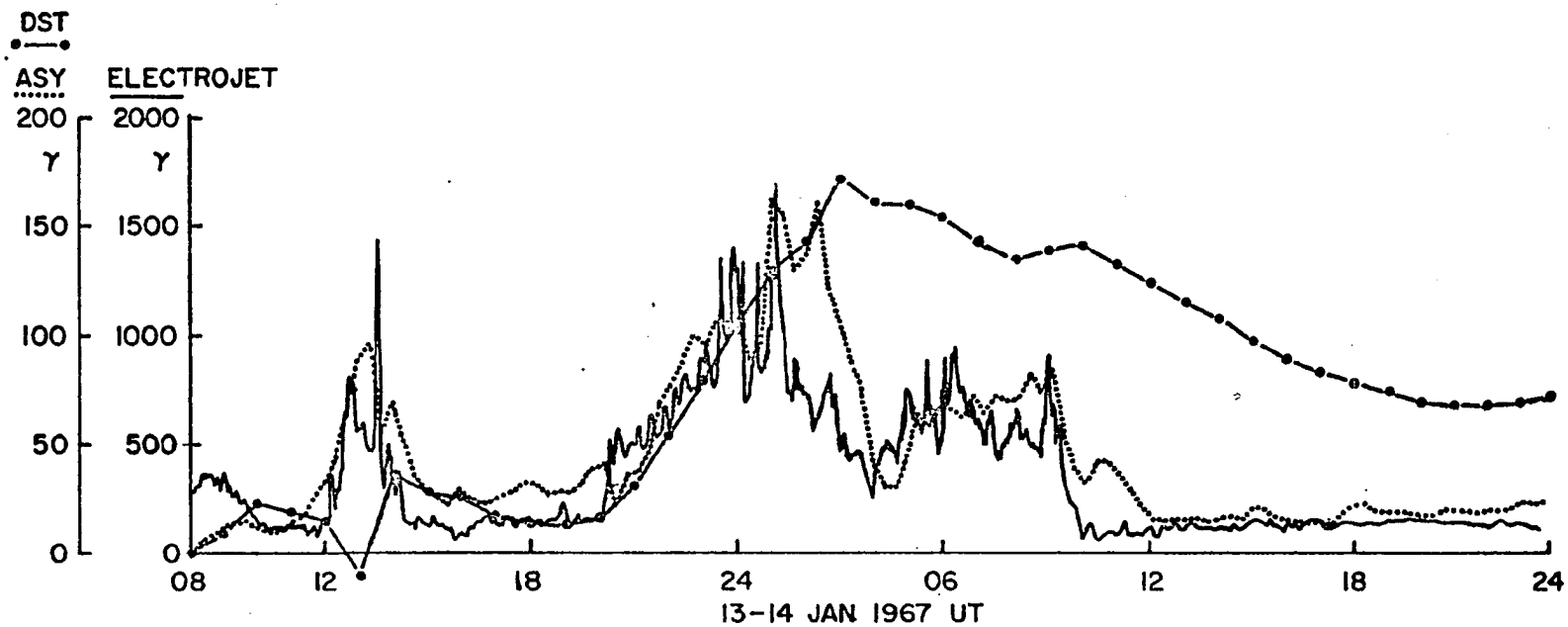

Fig. 3.5.c AL, ASY and Dst indices for the January 13-14, 1967, storm.

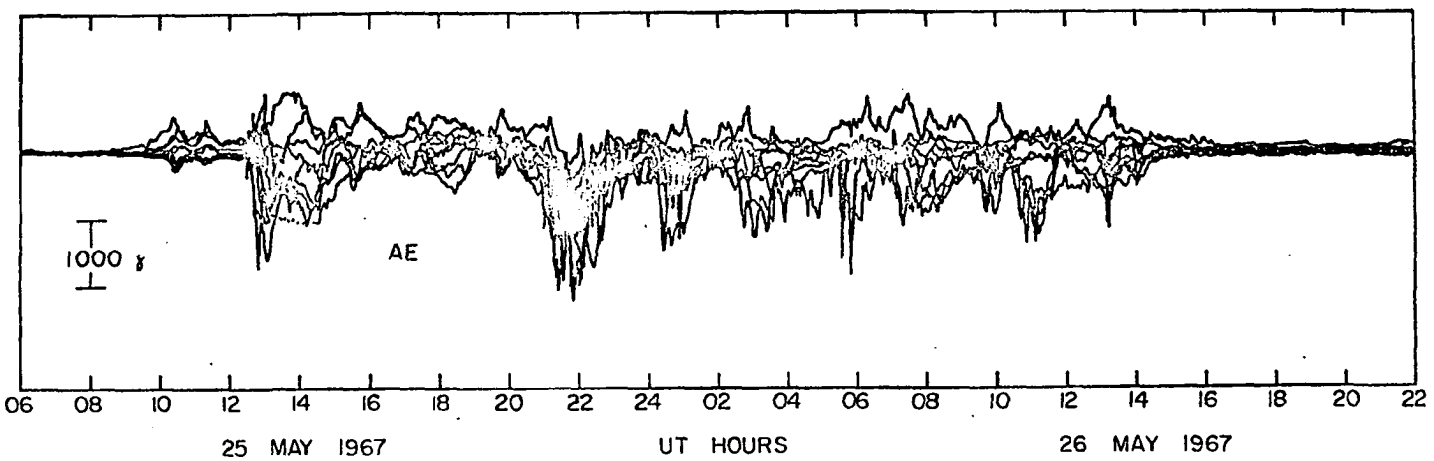

Fig. 3.6.a Superposition of H-component records of several high latitude stations during the May 25-26, 1967, storm.

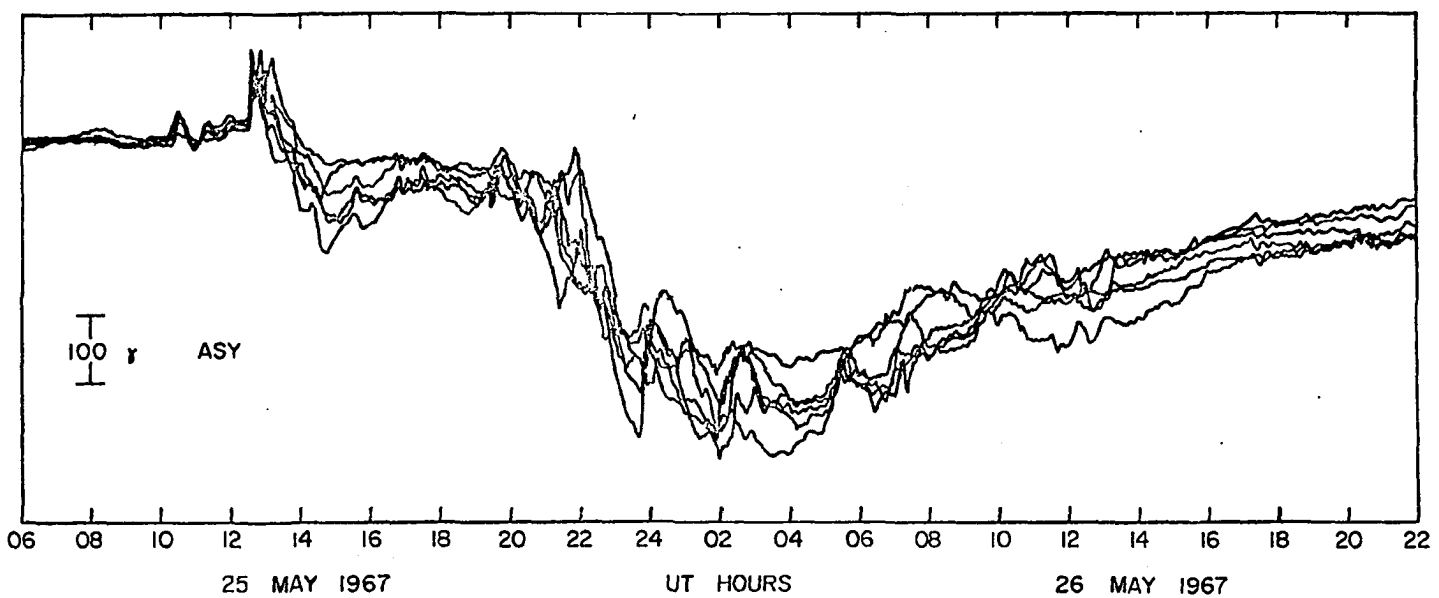

Fig. 3.6.b Superposition of H-component records of several low latitude stations during the May 25-26, 1967, storm.

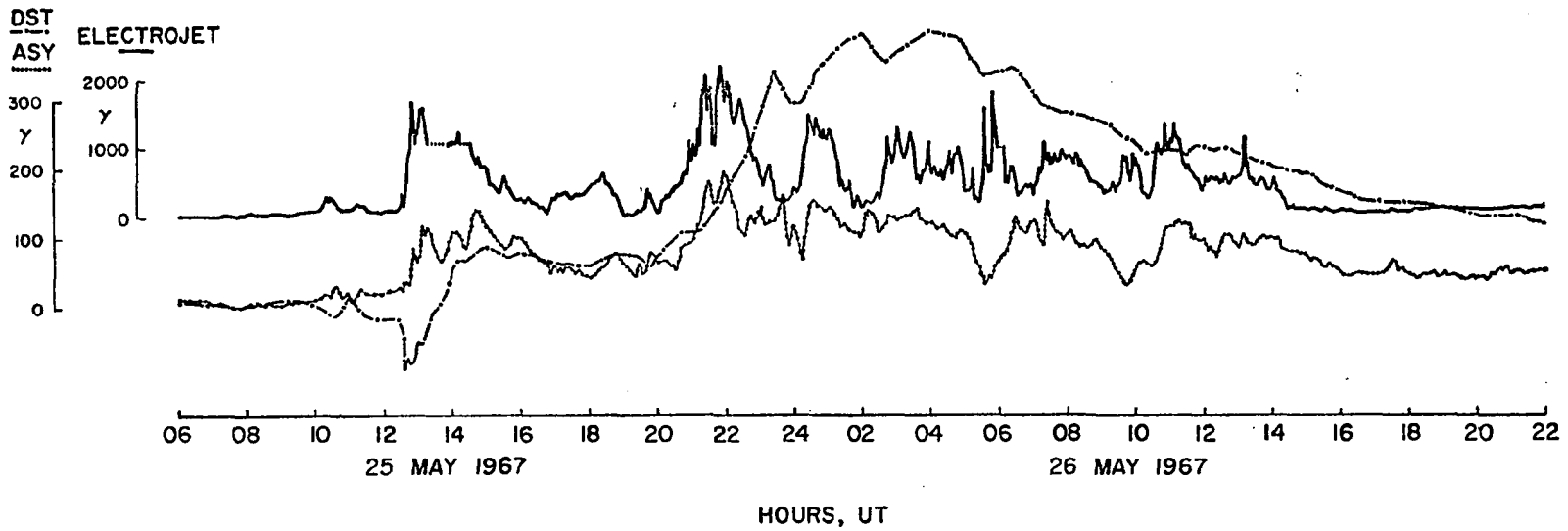

Fig. 3.6.c AL, ASY and Dst indices for the May 25-26, 1967, storm.

and ASY was fairly good up to 2200 UT on May 25. However, near the end of the substorm (~2300 UT) the electrojet intensity decreased to near the zero level while the asymmetry index remained relatively high.

At 2345 UT, when a new substorm began and the AL index increased, the degree of asymmetry was low and remained so for about half an hour before rising; at about 0010 UT on May 26, the asymmetry reached a minimum while the electrojet intensity had approached its peak value. The decrease of asymmetry was associated with a large positive increase at Quetta (which is the bottom trace of Figure 3.6b at 2300 UT, May 25. This positive change was also responsible for a small, temporary recovery in the Dst index.

Significant anti-correlations are also seen during polar substorm activities which began at 0500 UT and 0845 UT. In particular, during the substorm which began at about 0500 UT, most of the low latitude stations except M'Bour (upper trace in Figure 3.6b at 0400 UT, May 26) recorded a positive change. This effect is again reflected in the Dst index which began to recover at about the same time. Similar but lesser anti-correlations can be seen at other times such as 0200 UT, 0700 UT and 1000 UT.

3.4.6 Other geomagnetic storms

The geomagnetic storms of January 7-8, 1967, February 7-9, 1967, February 15-18, 1967, May 1-4, 1967, June 25-27, 1967, and October 31-November 1, 1968, have also been analyzed in the manner outlined above. The results are presented in Figures 3.7 through 3.12. Line plots of these storms and several others are compiled in Appendix A.

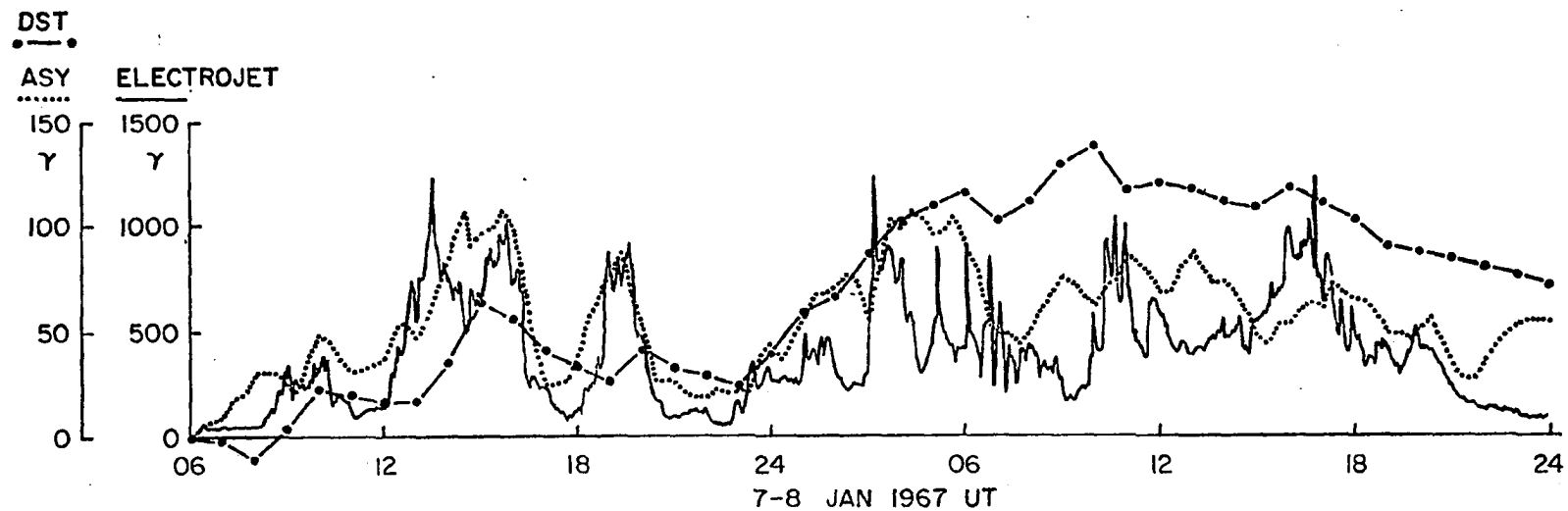

Fig. 3.7. AL, ASY and Dst indices for the January 7-8, 1967, storm.

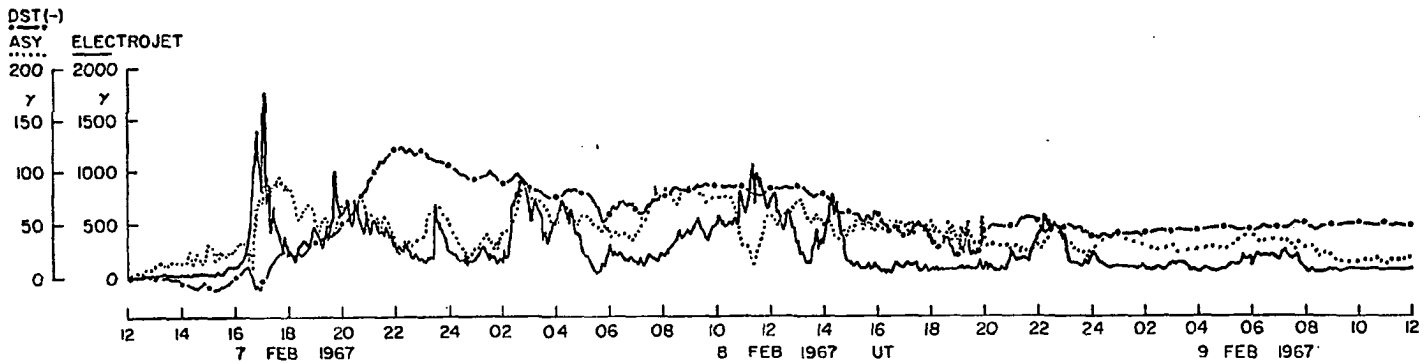

Fig. 3.8. AL, ASY and Dst indices for the February 7-9, 1967, storm.

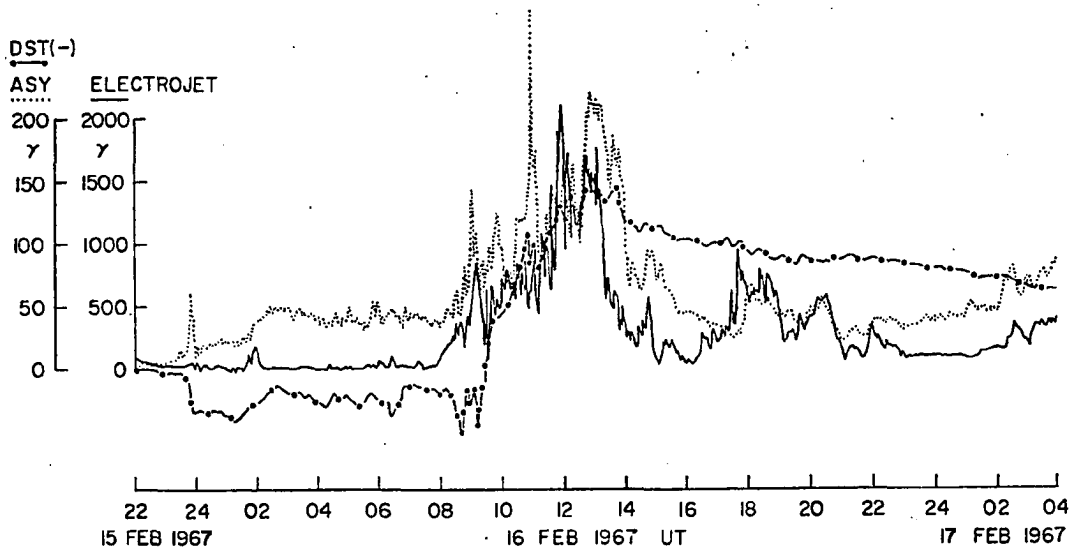

Fig. 3.9.a AL, ASY and Dst indices for the February 15-18, 1967, storm.

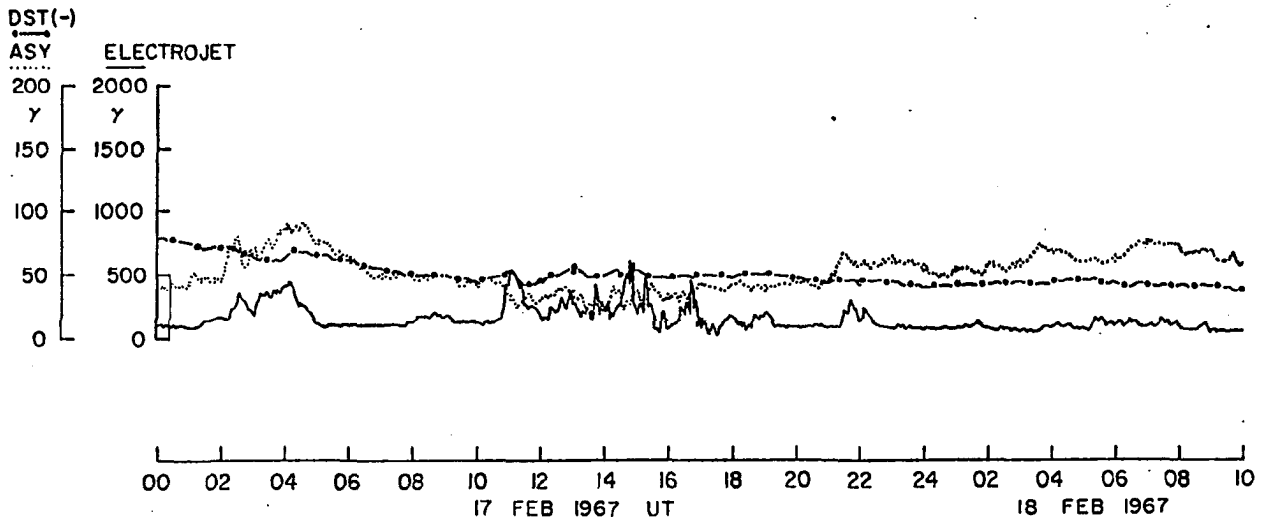

Fig. 3.9.b AL, ASY and Dst indices for the February 15-18, 1967, storm.

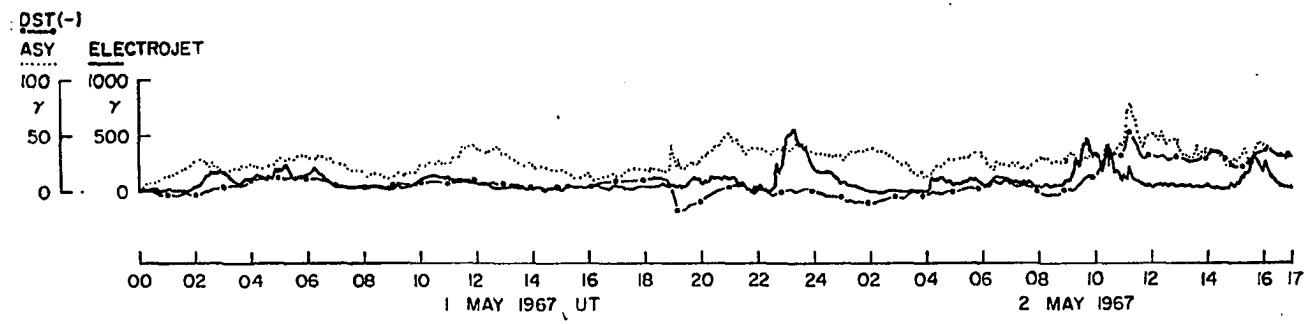

Fig. 3.10.a AL, ASY and Dst indices for the May 1-4, 1967, storm.

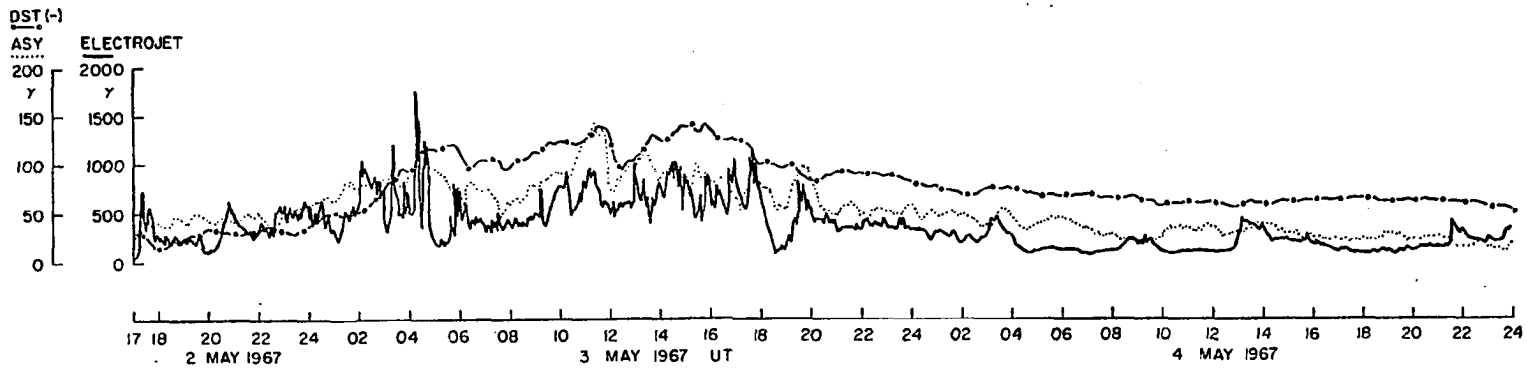

Fig. 3.10.b AL, ASY and Dst indices for the May 1-4, 1967, storm.

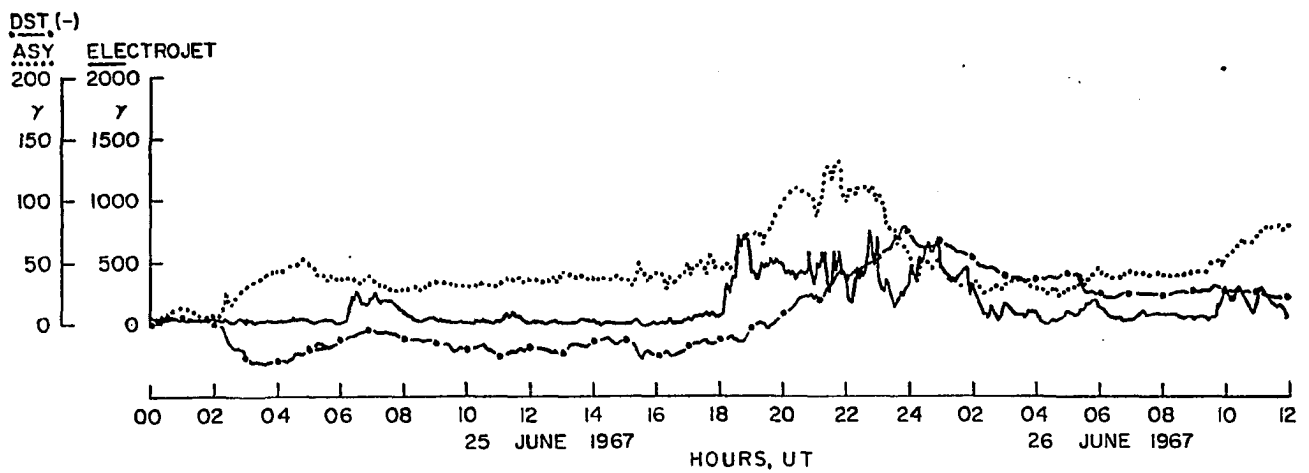

Fig. 3.11.a AL, ASY and Dst indices for the June 25-27, 1967, storm.

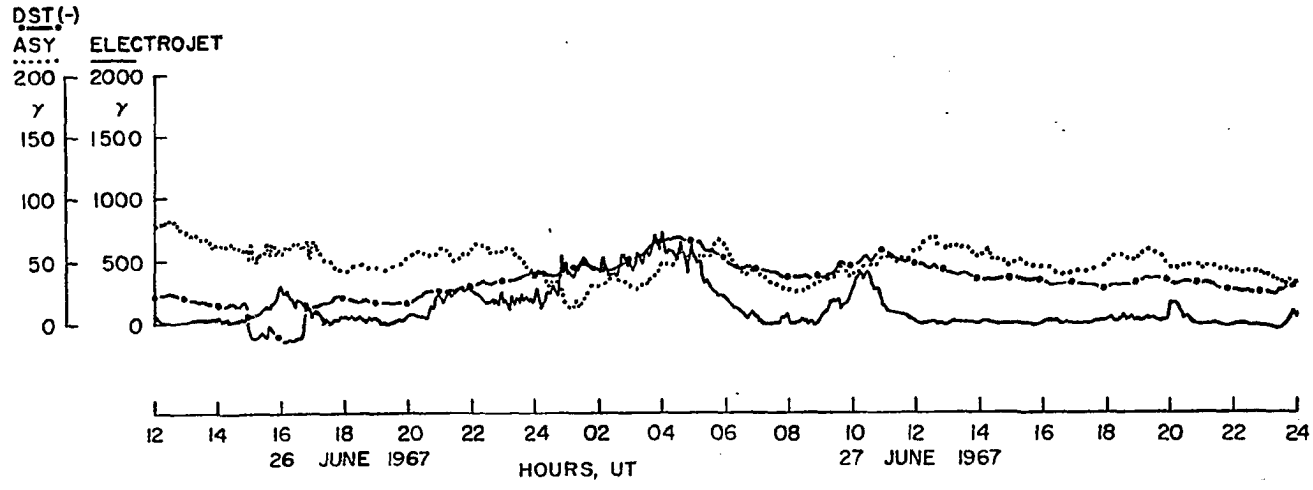

Fig. 3.11.b AL, ASY and Dst indices for the June 25-27, 1967, storm.

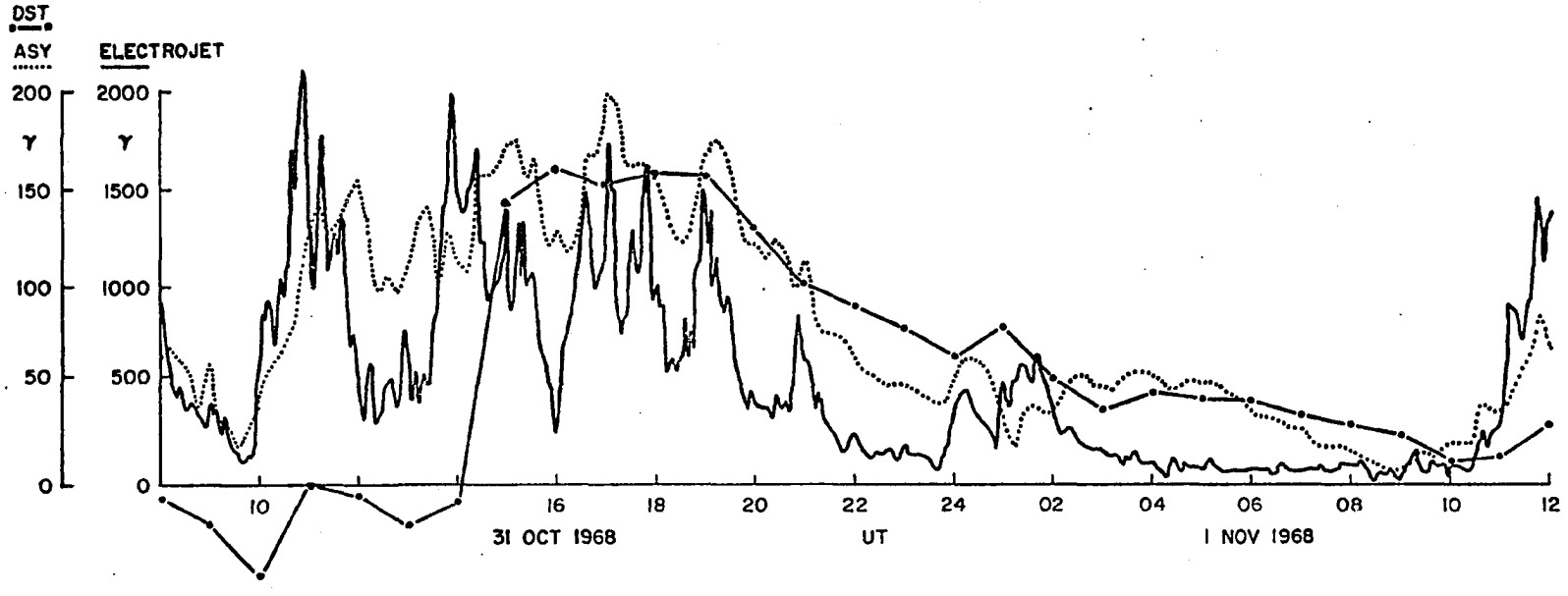

Fig. 3.12. AL, ASY and Dst indices for the October 31-November 1, 1968, storm.

It is seen in these Figures, that there is a high correlation between the ASY and AL indices during many periods of activity; however, significant anti-correlations also exist. The latter appear to be chiefly a result of the positive-type changes in the evening-midnight sector discussed in Sections 3.4.1 through 3.4.5 above.

It is clear that the Dst index does not correlate very well in these and the previous examples with either the ASY or AL indices. The Dst index merely delineates the period during which it is likely that polar substorms occur.

3.5 ISO-INTENSITY CONTOURS OF THE GEOMAGNETIC STORM OF SEPTEMBER 21-23, 1963

For a more complete treatment of the low latitude asymmetric component of the geomagnetic storm field of the September 21-23, 1963, storm (see Section 3.4.2), iso-intensity contours of the D(H) component have been constructed for several selected times; these are presented in Figures 3.13a through 3.13t. The contour traces are computer calculated and reveal some interesting details of asymmetry not fully noted in earlier studies of this type.

The iso-intensity contours begin at 1400 UT, September 22, which is a relatively inactive period just prior to the second main phase decrease. This major decrease begins after 2000 UT, September 22, (see the Dst index, Figure 3.3c).

At 2106 UT (Figure 3.13d) a fairly large, positive disturbance was recorded in the Asian sector, which was then in the early morning hours. At the same time, a large negative decrease was recorded at

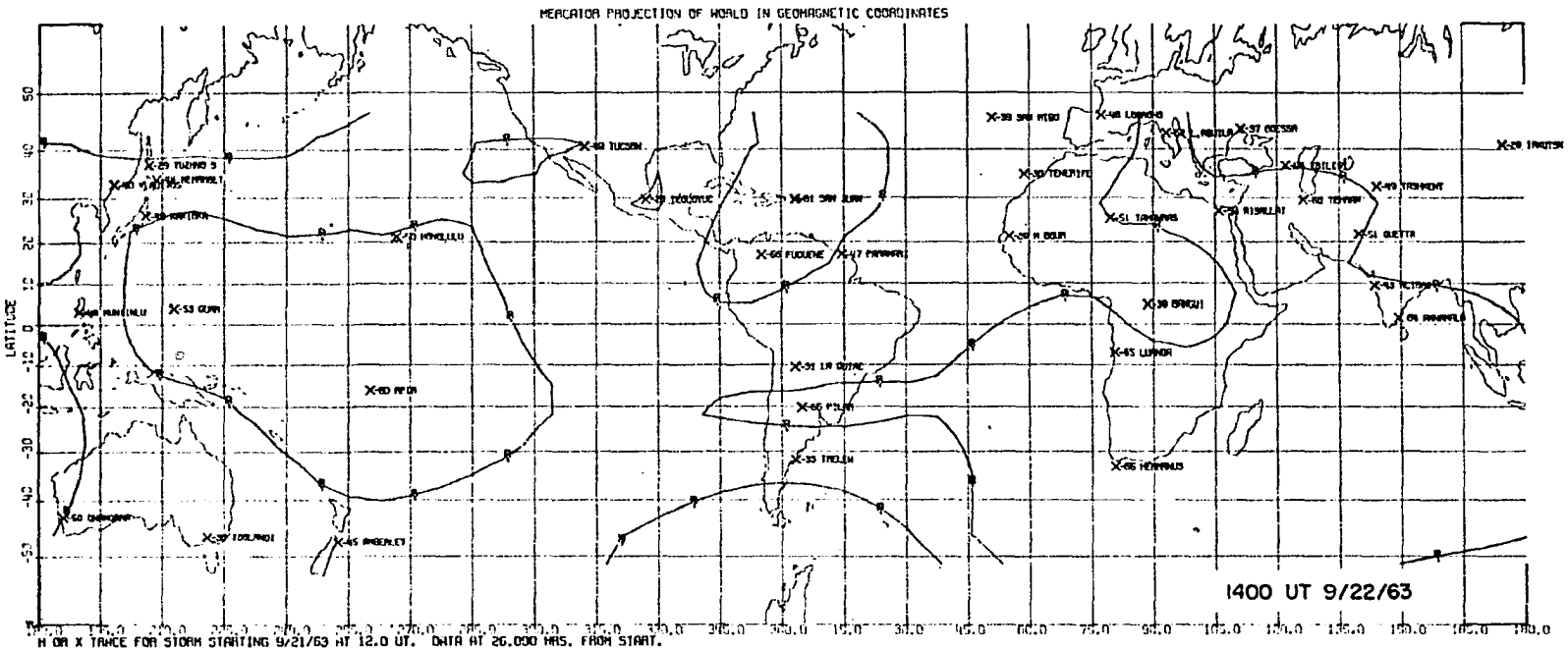

Fig. 3.13.a

Fig. 3.13.a through t Iso-intensity contours of H-component records of low and mid-latitude stations at several selected times during the September 21-23, 1963, storm.

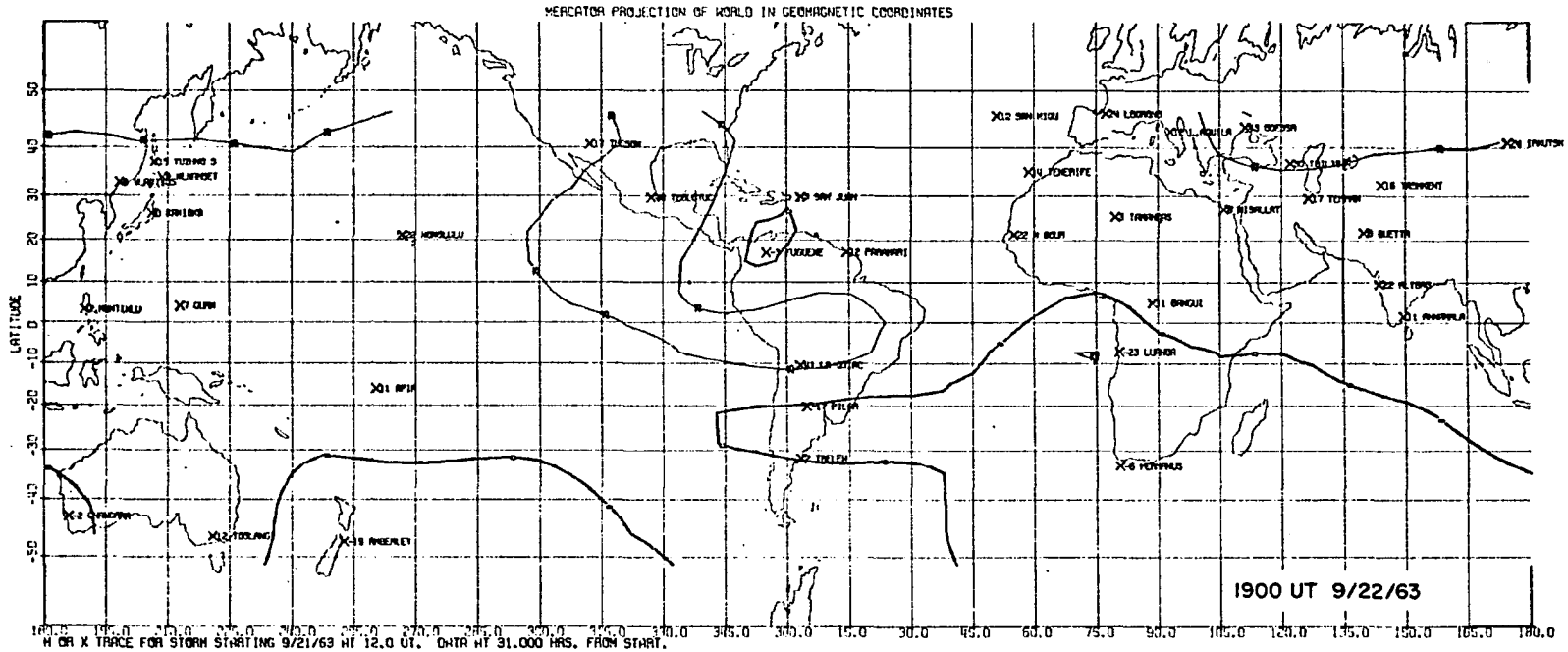

Fig. 3.13.b

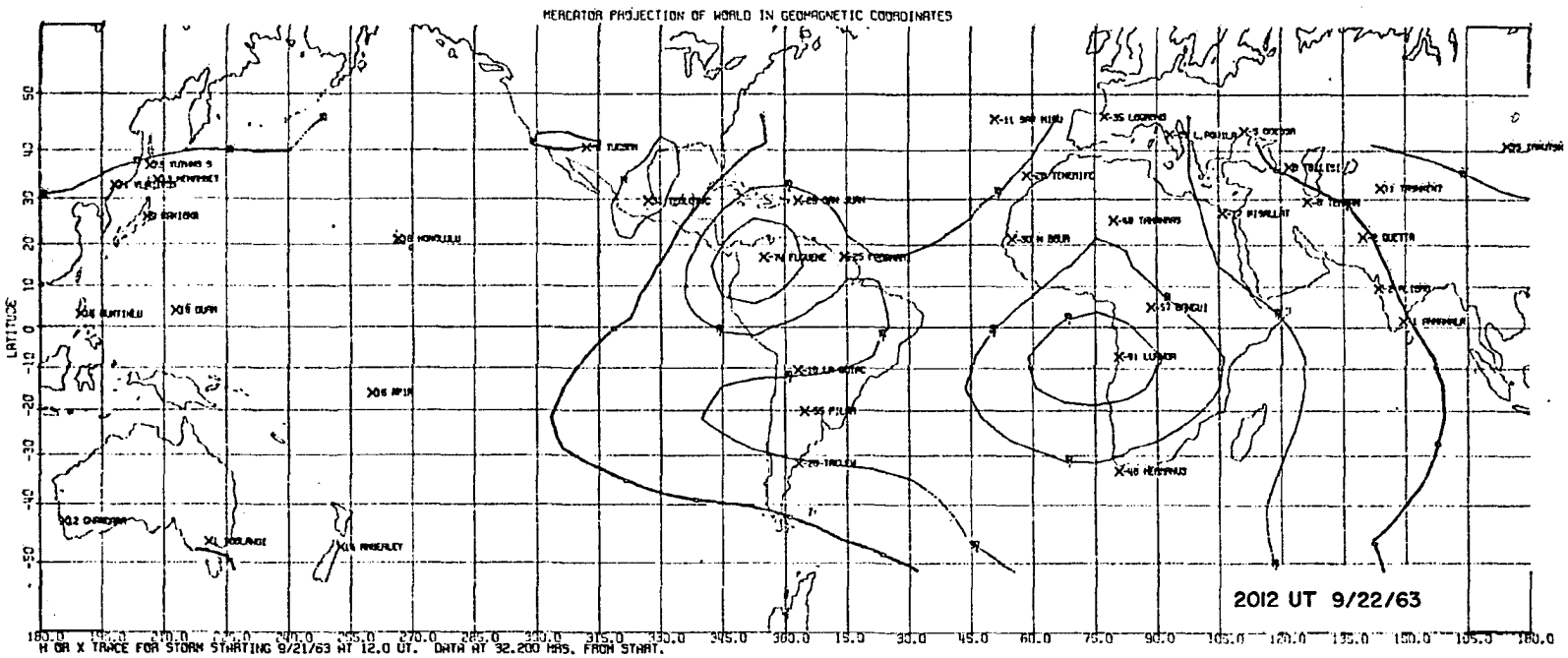

Fig. 3.13.c

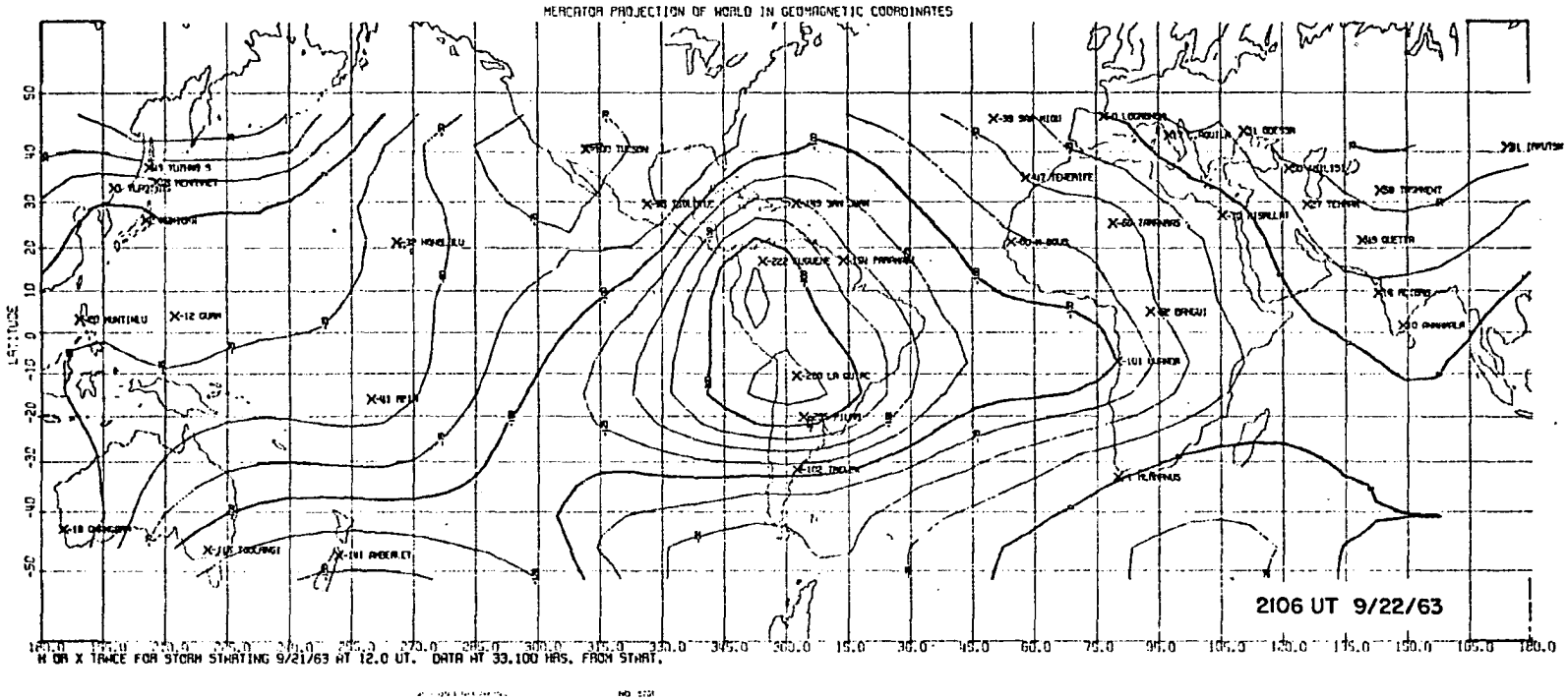

Fig. 3.13.d

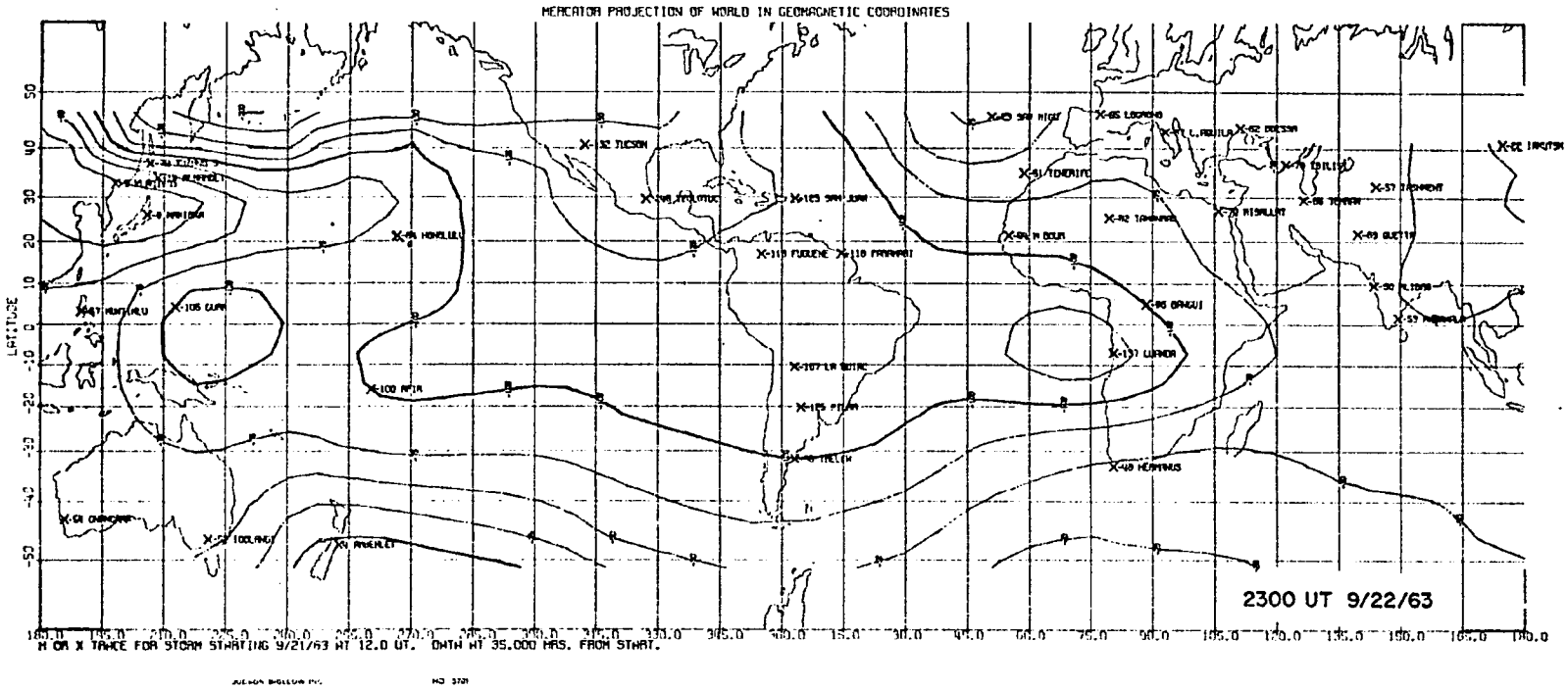

Fig. 3.13.e

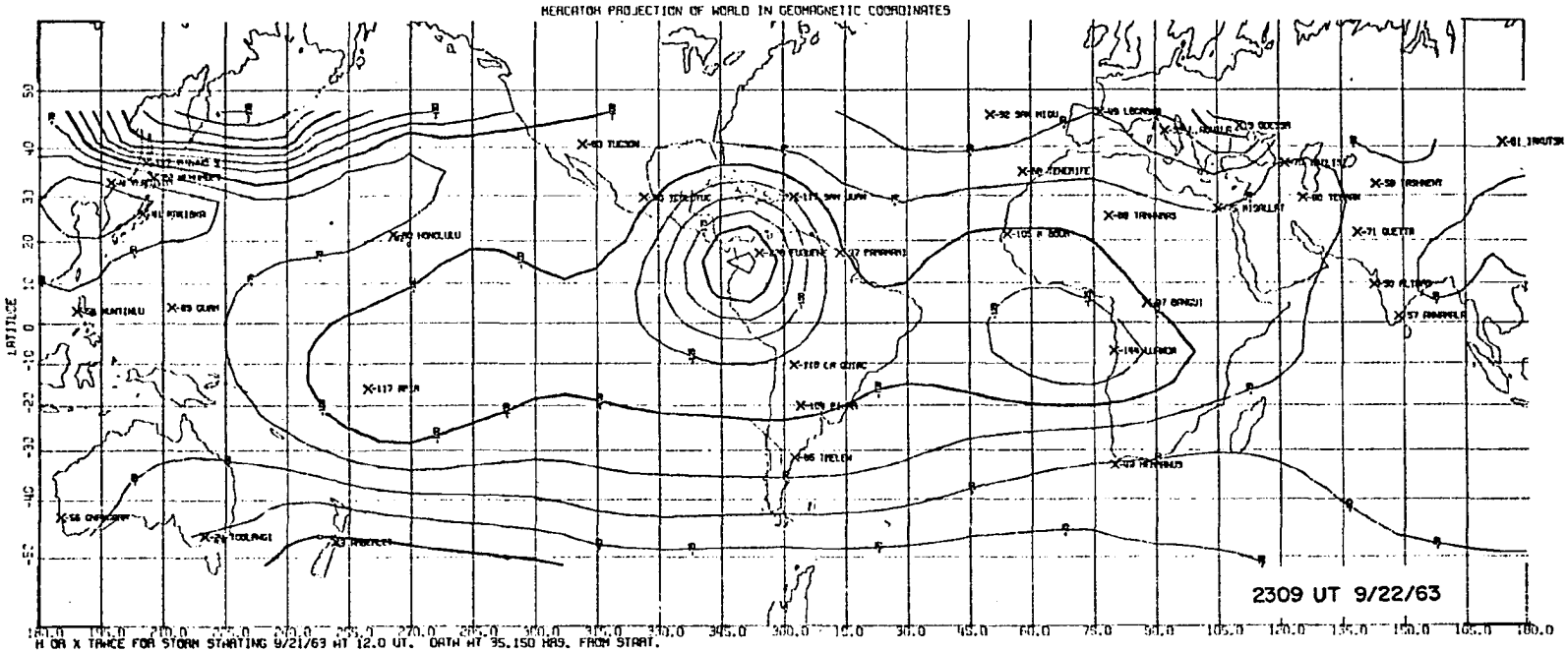

Fig. 3.13.f

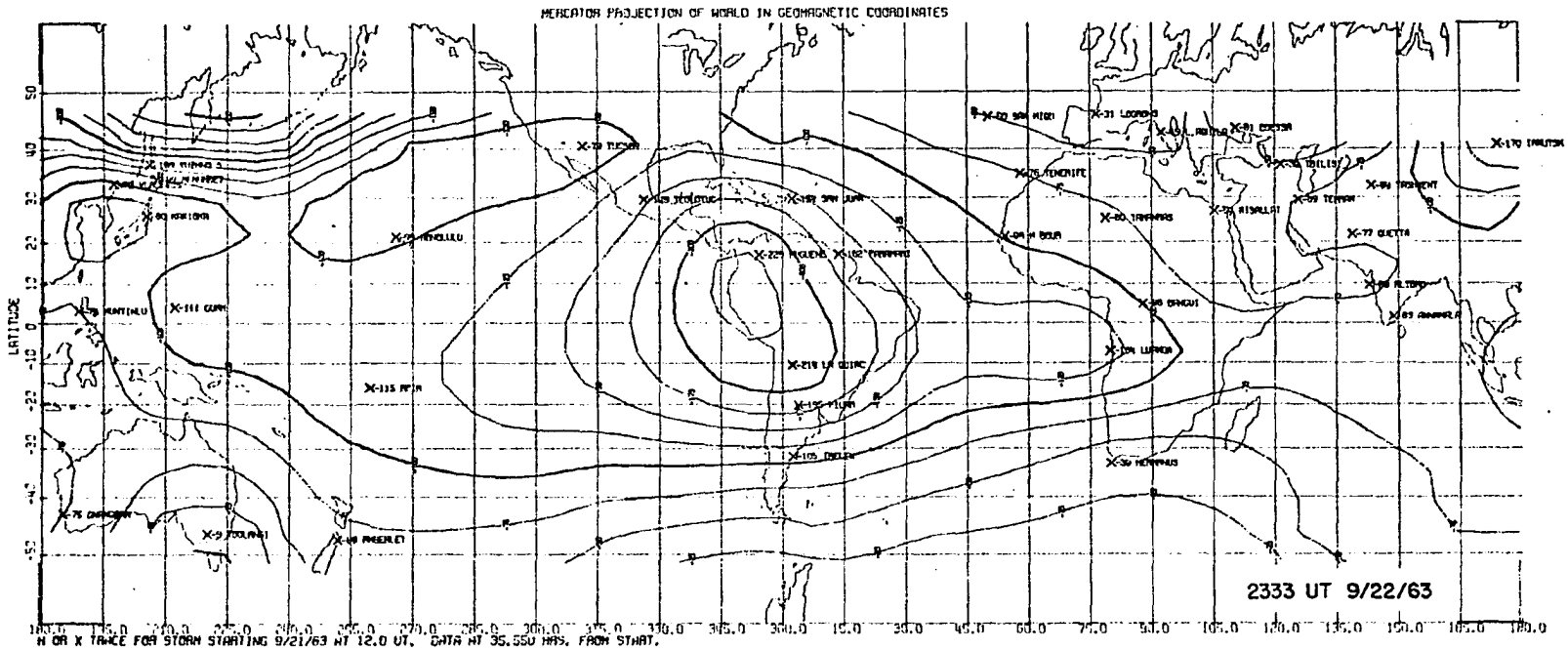

Fig. 3.13.g

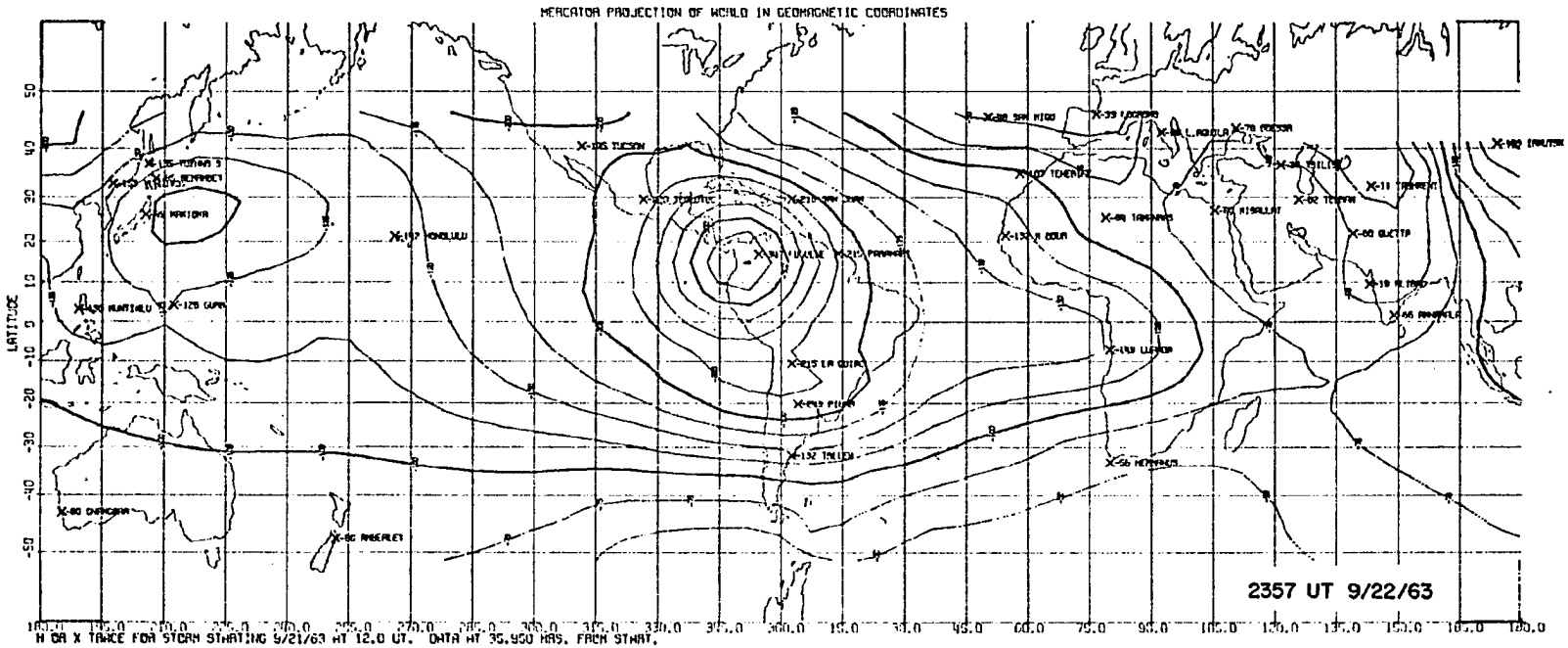

Fig. 3.13.h

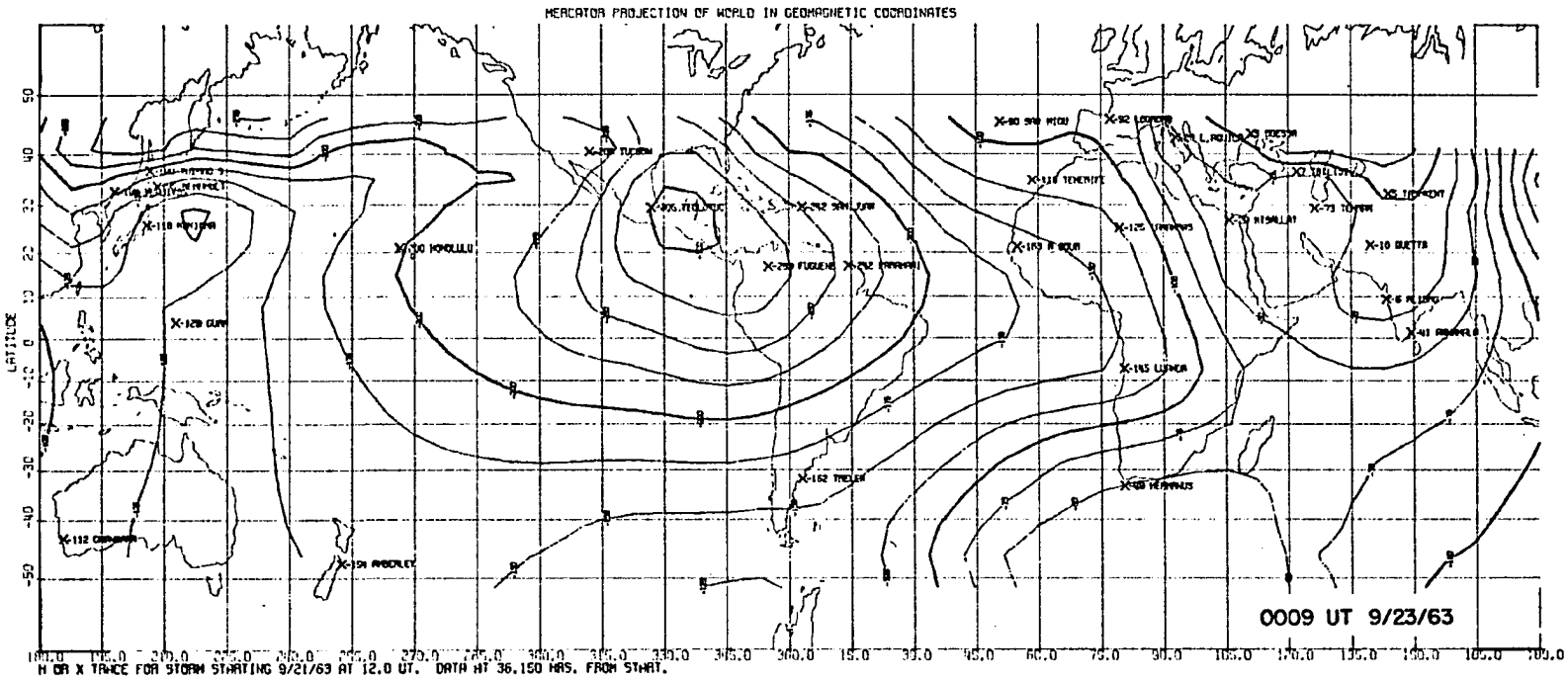

Fig. 3.13.i

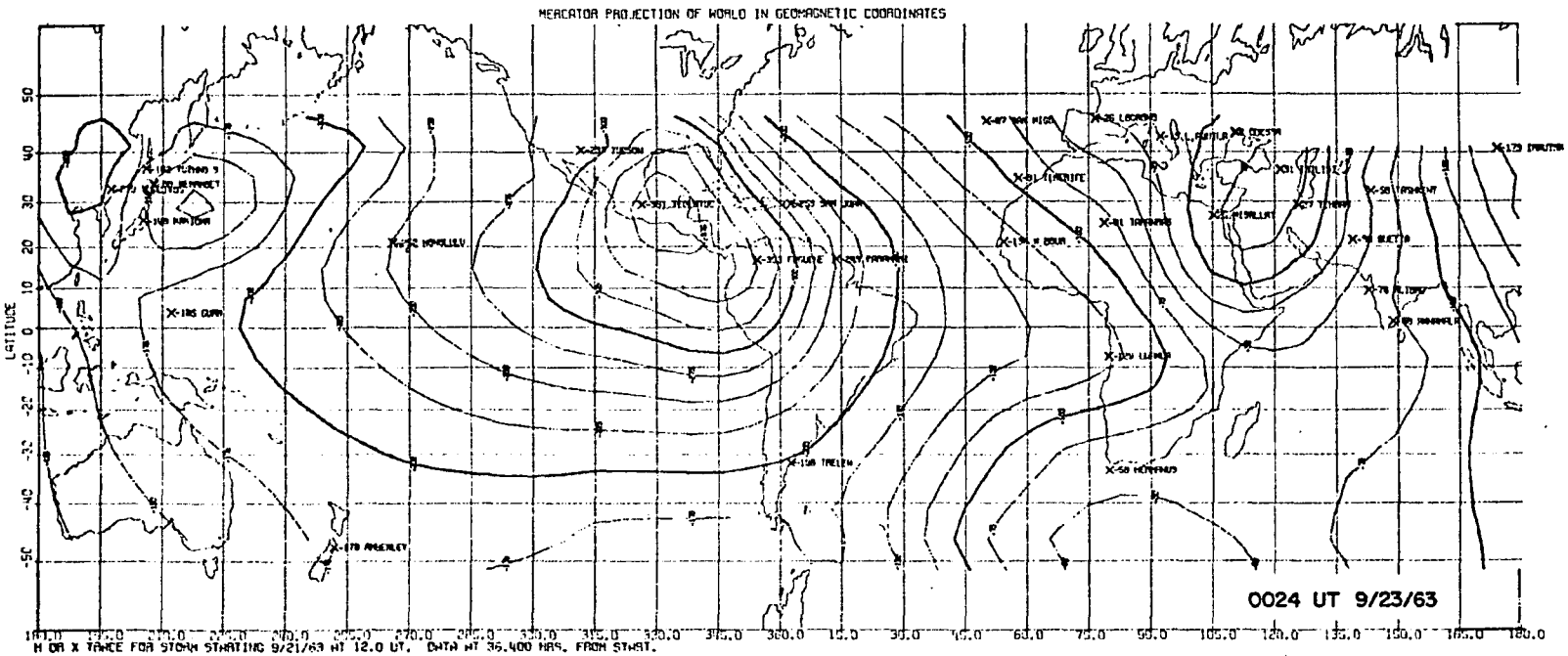

Fig. 3.13.j

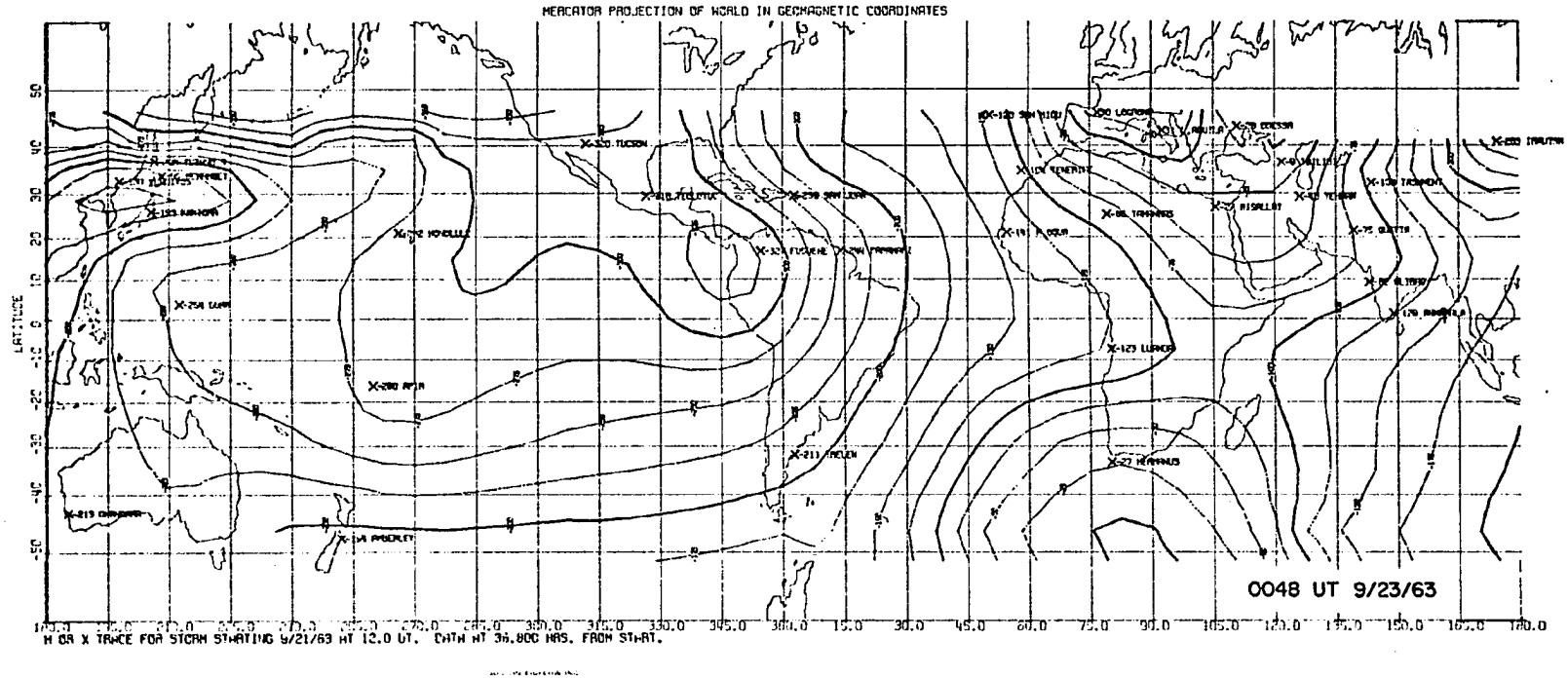

Fig. 3.13.k

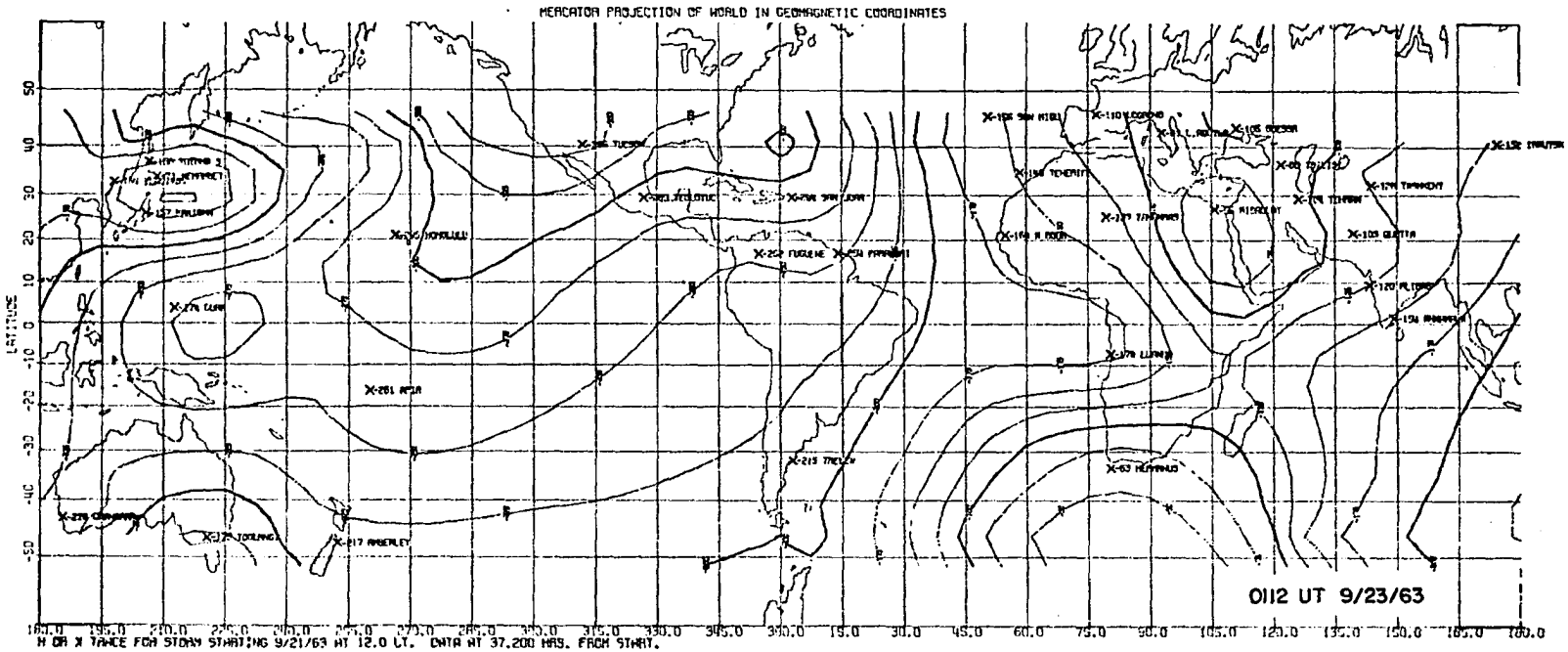

Fig. 3.13.1

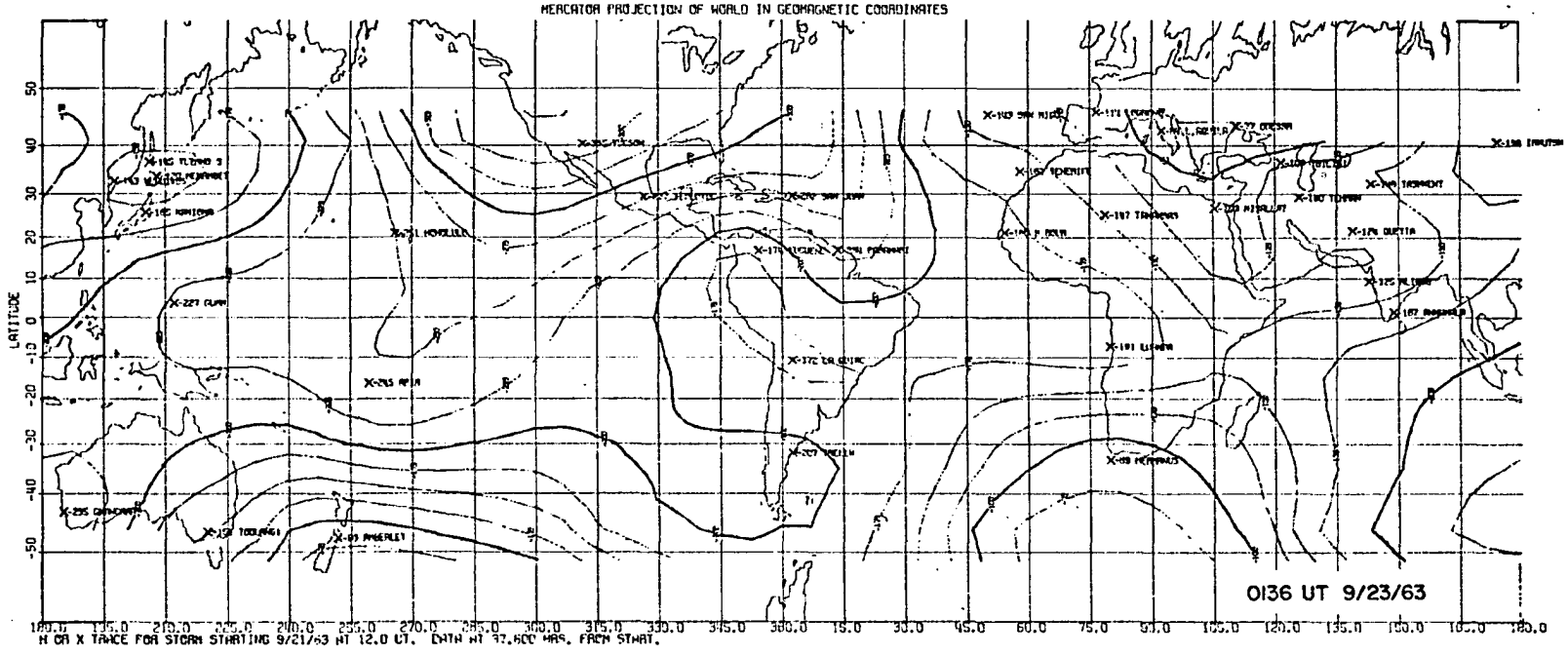

Fig. 3.13.m

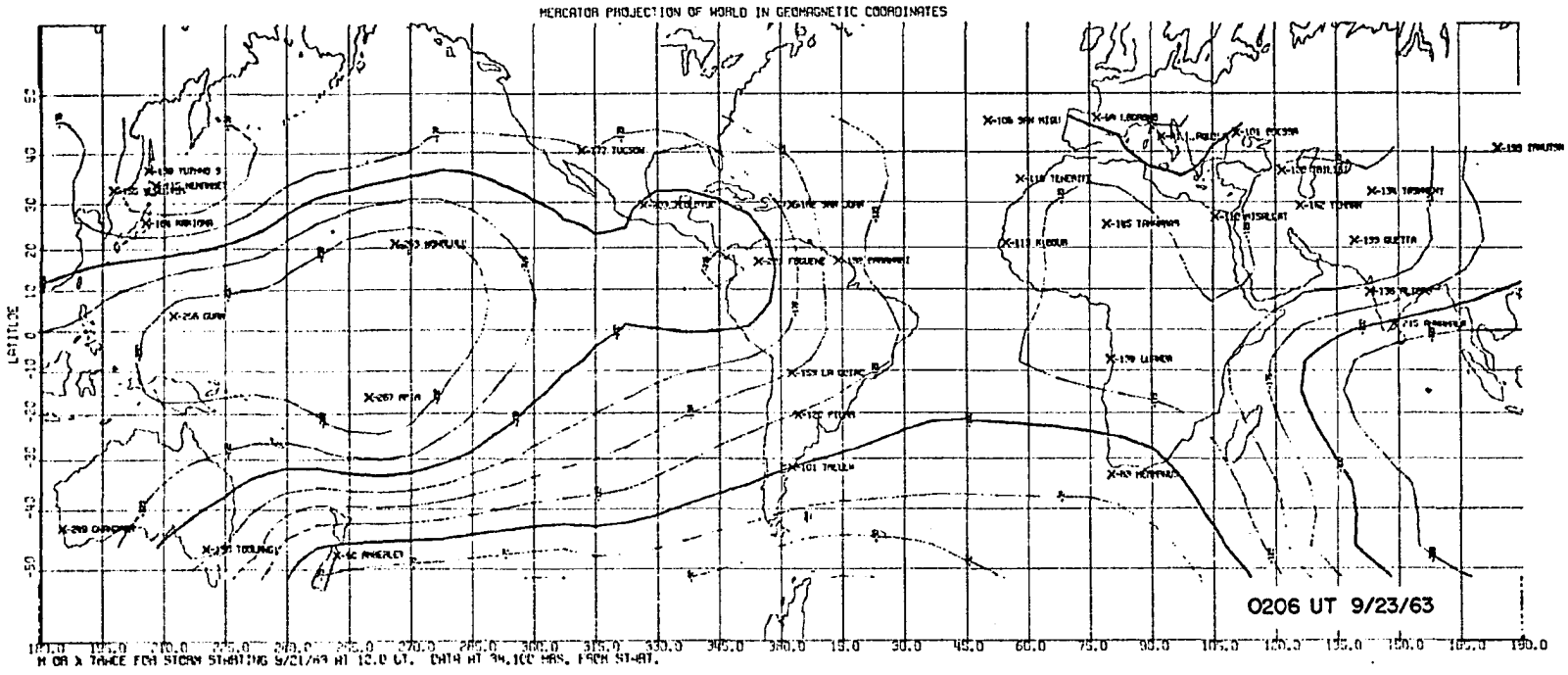

Fig. 3.13.n

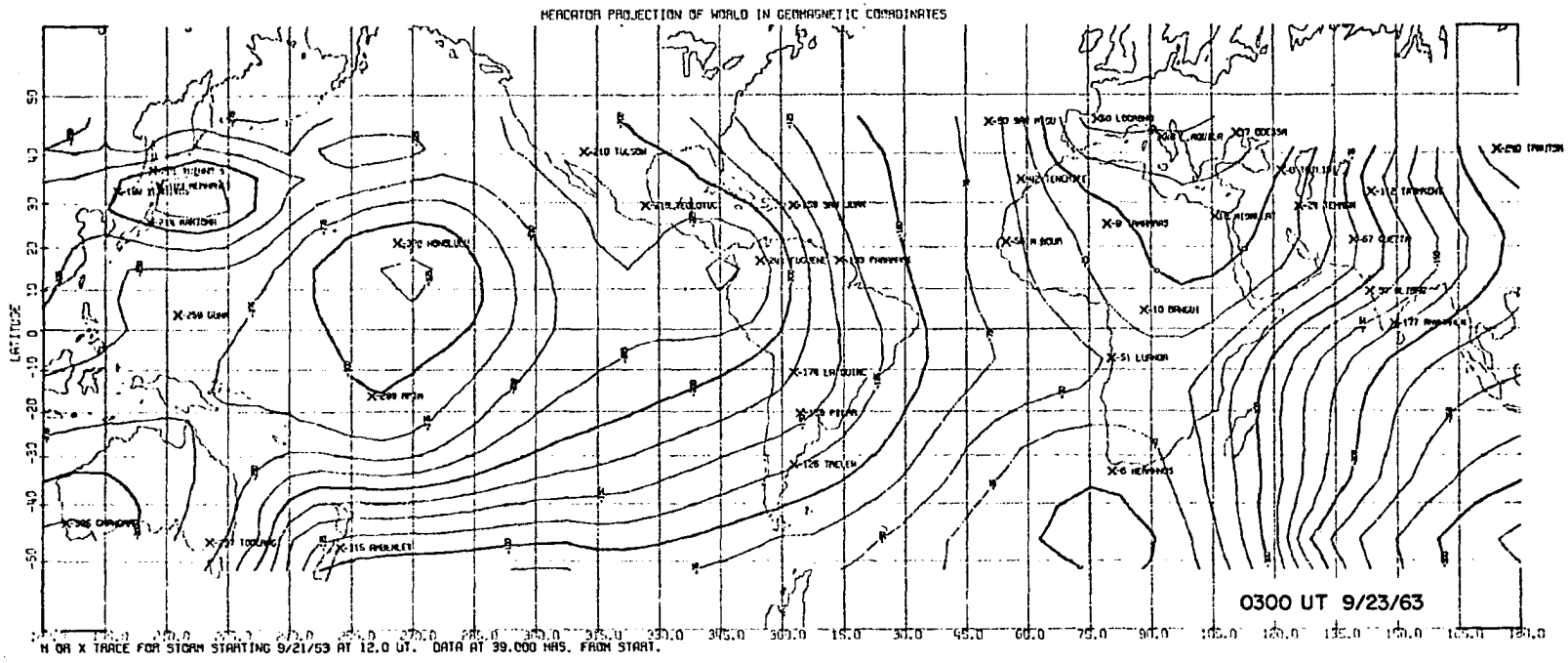

Fig. 3.13.o

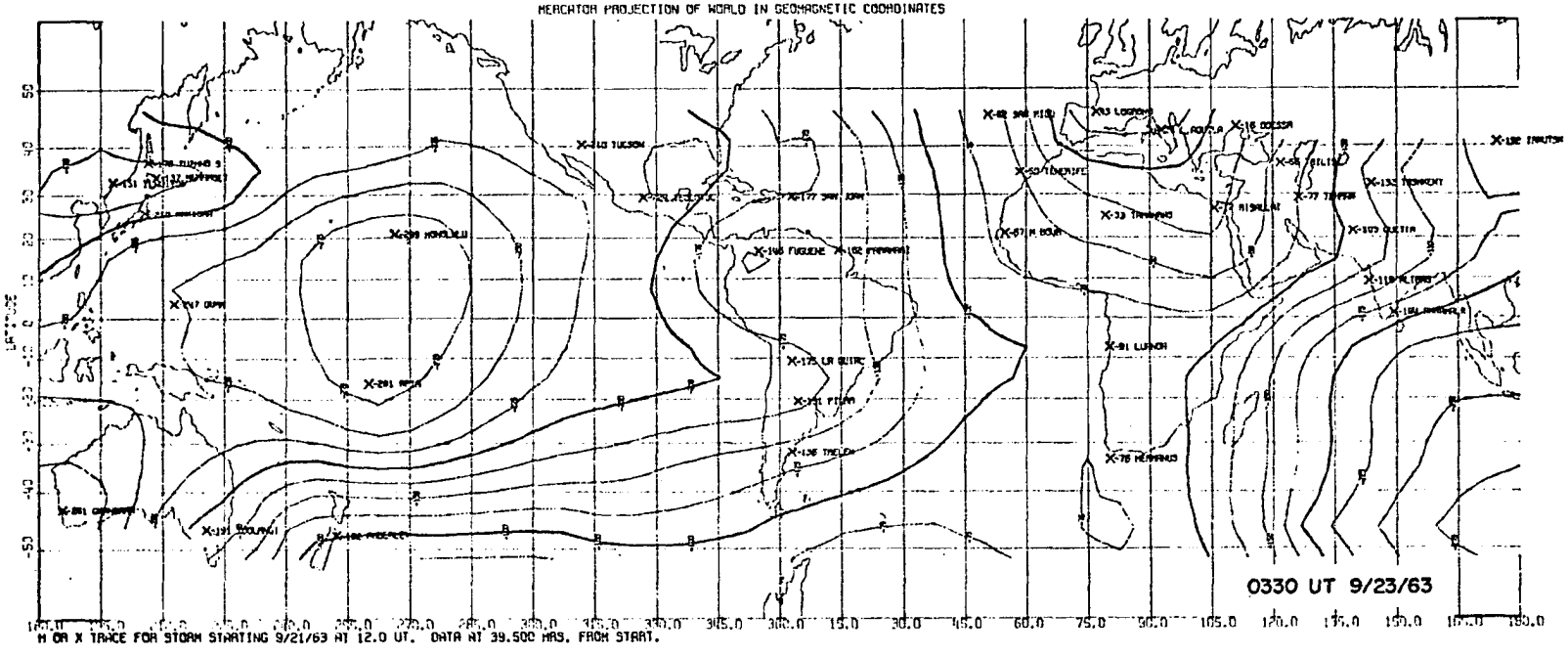

Fig. 3.13.p

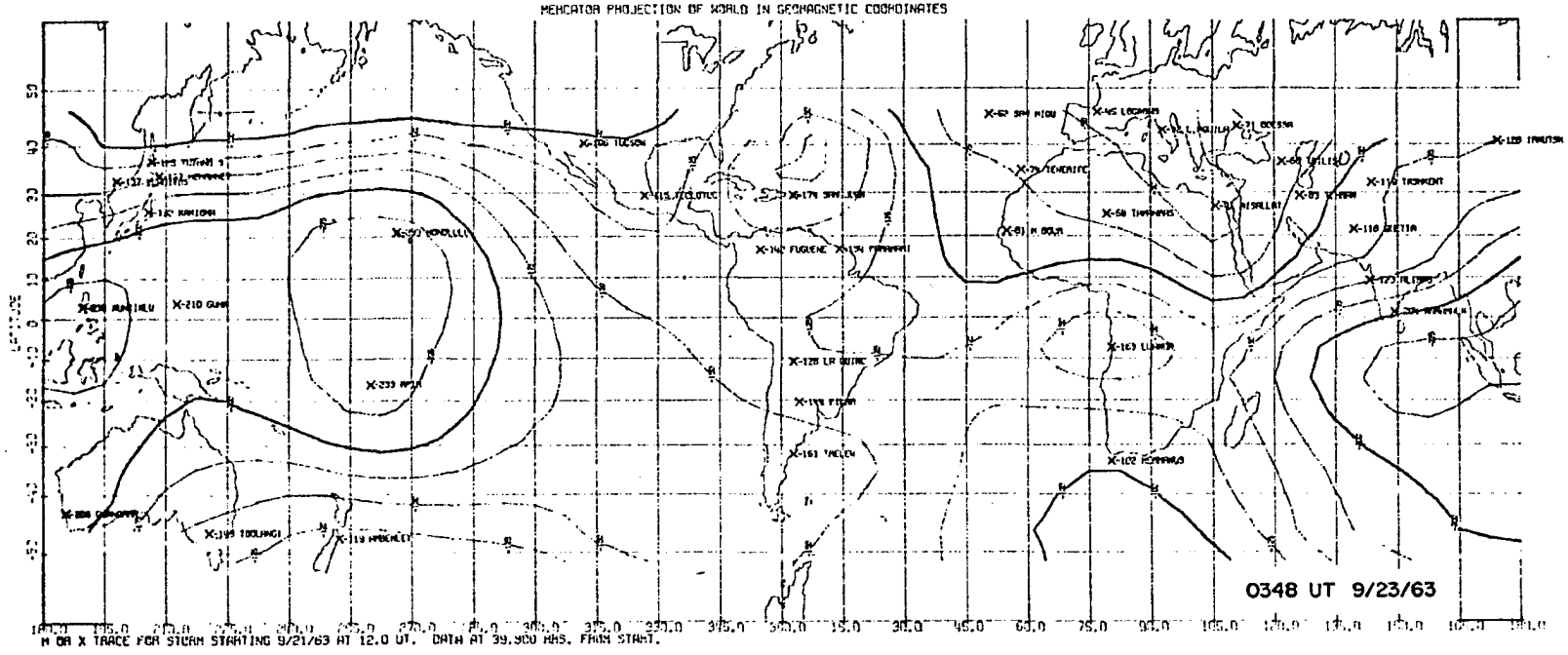

Fig. 3.13.q

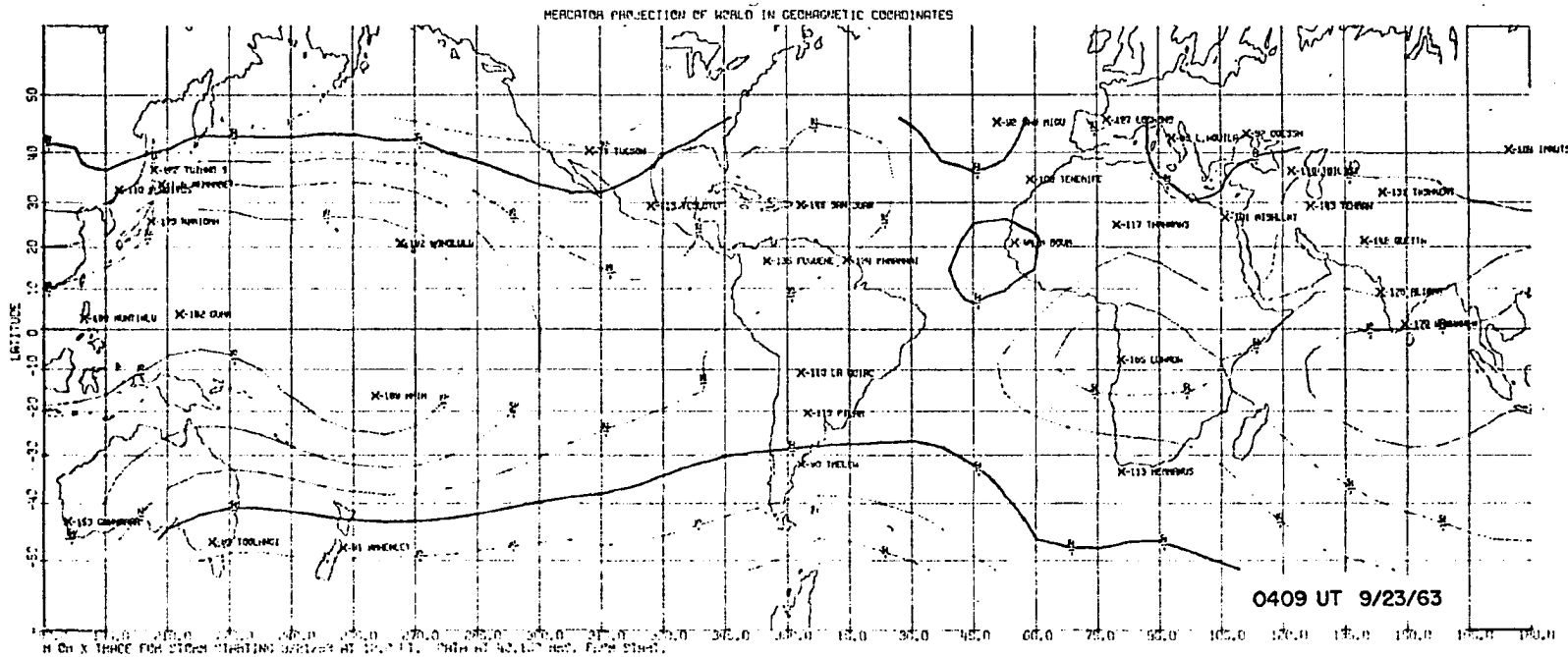

Fig. 3.13.r

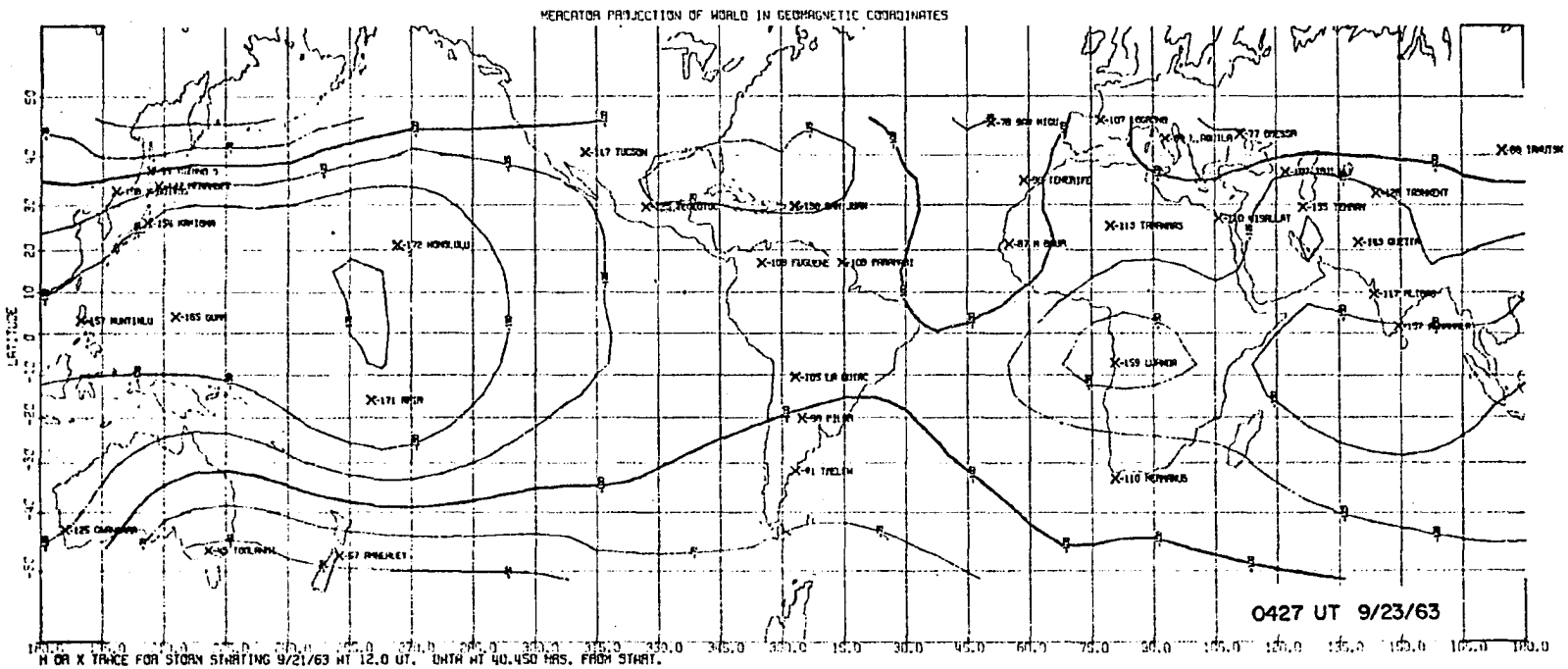

Fig. 3.13.s

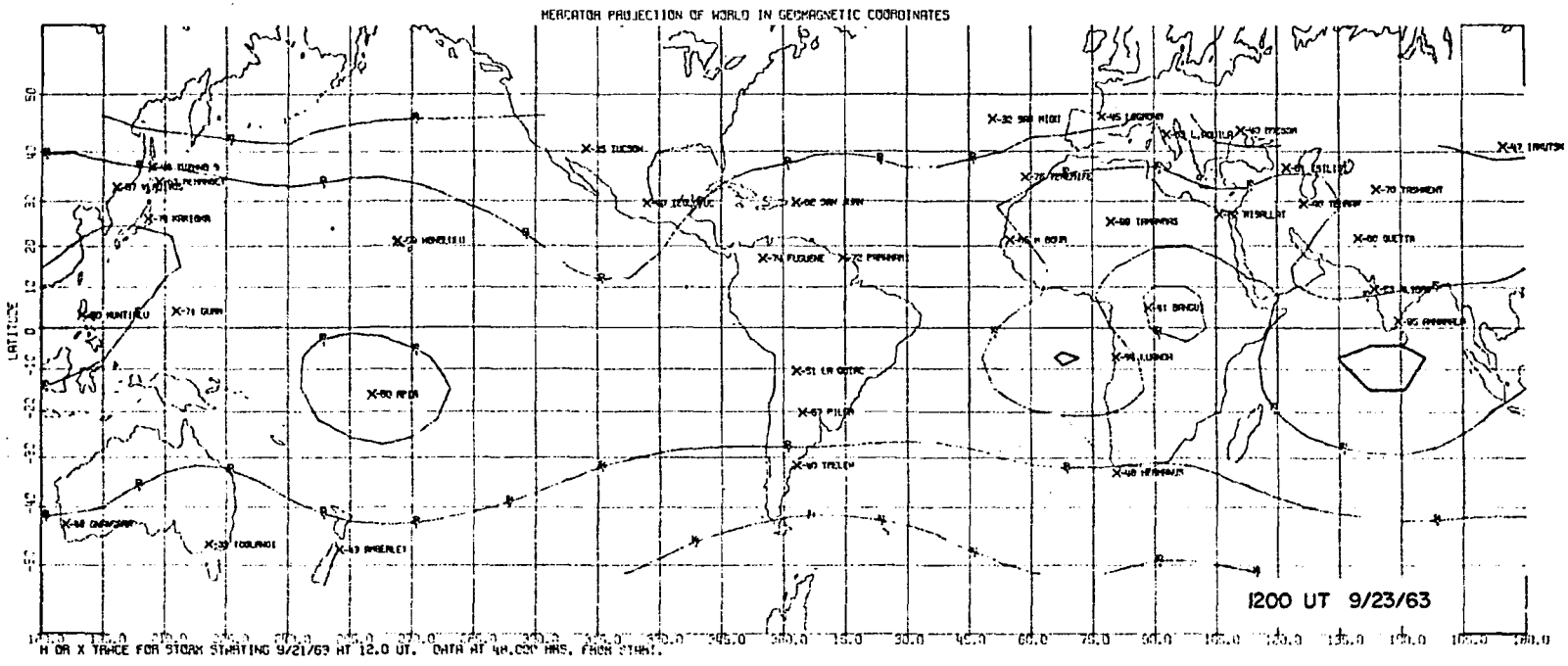

Fig. 3.13.t

South American stations where the field decreased to nearly -400 gammas. Between 2130 UT and 2300 UT (compare Figures 3.3 and 3.13e)there occurred a strong positive directed pulse in the records of American stations which were in the evening hours; the field became less asymmetric. However, by 2309 UT the field had once again deepened, reaching a minimum of over -300 gammas in the mid-Pacific region at about 0300 UT, September 23, (Figure 3.13o. The large positive change above the baseline level between about 0230 and 0430 UT which occurred at European and North African stations in the early morning hours should be noted. It is seen in Figure 3.13t that by 1200 UT, September 23, the field had nearly become symmetric (iso-intensity contours began to parallel the latitudes).

There are two points of interest to be noted in this storm. Firstly, the iso-intensity contours show that there is a gradual shifting to the west of both the regions of maximum decrease and minimum decrease. The region of minimum decrease (in fact, in some cases having above baseline values) is in the early morning hours, while the region of maximum decrease is in the evening hours for this storm. This confirms the earlier work of Akasofu and Chapman (1964). In between large increases in asymmetry for this storm, brief periods occur in which the field tends to become symmetric (c.f. Figures 3.13e and 3.13n). Secondly, although this storm occurred during an equinoctial period, the regions of minimum and maximum decrease are a substantial number of degrees north of the geomagnetic equator. The possible causes of the north-south asymmetry will be discussed in the next section.

3.6 SUMMARY AND DISCUSSION

In this chapter, the growth and decay of several geomagnetic storms have been analyzed in detail by comparing the westward auroral electrojet index, AL, with what has been termed, herein, the asymmetry or ASY index.

The latter quantity is related to the DS component of the harmonically synthesized disturbance field, but has the advantage of retaining the more rapidly varying components. The term 'asymmetry index' has been chosen to imply that the quantity is primarily due to some longitudinally asymmetric distribution of currents, unlike the symmetric part which is thought to chiefly arise from a ring current encircling the earth.

The major results of the correlative study in the present chapter of the asymmetry, electrojet and Dst indices for several geomagnetic storms are as follows:

(a) There are definite periods when an almost exact one-to-one correspondence exists between the two indices, although the ratios of maxima-to-maxima and minima-to-minima are not necessarily equal.

(b) Definite periods, when the correlations are rather poor, also exist.

(c) Cases of good correspondence are more numerous than cases of poor correspondence.

(d) The Dst index is poorly correlated with polar substorm activity.

In addition, the following points should be noted:

(e) Positive changes, which tend to make the field more symmetric, occur at late evening stations where the main phase decrease prior to the positive change had the greatest main phase decrease; this confirms earlier studies (Akasofu and Chapman, 1964; Meng and Akasofu, 1967 and Akasofu and Meng, 1969).

(f) Negative changes generally in the noon-morning sector of the earth sometimes accompany the positive changes (thereby increasing the asymmetry index greatly at that time).

(g) Simultaneously occuring positive and negative bay-like disturbances observed at low latitude stations on opposite sides of the earth during a geomagnetic storm are always accompanied by polar substorms at high latitudes, even though such low latitude changes may not be significantly reflected in the asymmetry index.

(h) A point not previously mentioned is that there is often times a disappearance of positive type bays in the auroral zone records (see Figures 3.2a, 3.3a, 3.4a, 3.5a, and 3.6a) during a part of the main phase decrease observed at low latitudes.

(i) The iso-intensity contour study of the equinoctially occurring storm of September 21-23, 1963, suggests a substantial north-south asymmetry exists for both the regions of maximum and minimum main phase decrease which would not be expected for the case of a magnetic dipole coincident with the rotational axis of the earth.

The data presented in this chapter along with satellite data can be interpreted in the following manner:

(1) The relatively good correlation of the disturbance storm fields observed simultaneously at ATS-I and Honolulu suggests that a significant part of the low latitude storm fields arises from distant currents, rather than ones in the ionosphere. Hence, the asymmetry of the low latitude storm fields is likely to be due to an asymmetric distribution of distant currents.

(2) The occurrence of anti-correlation between the asymmetry and the electrojet indices also suggests that the DS component cannot be mainly due to ionospheric return currents. Crooker and Siscoe (1970) have also reached this conclusion.

(3) As mentioned previously, distant currents in the tail region of the magnetosphere, the ring current and magnetospheric boundary currents can contribute to the magnetic storm and to the DS component in general. Some evidence has been given that the enhanced boundary currents do continue to flow from the time of ssc to at least the maximum main phase decrease (Coleman and Cummings, 1971). However, since the magnitude of these currents is often small and since it is not probable that the field of these currents could have such large gradients across the surface of the earth as is observed for the DS component, the asymmetry must primarily be due to the combined effects of the magnetotail current and an asymmetric ring current.

(4) There is no way to determine the relative contribution of an asymmetric ring current and the magnetotail current to the DS component. From detectors aboard ATS-5, it has recently been demonstrated by DeForest and McIlwain (1970) that variations in the total energy of the particles at synchronous orbits do not correlate in any simple way with the magnetic field variations observed there. They suggested that both local and distant currents are the sources of the magnetic field variations at synchronous orbits.

(5) It is possible for a positive change to occur at synchronous orbits in the night sector if there is depletion of ring current particles, i.e., a decrease of diagmagnetism there. This is consistent with the observation of positive changes both at the surface of the earth and at the satellite. However, this is not consistent with the increase of the energy density of plasma particles (hence, diamagnetism) actually observed by ATS-5 during positive changes in the dark sector (DeForest and McIlwain, 1970). The only single current which is consistent with the observed positive changes at both the satellite position and on the nightside of the earth and the observed increase of the energy density of the plasma particles at the satellite is one which is located beyond the orbit of the satellite.

(6) In this chapter, it has been shown that a large decrease of the DS component (or ASY index) sometimes occurs during the

decreasing phase of a geomagnetic storm when large positive changes occur at nightside stations. The positive pulse type changes are most probably due to a sudden decrease of the strength of the magnetotail current and a subsequent increase.

(7) The electrojet intensity often increases when the DS component decreases. It may be speculated that the decrease of the magnetotail current suggested in (6) may be caused by a diversion of part of this current to the auroral oval along appropriate field lines. Since the magnetotail current density during disturbed periods is of the order of 35 mA/m (c.f. Beard et al., 1970), an electrojet intensity of 10^6 amperes could be generated, if the magnetotail current between R = 10 R_e and 15 R_e is completely diverted into the auroral oval.

(8) Fairfield and Ness (1970) have recently shown that the magnetotail field becomes more dipole-like during substorms than during quiet periods; this is not inconsistent with the diversion hypothesis.

(9) The only available observation which might be related to the diversion of the magnetotail current to the auroral oval is the remarkable decrease of the plasma energy density over the entire thickness of the plasma sheet observed during the early epoch of substorms (Hones, Asbridge and Bame, 1970).

(10) Although a substantial number of low latitude, DS-like events are explainable in terms of distant magnetotail currents, there are some which are not. Simultaneously occurring positive and negative low latitude bays suggest that either a) substantial near-earth or ionospheric return currents do occasionally flow or b) the magnetic effects of the auroral electrojets confined to the northern and southern auroral ovals are directly observed unattenuated except by distant at low latitude stations.

(11) The north-south asymmetry of the region of maximum and minimum main phase decrease as seen in the iso-intensity contours of the September 21-23, 1963, geomagnetic storm indicates that there is a north-south asymmetry in the currents causing the changes. Since the storm occurred during a period near the autumnal equinox, this asymmetry may be related to non-coincidence of the dipole axis to the rotational axis of the earth. It is suggested that the observed northern location of the region of maximum main phase decrease may be due in part to the 'tipping' of the geomagnetic equatorial plane toward the ecliptic plane. An alternative possibility is that the return currents of the boreal and austral auroral electrojets are influenced by an asymmetric distribution of conductivities. That is, return currents may be stronger in the northern hemisphere.

CHAPTER IV

GEOMAGNETIC STORM FIELDS NEAR A SYNCHRONOUS SATELLITE- THE RECOVERY PHASE OF A GEOMAGNETIC STORM

4.1 INTRODUCTION

In the previous chapter,the characteristics of geomagnetic storms observed at the surface of the earth have been described in some detail. To interpret the storm time disturbances at the surface of the earth, it is necessary that simultaneous satellite data be used. The data studied suggests that the non-symmetric part of the geomagnetic storm field during its decreasing phase can be mainly attributed to currents in the magnetotail, although at times additional near-the-earth sources of current may be required to adequately explain the phenomenon fully. In the present chapter, we will turn our attention to the behavior of the presumably simpler, recovery phase of a geomagnetic storm observed at synchronous altitudes and on the surface of the earth.

It is clear that the outer geomagnetic field must be considerably distorted during geomagnetic storms. For example, an auroral arc with a width of 10 km and a length of 1000 km in the auroral zone maps onto a region of about 300 km by 6000 km in the equatorial plane assuming a dipole configuration. Hence, such disturbances must be associated with wide scale distortions of the outer magnetosphere.

There are at least three current systems inside the magnetosphere which are responsible for the distortion. These are the ring current, the magnetotail current flowing in the plasma sheet from dawn to dusk and the auroral electrojet. The existence of the tail current in the

plasma sheet has been postulated from field and particle measurements (Ness, 1965; Williams and Mead, 1965) to account for the observed antisolar and solar directions of the magnetic field above and below the neutral sheet, respectively. The circuit is thought to be closed by cylindrical currents flowing on the surface of the magnetospheric tail. It is probable that the three currents are not dependent but connected by field aligned currents during disturbed periods. Hence, the division of the magnetospheric current system into the three separate current systems is somewhat arbitrary.

The existence of the ring current has long been postulated to account for the significant decrease of the horizontal (H) component of the geomagnetic field in low and middle latitudes during magnetic storms; this has only recently been confirmed by direct satellite observations by Cahill (1966)and Frank (1967). Behannon and Ness (1966) have shown that the magnetotail field increases during periods of geomagnetic storms, which suggests there is an enhancement of the magnetotail current during such disturbed periods. However, only recently have the storm-time variations of the ring current belt (i.e., the low energy proton belt) and of the plasma sheet been studied to any extent. A qualitative estimate of the storm-time variations of the outer geomagnetic field can now be made.

This chapter is mainly concerned with the storm field observations made by the synchronous satellite ATS-1. Coleman (1970) and Coleman and Cummings (1971) have recently reported that at the distance of the synchronous satellite ($r \approx 6.6\ R_E$), the main phase of geomagnetic

storms is much shorter than that observed at ground stations. The specific purpose of this chapter is to examine this relatively 'earlier recovery' of the main phase at synchronous orbit altitudes in terms of the storm-time variations of the ring current belt and the plasma sheet.

4.2 EXAMPLES OF AN 'EARLIER RECOVERY' OF THE MAIN PHASE AT THE ATS-I SATELLITE

Figures 4.1 through 4.5 illustrate examples of an 'earlier recovery' of the main phase at the ATS-I satellite as compared with ground stations. Each figure consists of an ATS-I storm day record and a typical quiet day record of the satellite H-component and the corresponding magnetic records from five to six low latitude stations; the solar quiet day variation, Sq, has been subtracted from each of the low latitude traces. The times of local midnight at ATS-I are marked by solid circles. These storms have been studied in the previous chapter and their asymmetry index (ASY), westward electrojet index (AL) and Dst indices given there.

It should be noted that at the synchronous orbit, the dayside changes during storm-time periods tend to have a higher value than the 'quiet' day levels. It is quite likely that the magnetosphere is 'compressed' by an intensified solar wind during at least the period from the ssc to the beginning of the recovery phase (Coleman and Cummings, 1971). On the other hand, nightside changes during storm time periods tend to have below-quiet-day-level values, suggesting an enhancement of the ring and/or magnetotail currents.

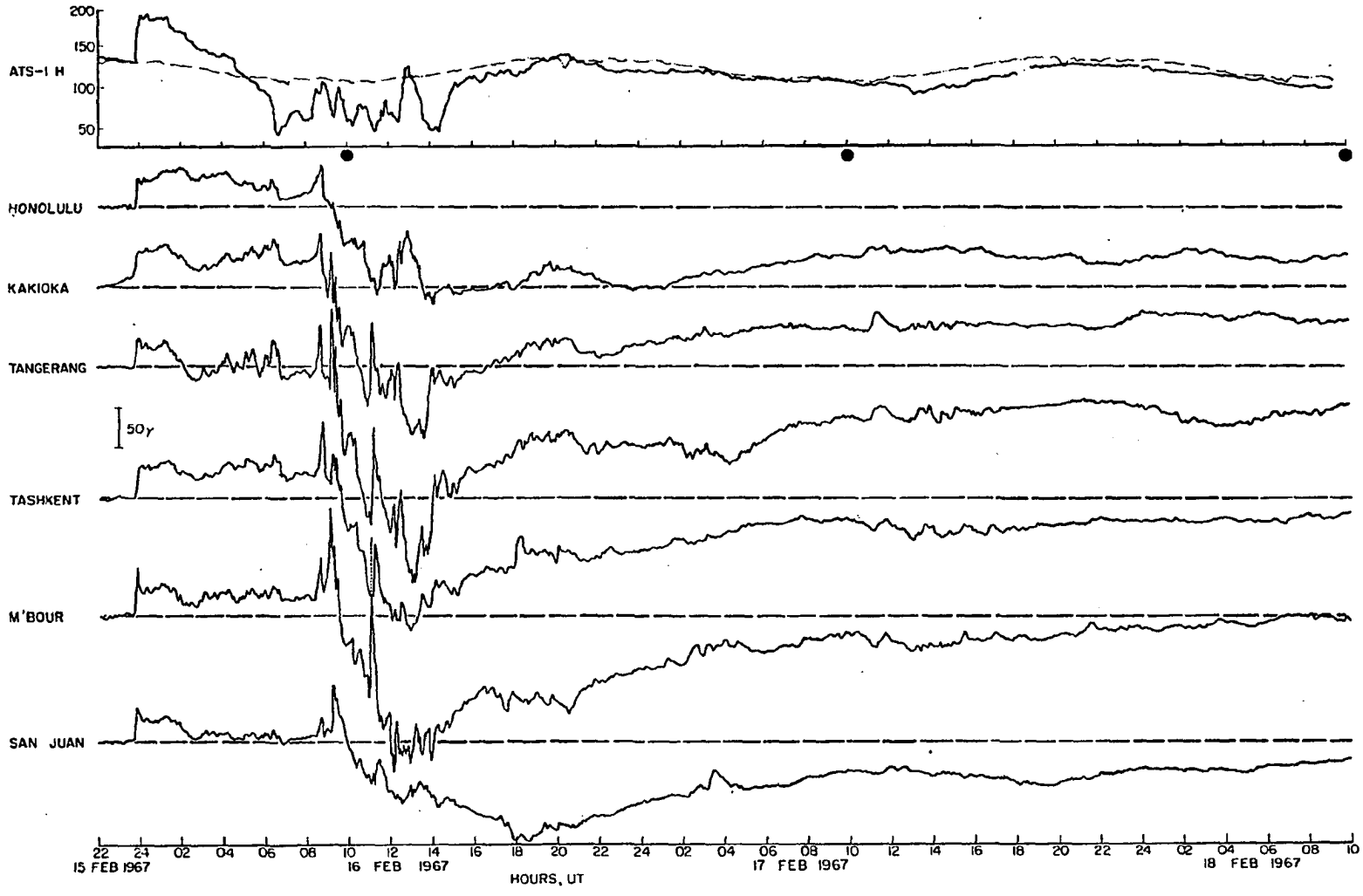

Fig. 4.1. Comparison of ATS-1 and low latitude H-component records during the geomagnetic storm of February 15-18, 1967. Local midnight at ATS-1 is marked by a closed circle.

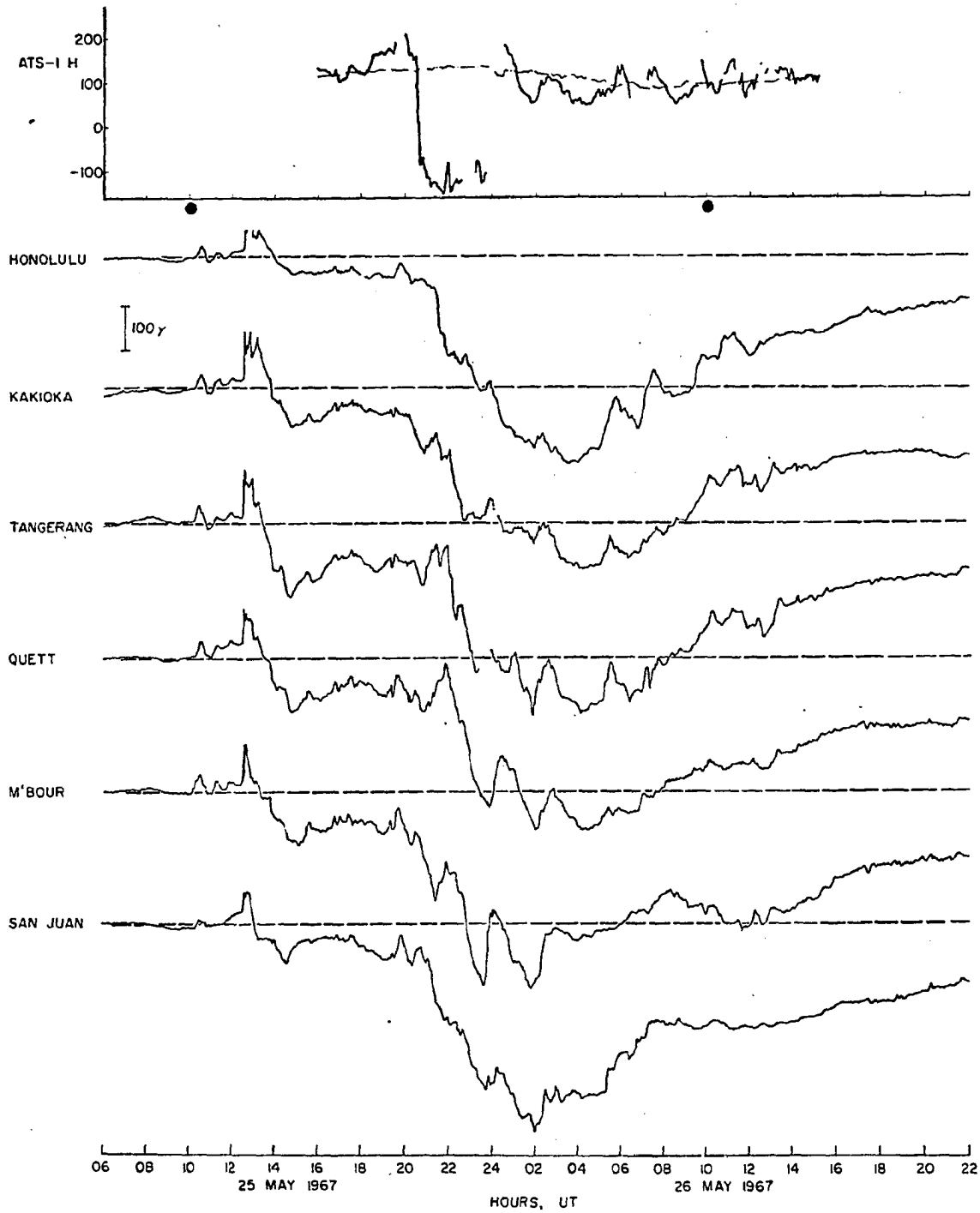

Fig. 4.2. Comparison of ATS-1 and low latitude H-component records during the geomagnetic storm of May 25-26, 1967. Local midnight at ATS-1 is marked by a closed circle.

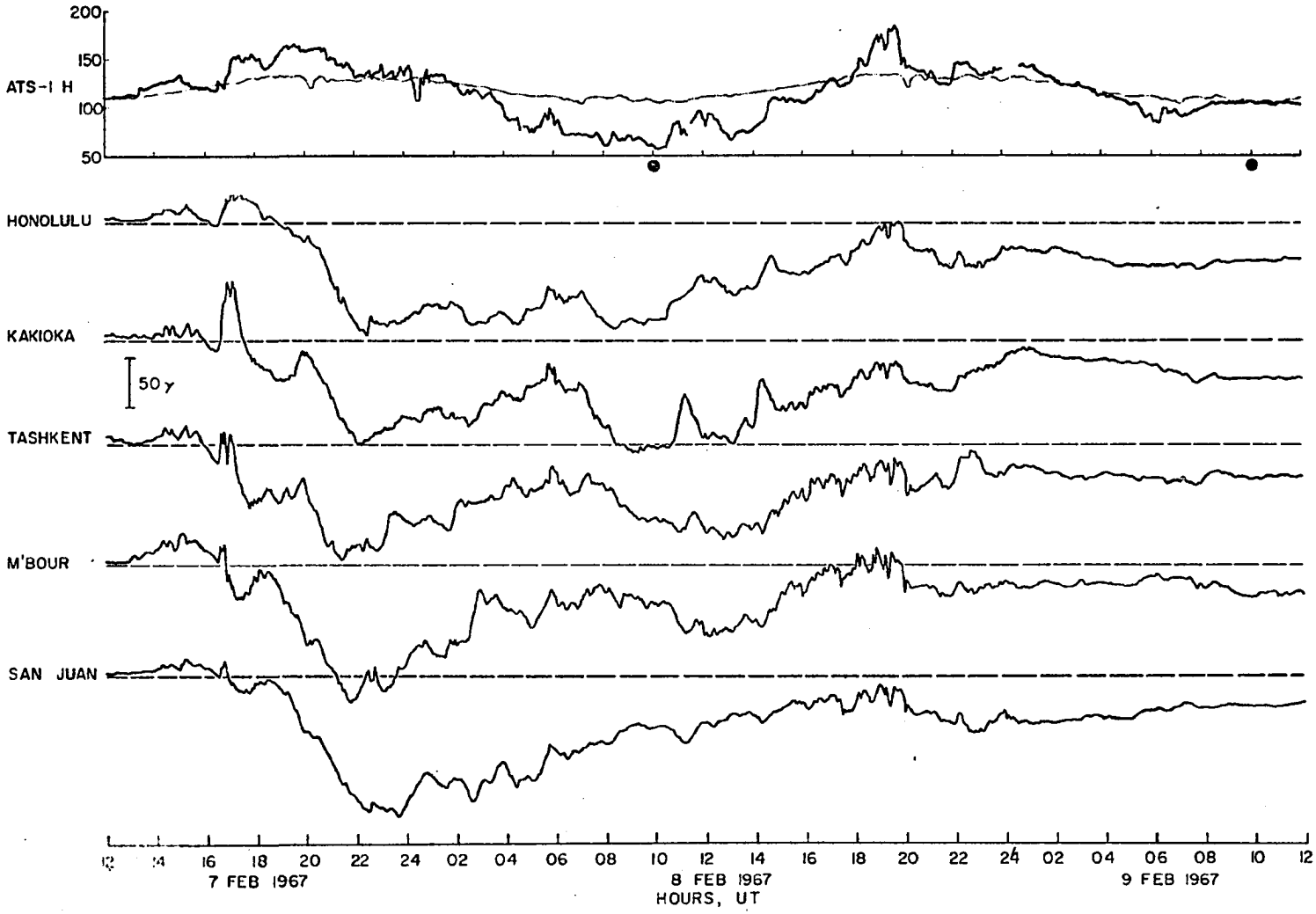

Fig. 4.3. Comparison of ATS-1 and low latitude H-component records during the geomagnetic storm of February 7-9, 1967. Local midnight at ATS-1 is marked by a closed circle.

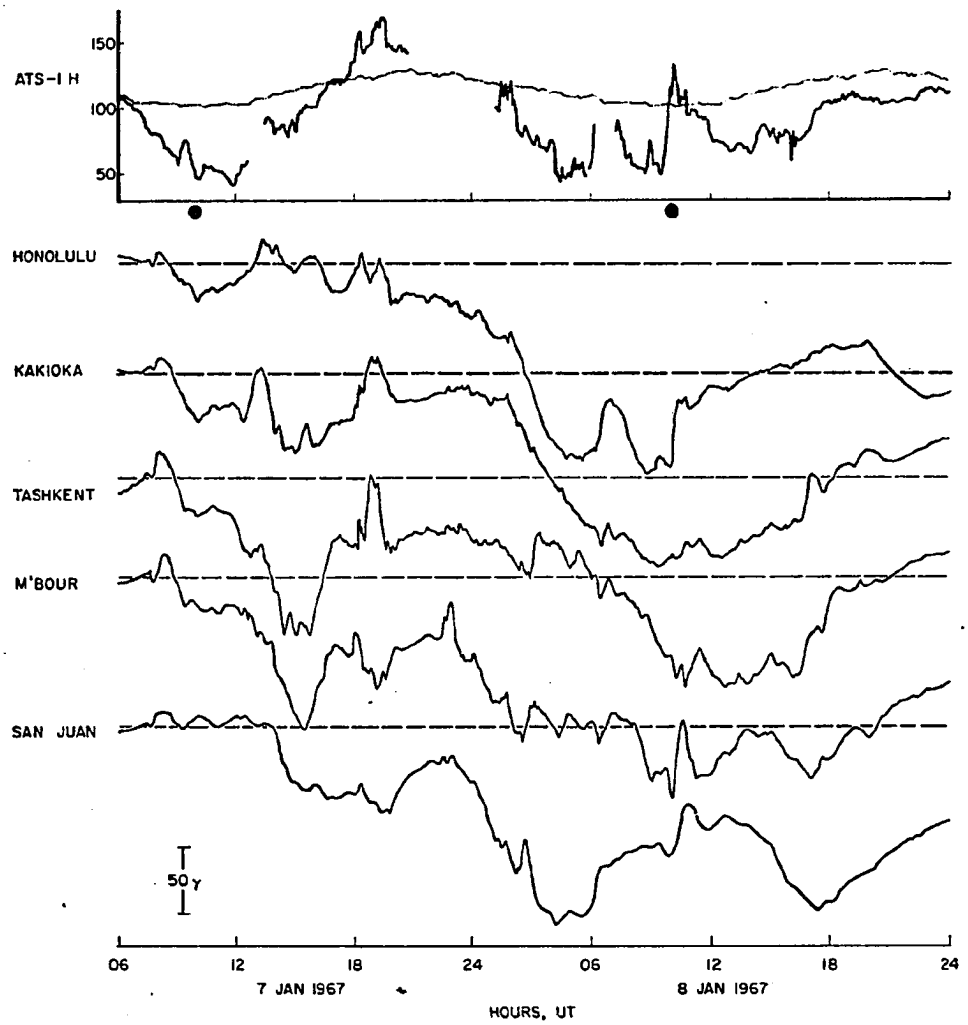

Fig. 4.4. Comparison of ATS-1 and low latitude H-component records during the geomagnetic storm of January 7-8, 1967.

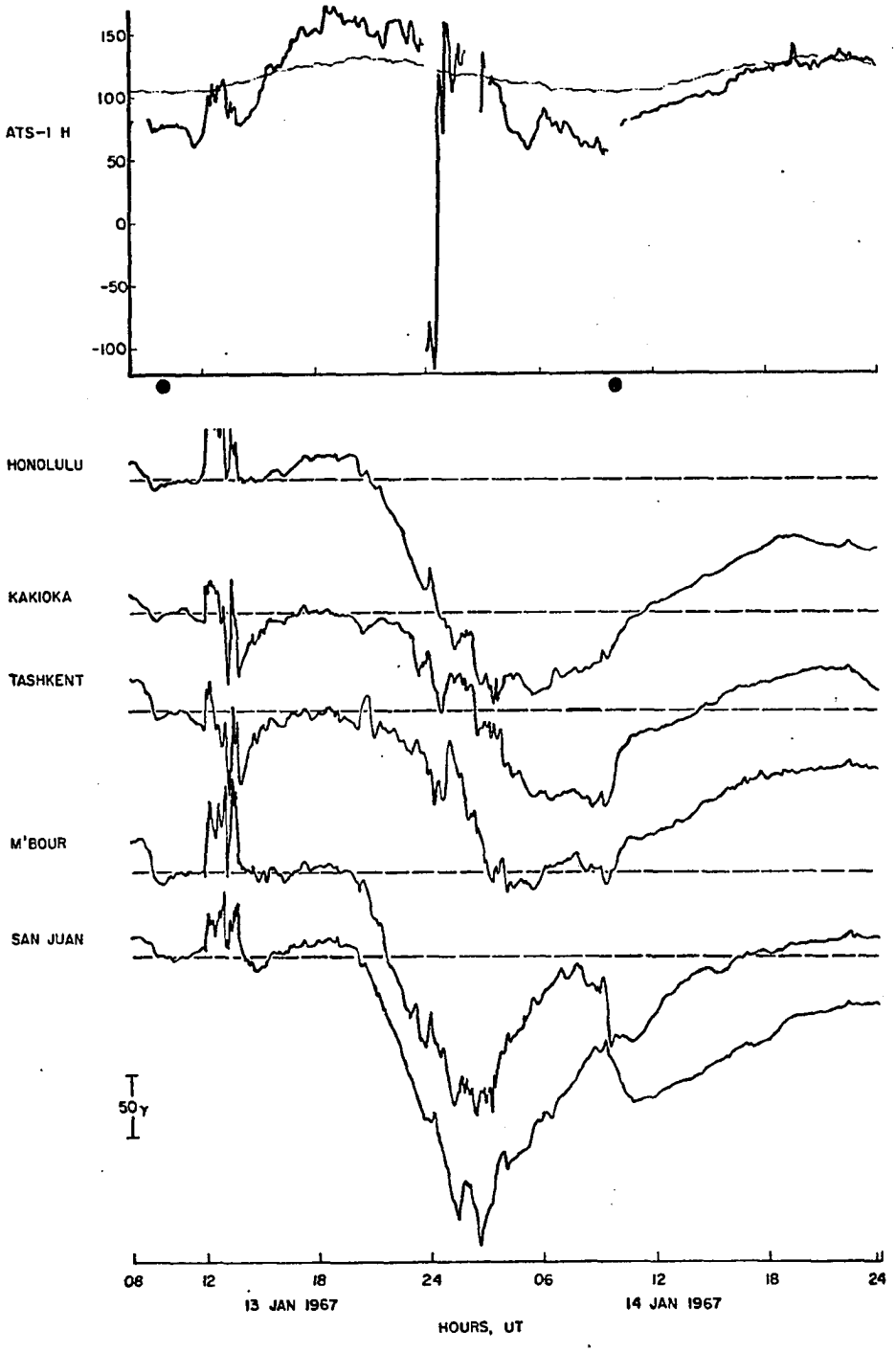

Fig. 4.5. Comparison of ATS-1 and low latitude H-component records during the geomagnetic storm of January 13-14, 1967.

1) In spite of this enhanced daily variation at the synchronous ATS-1 orbit, it is clear that the field at the ATS-1 returns to its 'quiet' day level much more quickly than does the comparable record of a ground observatory during the latter stages of a geomagnetic storm. That is, the main phase 'recovery' occurs earlier at the ATS-1 than on the ground. For example, during the recovery phase of the February 15-18, 1967, storm (see Figure 4.1) the field at the ATS-1 returned roughly to the quiet day level after 16 UT on February 16; on the other hand, the main phase depression on the ground was still appreciable even at 10 UT on February 18, 1967. In this case, it may well be that the return to the quiet level at 16 UT on February 16 was partly caused by the opposing effects of the compression by the enhanced solar wind and of the ring current. However, it is quite obvious that even during midnight hours (10 UT on February 17) the disturbance field at the ATS-1 was much weaker than that on the ground.

2) The early recovery is better illustrated in Figure 4.2 for the great storm of May 25/26, 1967. At the ATS-1, the field became almost normal at as early as 02 UT on May 26, in spite of the fact that a large main phase decrease was still developing on the ground.

3) Figure 4.3 shows another example of an 'early' recovery during the February 7-9, 1967, storm. Although, this example is not as clear as the previous one, it is seen that at 10 UT on February 9, the field at the ground was still quite depressed while at ATS-1,

the H-component had returned to its 'quiet' level. Another interesting feature of this storm are the compressions of the magnetosphere which occurred between 18 and 20 UT on February 8. It is clear that the magnetic variations at these hours are due to compressive effects since they were observed at all the ground stations and produced magnetic variations which were above the quiet day level in the dayside sector of the ATS-I orbit. A modulation of almost identical form was also seen in the 150 KeV electrons by particle detectors aboard the ATS-I.

Two more examples are presented in Figures 4.4 and 4.5. Unfortunately, the scalings of the low latitude records have not been extended sufficiently beyond the beginnings of the recovery phases of the two storms to clearly demonstrate the phenomenon; however, the data available for the latter periods of the storms also show the field at ground stations remains much depressed relative to that seen by ATS-I in the midnight sector during the recovery phases (see Figures 2 and 3, Coleman and Cummings, 1971).

4.3 COMBINED EFFECTS OF THE FIELDS OF THE RING CURRENT AND THE MAGNETOTAIL CURRENT

In this section the combined effects of the ring and tail current fields in the vicinity of a synchronous orbit will be briefly described. In Chapter 6, a simplified model of the magnetosphere will be given; the model can be used to qualitatively verify the description given in this section.

Along an equatorial radius, a proton belt (ring current) produces a negative (southward directed) field in the vicinity of the earth and

a positive (northward directed) field outside the distribution; for details of the ring current field distribution, see Akasofu and Chapman (1961), Sozou and Windle (1969), and Hoffman and Cahill (1968). On the other hand, the magnetotail current produces a negative field in the region earthward from the inner edge of the plasma sheet. Hence, there should be a limited region between the ring current belt and the inner edge of the plasma sheet in which their fields tend to cancel.

Coleman and Cummings (1971) suggested that as the recovery phase begins, the compression and the tail current return to their respective quiet day states and that an inward motion of the ring current produces a separation of the neutral sheet from the ring current. In this section, variations of the distribution of the magnetospheric current and their consequences are semi-quantitatively examined. More specifically, it is suggested that during the recovery phase of a geomagnetic storm, the inner edge of the plasma sheet recedes rapidly away from the earth while the ring current decreases, and that the synchronous satellite is often located in this region where the cancellation tends to occur.

Here, the results of a simple model calculation are presented which show somewhat qualitatively how such a situation can occur. The model consists of a distributed ring current (based on the work of Akasofu, 1966) and a tail sheet current which flows in the plasma sheet from dawn to dusk. The tail circuit is completed by cylindrical sheet currents from the dusk portion of the magnetotail

to the dawn part. More detailed and expanded calculations are presented in Chapter 6.

The ring current model of Akasofu (1966) consists of mono-energetic particles having a Gaussian distribution of number density and a special pitch angle distribution; the model is symmetric about the dipole axis.

The cross-section of the magnetotail is taken to be circular (radius = 16 R_E) in the plane perpendicular to both the equatorial and midnight meridian planes; the tail sheet current in the equatorial plane bisects the cyclinder. To simplify the computations, the magnetotail current was assumed to have constant density over the entire length of the tail (taken to be $\sim$ 10 to 30 R_E). A closed solution for the magnetic field was obtained for the plane sheet of current, while the contributions from the cylindrical parts were computed numerically.

This model should provide a reasonable qualitative approximation of the actual field. Ness (1965) and Behannon and Ness (1966) from IMP I data and Behannon (1968) from Explorer 33 data found that the field is relatively uniform over an approximately cylindrical cross-section of the tail, solar in direction above the solar-ecliptic plane and anti-solar below. These measurements also show the field slowly decreases with increasing distance down the tail and also that the cross-section becomes less cylindrical. In the model used here, the inner and outer edges of tail sheet and cylinder surfaces are singularities; however, for regions sufficiently far from these currents, the approximation is fairly good. Much like a long solenoid, the interior field is nearly uniform in each half of the bisected cylinder. Earthward in the equatorial plane, the magnitude of the field drops off rapidly, and

within a fraction of an earth radius,the field is primarily due to the integrated effects of the more distant parts of the tail currents.

The combined field of the ring and magnetotail currents are shown in Figures 4.6 and 4.7. (For definitions of the various parameters listed, see Chapter 6). Figure 4.6 represents the situation along the midnight meridian, equatorial radius which may exist during the latter part of the recovery phase. For a comparison, the magnitudes of the ring current and tail current fields are plotted inidividually. In Figure 4.6, the current intensities and locations are chosen such that the combined field is negative in the region of the synchronous orbit. In Figure 4.7, the equatorward edge of the plasma sheet begins at 9 R_E and with the ring current and tail current intensities each reduced by one-fourth of the values of Figure 4.6, it is seen that at the orbit of a synchronous satellite the combined field is nearly null. However, the combined fields in the vicinity of the earth are seen to add vectorially such that the magnitude there is still appreciable.

4.4 SUPPORTING EVIDENCE

By means of a simple model calculation,it has been shown in the in the preceding section that the combined fields of the ring and magnetotail currents can interact in such a way as to duplicate the observed early recovery of a geomagnetic storm at synchronous orbit altitudes in the night sector. Whether this model fits at least qualitatively the available particle and field observations in the region of the ring current and the magnetotail will now be discussed.

It has been shown by Frank (1970) that the plasmapause, the ring current belt and the inner edge of the plasma sheet tend to advance

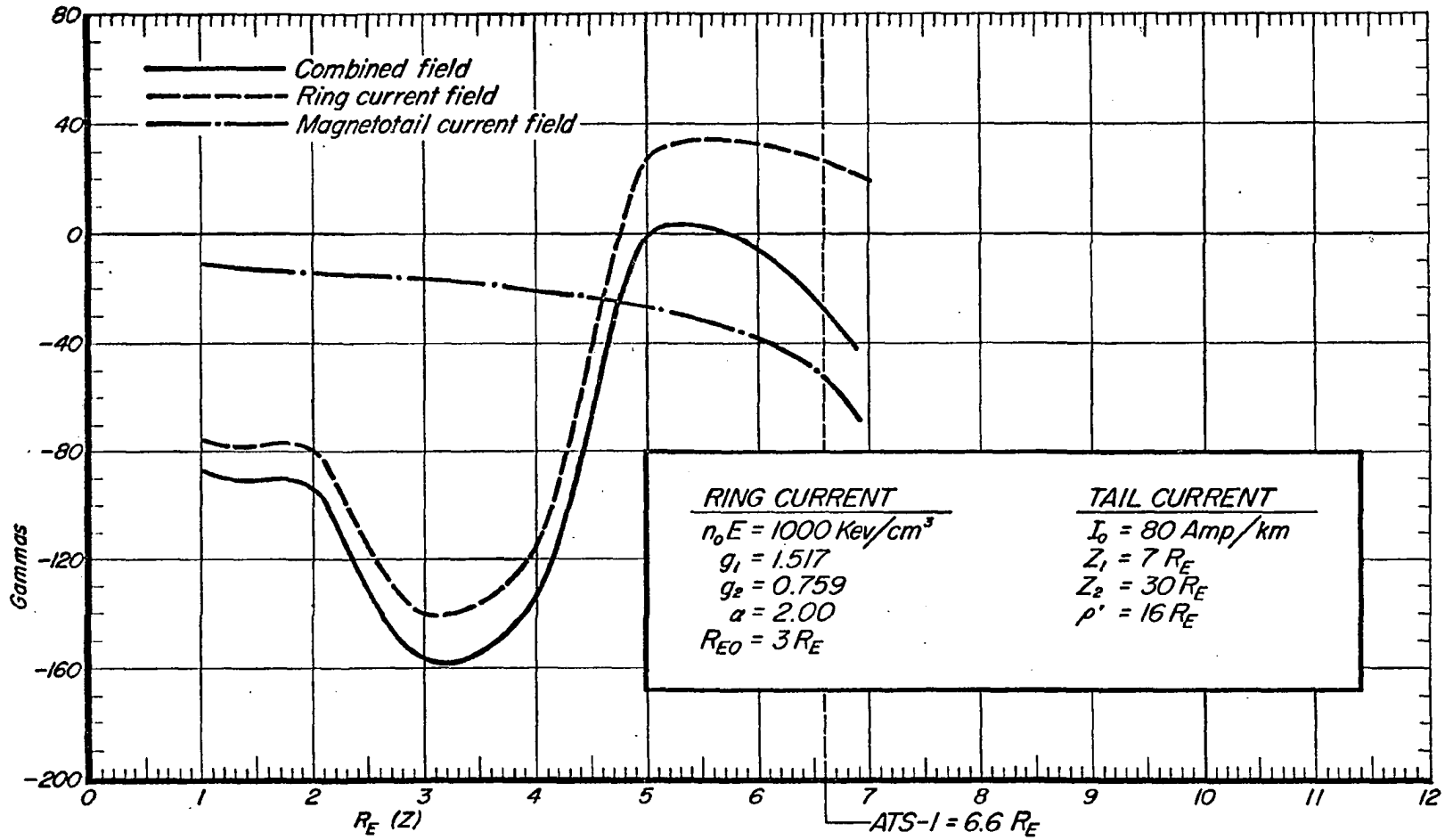

Fig. 4.6. Tail current, ring current and combined fields along the equatorial radius in the midnight meridian plane for the model simulating a moderate main phase decrease. For details of the calculations, see Chapter VI.

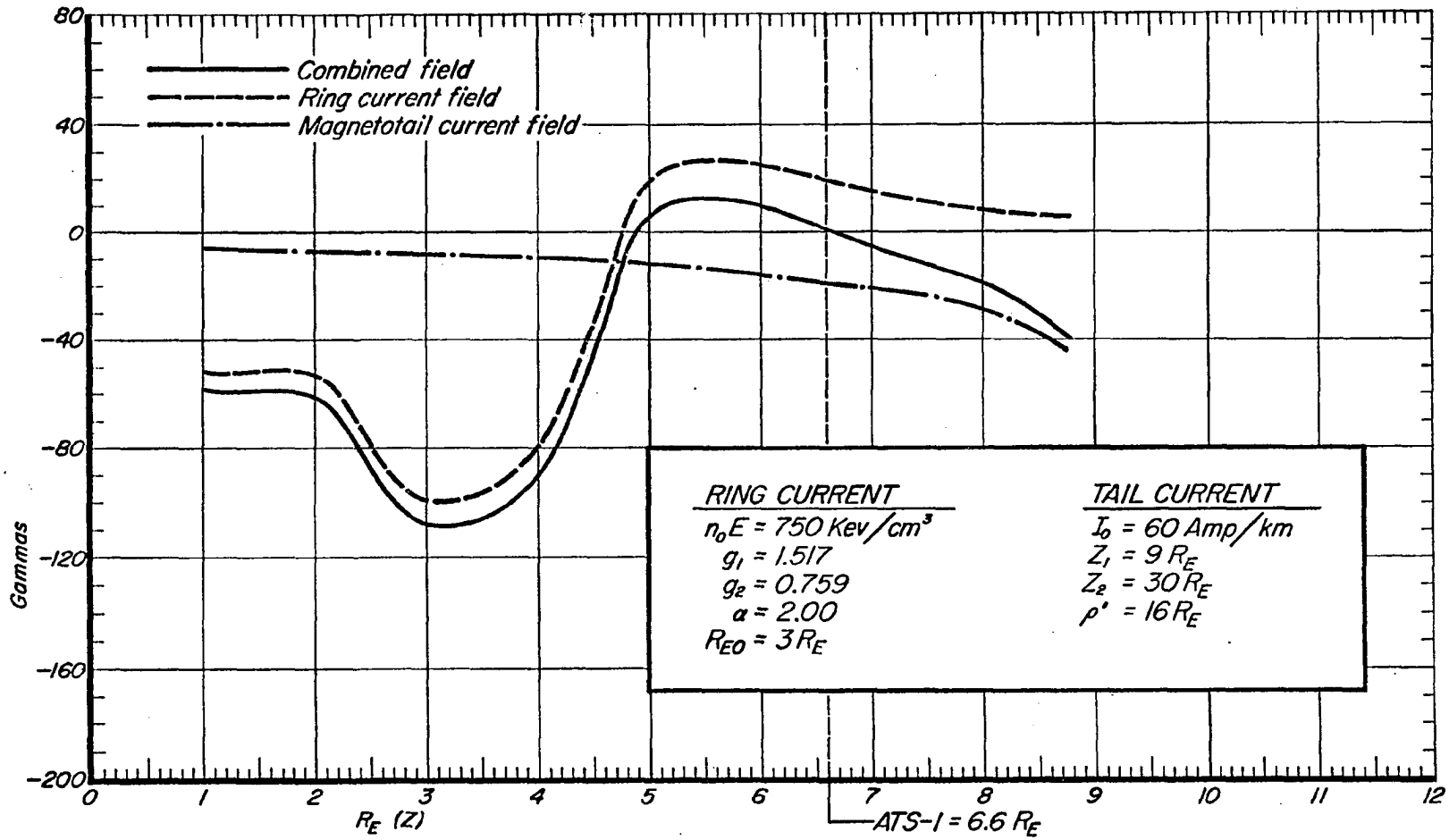

Fig. 4.7. Tail current, ring current and combined fields along the equatorial radius in the midnight meridian plane for the model simulating the recovery phase. For details of the calculations, see Chapter VI.

toward the earth during disturbed periods and recede away from the earth during quiet periods. A critical test of the interpretation of the ATS-I data proposed in this chapter is to determine whether the observed storm-time variations of the relative locations of the ring current belt and the plasma sheet fit the interpretation. One difficulty which arises in attempting to examine the data in this way is that both the ring current belt and the plasma sheet do not have simple geometries, so that the locations of the ring current belt and the edge of the plasma sheet are poorly defined (Frank, 1970).

Although the energy density of the low energy protons and electrons along the midnight equatorial radius can vary greatly throughout a magnetic storm, certain features of the distribution persist. With increasing radial distance, both the proton and electron energy density distributions rise exponentially, reach a peak and decrease drastically outside the trapping region (of higher energy electrons) during disturbed periods and more slowly during quiet periods. For the series of observations by the OGO-3 satellite studied by Frank (1970), the peak intensity of the ring current occurred nearer the earth than the peak of the electron energy densities. Within about 4 to 9 R_E, the energy densities densities of electrons range between 10^{-7} to 10^{-8} ergs/cm^3; the proton energy densities are about one order of magnitude larger throughout the interval.

Frank (1970) has given the following definitions for the earthward edge of the plasma sheet proper and the outer edge of the extraterrestrial ring current. The region in which the proton energy density greater than 10^{-8} erg/cm^3 begins to <u>increase</u> to the peak value with <u>decreasing</u>

radial distance is defined as the outer edge of the ring current. The inner edge of the 'plasma sheet proper' is defined as the region in which the electron energy densities begins to exponentially decrease from the peak value with decreasing radial distance. The term 'proper' is used by Frank to distinguish the electrons beyond the peak intensity from those earthward.

Figure 4.8 shows the locations of the ring current and the plasma sheet for the storm of June 25, 1966 (Frank, 1970). The location of the 'peak intensity' of the ring current belt is also shown. Figure 4.9 shows the corresponding low latitude magnetic records of Honolulu, Kakioka, Tashkent, M'Bour and San Juan. During a quiet period (June 23) prior to the storm, the peak of the ring current was located at about the synchronous (geo-stationary) orbit distance, and the edge of the plasma sheet proper was located about 0.4 R_E outside this distance. During the main phase (June 25), both the peak of the ring current and the edge of the plasma sheet proper were located inside the orbit of the synchronous satellite.

During the recovery phase (June 27), however, there occurred a large separation between the peak intensity of the ring current and the edge of the plasma sheet proper. The peak of the ring current belt moved away from the earth, but remained well inside the orbit of the synchronous satellite. The plasma sheet also moved away from the earth and was located even beyond the pre-storm location on June 23. It may well be that the residual ring current has a role in determining the location of the edge of the plasma sheet, since the effect of the

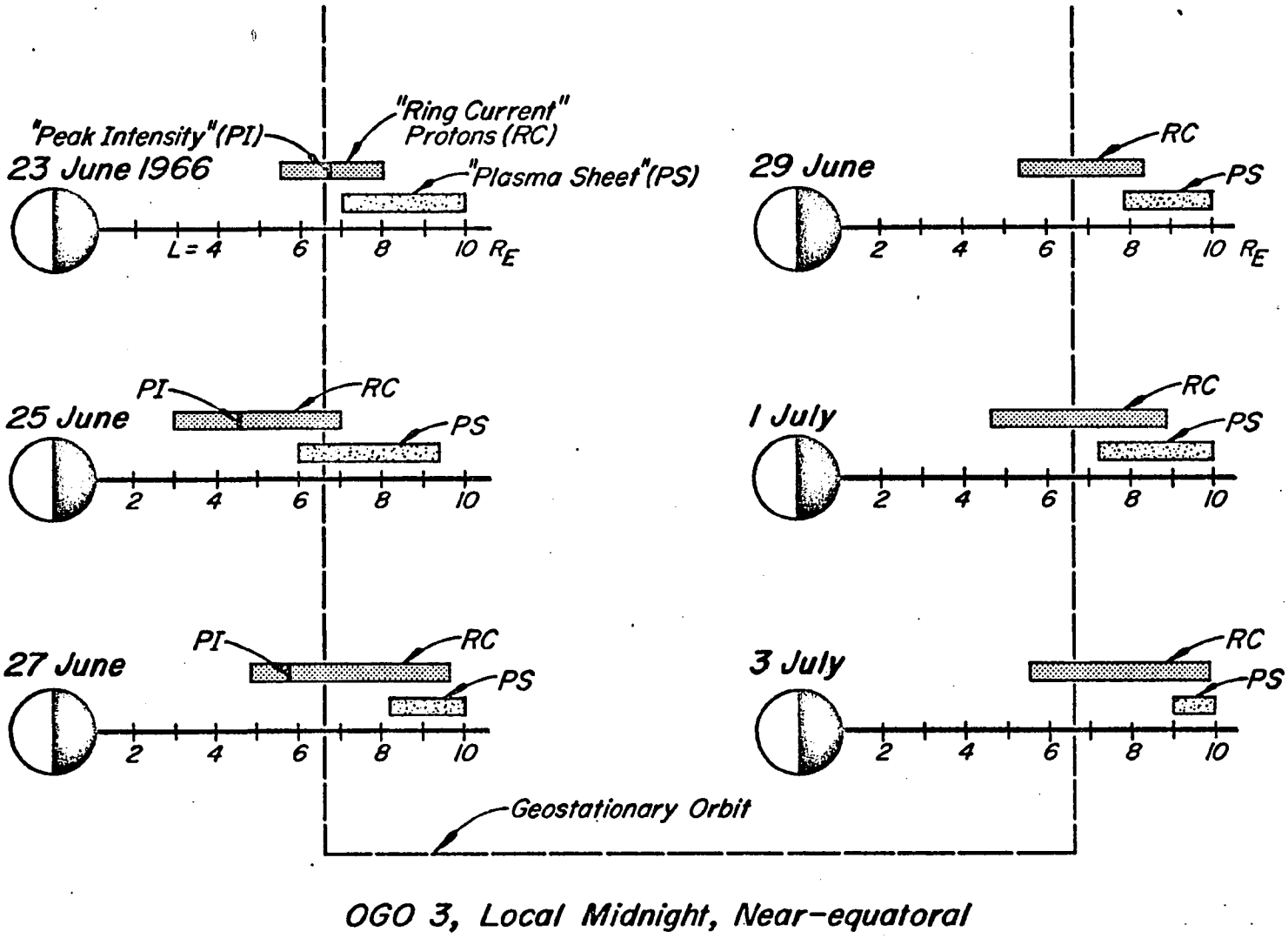

Fig. 4.8. Locations of the plasma sheet and ring current protons for six days during the period June 23-July 3, 1966. The location of the peak intensity of the ring current protons is also shown. (After Frank, 1970).

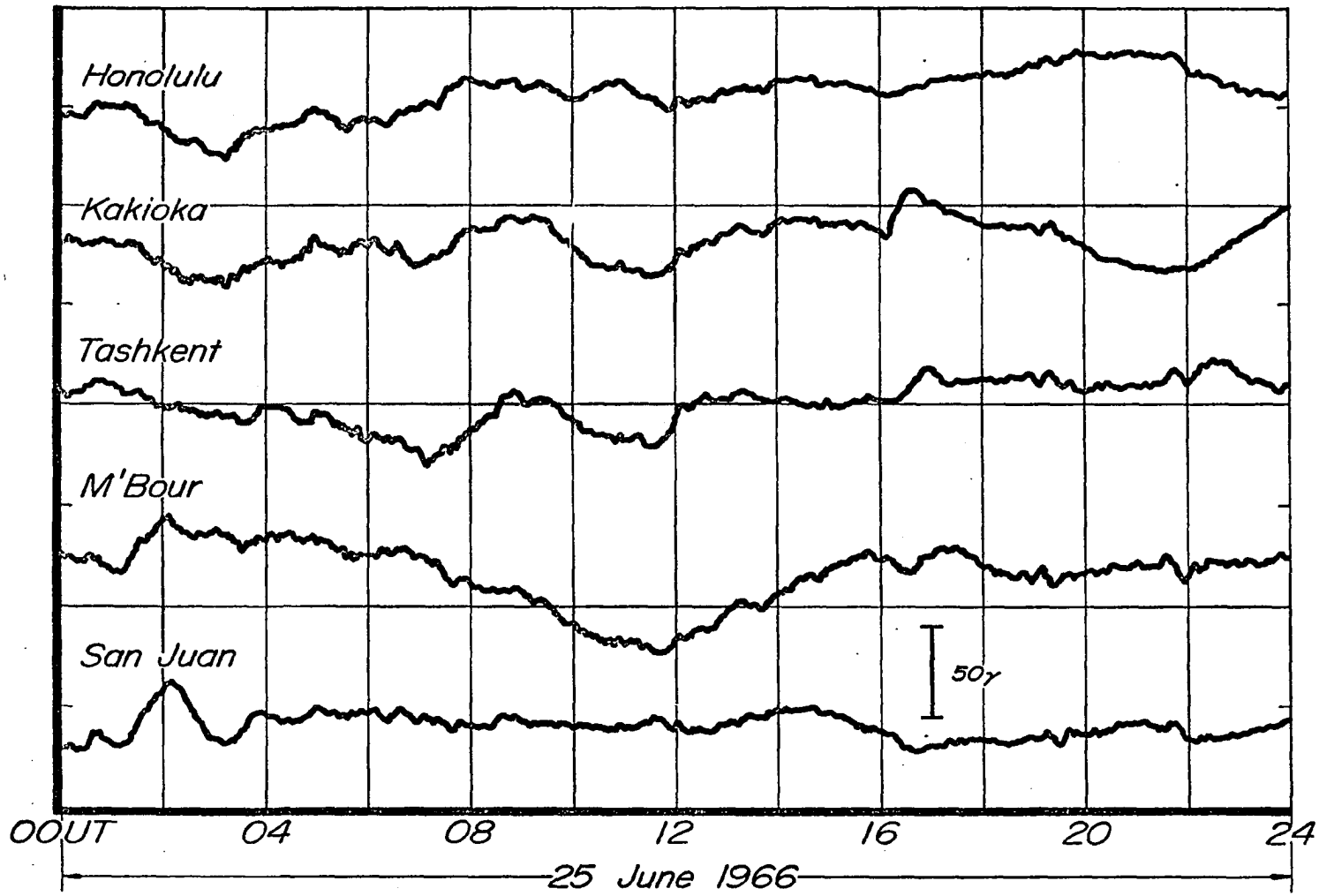

Fig. 4.9. Low latitude H-component records during magnetic storm of June 25, 1966.

ring current outside the trapping region is equivalent to increasing the magnetic moment of the earth. A sequence of events similar to the one above occurred during a relatively weak disturbance on June 29 - July 3, 1966. Therefore, these situations are qualitatively similar to the idealized model which was examined in Section 4.3. A more quantitative estimate of the combined field of the ring current and the magnetotail current on the basis of the observed particle distributions is, unfortunately, difficult to make. This is particularly the case with the latter current, because the actual current distribution (or, conversely, the field distribution) is not known and because a self-consistent estimate is required which takes into account the approximate equality of the plasma and magnetic pressures.

4.5 SUMMARY AND DISCUSSION

In this chapter, several examples of ATS-I and ground H-component data have been presented which indicate that the recovery phase of a geomagnetic storm proceeds more 'rapidly' at synchronous altitudes than at ground stations. Particle measurements in the tail region show that the earthward edge of the plasma sheet and the peak intensity of the ring current distribution recede away from the earth during the recovery phase of geomagnetic storms, while the current strengths also diminish. This tends to result in a cancellation of the magnetic fields of the ring current and magnetotail current at points between the peak of the ring current belt and the inner edge of the plasma sheet. The orbit of the synchronous satellite is located in the region, so that the main phase tends to 'recover' there even when the main phase as observed on the ground is still in progress.

Some preliminary results of a simple model calculation of the effects of the ring and magnetotail currents at the synchronous satellite altitudes and on the surface of the earth have been presented, which indicate that the fields can interact in such a way as to produce the observed 'early' recovery. Since the ring current contributes a significant northward directed field where the edge of the plasma sheet is located, the situation described by the model is a reasonable one.

CHAPTER V

A STUDY OF THE OCCURRENCE OF SIMULTANEOUS STORM SUDDEN COMMENCEMENTS AND POLAR MAGNETIC SUBSTORMS

5.1 INTRODUCTION

Since the advent of space probes, considerable efforts have been expended to determine which of the parameters of the solar-terrestrial environment are directly or indirectly related to the occurrence of magnetospheric substorm phenomena (Snyder, Neugebauer and Rao, 1963; Fairfield and Cahill, 1966; Fairfield, 1967; Rostoker and Fälthammar, 1967; Rostoker, 1968; Ballif and Jones, 1967; Schatten and Wilcox, 1967; Wilcox, Schatten and Ness, 1967). Most of the studies have indicated that, as suggested by Dungey (1961, 1963), the existence of a southward-directed interplanetary field is a necessary or favorable but insufficient condition for the generation of magnetospheric substorms (cf. Rostoker, 1968, p. 4383).

There have also been various correlative studies made on the discontinuities of the solar wind and the occurrence of sudden compressions of the magnetosphere (see the review article by Burlaga, 1970). Sudden compressions observed in the world-wide H-component of the geomagnetic field as a sudden change have been classified into two categories: storm sudden commencements (ssc's) and sudden impulses (si's). An si is not followed by an appreciable increase in activity while the opposite is the case for an ssc. There are both positive and negative ssc's and si's. (For more exact definitions, see the Provisional Atlas of Rapid Variations (1957)).

Tangential and fast shock discontinuities have been identified in the solar wind. It has been found that fast shock and tangential

discontinuities tend to cause ssc's and si's (Burlaga, 1970). Shock discontinuities are, in general, associated with the more intense activity of a geomagnetic storm.

It is generally acknowledged that a polar magnetic substorm (bays) are a result of some kind of instability in the magnetosphere. Sudden compressions may produce large-scale changes in the configuration of the magnetosphere, and, therefore, may provide the necessary conditions for the immediate onset of a polar substorm. This chapter is a study of such 'simultaneously occurring ssc's and polar magnetic substorms'.

5.2 EXAMPLES OF SIMULTANEOUS STORM SUDDEN COMMENCEMENTS AND POLAR MAGNETIC SUBSTORMS

Figures 5.1, 5.2 and 5.3 show the reproduction of parts of magnetic records from Honolulu, a typical low latitude station, and from College, a typical auroral zone station, for periods which registered storm sudden commencements (ssc). In the first example in Figure 5.1, the ssc of the storm of September 22/23, 1957, occurred at 1344 UT on September 22. It is clearly seen in the Honolulu record as a step-function-like positive change at that time.

The corresponding College magnetic record is shown below the Honolulu record. An extremely intense negative bay of order 1000 gammas began at the time when the ssc was registered at Honolulu; note that two kinds of College records, insensitive and normal, are used in Figures 5.1, 5.2 and 5.3; when substorms were too intense to be shown clearly in normal records, insensitive records have been used. Auroral activity during this particular substorm was studied by Akasofu (1962), who showed that it was typical of an auroral substorm.

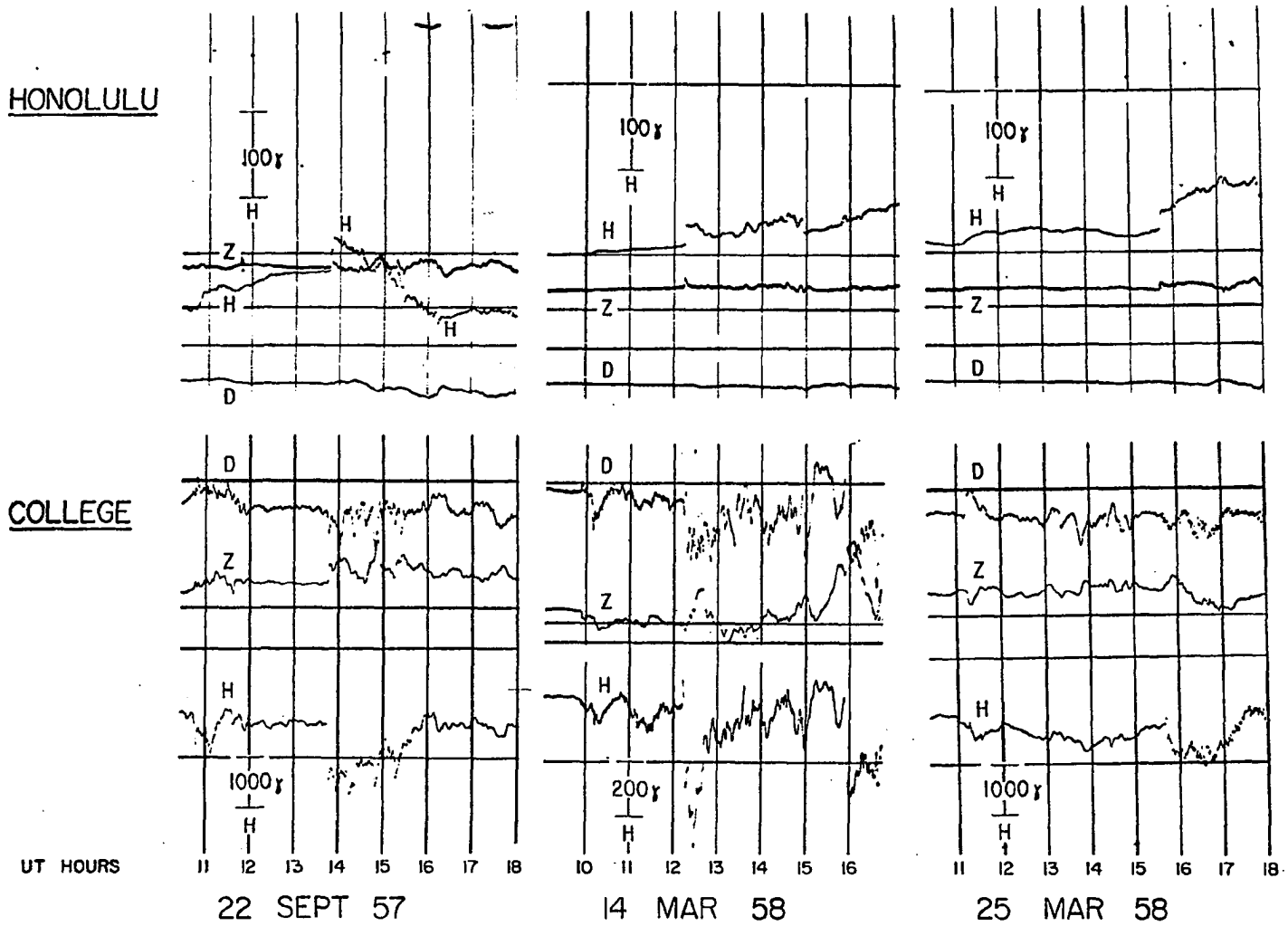

Fig. 5.1. Magnetic records from Honolulu and College showing examples of simultaneous ssc and polar magnetic substorms.

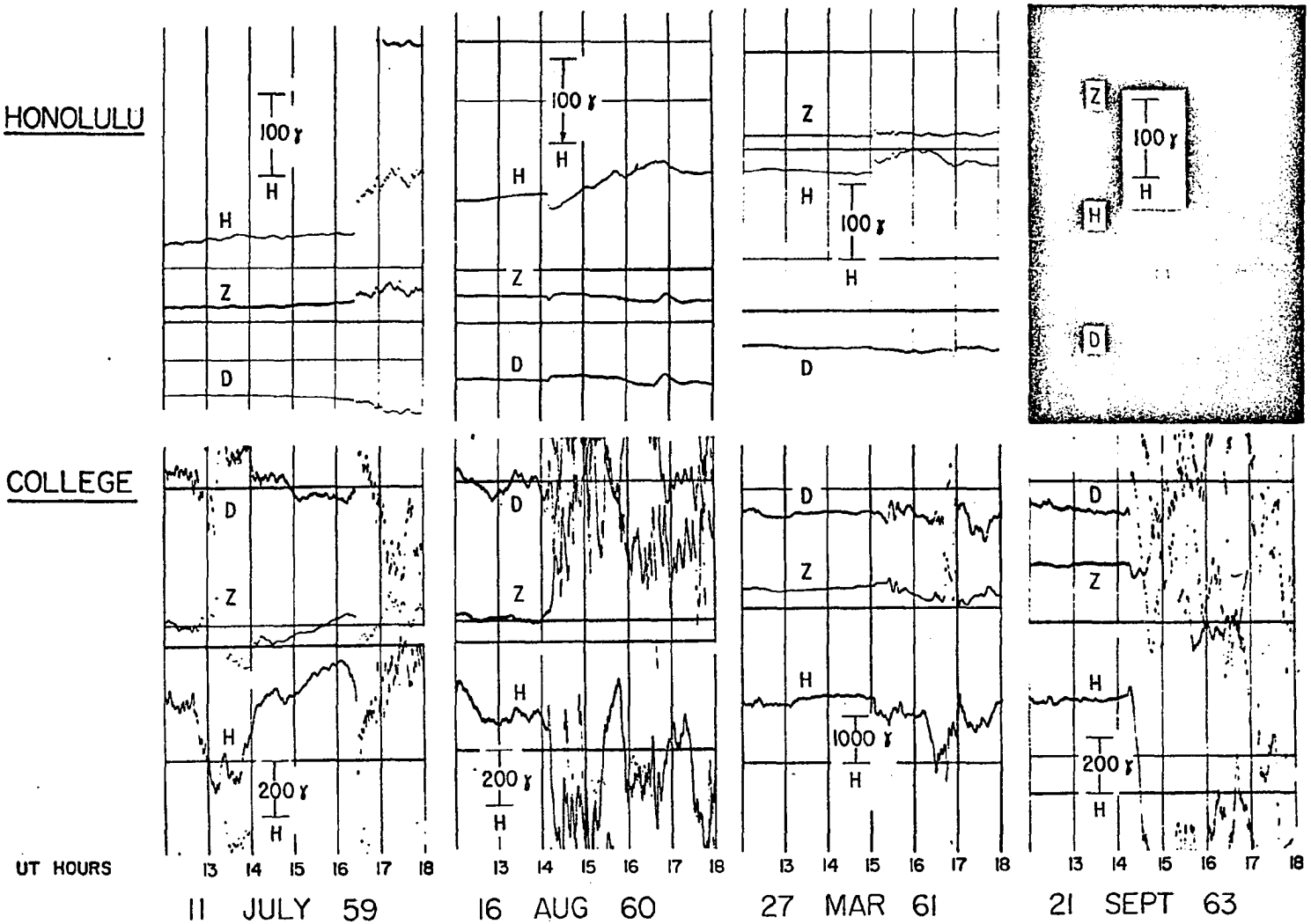

Fig. 5.2. Magnetic records from Honolulu and College showing examples of simultaneous ssc and polar magnetic substorms. The Honolulu H-component record of August 16, 1960 is positive in the downward direction.

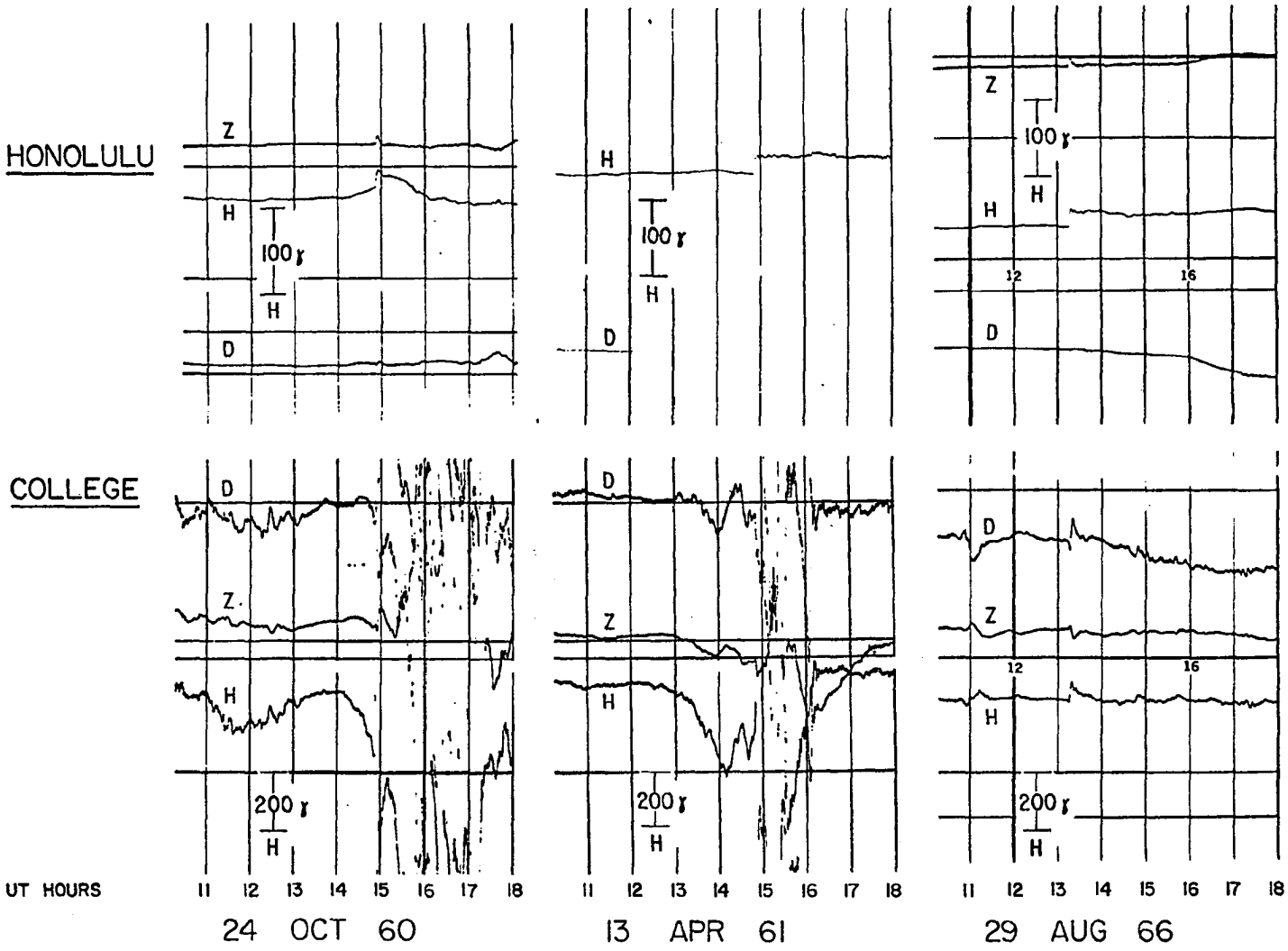

Fig. 5.3. Two examples of simultaneous ssc and polar magnetic substorms observed in the Honolulu and College magnetic records, and a third example showing a non-simultaneous event.

In the second example, an ssc occurred at 1212 UT on March 14, 1958. The corresponding College record indicates an impulsive positive change at 1213 UT which was immediately followed by a negative bay of order 400γ; in such rapid changes, the simultaneous rapid-run magnetic record was also used to obtain exact onset times of various phenomena. The third example of Figure 5.1 is similar to the second one; the College record is an insensitive one.

In Figures 5.1, 5.2 and 5.3, the other illustrated ssc's occurred at 1540 UT, March 25, 1958; 1626 UT, July 11, 1959; 1409 UT, August 16, 1960; 1452 UT, October 24, 1960; 1451 UT, April 13, 1961; 1503 UT, March 27, 1961; 1413 UT, September 21, 1963 and 1316 UT, August 29, 1966. Except for the last example in Figure 5.3, all the ssc's were accompanied by negative bays at College, although in some cases College was not located at the most suitable location to register the substorms. In some of the examples presented, the ssc-associated substorm can be clearly identified, in spite of the fact that substorms were already in progress.

For the examples shown, the polar substorms occurred within about two minutes after the onset of the ssc. All of the simultaneous events studied in the following Section (5.3) occurred within about three minutes of each other.

Magnetic field variations associated with ssc's at auroral zone stations were studied in detail by Wilson and Sugiura (1961). They showed that ssc variations often have oscillatory features at auroral zone stations and that such variations could be interpreted in terms

of the arrival of hydromagnetic waves with certain polarization patterns. It is likely that the initial impulsive positive change in the horizontal component is an indication of the arrival of hydromagnetic waves. However, the waves were masked by a powerful negative bay disturbance which followed soon after the arrival of the waves.

The examination of magnetic records from a single auroral zone station clearly indicates that the occurrence of negative bays at the time of ssc is a local midnight-morning phenomenon. Thus, negative bays which are simultaneous to ssc's have the same evening-midnight-morning asymmetry of occurrence frequency as do non-associated negative bays. Oscillatory changes are most often observed during ssc's which occur in afternoon hours; for such examples, see Wilson and Sugiura (1961). Therefore, the examination of the occurrence of a negative bay at the time of a particular ssc requires a study of magnetic records from stations which are distributed along the auroral zone.

In the next section, the results of a statistical study are described.

5.3 SOME STATISTICAL RESULTS ON THE OCCURRENCE OF SIMULTANEOUS EVENTS

For the statistical study, magnetic records from College, Meanook, Ft. Churchill, Leirvogur, Kiruna, Cape Chelyuskin, Dixon,, and Cape Wellen were used. All the ssc's, which are listed in the IAGA Bulletin for the years of the IGY (July 1957-December 1958) and of the IQSY (1964 and 1965),108 and 72 cases, respectively, were examined for the simultaneous occurrence of negative bays at the above listed auroral zone stations.

The instrumentation at most high latitude stations is insensitive to magnetic field changes of the order of 50 to 100 gammas. Accordingly, events were considered simultaneous only when the value of the bay was at

least -50 gammas or so. For isolated events, even for this level of change, it is often clear whether a bay is associated with an ssc. However, if an ssc occurs during a time of considerable activity, the identification of an ssc-associated, bay event becomes difficult to make.

In this study the ssc's have been classified into four categories: simultaneous or yes events (Y), non-simultaneous or no events (N), doubtful yes events (Y?) (events which occurred during substorms and/or with only very small negative bays), and events with incomplete data (?). The results are summarized in Table 5.1.

During the IGY, 49% of all the ssc's were accompanied by polar substorms, but the percentage decreased drastically to less than 3% during the years of minimum solar activity, 1964-1965. The last example in Figure 5.3 is an illustration of an ssc which was not accompanied by a negative bay, although College was suitably located to observe a negative bay.

In order to examine whether or not the occurrence of substorms are related to the degree of disturbances before ssc's, the Kp index prior to the 3-hour interval which registered ssc's was examined for all the ssc's of this study. For this data, no relation between prior activity and the occurrence of substorms simultaneous to ssc was observed.

Similarly, the sums of two, four and eight Kp indices prior to the 3-hour interval which registered ssc's were examined, with the same result. This can be seen in Figure 5.4, which gives the ratio of the number of yes or simultaneous events, including doubtful ones, to the total number of events studied during the 1957-1958 period

TABLE 5.1

	TOTAL SSC	YES EVENTS (Y)	NO EVENTS (N)	DOUBTFUL YES EVENTS (Y)	INCOMPLETE DATA
IGY (1957-1958)	108	51(48.6%)	35(33.3%)	19(18.1%)	3(not included)
IQSY (1964-1965)	72	2(2.8%)	51(70.8%)	19(26.4%)	0

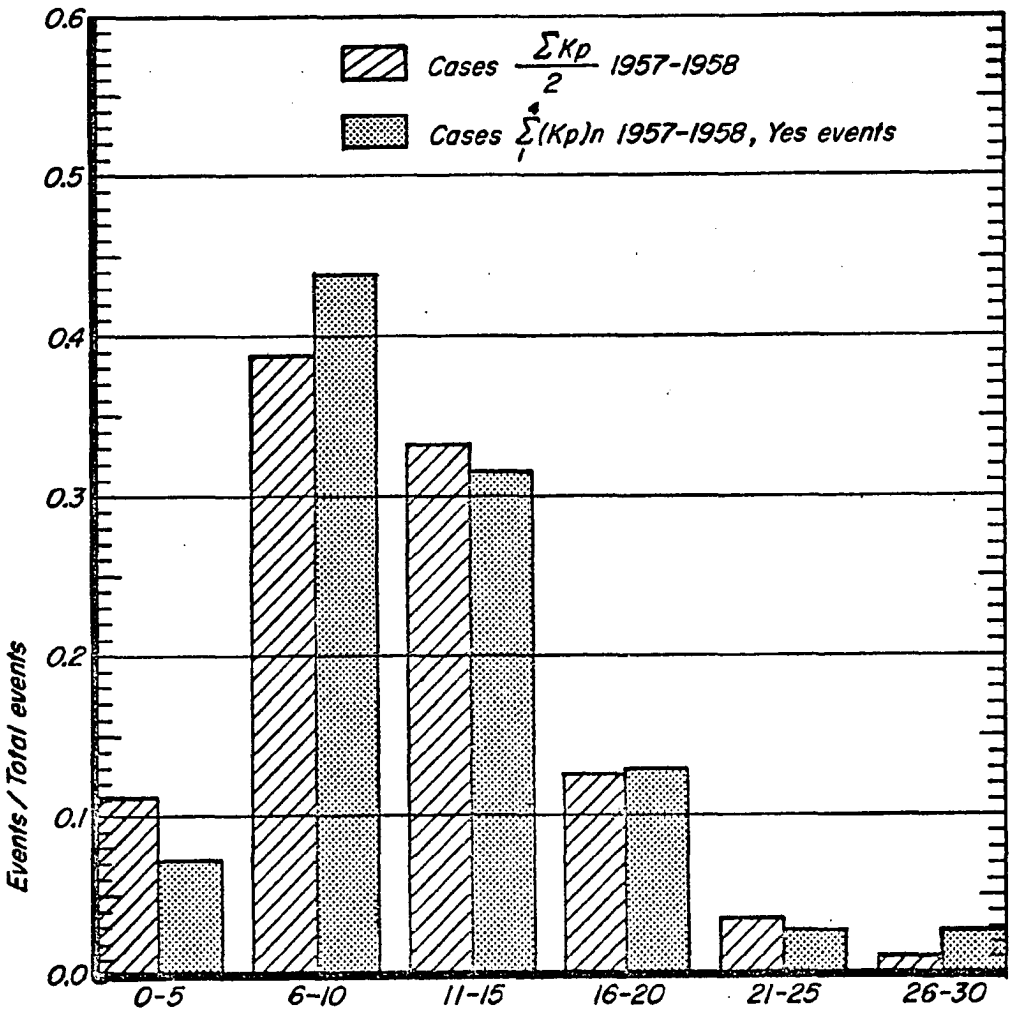

Fig. 5.4. Normalized distribution of the sum of Kp of the four 3-hourly Kp indices prior to the 3-hourly interval containing the ssc versus Kp intervals for yes events (Y) during July, 1957 to January, 1959. For comparison the normalized distribution of the sum of Kp divided by two for all days during this period versus Kp intervals is also given.

plotted against the sum of the prior four Kp indices. Figure 5.4 also gives the ratio of the number of cases of the daily sum of Kp divided by two for all days during the 1957-1958 period to twice the total number of days during the period plotted against intervals of Kp; for example, a daily sum of Kp of 28 yields two cases with sum 14. Although the number of cases in each plot is not large statistically, it is seen that there is no strong tendency for the yes event distribution to be different from the distribution of all days during the period.

Therefore, this study shows there is no definite tendency for a highly disturbed magnetosphere to respond more readily by generating substorms simultaneous to an ssc-associated interplanetary disturbance than a quiet magnetosphere.

It is thus suggested that the drastic difference of the occurrence of substorms associated with ssc's between the IGY (1957-58) and IQSY years (1964-65) could partly be due to differences of the types and/or intensities of interplanetary disturbances (or interplanetary discontinuities).

Figure 5.5a is a histogram of the total number of events versus the average amplitude of the ssc of three low latitude stations, Tashkent, San Juan and Honolulu during the 1957-1958 period. It is clear that smaller amplitudes dominate the distribution even though smaller amplitude changes are often not easily recognizable as world-wide events. Figure 5.5b are histograms of yes (including doubtful events) and no events plotted against the average amplitudes at the three stations. Above 30 gammas there is only one no event; clearly, there is a tendency for larger amplitudes to be associated with yes events.

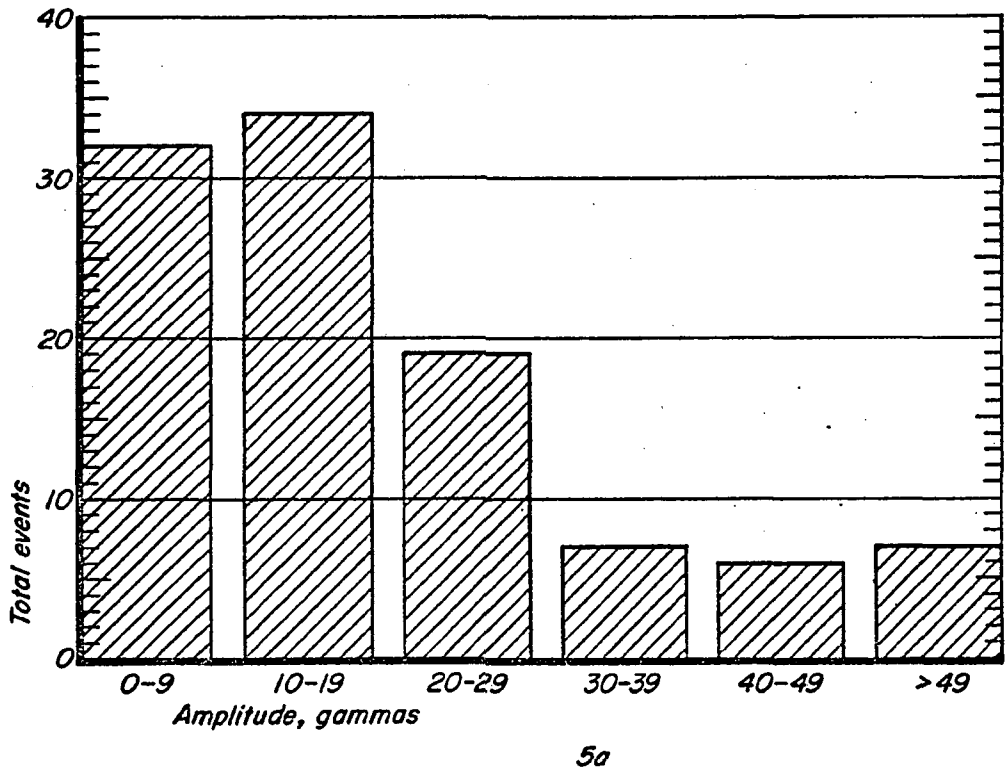

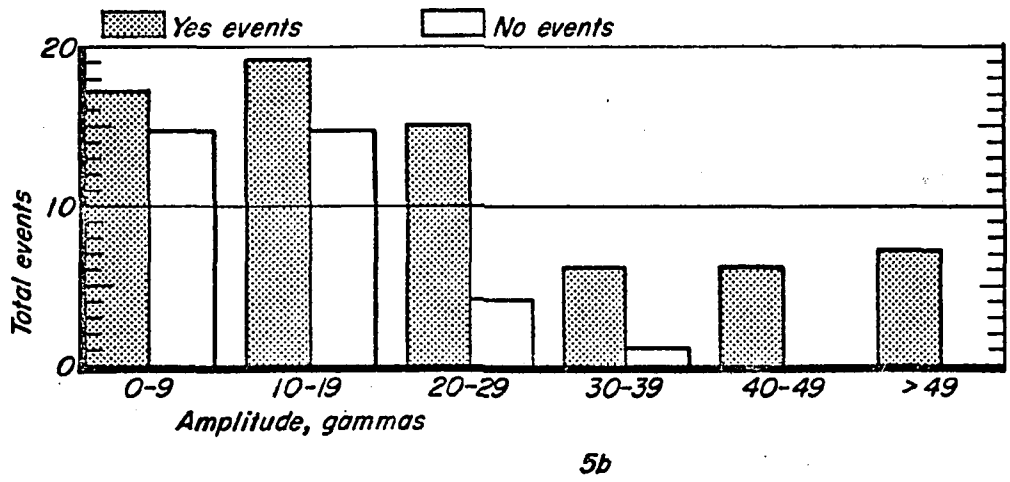

Fig. 5.5. a) Distribution of events versus amplitude intervals in gammas.
b) Distribution of simultaneous (Y) and non-simultaneous (N) event versus amplitude intervals in gammas.

After the work of this section was completed, a paper by Schieldge and Siscoe (1970) came to the attention of this writer. They reported that the probability for simultaneous sudden compressions of the magnetosphere and negative bays to occur is larger for larger compression amplitudes. This result is in substantial agreement with the result presented here. They also state that the probability of a yes event to occur is independent of Kp. Although it is not specifically stated, it appears that they have compared the distribution of yes events and total events against the Kp of the three-hourly periods which contain the events. Thus, the result presented here, that the state of the magnetosphere prior to the onset of an ssc, as implied by the Kp indices, does not make the occurrence of simultaneous events more probable, is a new one.

5.4 INTERPLANETARY DISCONTINUITIES AND THE OCCURRENCE OF SIMULTANEOUS EVENTS

The almost simultaneous occurrence of magnetospheric substorms at the time of some ssc's strongly suggests that some interplanetary discontinuities possess necessary and sufficient parameters for generating magnetospheric substorms. An accurate determination of the types of discontinuities and of the variables associated with them is essential for studying the relatonship between the solar wind changes and their subsequent effects on the magnetosphere. Through relatively complete magnetic measurements in the solar wind, evidence has been obtained for the existence of several different types of the magnetohydrodynamic discontinuities. Unfortunately, there is no comparable set of data of the density, temperature and velocity of the solar wind for the time scale and accuracy required to definitely identify all the types of

discontinuities thought to exist (Burlaga, 1970). In this section, a study of some satellite observations of discontinuities and their relationship to magnetospheric substorms is presented. The results can be re-examined when more accurate measurements of the solar wind plasma parameters adjacent to discontinuities become available.

On the basis of IMP 3 data, Taylor (1969) has examined 36 interplanetary discontinuities which produced ssc's; he has identified 26 of these as interplanetary shocks. For these ssc's, the simultaneous occurrences of substorms along auroral zone stations have been examined. Ten were clearly accompanied by negative bays; six of the ten were shocks associated with polar substorms, as well as ssc's. Figures 5.6, 5.7 and 5.8 show such examples. The ssc's on July 27, 1966 (Figure 5.6) and on September 3, 1966 (Figure 5.7) were caused by interplanetary shock waves, but the ssc on July 7, 1965 (Figure 5.8) was caused by a different type of discontinuity,

Since the solar wind parameters were not available, only the direction of interplanetary electric currents have been examined in the present work. Some interplanetary discontinuities may be considered to be produced by electric current sheets, if curl $\underline{B} \neq 0$ across the discontinuities (Siscoe et al., 1968; Burlaga and Ness, 1968). The current vector in the current sheet is related to changes of $\underline{B}$ across the sheet by

$$(\underline{B}_2 - \underline{B}_1) \times \hat{n} = \mu_o \underline{I}$$

where $\underline{B}_1$ and $\underline{B}_2$ are total vector fields measured in the region in front of and in back of the discontinuity, respectively, $\hat{n}$ is a unit normal to

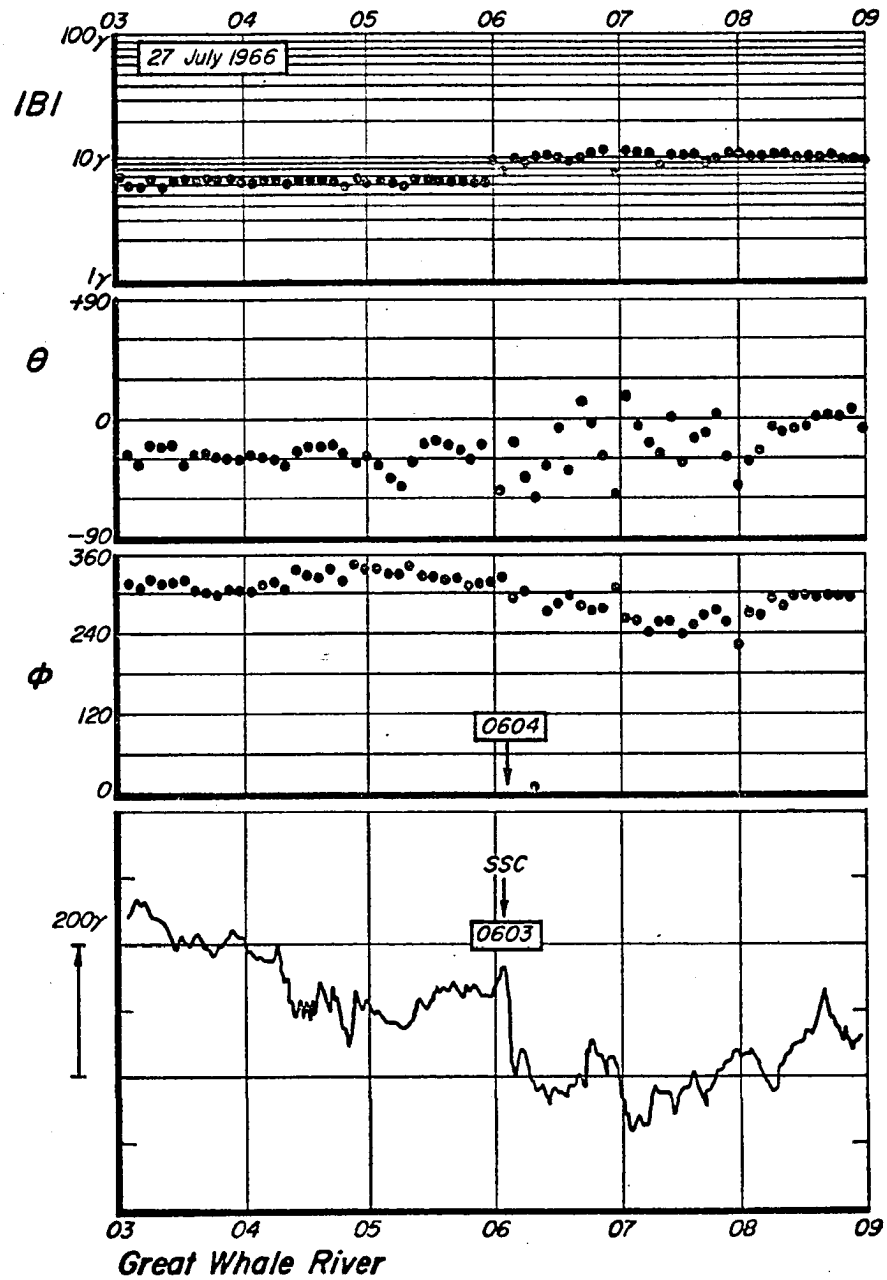

Fig. 5.6. Polar magnetic substorm observed in Great Whale River which began simultaneously to an ssc at 0603 UT, July 27, 1967. Satellite data (top three traces) indicates the discontinuity was a shock.

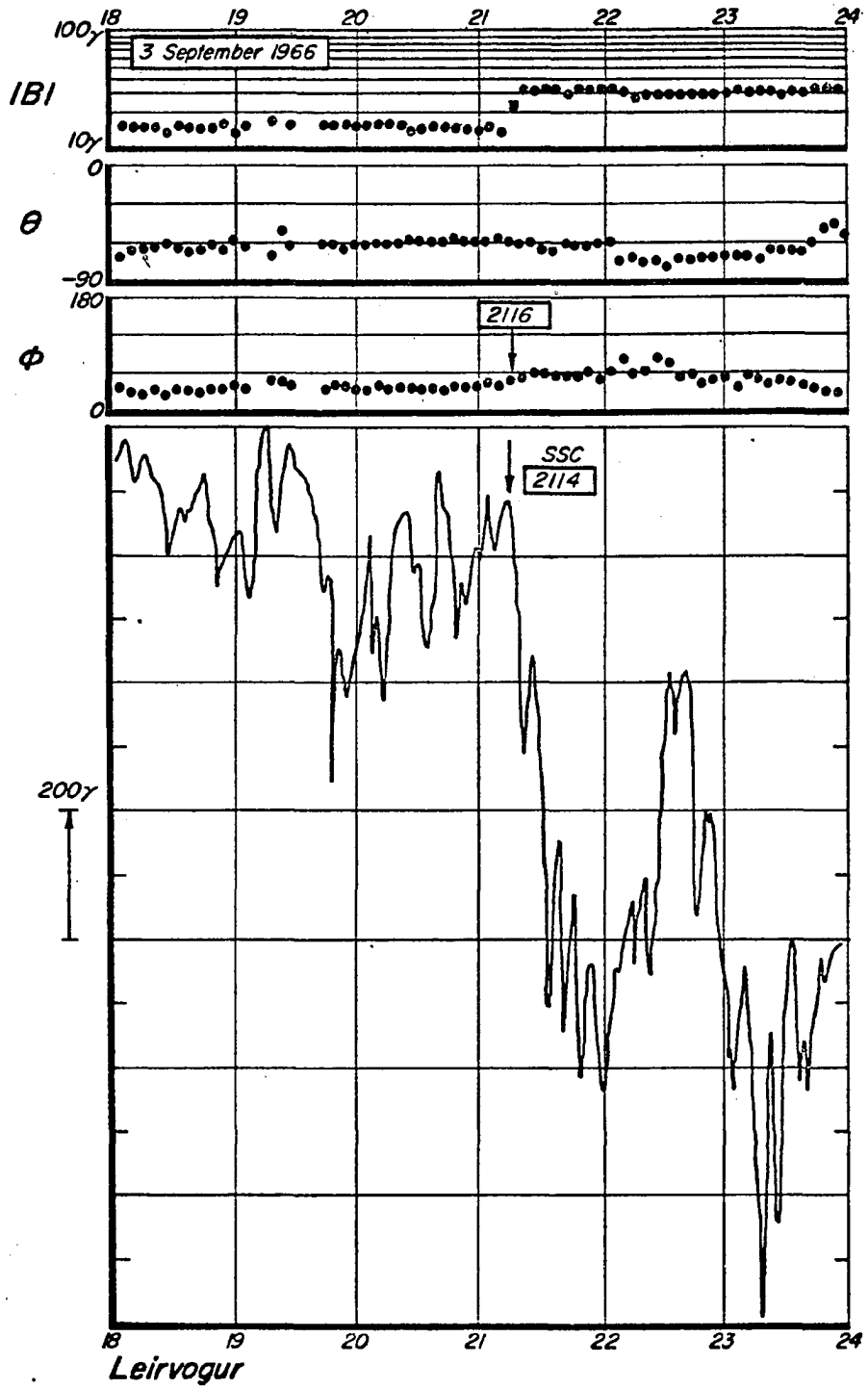

Fig. 5.7. Polar magnetic substorm observed at Leirvogur which began simultaneously to an ssc at 2114 UT, September 3, 1966. Satellite data indicates the discontinuity was a shock.

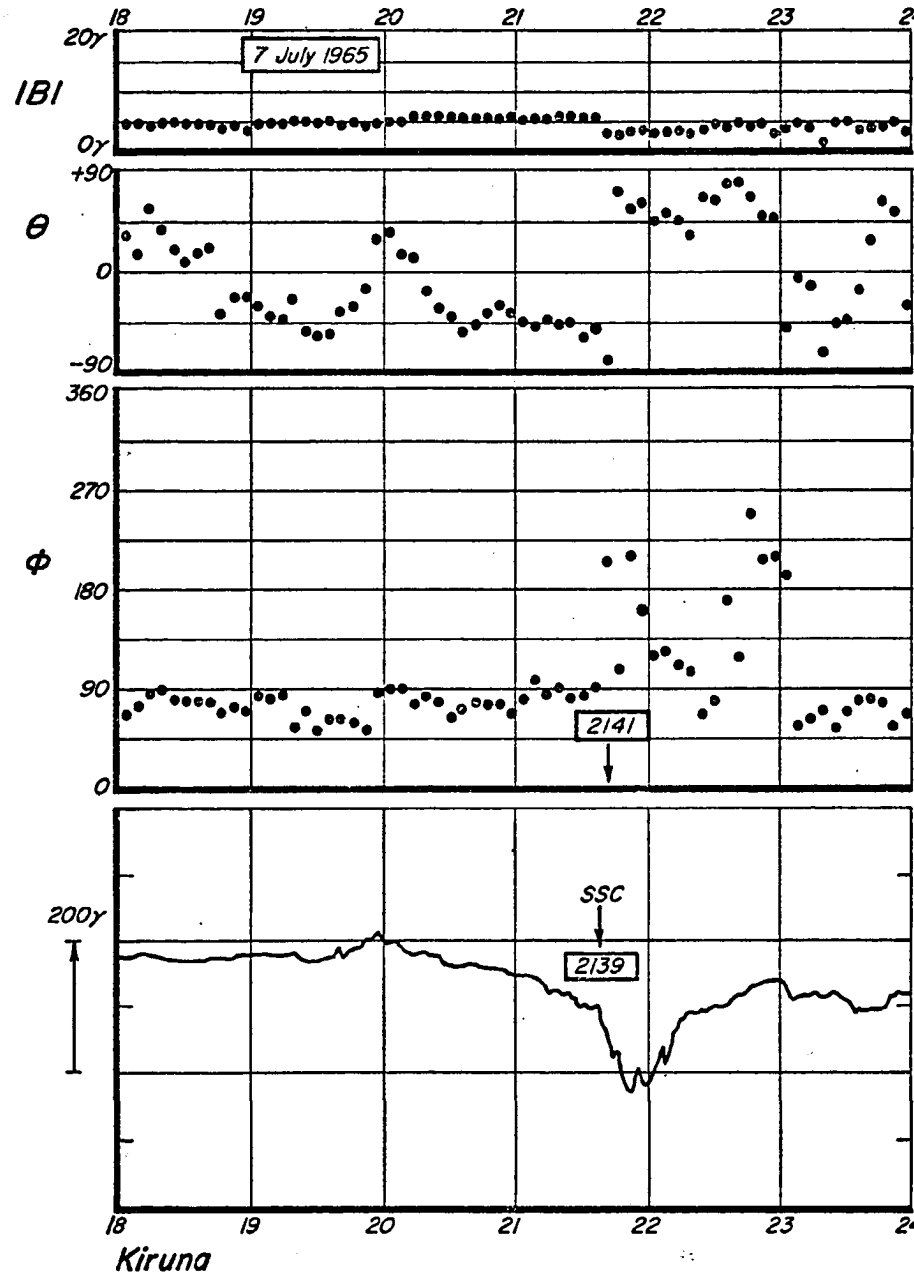

Fig. 5.8. Polar magnetic substorm observed at Kiruna which began simultaneously to an ssc at 2139 UT, July 7, 1965. Satellite data indicates the discontinuity was not a shock.

the discontinuity pointing into region 1, and $\underline{I}$ is the vector sheet current density (amp/meter) in the discontinuity.

Table 5.2 lists the three components of the current vectors in the discontinuities, calculated on the basis of Taylor's Table 1. The current vectors are given in the geocentric solar eliptic coordinate system (the x coordinate points toward the sun, z toward the north ecliptic pole, and y toward the dusk meridian). Table 5.2 also shows whether the event was simultaneous (Y) or not (N).

It should be noted that a positive y component of the current is responsible for a $\Delta\underline{B} = (\underline{B}_2 - \underline{B}_1) < 0$ and that the magnetotail current in the plasma sheet also flows in the positive y direction. It can be seen in Table 5.2 that only two cases out of ten substorm-associated discontinuities were associated with a positive y component of interplanetary current.

The occurrences of substorms have also been examined for nine interplanetary shock waves which were identified on the basis of Vela satellite data (A. J. Hundhausen, private communication, 1971). Only three of these shocks were associated with substorms, so that a sudden compression of the magnetosphere is apparently not the necessary and sufficient condition for the occurrence of substorms. Further,none of six tangential discontinuities examined in detail by Burlaga and Ness (1969) were associated with substorms.

However, it is obviously not possible to make a conclusive study of the relationships between interplanetary discontinuities and substorms from such a limited amount of interplanetary data. It

TABLE 5.2

Number*	Date	I ($\times 10^{-3}$ amp/m) I_x	I_y	I_z	Simultaneous Event (Y or N)
2	6/17/65	2.80	-1.98	1.45	Y
3	7/6/65	-8.95	-6.09	-0.49	Y
4	7/7/65	-5.23	-2.46	-2.10	Y
12	10/7/65	2.91	4.33	-1.39	N
20**	7/8/66	-1.56	-0.33	-5.28	Y
22	7/27/66	1.53	2.72	-1.46	Y
24	8/29/66	2.65	-1.27	-4.89	N
25	8/30/66	-1.10	-0.69	-0.76	Y
26	9/3/66	5.70	11.15	7.00	Y
28	9/19/66	-5.46	-3.18	-1.35	Y
29	9/23/66	-1.72	-1.61	3.26	N
31	10/15/66	-3.63	1.35	-1.62	N
35**	1/7/67	-3.94	-1.55	2.10	Y
36	1/13/67	-4.91	-2.26	-4.56	Y

*Events are listed according to Taylor's original numbering scheme (Taylor, 1969).

**The correct value for B_{2y} is -16.9; ***The correct value for B_{2x} is -6.2 (Taylor, private communication, 1971). Besides the ten substorm-associated discontinuities, four additional discontinuities not associated with substorms are listed for the purpose of comparison.

is urged, in this connection, that an extensive list of interplanetary discontinuities be compiled and made available in the future for further study along this line.

5.5 SUMMARY AND DISCUSSION

During the 18 months of the IGY (see Table 5.1) there occurred 108 storm sudden commencements which are listed in the IAGA Bulletin. Approximately 49% of these were associated with simultaneous polar magnetic substorms of magnitude 50 gammas or greater. Comparable data for the IQSY period were 72 ssc's, of which less than 3% were simultaneous with polar substorms.

Schieldge and Siscoe (1970), in a similar analysis of IGY data, obtained a value of only 18.7% for the percentage of simultaneous events. This is in part due to the higher threshold (200 gammas) which they used as a lower limit for the identification of a negative bay, and also in part due to the inclusion of si's in their analysis.

In agreement with Schieldge and Siscoe (1970), it has been found that larger amplitude, sudden compressions of the magnetosphere have a greater tendency to produce simultaneously occurring polar magnetic substorms.

Within the large statistical uncertainty of the limited number of events available for study, it has been shown in Section 5.3 that the pre-existing state of the magnetosphere does not affect the probability of the occurrence of simultaneous ssc and polar magnetic substorms. This suggests that the mechanism which produces a simultaneous event is either contained within the discontinuity (or in a limited region behind it) or related to some parameter of the magnetosphere which has little

or no effect on the Kp indices.

The limited number of discontinuities and polar magnetic substorms studied in Section 5.4 excludes any statistically valid conclusions based on this work. It is interesting to note, however, that only two of the simultaneous events were associated with discontinuity current flowing in the positive y-direction, that is, associated with discontinuities which produce a decreased northward or an increased southward-directed component of the field behind the discontinuity. This does not agree with the statistically derived result that the interplanetary field, changing to a southward orientation, tends to produce geomagnetic activity. The explanation for this discrepancy must await more exact and numerous interplanetary observations of the plasma and magnetic parameters of the discontinuities in the solar wind.

CHAPTER VI

MODEL CALCULATIONS OF THE QUIET AND DISTURBED MAGNETOSPHERE

6.1 INTRODUCTION

The quiet-time state of the magnetic field at the surface of the earth with regard to non-ionospheric sources has been discussed in Chapter II. Aspects of the disturbed state of the magnetosphere have been covered in Chapters III, IV and V. In this chapter, two, three-dimensional, magnetospheric current system models are presented which can reproduce the observed changes occurring at a particular instant during a geomagnetic storm.

The first model consists of a ring current, field-aligned currents and auroral electrojet currents. The second model includes the boundary currents and the tail current, but not field-aligned and auroral electrojet currents. The parameters in this model can be varied so as to represent the 'quiet' state of the magnetosphere, and also the disturbed magnetosphere during quasi-steady periods when polar magnetic substorms are absent such as during the recovery phase. Observations of the current and particle parameters in the tail and ring current regions have been briefly discussed in Chapters III and IV.

6.2 THE COMPUTED DISTRIBUTION OF GEOMAGNETIC DISTURBANCE VECTORS OF A SIMPLE, THREE-DIMENSIONAL CURRENT SYSTEM MODEL

6.2.1. Introduction

The model presented here consists of an asymmetric ring current belt, current along the field lines from the pre-dawn quadrant of the ring current to the northern and southern auroral ionsopheres, ionospheric current along the auroral ovals (the auroral electrojets), and

current along the field lines from the pre-midnight quadrant of the auroral electrojets back to the ring current. This model is based on the work of Kirkpatrick (1952). The basic current distribution was schematically shown by Akasofu (1969) and Meng and Akasofu (1969).

Computations of the surface disturbance field for particular functions of the various currents of this model have been presented by Akasofu (1970) and for a similar model by Bonnevier, Boström and Rostoker (1970). The present study is based on the work of Akasofu (1970), but here Kirchoff's laws are applied for the complete circuit (that is, div $\underline{j} = 0$). Some preliminary results have already been presented (Kawasaki and Akasofu, 1971).

The model is intended to represent the main features of the disturbance field both at the ground and in space. It is an equivalent current system, but one which conforms more realistically to recent observations of the ring and field-aligned currents.

6.2.2. The model

The dependence of the currents of the basic model on local time is tablulated below as Model A. Model B contains a constant, eastward flowing ring current all around the earth. When this eastward current is superposed on the westward flowing ring current (which has the same dependence on local time as Model A), the resulting current is westward in the day sector and portions of the dusk and dawn sectors, but eastward in the midnight sector of the ring current belt. This net eastward flowing current in the dark sector is intended to represent the removal of the diamagnetic effect of ring current particles, which has been observed in that sector during magnetospheric substorms by the

ATS-I satellite (Cummings, Barfield and Coleman, 1968).

The expressions for the currents as functions of the longitudinal angle ϕ measured positive eastward from the 06 hour meridian are:

MODEL A

Field-Aligned current/radian	$I = 0,$	$0 \leq \phi \leq \pi$
	$I = I_o \sin 2\phi,$	$\pi \leq \phi \leq 2\pi$
Electrojet	$I = 0,$	$0 \leq \phi \leq \pi$
	$I = -I_o \sin^2\phi,$	$\pi \leq \phi \leq 2\pi$
Ring Current	$I = -2I_o,$	$0 \leq \phi \leq \pi$
	$I = -2I_o \cos^2\phi,$	$\pi \leq \phi \leq 2\pi$

MODEL B

Field-aligned current/radian	$I = 0,$	$0 \leq \phi \leq \pi$
	$I = I_o \sin 2\phi,$	$\pi \leq \phi \leq 2\pi$
Electrojet	$I = 0,$	$0 \leq \phi \leq \pi$
	$I = -I_o \sin^2\phi,$	$\pi \leq \phi \leq 2\pi$
Ring Current	$I = -2I_o + I_o,$	$0 \leq \phi \leq \pi$
	$I = -2I_o \cos^2\phi + I_o,$	$\pi \leq \phi \leq 2\pi$.

I_o is taken to be 10^6 amperes. The field-aligned current flows along the field lines which cross the equatorial plane at a geocentric distance of $r_e = 6.55$ earth radii. Thus, the auroral electrojets are located at latitudes of $\theta = \pm 66.81°$ in the auroral ionosphere taken to be at an altitude of 100 km.

The combined effects of the three parts of the current system have been numerically calculated. The results are presented in 6.2.3 and 6.2.4. A complete listing of the program for model B appears in

Appendix 2.

6.2.3. Distribution of disturbance vectors on the surface of the earth

Figure 6.1 shows a polar plot of the resultant disturbance vectors for model A on the northern hemisphere of the earth. Note the differences in scale between the 0-60° and 60-90° dp lat regions. The vectors pointing away from the pole represent southward (i.e., a decrease in the H-component) directed field. There is only a small southward directed component of the disturbance field at low latitudes in the midnight sector.

The model A surface disturbance vectors should be compared with those of model B, Figure 6.2. There, the addition of the eastward directed current has reversed the field at low latitudes in the midnight sector to the north. The field is still southward (or negative) over much of the low latitude regions of the earth, but it is somewhat smaller in magnitude. The magnitudes of the 'dayside' and 'nightside' disturbance vectors are now approximately equal. At high latitudes the effects of the eastward current are negligible because of the dominance of the intense and relatively nearby auroral electrojet.

As has been mentioned in Section 3.6(f), at low and middle latitudes there can exist both positive and negative departures of the geomagnetic field of relatively short duration (1-3 hours) from the mean or Dst value during a geomagnetic storm. Qualitatively, at least, the disturbance vectors of model B simulate such changes. However, these changes occur while Dst is usually much below zero, and hence, a net southward component of the storm fields is required in

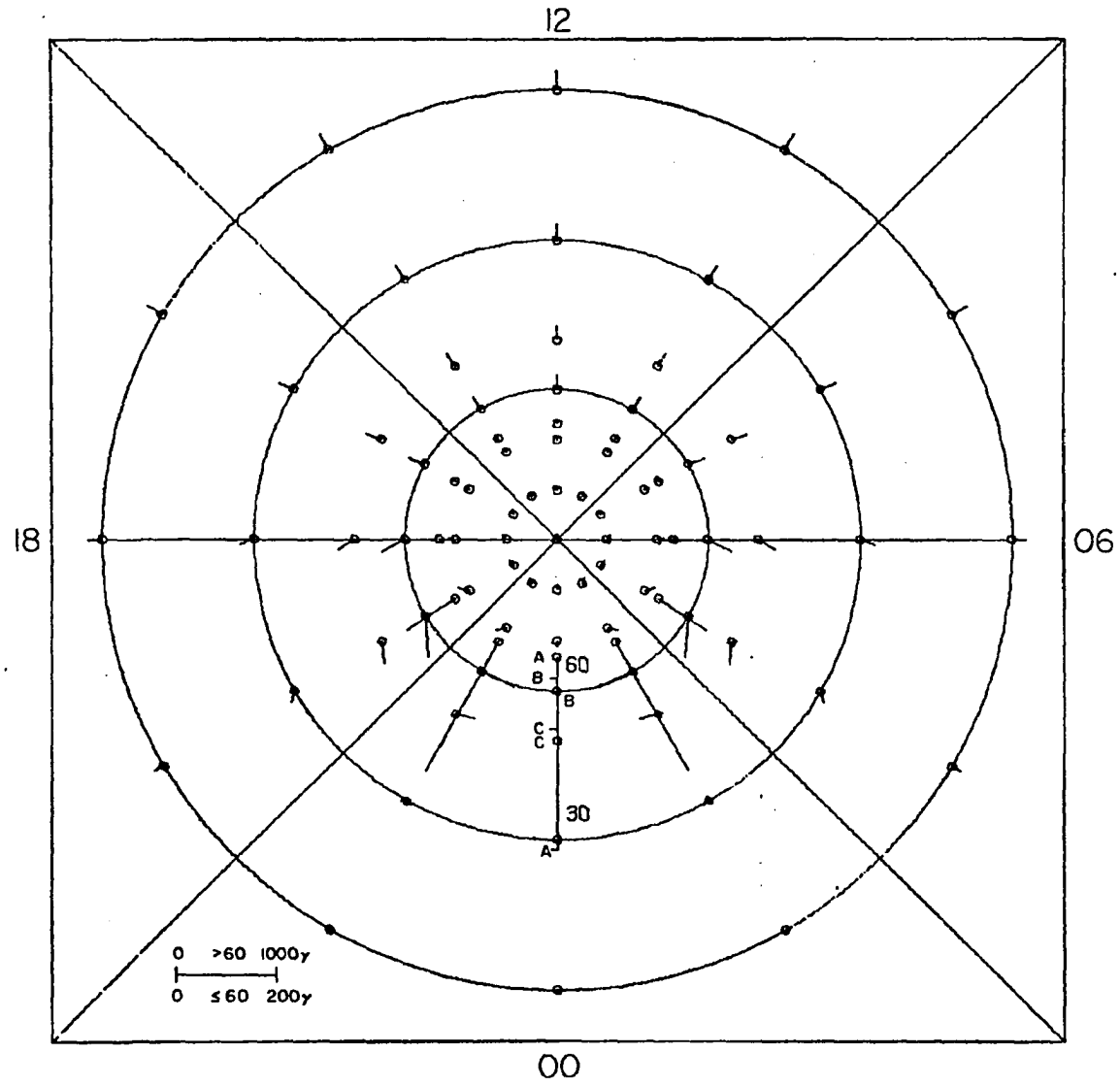

Fig. 6.1. Polar plot of horizontal disturbance vectors of a simple, three-dimensional current model: Model A.

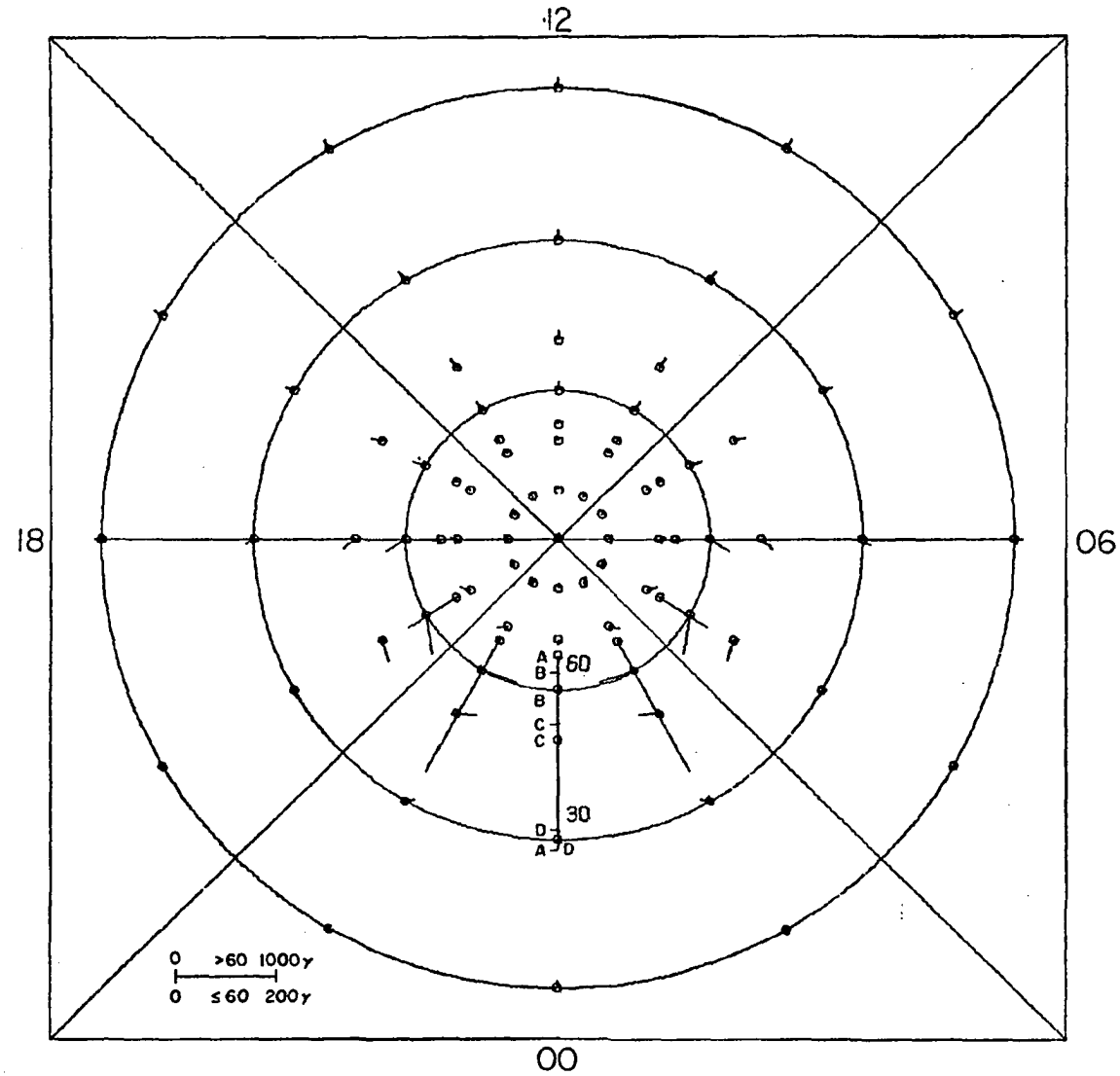

Fig. 6.2. Polar plot of horizontal disturbance vectors of simple, three-dimensional current model: Model B. *There is a net <u>eastward</u> ring current in the midnight sector.*

the vicinity of the earth. The tail current field and/or a more substantial westward ring current field could produce the necessary negative Dst component. It should be noted, in this regard, that the disturbance vectors of model A can also qualitatively reproduce the observed changes if a larger southward directed field is superposed on the disturbance vector model. Both models A and B can produce relative changes which are similar to the sometimes observed features of the DS component of a geomagnetic storm field, namely, a positive pulse in the night sector and a negative one in the day sector.

The H and D components at the surface of the earth for model B are plotted separately in Figures 6.3, 6.4, and 6.5 as functions of local time for several latitudes. These show more clearly the H-component disturbance vector field. It can be seen from Figure 6.3 that the H-component of the disturbance vectors have a very similar dependence on longitude (time) at all latitudes from 0° to 50° dp lat. Above 50°, the disturbance vectors are strongly influenced by the auroral electrojet.

Both the H and D component vectors at low and middle latitudes (Figures 6.3 and 6.4) agree fairly well with those obtained by Silsbee and Vestine (1942), Akasofu and Meng (1969) and Meng and Akasofu (1969), who analyzed records of geomagnetic 'bay' disturbances. At higher latitudes, however, the agreement is not very good.

Models A and B are intended to represent the disturbance field on the earth at a particular instant during a 'bay' (magnetic substorm). Since a magnetic substorm may last from 1 to 3 hours, it might be

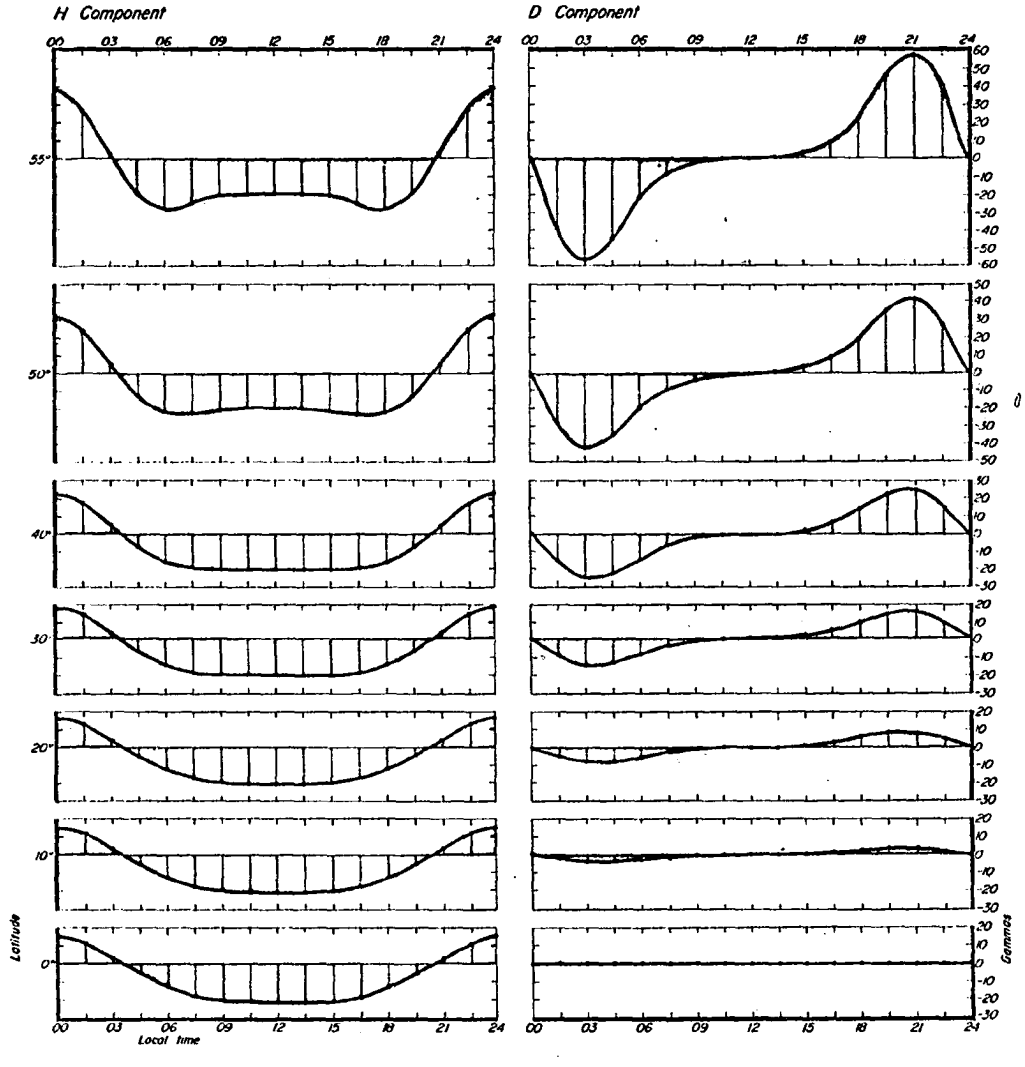

Fig. 6.3. H and D component disturbance vectors of model B in 0^{o}-55^{o} latitude range on surface of earth plotted as a function of local time (longitude).

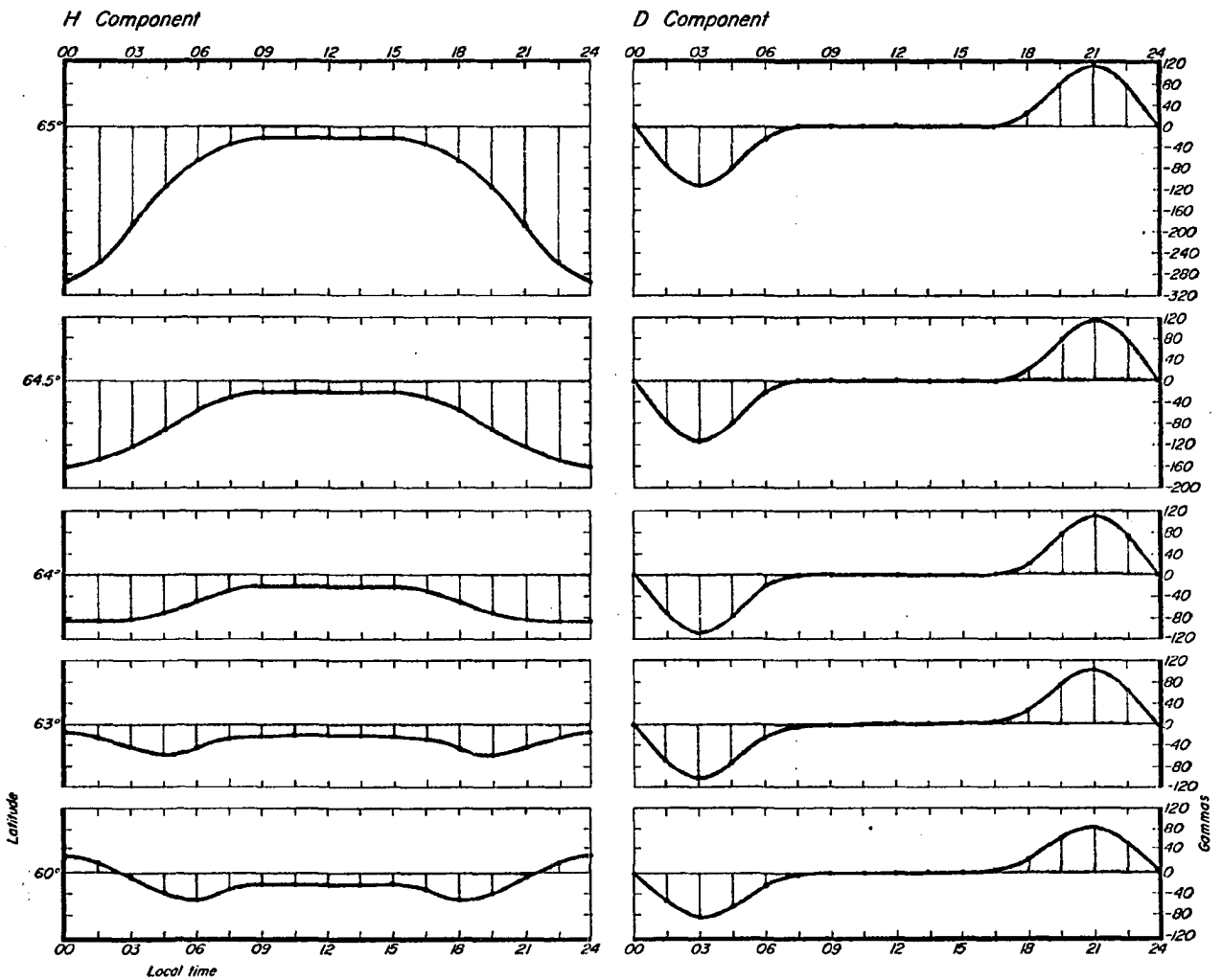

Fig. 6.4. H and D component disturbance vectors of model B in 60°-65° latitude range on surface of earth plotted as a function of local time (longitude).

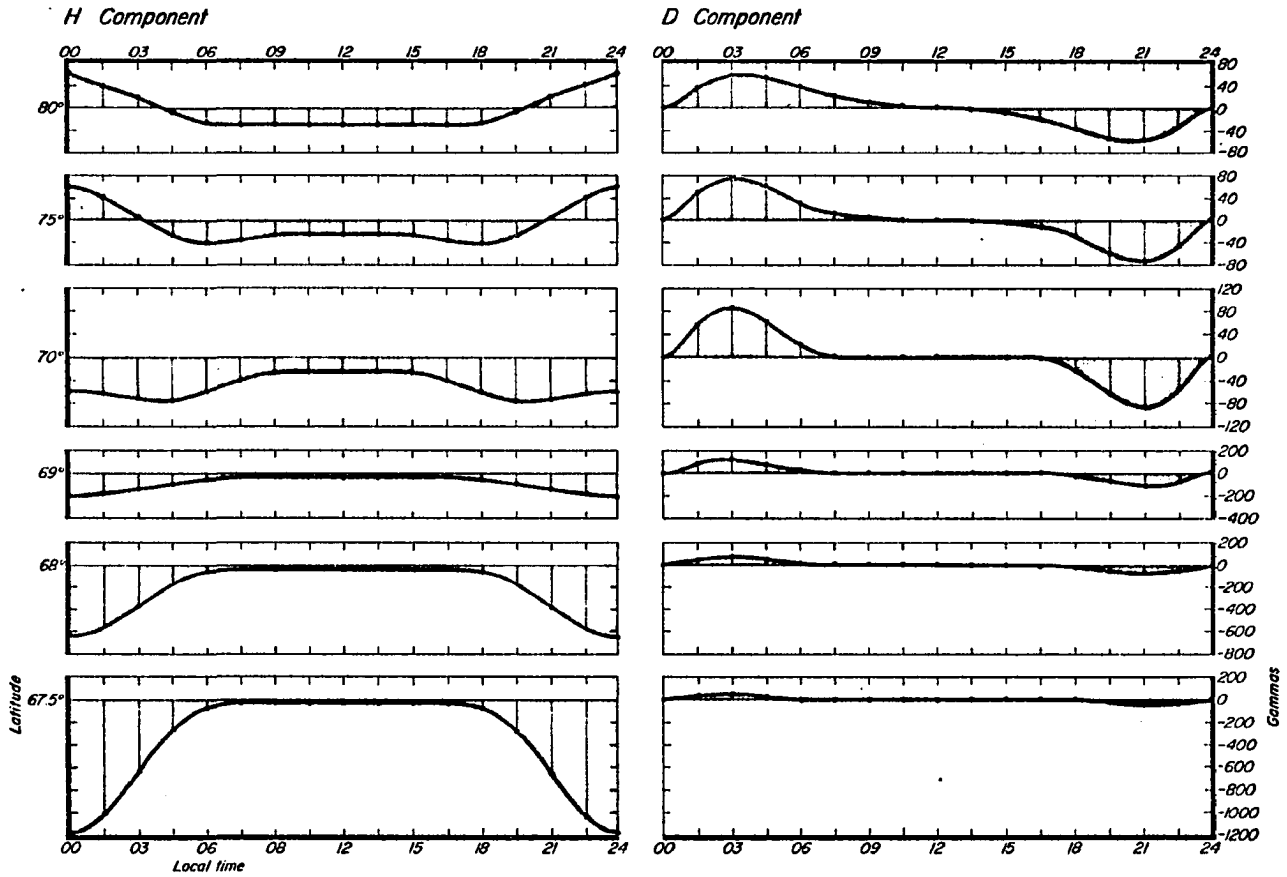

Fig. 6.5. H and D component disturbance vectors of model B in 67.5°-80° latitude range on surface of earth plotted as a function of local time (longitude). Note scale change between 69° and 70°.

expected that a station at low latitudes occasionally traverses a region of field reversal. Specifically, Figure 6.3 shows that if a low latitude station is located at about 03 hours local time when a substorm occurs, a positive field is observed; two hours later, if the substorm is still in progress, the field is negative with respect to the Dst value. Examples of such changes may be best seen in Figure 3.4b between 06 and 08 UT April 17, 1965, and between 14 and 16 UT April 18, 1965.

For a more accurate comparison between the observed and computed distribution of disturbance vectors, the effects of induction currents must be taken into account (Ashour, 1971). However, for the time-rate change of the primary inducing field involved, induction currents cannot seriously alter the gross features of the disturbance field at low and middle latitudes..

6.2.4. Magnitude of disturbance vectors adjacent to the field-aligned sheet current

The magnitudes of the H, D and Z components of the disturbance field produced by model B at points adjacent to the field-aligned current sheets have also been computed. Figure 6.6 shows the disturbance vectors for H, D and Z in the northern magnetosphere at various local times and longitudes along field lines passing through the equatorial plane at $r_e = 5.55\ R_E$. The field-aligned sheet currents flow on the surface generated by the field lines passing through the equatorial plane at $r_e = 6.55\ R_E$. The disturbance vectors have also been computed along field lines external ($r_e = 7.55\ R_E$) to the field-aligned sheet current; these are shown in Figure 6.7.

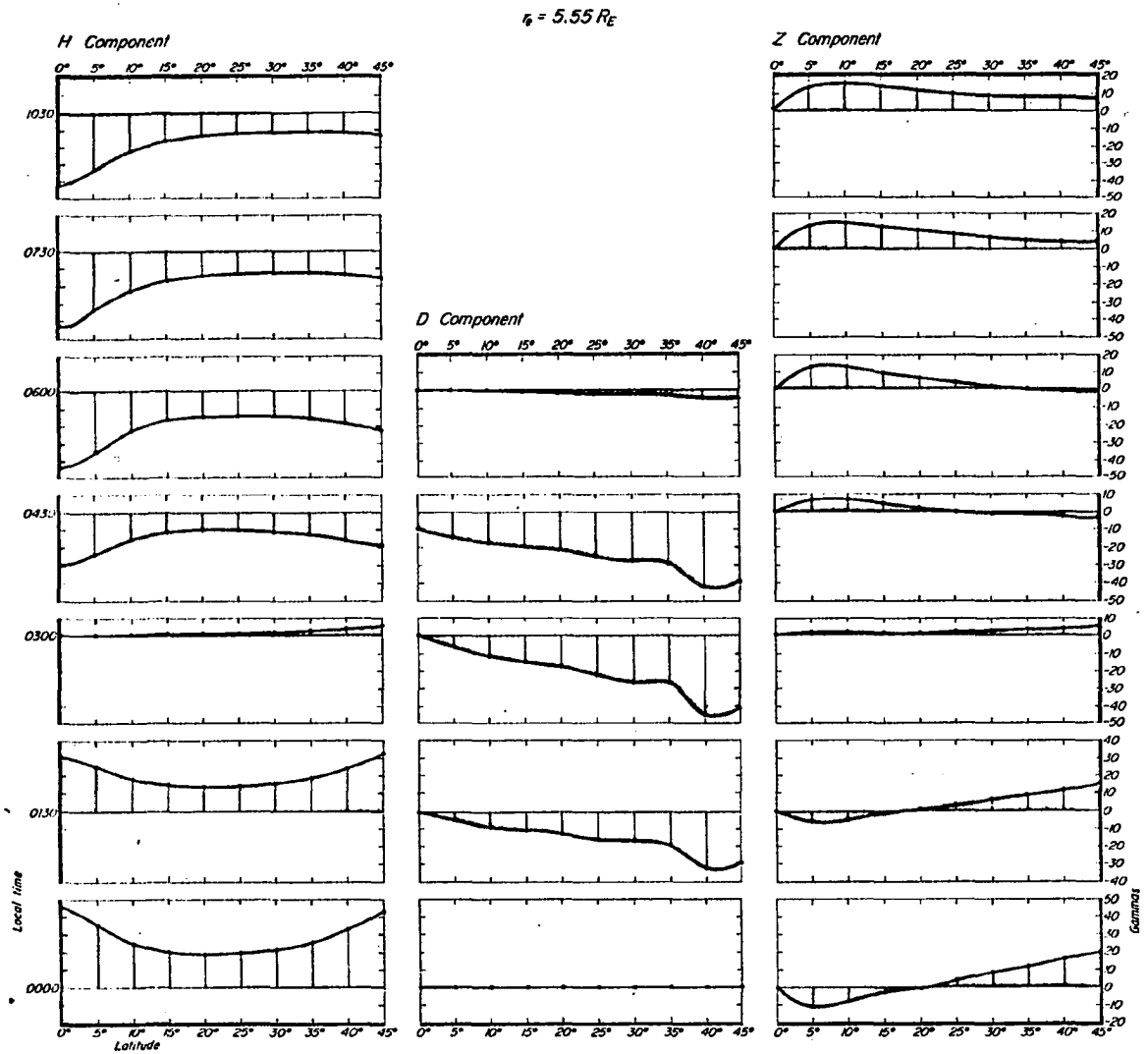

Fig. 6.6. Plot of H, D and Z component disturbance vectors of model B in magnetosphere at various selected latitudes and local times (longitudes) along interior field lines passing through $r_e = 5.55\ R_e$.

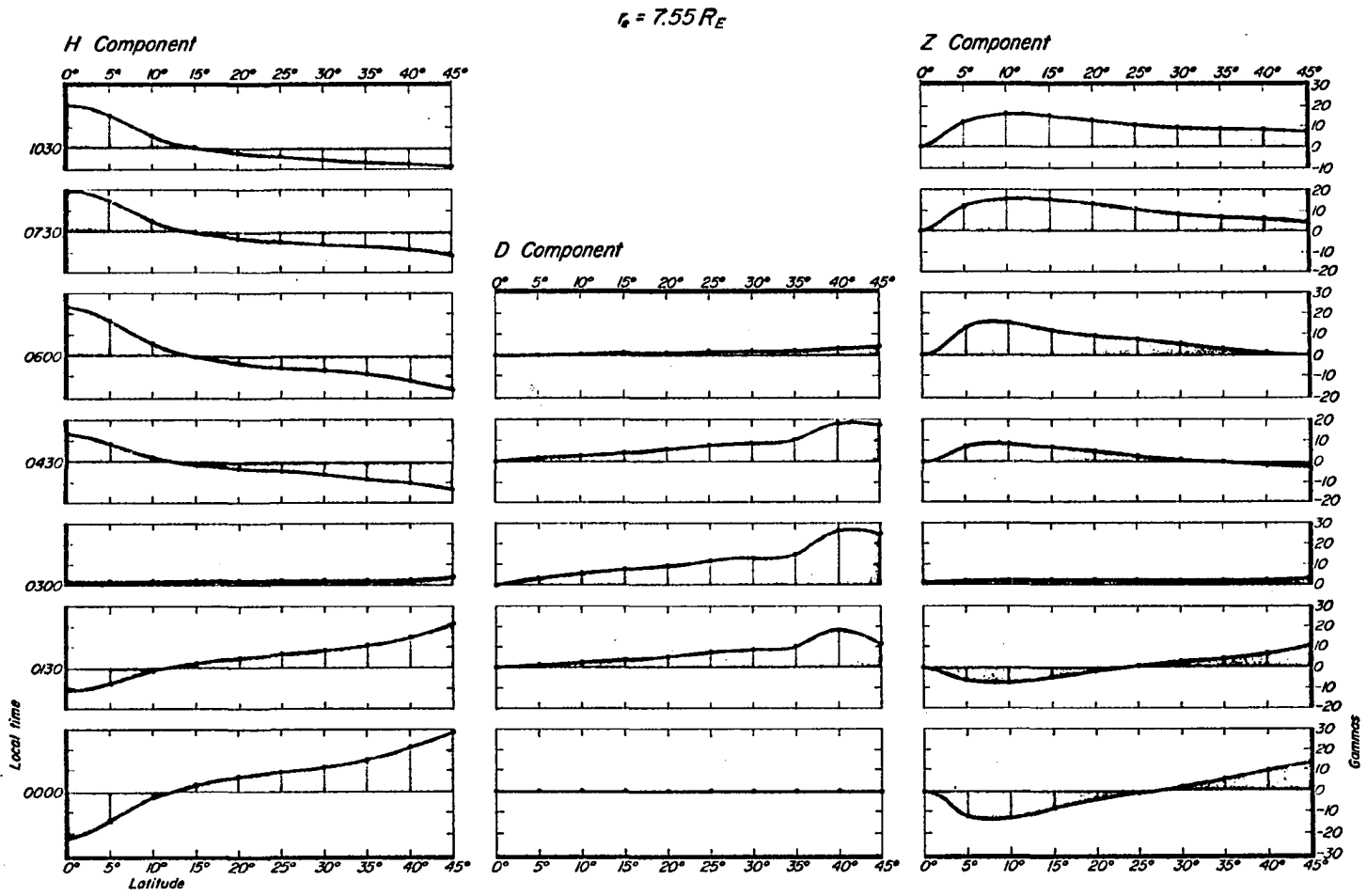

Fig. 6.7. Plot of H, D and Z component disturbance vectors of model B at various selected latitudes and local times (longitudes) along exterior field lines passing through $r_e = 7.55\ R_e$.

It should be noted that all three of the primary currents of the model will in general contribute to each component (H, D and Z) since the current intensities are taken as functions of local time. However, it is seen in Figures 6.6 and 6.7 that the D component in the early morning sector is westward on the interior field lines (the r_e = 5.55 R_E field lines) and eastward on the exterior lines (the r_e = 7.55 R_E field lines), which indicates that the field-aligned currents dominate there over the contributions from the asymmetric ring and the auroral electrojet currents. In the evening sector, the D-component will be eastward interior and westward exterior to the field-aligned currents.

The change in the H and Z component directions (Figures 6.6 and 6.7) at the 03 hour local time meridian is due to the change from a net eastward flow in the 00 to 03 hours local time meridian of the ring current to a net westward flow from 03 to 06 hours.

It is evident from these figures that the field distribution in space of even the simple model presented here is not easy to visualize since the integrated effects of distant portions of the circuit must be taken into account. However, the model may provide a basis for a study of the actual field during polar substorms should satellite data become available. Field-aligned current will be discussed more fully in 6.3.4.

6.3 THE COMBINED FIELDS OF THE GEOMAGNETIC DIPOLE, BOUNDARY CURRENTS, RING CURRENT, AND MAGNETOTAIL CURRENT

6.3.1. Introduction

In Section 6.2, a simple model which reproduces the major

features of the disturbance field at low and middle latitudes during polar magnetic substorms has been presented. The purpose of this section is to present a more sophisticated model which takes into account the effects of the boundary and tail currents, as well as the ring current. Some preliminary results of the model have been given in Chapter IV. The model can also be used to represent the state of the quiet magnetosphere.

The model consists of a symmetric ring current, a tail sheet current flowing from the dawn to dusk portion of the magnetotail (completed by cylindrical sheet currents from dusk to dawn), and boundary currents, whose effects are approximately simulated by a large dipole interacting with the earth's dipole field.

6.3.2. Equations of the individual fields

6.3.2.1. Ring current

The distribution of the field of a symmetric ring current has been calculated using the model of Akasofu (1966). This model consists of mono-energetic particles with a Gaussian distribution of number density and a simple pitch angle distribution.

The number density $n(r_e)$ at a distance r_e along a radius in the equatorial plane and the pitch angle distribution $H(\alpha,p)$ of the ring current model are assumed to have the following forms:

$$n(r_e) = n_o e^{-g^2 z^2}$$

and $$H(\alpha,p) = A(p) \sin^{p+1}\alpha$$

respectively, where $z = (r_e - r_{eo})/R_e$, r_{eo} denotes the equatorial distance at which n attains its maximum value n_o, R_e denotes the earth's radius,

α is the pitch angle, p is a constant, and A(p) is a normalizing factor. The factor g is a measure of the radial extent of the ring current belt and we take $g = g_1$ for $z < 0$ (inner part of the belt) and $g = g_2$ for $z > 0$ (outer part of the belt). Thus the number density distribution can be independently varied on either side of the peak of the distribution by choosing different values of g on either side. Parker (1957) has shown that if the pitch angle distribution $H(\alpha,p)$ on the equatorial plane is of the form shown above, the distribution has this same functional relationship all along a field line. The current is also proportional to the pressure of the gas formed by the particles and, hence, to the energy ε.

In a steady distribution of particles symmetric about a dipole field, a current vector may be obtained at each point along a field line from the values of the currents in the equatorial plane (see Akasofu and Chapman, 1961 and Akasofu, 1966 for details). The magnetic field may then be calculated from the current.

Thus, the ring current magnetic field at a particular point r_1 from the earth and at a latitude θ_1 has the functional relationship:

$$\underline{\Delta B} = \underline{\Delta B}(r_1, \theta_1; r_{eo}, g_1, g_2, p, n_o, \varepsilon)$$

The procedure used in the computation is to first calculate the current $I(r,\theta)$ from the assumed number density $n(r_e)$ and pitch-angle distribution, and then numerically calculate the field $\underline{\Delta B}$ at a point r_1 and latitude θ, from each element of current in the ring current belt.

The equations developed by Akasofu and Chapman (1961) and Akasofu

(1966) give the values of ΔB_x and ΔB_z, which are the magnetic field components in a magnetic meridian plane perpendicular (positive northward) and parallel (positive outward from the earth) to the equatorial plane. In a coordinate system centered in the earth with the positive x-coordinate northward parallel to the spin axis, the z-axis aligned parallel to the sun-earth line and positive in the nightside, and the y-axis positive toward the dusk meridian, the field components at a point (x, y, z) can be obtained from:

$$B_{rx} = \Delta B_{x'}$$

$$B_{ry} = \frac{y}{\sqrt{y^2+z^2}} \Delta B_{z'}$$

$$B_{rz} = \frac{z}{\sqrt{y^2+z^2}} \Delta B_{z'}$$

6.3.2.2. Boundary currents

The effects of boundary currents can be approximated by an image dipole of the earth's dipole (Hones, 1963). The magnetic scalar potential V due to the two parallel but unequal dipoles placed a distance d apart is given by:

$$V = -M\left\{\frac{x}{(x^2+y^2+z^2)^{3/2}} + \frac{nx}{(x^2+y^2+z^2+2dz+d^2)^{3/2}}\right\}$$

Here M is the dipole moment of the earth and n is the ratio of the dipole moment of the large dipole to the earth's dipole. The center of the earth is the center of the coordinate system with the x-axis coincident to the spin axis of the earth positive northward, z positive

toward the nightside along the sun-earth line, and y positive toward the dusk meridian. The image dipole moment is taken to be parallel to the earth's dipole moment and anti-parallel to the x-axis. The plane containing both dipoles is the z-y plane.

The components of the total magnetic field at an observation point (x,y,z) due to the dipoles are:

$$B_{bx} = -\frac{\partial V}{\partial x} = M\left\{\frac{y^2+z^2-2x^2}{(x^2+y^2+z^2)^{5/2}} + \frac{n(y^2-2x^2+z^2+2dz+d^2)}{(x^2+y^2+z^2+2dz+d^2)^{5/2}}\right\}$$

$$B_{by} = -\frac{\partial V}{\partial y} = -3M\left\{\frac{xy}{(x^2+y^2+z^2)^{5/2}} + \frac{nxy}{(x^2+y^2+z^2+2dz+d^2)^{5/2}}\right\}$$

$$B_{bz} = -\frac{\partial V}{\partial z} = -3M\left\{\frac{xz}{(x^2+y^2+z^2)^{5/2}} + \frac{nx(z+d)}{(x^2+y^2+z^2+2dz+d^2)^{5/2}}\right\}$$

Hones (1963) used an image dipole some 28 (=n) times as intense as the earth's dipole moment and separated by a distance of 28 R_e (=d). The resulting model gave a neutral point latitude of about 79-80°.

6.3.2.3. Magnetotail current

A simple geometry and constant current density have been chosen for the magnetotail current. The model consists of a rectangular sheet of current in the equatorial plane flowing from dawn to dusk and cylindrical sheet currents flowing from dusk to dawn. The cross-section perpendicular to the sun-earth line of the cylindrical parts of the tail current is a circle of radius ρ bisected by a cross-section of the plane sheet current in the equatorial plane.

Williams and Mead (1965) and Antonova and Shabanskiy (1968)

have obtained the configuration of the magnetosphere when a plane sheet of current is included in the magnetotail. Beard et al., (1970) included both plane sheet and cylindrical surface currents for a current varying with distance along the tail, but did not include boundary and ring currents in the model.

A solution for the magnetic field of the sheet current with constant current density analytic everywhere except at the edges of the sheet may be obtained. With the geocentric coordinates, x positive northward and parallel to the spin axis, z positive along the nightside extension of the sun-earth line and y the remaining coordinate of the right-handed system, the magnetic field due to the plane sheet of current directed in the positive y direction and located at ($x' = 0$, $-\rho' \leq y' \leq \rho'$, $z_1 \leq z' \leq z_2$) is given by:

$$\underline{B}_s = B_{so} \int_{z_1}^{z_2} \int_{-\rho'}^{\rho'} \frac{\underline{j}\, dy' \times \underline{r}\, dz'}{r^3}$$

where B_{so} is a constant which includes the constant linear current density per length of tail (I_o), the primes denote the source coordinates, and $\underline{r}$ denotes the vector from the source point (x',y',z') to the observation point (x,y,z). After integration, the following field components are obtained:

$$B_{sx} = -B_{so} \log \left[\frac{\left[\sqrt{x^2+(y-\rho')^2+(z-z_2)^2}-y+\rho'\right]}{\left[\sqrt{x^2+(y-\rho')^2+(z-z_1)^2}-y+\rho'\right]} \cdot \frac{\left[\sqrt{x^2+(y+\rho')^2+(z-z_1)^2}-y-\rho'\right]}{\left[\sqrt{x^2+(y+\rho)^2+(z-z_2)^2}-y-\rho'\right]} \right]$$

$$B_{sz} = B_{so}\left[\tan^{-1}\left(\frac{(z-z_2)(y+\rho')}{x\sqrt{x^2+(y+\rho')^2+(z-z_2)^2}}\right)\right.$$
$$-\tan^{-1}\left(\frac{(z-z_1)(y+\rho')}{x\sqrt{x^2+(y+\rho')^2+(z-z_1)^2}}\right)$$
$$-\tan^{-1}\left(\frac{(z-z_2)(y-\rho')}{x\sqrt{x^2+(y-\rho')^2+(z-z_2)^2}}\right)$$
$$\left.+\tan^{-1}\left(\frac{(z-z_1)(y-\rho')}{x\sqrt{x^2+(y-\rho')^2+(z-z_1)^2}}\right)\right]$$

It is not possible to find closed solutions for the components of the magnetic fields of the cylindrical sheet currents, since the integrals involved are of elliptic form. Here, the relevant equations are reduced to forms suitable for numerical integrations.

Unfortunately, the geometry of the cylindrical parts is such that it does not lend itself very well to calculations in a Cartesian coordinate system as has been used in the plane sheet part. Instead, the integrals will be written in a cylindrical coordinate system; after numerical integration, the components may easily be converted to Cartesian coordinates. The coordinates of the source and observation points are (ρ',ω',z') and (ρ,ω,z), respectively. ρ' is the radius of the cylinder. Again z is aligned along the sun-earth line, positive to the nightside, ρ is the radial distance from the axis of the cylinder, and ω is the angle of the radius vector $\underline{\rho}$ measured positive from the dusk half of the plane sheet of current. The components due to the northern half of the cylindrical current sheet are given by:

$$B_{cz} = -\frac{B_{so}}{2}\int_0^{\pi}\int_{z_1}^{z_2}\frac{\rho'[\rho'-\rho\cos(\omega-\omega')]\,d\omega'dz'}{[\rho^2+\rho'^2+(z-z')^2-2\rho\rho'\cos(\omega-\omega')]^{3/2}}$$

$$B_{c\omega} = \frac{B_{so}}{2}\int_0^{\pi}\int_{z_1}^{z_2}\frac{\rho'[(z-z')\sin(\omega-\omega')]\,d\omega'dz'}{[\rho^2+\rho'^2+(z-z')^2-2\rho\rho'\cos(\omega-\omega')]^{3/2}}$$

$$B_{c\rho} = -\frac{B_{so}}{2}\int_0^{\pi}\int_{z_1}^{z_2}\frac{\rho'[(z-z')\cos(\omega-\omega')]\,d\omega'dz'}{[\rho^2+\rho'^2+(z-z')^2-2\rho\rho'\cos(\omega-\omega')]^{3/2}}\ .$$

The contributions from the southern half are similar except for the change in sign of the direction of the current in the range of integration $\pi \leq \omega \leq 2\pi$. After integration over both halves of the cylinder, the result obtained for $B_{c\omega}$ is:

$$B_{c\omega} = -\frac{B_{so}}{\rho}\left[-\sqrt{\rho^2+\rho'^2+2\rho\rho'\cos\omega+(z-z_2)^2}\right.$$
$$-\sqrt{\rho^2+\rho'^2-2\rho\rho'\cos\omega+(z-z_2)^2} - \sqrt{\rho^2+\rho'^2+2\rho\rho'\cos\omega+(z-z_1)^2}$$
$$\left.+\sqrt{\rho^2+\rho'^2-2\rho\rho'\cos\omega+(z-z_1)^2}\right]$$

For the remaining components, B_{cz} and $B_{c\rho}$, the integration over z' may be carried out. Thus we have:

$$B_{cz} = -\frac{B_{so}}{2}\,\rho' \int_0^{2\omega} \frac{[\rho'-\rho\cos(\omega-\omega')]}{[\rho^2+\rho'^2-2\rho\rho'\cos(\omega-\omega')]}$$

$$\left(\frac{z-z_1}{\sqrt{\rho^2+\rho'^2-2\rho\rho'\cos(\omega-\omega')+(z-z_1)^2}} \right.$$

$$\left. - \frac{z-z_2}{\sqrt{\rho^2+\rho'^2-2\rho\rho'\cos(\omega-\omega')+(z-z_2)^2}} \right) d\omega'$$

$$-\frac{B_{so}}{2}\,\rho' \int_0^{2\omega} \frac{[\rho'+\rho\cos(\omega-\omega')]}{[\rho^2+\rho'^2+2\rho\rho'\cos(\omega-\omega')]}$$

$$\left(\frac{z-z_2}{\sqrt{\rho^2+\rho'^2+2\rho\rho'\cos(\omega-\omega')+(z-z_2)^2}} \right.$$

$$\left. - \frac{z-z_1}{\sqrt{\rho^2+\rho'^2+2\rho\rho'\cos(\omega-\omega')+(z-z_1)^2}} \right) d\omega'$$

and

$$B_{c\rho} = -\frac{B_{so}}{2}\,\rho' \int_0^{2\omega} \cos(\omega-\omega') \left[\frac{1}{\sqrt{\rho^2+\rho'^2+2\rho\rho'\cos(\omega-\omega')+(z-z_2)^2}} \right.$$

$$- \frac{1}{\sqrt{\rho^2+\rho'^2-2\rho\rho'\cos(\omega-\omega')+(z-z_1)^2}}$$

$$- \frac{1}{\sqrt{\rho^2+\rho'^2+2\rho\rho'\cos(\omega-\omega')+(z-z_2)^2}}$$

$$\left. + \frac{1}{\sqrt{\rho^2+\rho'^2+2\rho\rho'\cos(\omega-\omega')+(z-z_1)^2}} \right] d\omega'$$

Note that the range of integration for ω' is from 0 to 2ω. It can be seen from the symmetry of the geometry that the contributions to B_{cz} and $B_{c\rho}$ of the currents in the interval ranges $2\omega \leq \omega' \leq \pi$ and $2\omega+\pi \leq \omega' \leq 2\pi$ will cancel.

It should be noted that the field possesses singularities on the edges of the plane and cylindrical sheet currents, and that the field equations given above are not applicable on the current sheets themselves. However, at distances 'sufficiently far' from these currents, the field should give a fairly reasonable approximation of the actual field of the magnetotail current.

6.3.2.4. Combined fields in midnight magnetic meridian plane

In the previous three subsections, the equations for the individual fields of ring, boundary and tail currents have been given for an arbitrary point within the magnetosphere. In the noon-midnight magnetic meridian plane, the field will be two-dimensional, consisting of only the B_x and B_z components. The equations for these combined components will not be repeated here, but it should be noted that there will be some simplification of the equations. In the midnight meridian plane,

$$y = 0,\ \omega = \pi/2 \text{ and } B_{c\rho} = B_{cx},$$

so that,

$$B_x = B_{rx} + B_{bx} + B_{sx} + B_{c\rho}$$

$$B_y = 0$$

$$B_z = B_{rz} + B_{bz} + B_{sz} + B_{cz}$$

where the subscripts r, b, s and c refer to the ring, boundary, plane sheet and cylindrical sheet currents, respectively.

A listing of the computer program which calculates each of these components and their sums is given in Appendix 3.

6.3.3. Some results of the calculations

The program listed in Appendix 3 has been used to obtain the results presented in 4.3 on the combined fields of the ring and tail current along an equatorial radius in the midnight magnetic meridian plane. In Section 4.3, the combined field of the ring and tail currents was computed for two sets of values of the parameters of the model. In the first calculation, it was found that for values of the parameters consistent with the observed strengths and locations of the ring and tail currents, the model could represent a moderate main phase decrease of a geomagnetic storm both at the ground and synchronous satellite positions. In the second calculation, the parameters were adjusted to represent the recovery phase of a storm; that is, the current strengths were reduced and the earthward edge of the tail current placed further out. The values of the second set of parameters were also compatible with satellite observations of the latter phases of a storm. The combined field due to this choice of parameters was found to be nearly zero in the midnight region where a synchronous satellite is located. However, the field was still of appreciable magnitude on the surface of the earth. Thus, suitable choices of the parameters can be made such that the model reproduces the 'earlier recovery' of a geomagnetic storm observed at synchronous orbits relative to ground stations.

The currents depend on several different parameters. For completeness, their definitions are repeated here. The ring current field

depends on: n_o, the peak number density of particles; ε, the energy of a particle; r_{eo}, the location of the peak of the number density in the equatorial plane; g_1 and g_2, which are measures of the width of the number density distribution earthward and outward from the peak, respectively; and p, which governs the form of the pitch angle distribution. Boundary currents are simulated by an image dipole to the earth whose parameters are: d, the distance between the image and earth dipoles; M, the dipole moment of the earth; and n, the ratio of the image dipole moment to the earth's moment. The tail current field depends on the parameters: ρ', the radius of the cylinder which approximates the shape of the cross-section of the tail of the magnetosphere; z_1 and z_2, which are the earthward and outer edges of the tail current, respectively; and B_{so}, a constant which includes the constant current density per unit length of tail.

Thus, the contributions to the total field from each of the currents have the following functional relationships to the parameters:

$$\text{ring current: } \underline{B}_r = \underline{B}_r(x,y,z;\ r_{eo},\ g_1,\ g_2,\ p,\ n_o,\ \varepsilon)$$

$$\text{boundary current: } \underline{B}_b = \underline{B}_b(x,y,z;\ M,\ d,\ n)$$

$$\text{tail current: } \underline{B}_s = \underline{B}_s(x,y,z;\ B_{so},\ \rho',\ z_1,\ z_2)$$

$$\text{and } \underline{B}_c = \underline{B}_c(x,y,z \text{ or } \rho,\omega,z;\ B_{so},\ \rho',\ z_1,\ z_2).$$

The parameters can be varied so as to represent a wide variety of situations. For example, one may start with a step function increase in the boundary currents with the ring and tail currents at relatively low values. Then, keeping the boundary current value constant, one may change the ring and tail current parameters in such a way that the net

field at the earth is decreased below the quiet level. In this way the ssc and initial and decreasing phases of a geomagnetic storm can be reproduced. The value of the parameters must be such that not only do the currents simulate ground observations of a geomagnetic storm, but they also must be consistent with the available satellite data.

In the absence of polar magnetic substorms, which are presumably a consequence of field-aligned currents flowing from the region of the ring current and beyond, this model can satisfactorily reproduce the quasi-steady conditions of a geomagnetic storm. The effects of field-aligned currents will be discussed in 6.3.4.

A field line tracing program to be used in conjunction with the fields of the boundary, ring and tail currents calculated at points in the midnight equatorial plane is also included in Appendix 3.

Figure 6.8 is a plot of a few field lines in the magnetic midnight meridian plane for the following values of the parameters:

ring current, $n_o\varepsilon = 1000$ Kev/cm^3

$g_1 = 1.517$

$g_2 = 0.759$

$p = 2.00$

$r_{eo} = 3\ R_e$

boundary current, $M = 0.31$ gauss (for x,y,z measured in units of R_e)

$d = 28\ R_e$

$n = 28$

and tail current, $B_{so} = 2 \times 10^{-5}$ gauss (or $I_o = 20$ amps/km)

$z_1 = 10\ R_e$

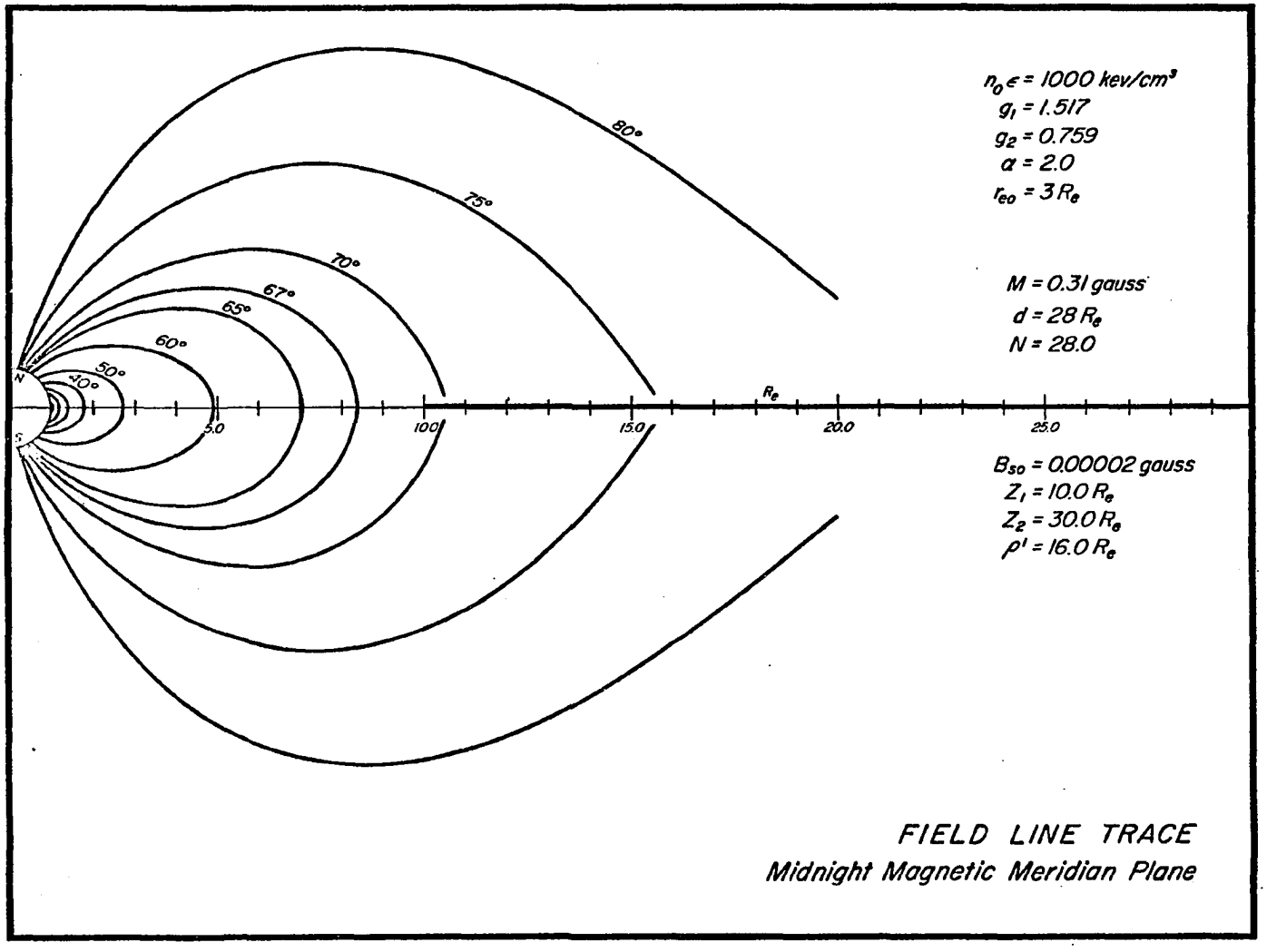

Fig. 6.8. Field line tracings of model containing ring, tail and boundary currents in midnight magnetic meridian plane for moderately disturbed magnetosphere.

$$z_2 = 30\ R_e$$

$$\rho' = 16\ R_e$$

These parameters are representative of a moderately disturbed magnetosphere. At the earth, the combined field of the ring and tail currents is in the order of 80 gammas directed southward. In the tail, the combined field is primarily directed in the solar direction above the neutral sheet and in the anti-solar direction below the sheet; the magnitude of the combined field in the tail is in the order of 20 γ at $z = 20\ R_e$.

Figure 6.9 shows field lines in the magnetic midnight meridian plane for ring and tail current densities larger than those listed for Figure 6.8, but with the same geometric factors. Here, $B_{so} = 6 \times 10^{-5}$ gauss (or $I_o = 60$ amps/km) and $n_o\varepsilon = 1500$ kev/cm^3. The combined field of the ring and tail currents for these values at the surface of the earth is about -130 gammas. The magnitude of the combined field in the tail is about 35 gammas at 20 R_e.

Comparing Figure 6.8 with Figure 6.9, it can be seen that the effect of the stronger tail current is to 'stretch' the field lines into a direction more parallel to the sheet current. In Figure 6.9, in the region between the peak density of the ring current belt ($r_{eo} = 3.0\ R_e$) and the tail current, the field of the ring current begins to be directed northward, while the tail current field magnitude increases with distance. The combined fields of these currents plus the earth's dipole-image dipole fields approaches a null in the region between 9 and 10 R_e. The field line starting at a latitude of 66.5° on the

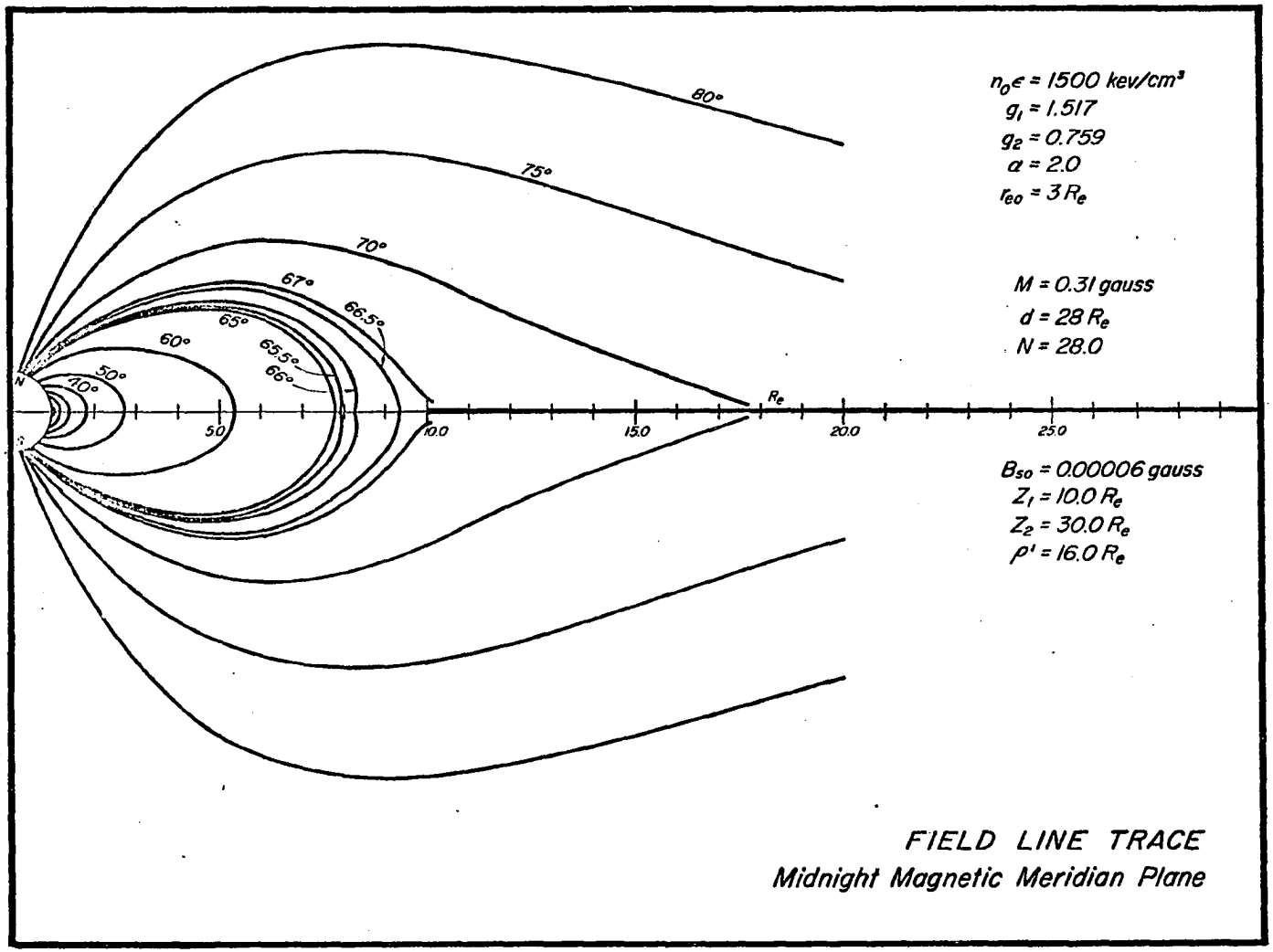

Fig. 6.9. Field line tracings of model containing ring, tail and boundary currents in midnight magnetic meridian plane for strongly disturbed magnetosphere.

earth is 'closed'; the field line beginning at 67° is 'open'. On the other hand, the 67° latitude field line is 'closed' in Figure 6.8. Here, the term 'open' is used in a very loose sense to denote field lines which extend into the tail region.

6.3.4. Effect of field-aligned currents

Magnetic field variations transverse to the expected magnetic field direction in and above the auroral zone ionosphere have been detected (Zmuda et al., 1966; Zmuda et al., 1967; Cloutier et al., 1970; Zmuda et al., 1970; Armstrong and Zmuda, 1970). These localized fluctuations have been interpreted to be due to field-aligned currents flowing into and out of the auroral ionosphere in the same longitudes but slightly displaced in latitude. In the ionosphere, the circuit of the two-sheet model of field-aligned currents is completed by meridional Pedersen currents.

The field-aligned current portion of the model presented in Section 6.2 does not agree with the two-sheet field-aligned current interpretation of the transverse magnetic variations above the auroral regions. However, the two-sheet model is inconsistent with large-scale ground observations of the magnitude of the middle-latitude D component, since little contribution to the disturbance field can be expected there from the two-sheet model. The D-component disturbance field at low latitudes in the midnight-morning sector has been shown to be qualitatively consistent with single-sheet field-aligned currents in the magnetosphere by Akasofu and Meng (1969) and Meng and Akasofu (1969). It may be that small-scale transverse fluctuations detected

by satellites above the auroral ionosphere are only occasionally due to field-aligned currents of the two-sheet-type in the midnight-morning sector.

No attempt has been made to include field-aligned currents in the model presented in this section. If these currents are included, the general distribution of the magnetic field vectors throughout the magnetosphere will be considerably modified.

It has been suggested in Section 3.6 that field-aligned currents arise when a part of the magnetotail current is diverted earthward in the midnight-morning sector. Observations of the magnetic field and plasma energy density in the tail are not inconsistent with such a hypothesis. Presumably, the circuit of the earthward directed current would be connected to an electrojet current westward along the auroral oval and a current flow back toward the tail along field lines. The circuit is completed by current flowing from dusk to dawn on the surface of the tail.

The geometry of such a model of field-aligned currents is complex and difficult to visualize. However, the distribution of disturbance vectors due to such field-aligned currents flowing out of and into the tail will be very similar to those obtained for the rather simple model presented in Section 6.2.

6.4 DISCUSSION

The simple three-dimensional current model presented in Section 6.2 can reproduce the major features of a geomagnetic storm over the surface of the earth in the latitudinal belt between the auroral zones. The

model is not satisfactory in the polar cap region.

In Section 6.3, a more realistic model has been presented. This model can reproduce the major features of a magnetic storm, if polar substorms (and, hence, field-aligned and auroral electrojet currents), which generally occur during the decreasing phase of a geomagnetic storm, are absent. The model is more realistic in the sense that boundary and tail currents are included and thus, it can be used to investigate magnetic field changes throughout the magnetosphere. Incorporation of field-aligned and electrojet currents will complete the model.

The model can also be used to represent the state of the magnetosphere during quiet times. Reducing the intensity parameters of the boundary, ring and tail current should yield an approximation of the quiet magnetosphere which can be compared with satellite observations.

In both of the models, neither induced currents in the earth nor ionospheric return currents have been considered. A more complete treatment, which incorporates these currents plus field-aligned and auroral electrojet currents in the second model, may explain all the major features of a geomagnetic storm over the surface of the earth, and throughout the magnetosphere.

CHAPTER VII

DISCUSSION AND CONCLUSION

7.1 Summary of Results

(a) Following a brief review of ground and satellite-based observations of the disturbed geomagnetic field in Chapter I, a summary and study of quiet day magnetic variations were presented in Chapter II. In particular, recent analyses of the quiet day variations at high latitudes (S_q^p) were reviewed for the purpose of finding an explanation for the phenomenon. The major features which distinguish this phenomenon from other quiet day variations are its relatively large amplitude and its sunward-directed component in the region above 80° dp lat.

A model consisting of negatively and positively charged particles on the 80° dp lat., dayside semi-circle in the ionosphere and the expected Hall current circuit satisfactorily reproduces the variation below 80° dp lat., but does not conform to the S_q^p pattern poleward of this region. The choice of this model was prompted by theoretical considerations and observations which suggest the neutral point of the magnetosphere is actually a neutral line; just exactly how such a semi-circular charge distribution in the ionosphere can be maintained is unknown. Recently, Frank and Gurnett (1971) from Injun 5 data have reported the existence of such a space charge in the vicinity of the auroral oval.

None of the other acknowledged, ionospheric and non-ionospheric sources of quiet day geomagnetic variations appear to have the correct magnitudes and/or directions to account for the anomalous S_q^p variation

in the region of the polar cap.

(b) The subsequent two chapers (III and IV) deal with ground and satellite observations of the disturbance magnetic field. The magnetic records of representative low and high latitude stations were superposed to yield the asymmetry (ASY) and westward auroral electrojet (AL) indices, respectively, for several magnetic storms. A comparison of these indices indicated that periods of poor correlation existed. It was pointed out that in fact correlations should exist if the current circuit of auroral electrojets were chiefly completed through the lower latitude ionosphere. On the other hand, satellite observations in the midnight sector of the magnetosphere at synchronous altitudes have shown that magnetic field variations there are often very similar to those at the ground station Honolulu. Thus, it was concluded that the source of some low and middle latitude positive bay-like disturbances during magnetic storms must be located outside the orbit of the synchronous satellite in the region of the geomagnetic tail. Certain particle observations in the vicinity of a synchronous satellite in the midnight region of the magnetosphere are consistent with such an interpretation.

Numerous examples of a relatively high degree of correlation between ASY and AL were also found, and thus, it was suggested that other sources such as return currents of the auroral electrojets in the ionosphere may also be important in producing bay-like changes at low latitudes during a magnetic storm.

The storms studied exhibit typical morphological features, which have been noted in other studies. The maximum rate of decrease and maximum main phase decrease occurred at stations in the afternoon-

evening sector. The westward shift (with respect to a frame of reference rotating with the earth) of the region of maximum H-component field decrease at a particular instant of the storm is best illustrated in the iso-intensity contours of the storm of September 21-23, 1963. The asymmetrical distribution of distant currents, as evidenced by large values of the ASY index, is noted to be only generally associated with the occurrence of polar magnetic substorms. Finally, it has been shown that the Dst variations do not follow the polar substorm time variations very closely and in fact tend to lag behind it.

In the vicinity of the synchronous satellite in the midnight sector, the maximum value of the main phase decrease of a magnetic storm has been noted to be smaller than that observed at ground stations. This observation plus the observed similarity of changes at the two locations lead to the interpretation that the observed ' earlier recovery' of a storm at synchronous altitudes, over that observed at the ground, is due to the combined effect of the ring and tail currents. Several examples of ground and ATS-I satellite magnetic records were presented which clearly show the 'earlier recovery'.

Preliminary calculations for a simple model for the ring and tail current fields were presented which show that the net field in the midnight region of the synchronous satellite orbit could be made to approach the reference field level (that is, the net ring and tail fields approach zero) by choosing a set of parameters consistent with the observed locations of the particles which constitute the two currents. The location of the satellite is between the tail and ring currents in the magnetic midnight meridian plane. For the values of

the parameters chosen, the combined field is substantial in the vicinity of the earth even though the field near the satellite is very small. Thus, the model can be made to reproduce an instant of the recovery phase at both locations.

(c) A statistical study on the occurrence of storm sudden commencements (ssc) associated with polar magnetic substorms was made in Chapter V. Here, a polar magnetic substorm is regarded as 'simultaneous' to an ssc, if it occurs within a few minutes (<5 min.) and has an amplitude of greater than 50 gammas. Several examples of such events are presented to illustrate more precisely what is meant by 'simultaneous storm commencements and polar magnetic substorms' or 'ssc-associated polar magnetic substorms'. The study is prompted by the fact that an ssc is associated with a rather large-scale and sudden change in the magnetospheric configuration and, thus, it may lead to instabilities in the magnetospheric plasma.

The statistical study of 108 ssc's during the IGY shows that the state of the magnetosphere prior to the ssc as determined from the Kp indices does not significantly affect the occurrence frequency of simultaneous events. That is, the occurrence of simultaneous events is not influenced by whether or not the magnetosphere is highly disturbed prior to the ssc event. However, amplitude dependence is found; larger ssc's tend to be associated with polar magnetic substorms. It is found that approximately 49% of the IGY ssc's were substorm-associated events, while only 3% of ssc's during the IQSY were so associated.

A few (36) interplanetary discontinuities, detected by the IMP 3 satellite and known to subsequently cause ssc's, were also examined for the simultaneous occurrence of polar substorms. The current directions in the discontinuities were also calculated for a few cases; no definite tendency for relating the current directions and the occurrence of substorms could be found. However, this result cannot be taken as statistically significant, since so few discontinuities were examined.

(d) Two models incorporating three-dimensional currents in the magnetosphere were discussed in Chapter VI. The models are primarily intended to simulate the distribution of the disturbance vectors in the vicinity of the earth, but the parameters of the second, more realistic model can be readily varied to yield an approximation of the fields of known non-ionospheric sources of quiet day magnetic variations.

The first model basically consists of a westward ring current in the equatorial plane varying in intensity with longitude, field-aligned sheet currents from the pre-dawn quadrant of the ring current flowing into the auroral regions, westward auroral electrojets, and field aligned sheet currents from the auroral regions back into the pre-midnight quadrant of the ring current. (The currents of this model obey Kirchoff's rules). This model gives a distribution of field on the earth similar to the observed one except in the region of the polar cap. Modification of this model by addition of a constant eastward flowing component of ring current gives a net flow eastward in the midnight sector; this simulates the removal of the diamagnetic effect of the ring current particles observed by the ATS-I satellite. The modified model also produces a distribution of disturbance vectors

very similar to the observed one, but again the field in the polar regions is not in agreement with the actual disturbance field. The modified model differs from the original in that the field direction is northward rather than southward in low latitudes in the midnight sector, which is due to the dominance of the eastward current in this region. For both models, the relative differences between the low latitude noon sector vectors and low latitude midnight sector vectors are, however, in the correct sense and magnitude to reproduce the often observed positive and negative bay-type disturbances at low latitudes during a magnetic storm.

Field calculations for the modified model were also made along a field line adjacent and interior to the field-aligned currents at several magnetic meridians. A similar calculation was carried out for an externally adjacent field line. The chief utility of these calculations is that they may be compared with satellite observations of field-aligned currents should they become available.

The second model takes into account the boundary and tail currents in addition to the ring current and is more realistic in this sense than the simpler model discussed above. The effects of boundary current are simulated by an image dipole, while the tail current consists of a plane sheet of current from the dusk portion of the tail to the dawn part with cylindrical sheet currents back to the dawn side completing the circuit. The ring current consists of a distribution of particles symmetric around the axis. The relevant equations for the individual fields are developed. The combined field of the ring and tail current parts of the model have been used to obtain the results presented in Chapter IV, which may account for the earlier recovery of a storm at synchronous altitudes.

7.2 Further Discussion of Results and Conclusions

The results and conclusions of this dissertation have already been discussed. Here, we wish to present an overall view of the results and conclusions bearing in mind some of the major questions which remain unanswered in this dissertation and in the theory of geomagnetic storms in general.

(a) During a typical main phase decrease, the estimated energy stored in the ring current belt is of order 10^{22} to 10^{23} ergs. The estimated energy associated with polar magnetic substorms is 1 to 2 orders of magnitude less than this. The long-term dependence of the occurrence of magnetic storms on solar activity leaves little doubt that the sun is the ultimate source of this energy.

The energy rate of electromagnetic radiation primarily in the visible range incident upon the earth is in the order of 10^{25} ergs/sec. A part of this energy goes into maintaining the ionosphere of the earth, which is important in any theory of magnetic storms and in ionospheric sources of quiet day variations. Although the rate of energy input is large, it is very doubtful that solar electromagnetic radiation participates in any direct manner in the production of magnetic storms.

Measurements of the solar wind parameters and the observed delay times between the onset of solar flares and the onset of magnetic storms (Akasofu and Yoshida, 1967) leave very little room for doubt that the particles of the solar wind are intimately related to the occurrence of geomagnetic storms. The energy rate across an area equivalent to the cross-section of the magnetosphere exposed to the solar wind is in the order of 10^{20} ergs/sec. In 10 hours, which is

the required time for a typical maximum main phase decrease from onset time, the time-integrated energy of the solar wind over a cross-section of the magnetosphere is in the order of 10^{24} to 10^{25} ergs. This is more than enough energy to produce a main phase decrease. However, a rather efficient and rapid mechanism is required to bring the solar wind energy across the magnetospheric boundary and deep into the magnetosphere, since the total energy residing in the ring current is of order 10^{22} to 10^{23} ergs. An adequate theory has yet to be developed to explain this transfer of solar wind energy. It is probable that a significant portion of the required energy is already stored within the magnetosphere in the plasma and neutral sheets of the magnetotail or some other reservoir of particles.

(b) Satellite magnetic field measurements at the boundary of the magnetosphere (Cahill and Amazeen, 1963) show the Chapman-Ferraro theory of boundary formation is essentially correct. It predicts a field, which is larger than the dipole field, just inside the boundary. That is, currents are set up such that the dipole field is excluded from solar wind, while they add to the dipole field interior to the boundary.

Enhancement of the energy of the ring current belt produces the main phase decrease of a magnetic storm (Frank, 1967, 1970). Differential energy spectrum measurements of the ring current particles indicate that the enhancement is the result of an increase in number density of the particles. Just exactly how such large numbers of particles can be introduced so deeply into the magnetosphere is the subject of much conjecture.

One suggestion is that the ring current particles are originally

stored in the neutral and plasma sheets of the tail. The tail is a permanent feature of the magnetosphere; it has been ascribed to the 'viscous' or 'frictional' force of the solar wind or to the effects of the merging of the geomagnetic field lines to the interplanetary field lines. Presumably, during storms, some mechanism acts to cause the flow of tail particles earthward. Ultimately, a part of the magnetotail particles ends up as ring current particles deep in the trapping region, while a portion flows along field lines into the auroral region and produces auroral and polar magnetic substorms. This interpretation fits the 'splash catcher' model of O'Brien (1962).

Thus, the existence of the storm-time ring current belt is closely related to the existence of the neutral and plasma sheets in the tail. Recent satellite observations indicate that time variations of the tail sheet are also closely related to the occurrence of polar magnetic substorms (see for example, Hones, et al., 1970).

(c) In this dissertation questions concerning the actual mechanisms causing magnetic storms have been avoided. However, it has been endeavored to coherently present and discuss models, which are consistent with a wide variety of satellite and ground observations. A few difficulties encountered in the topics included in this dissertation are important enough to warrant further discussion.

(d) The observed polar solar quiet day geomagnetic variation (S_q^p) is not in agreement in the polar cap with the model presented in Chapter II. The very location of this anomalous variation suggests that it must somehow be related to the magnetospheric tail. Piddington (1964) suggested that the full force of the solar wind on the polar

cap field lines is transferred to polar regions; this force gives a field in the proper sunward direction, but the field is one to two orders of magnitude too small to account for polar cap S_q^p. In any event, this mechanism is clearly related to the formation of the magnetospheric cavity and hence, to boundary currents which produce only a small contribution to quiet day variations.

The barium cloud experiments of Heppner et al. (1970) indicate that the polar cap electric field is directed approximately from dawn to dusk during low to moderately disturbed periods. It is interesting to note that this is precisely the direction predicted by the ionospheric charge distribution model for S_q^p of Chapter II, which gives the proper direction for S_q^p field equatorward of the polar cap region.

Heppner et al. (1970) show that the magnetic disturbance vector directions in the polar cap at the time of the electric field measurements are incompatible with the expected Hall and Pedersen current directions. They thus invoke a mechanism for the observed magnetic disturbance directions consisting of a net current flowing earthward in the late morning sector and an upward net current in the late evening sector. Both of these currents are located just equatorward of the polar cap delineated by the auroral oval. It should also be noted that the agreement between the magnetic field produced by the Hall and Pedersen currents expected of the electric field and the observed disturbance directions is made worse by addition of the expected S_q^p field to the disturbance field.

In Chapter II, it was concluded a priori that the mechanism producing S_q^p is unrelated to the mechanism producing the polar electrojet

pattern. This conclusion was based on the drastic difference observed between the two patterns (Kawasaki and Akasofu, 1967; Feldstein and Zaytsev, 1967). If, for example, it is assumed that the mechanism of Heppner et al. (1970) is correct for polar cap magnetic disturbances and is an intensification of the S_q^p pattern, it would require a rotation of some 90° westward in the northern polar cap for the locations of the upward and downward net currents. On the other hand, there does not appear to be a smooth transition from the S_q^p pattern to the pattern during disturbed periods. Furthermore, unlike negative bays, which are the primary mode of magnetic disturbances in the auroral regions, S_q^p has a strong seasonal dependence; the S_q^p variation is much larger in the polar cap summer than in the winter. Thus, it is suggested that the mechanism producing S_q^p in the polar cap is fundamentally different from that producing field changes during disturbed periods.

At the present time no explanation is offered for polar cap S_q^p. Whatever the mechanism invoked, it must explain not only the pattern of S_q^p, but also its seasonal dependence as well.

(e) In Chapter III, it has been demonstrated that the characteristics of some low latitude DS changes are consistent with the interpretation that they are primarily due to distant sources. Aside from the obvious similarities between the ATS-I and Honolulu records, particularly during geomagnetic storms in the midnight sector (Coleman and Cummings, 1968), the conclusion was based on the significant anticorrelations observed between the asymmetry index and the westward electrojet index. The occurrence of such anticorrelations can be taken to mean that there is no direct relationship between the two phenomena,

and thus, that return currents through the low latitude ionosphere do not contribute significantly to low latitude DS changes.

However, the existence of correlations between ASY and AL on some occasions does suggest a connection. It has been pointed out that under certain cconditions both a mechanism involving return currents and a mechanism involving a combination of the fields of auroral electrojets and a partially depleted ring current in the midnight sector are consistent with the correlated changes. Based on a simple three-dimensional current model, explicit calculations for the latter mechanism were made in Chapter VI. More specifically, it was shown that the low latitude positive pulse in the night sector and negative pulse in the day sector could be reproduced by the model. The second, more realistic model, in Chapter VI can also be made to be consistent with the similarity of the H-component ATS-I and Honolulu records, if we require that the positive change is due to a decrease in the strength of the tail current by a diversion of the current into the early morning auroral oval. In this case, the current flows along the oval and back into the dusk part of the tail.

We thus submit that positive and negative DS changes from the Dst level are primarily due to a combination of a sudden weakening of the tail field and the simultaneous strengthening of the auroral electrojets, rather than ionospheric return currents. The effect of the electrojets is to add to the dayside low latitude Dst component, while decreasing the nightside value. Simultaneously, of course, the Dst value will decrease because the tail field decreases, but since the auroral electrojets are closer to the observing region, they dominate the distribution of the disturbance field.

(f) Coleman (1970) has suggested that the observed rapid recovery of a geomagnetic storm at synchronous altitudes relative to the recovery phase observed at the surface of the earth and the lack of a substantial D-component could be taken as evidence for an inward movement of the ring current plasma. There are some observations which conflict with such an interpretation. Paramount among these are the observations of Frank (1970), who indicates there is actually an outward movement of the peak location of ring current particles during latter stages of a storm. The net effect of the ring current should be to increase the field above the quiet day level at the satellite all along its orbit. The ATS-1 observations do not indicate that this is the case.

According to Coleman (1970), the lack of an appreciable D-component during the recovery phase of a storm can be attributed to a decrease of the tail field back to its quiet day level. However, Coleman also suggested an alternative explanation in terms of field-aligned currents might be required to explain the D-component changes in the midnight sector during the main phase decrease. We favor this latter view, and thus, that a lack of an appreciably enhanced D-component does not necessarily mean the tail field has returned to its quiet day level. Also, there is no a priori reason to believe that the tail field returns to its quiet day level faster than the ring current field does.

Implicit in the interpretation presented in Chapter IV of the recovery phase at syncrhonous altitudes is the existence of an appreciable tail field during the recovery phase. This enhanced tail field can account for the required southward directed field needed to cancel the northward component of the ring current field throughout the

synchronous satellite orbit. There is a tail field gradient across the orbit of the synchronous satellite which produces a difference in field strengths between points on the orbit, but for a long tail located well outside the orbit this is not appreciable. Also, a slightly asymmetric quiet time ring current stronger on the nightside may provide a gradient of field which can cancel the oppositely-directed tail gradient.

(g) The occurrence of polar magnetic substorms simultaneous to ssc's clearly indicates that the particles causing the polar substorm are already deep within the magnetosphere. Otherwise, we are forced to conclude that solar wind particles have nearly immediate (within a minute, in some cases) access to the midnight-morning auroral ionosphere, where the simultaneous polar magnetic substorms are observed. It is not very likely that any mechanism invoking a turbulent diffusion process for solar particles through the magnetopause can be found to explain these simultaneous events.

Alternatively, direct entry through the neutral point (or 'neutral band') of the solar particles or some other mechanism such as the neutral hydrogen hypothesis might also account for the simultaneous events. However, in these cases, one would be hard put to understand why the magnetic substorm changes are greatest on the nightside of the earth rather than the sunward side.

It is suggested that the ssc renders magnetospheric plasma unstable via some unknown mechanism. The amplitude dependence of the occurrence of simultaneous events shown in Chapter V (see also Schieldge and Siscoe, 1970), supports this view.

Just precisely where the particles causing the simultaneous substorms

originate is unknown, but it should be pointed out that anticorrelation between the prior Kp and the events does not necessarily imply that the substorm-producing particles do not originate in the ring or tail current regions. In fact, a brief examination of a few examples indicates that low latitude stations exhibit changes of the positive and negative DS-type described in Chapter III and Section 7.2(e). That is, immediately after an ssc, there is a tendency for stations located in the midnight-morning sector to record a positive or zero net change from the ssc level, while those in the noon-afternoon sector record a negative relative value. (See Chapter V and Appendix I for numerous examples). Thus, it is suggested that simultaneous polar magnetic substorms appear via field-aligned currents from the tail or ring current region. The lack of dependence on prior Kp of these events also suggests that the instability arises regardless of whether or not the ring and tail current particles are in their respective quiet time states.

Of the solar wind discontinuity parameters investigated in Chapter V, namely pressure by means of the amplitudes of ssc's and solar wind discontinuity field and associated current directions, only the pressure has a very positive correlation for the occurrence of simultaneous events. The actual number of interplanetary discontinuity observations used in the study was so small that even the statistically valid result that a southward directed interplanetary field tends to produce magnetic storm activity was not found. It is further suggested that a one-to-one correspondence might be found in direct measurements of the pressure changes associated with interplanetary solar wind discontinuities and the occurrence and magnitude of simultaneous polar magnetic substorms.

(h) Although either and/or a combination of the models presented in Chapter VI are consistent with the major features of the geomagnetic disturbance field at low and middle latitudes and at various points in space, there remains a major difficulty. We have suggested that the low latitude fields are fairly well reproduced by the simple three-dimensional current model presented in Section 6.2. However, in the polar cap, the field directions contain a significant contribution from the field-aligned currents, which tends to make agreement with the actual polar disturbance field rather poor. One way to remedy the model is to assume a narrower longitudinal extent for the polar electrojet and hence the field-aligned currents. Then the transverse components of these currents will have more of a tendency to cancel in the polar regions.

One can forsee less of a problem with the distribution of field for the field-aligned currents from the tail which should be incorporated into the second, more realistic model. If current is diverted from the tail in the dawn part of the tail sheet toward the earth and returns to the dusk part via field lines and the auroral electrojets, then the 'stretched' geometry of the field-aligned currents will be such that the transverse components of the fields will be more effectively cancelled in the polar cap. At lower latitudes, it is evident that this model will still retain the essential features of the disturbance field (Meng and Akasofu, 1969).

Alternatively, the models might be modified by including a two sheet model for the field-aligned currents as suggested by Armstrong and Zmuda (1970) (see Section 6.3.4) or two single sheets of the type discussed by Heppner et al. (1970) (see Section 7.2d). In either case, the agreement with the actual lower latitude disturbance field would not be good.

7.3 Recommendations

This dissertation covers a rather wide range of topics. Consequently, some aspects have been treated somewhat superficially. As an extension of this dissertation, the following recommendations for future work are made.

(1) It is suggested that a few other magnetically quiet days be explicitly investigated to definitely show that the pattern of magnetic disturbances in the polar cap is not merely an intensification of the S_q^p pattern.

(2) Field-aligned and auroral electrojet currents should be incorporated into the model consisting of the tail, boundary and ring currents.

(3) In any future model calculations of the effects of magnetospheric currents, the effects of the currents induced in the earth must be taken into account. Ashour (1971) has given equations for the field of the induced currents once the effects of the primary field are known. The forms of these equations are particularly suitable for incorporation into the models presented in Chapter VI.

(4) It is recommended that a more realistic tail current be incorporated into the second model presented in Chapter VI.

(5) A series of computations should be made for the models presented in Chapter VI or for other models using various values for the parameters. A sequence of sets of parameters may be established, which may reproduce a magnetic storm

in its entirety both on the ground and throughout the magnetosphere. In this way, the values of some of the parameters associated with the quiet and disturbed magnetosphere may be deduced, and hence, may provide a basis for a better understanding of magnetospheric phenomena.

APPENDIX I

Presented here is an extensive compilation of H-component magnetic storm records. In general, the records are of low latitude stations with mean dp lat $\sim 25°$ and high latitude stations with mean dp lat $\sim 66°$. The stations are widely dispersed in longitude. The low-latitude H-component disturbance field is an indication of the strengths of the ring and magnetotail currents, while that of high latitude stations is generally indicative of the auroral electrojet current strength.

A few combined storm-time records of low and high latitude stations are also given. These give the asymmetry (ASY) and auroral electrojet indices (AE), respectively (see Chapter III, Section 3.3).

H-component records of 44 stations during the great magnetic storm of March 8, 1970 are also shown. These are grouped according to longitudinal sector and latitudinal range. A few southern hemisphere stations are also included.

A complete list of dates follows on page 197 a.

LIST OF DATES

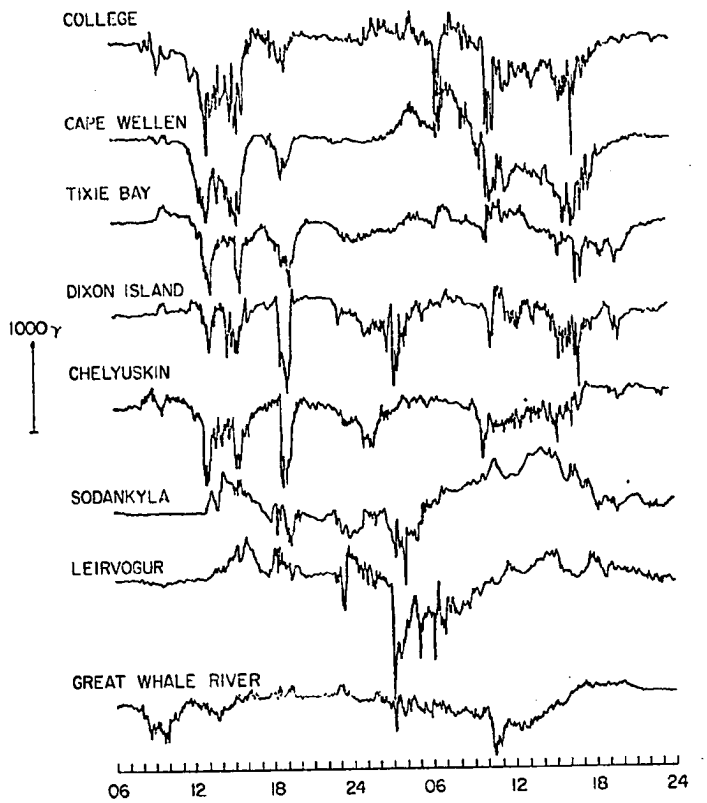

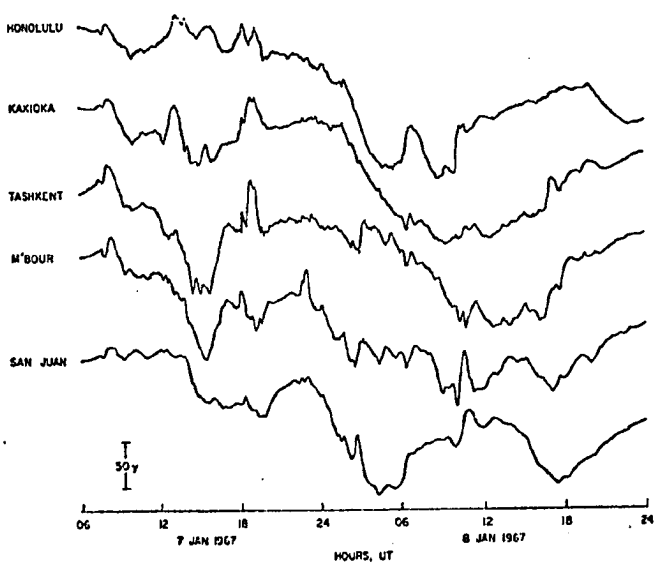

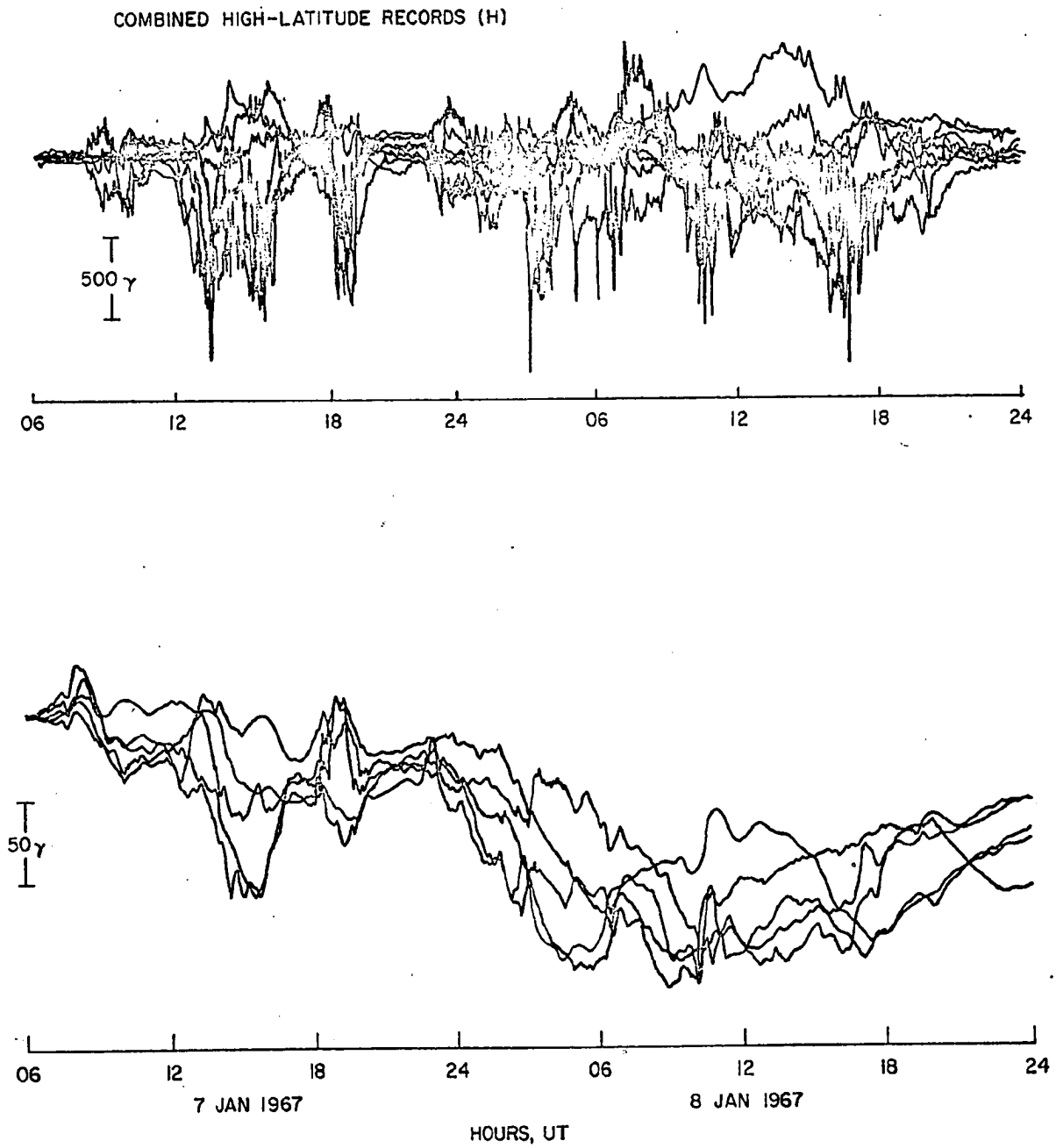

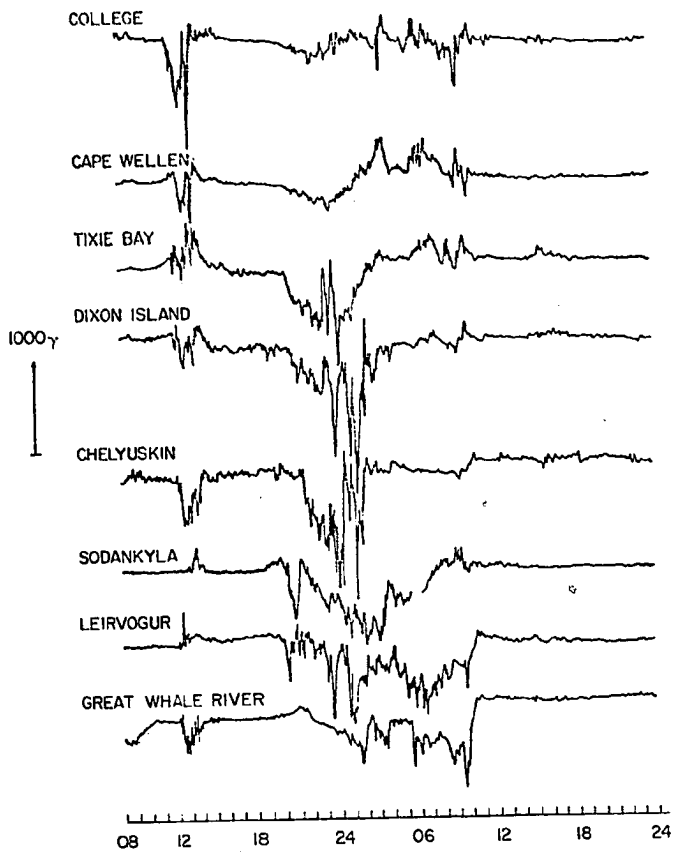

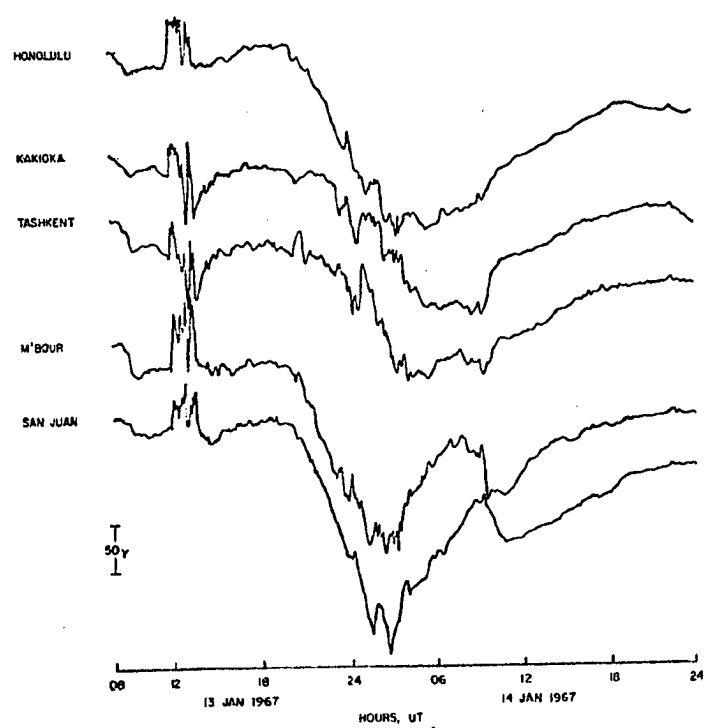

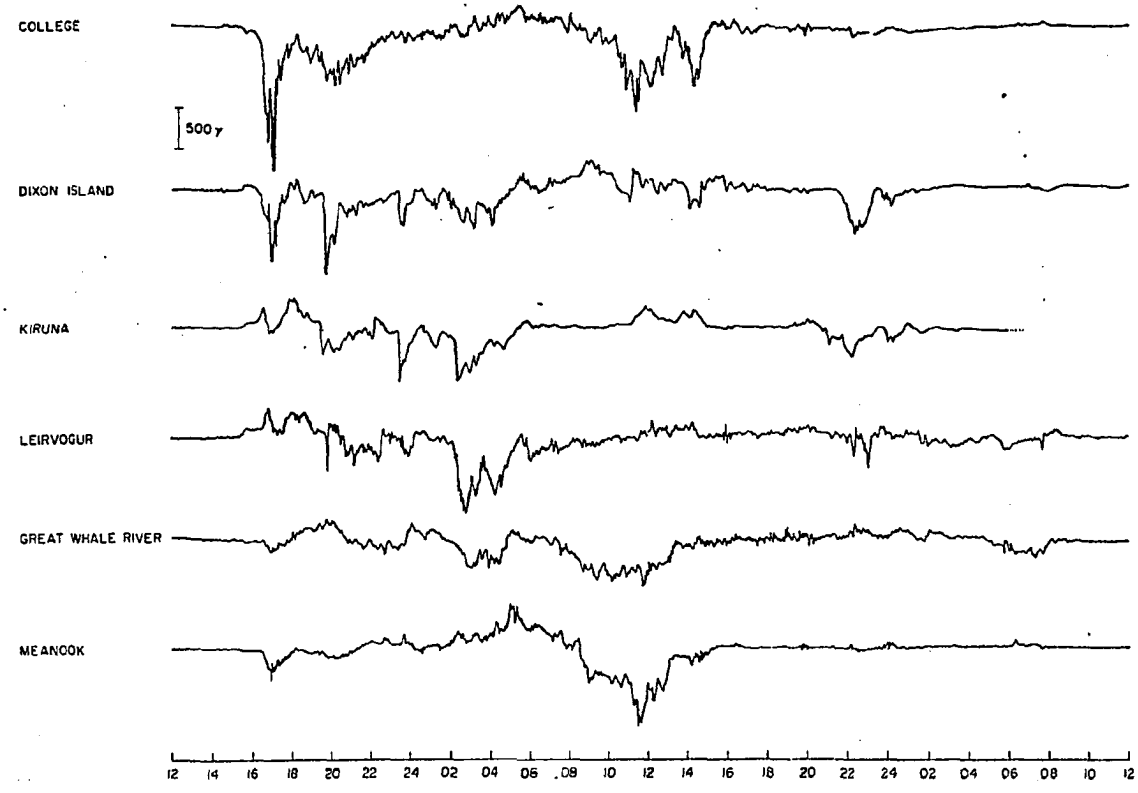

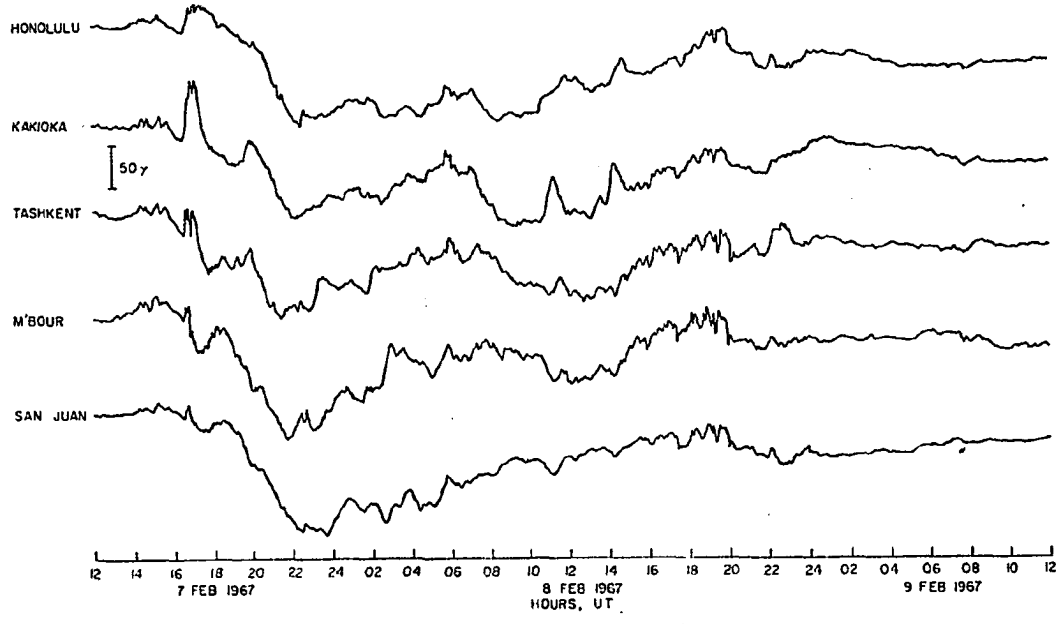

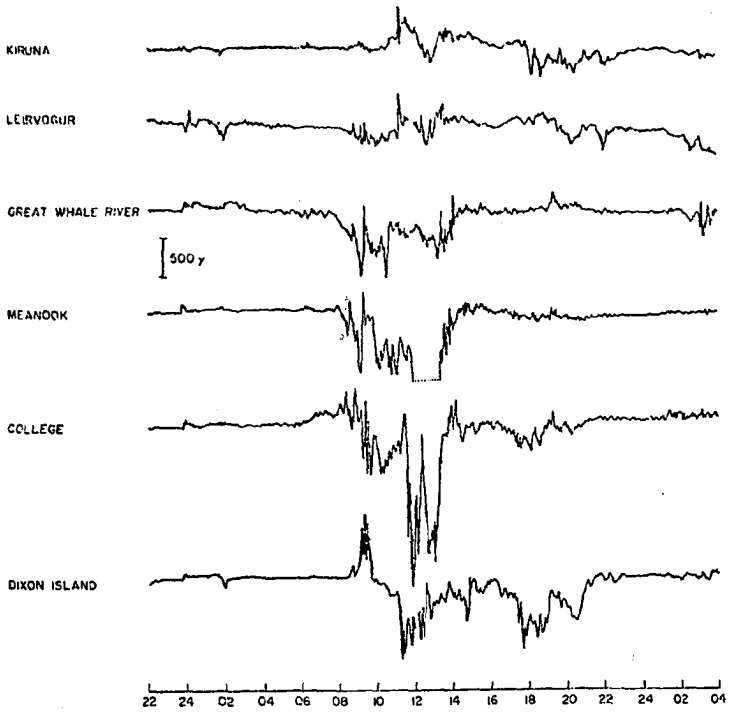

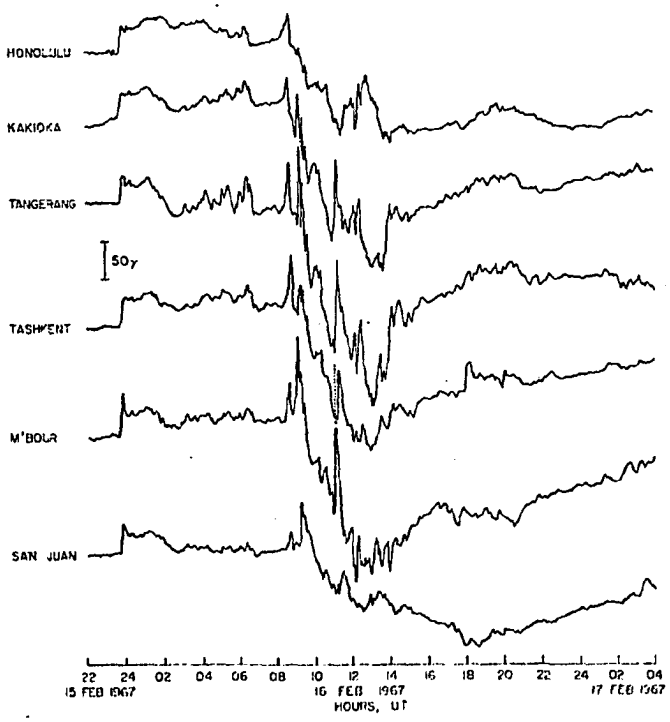

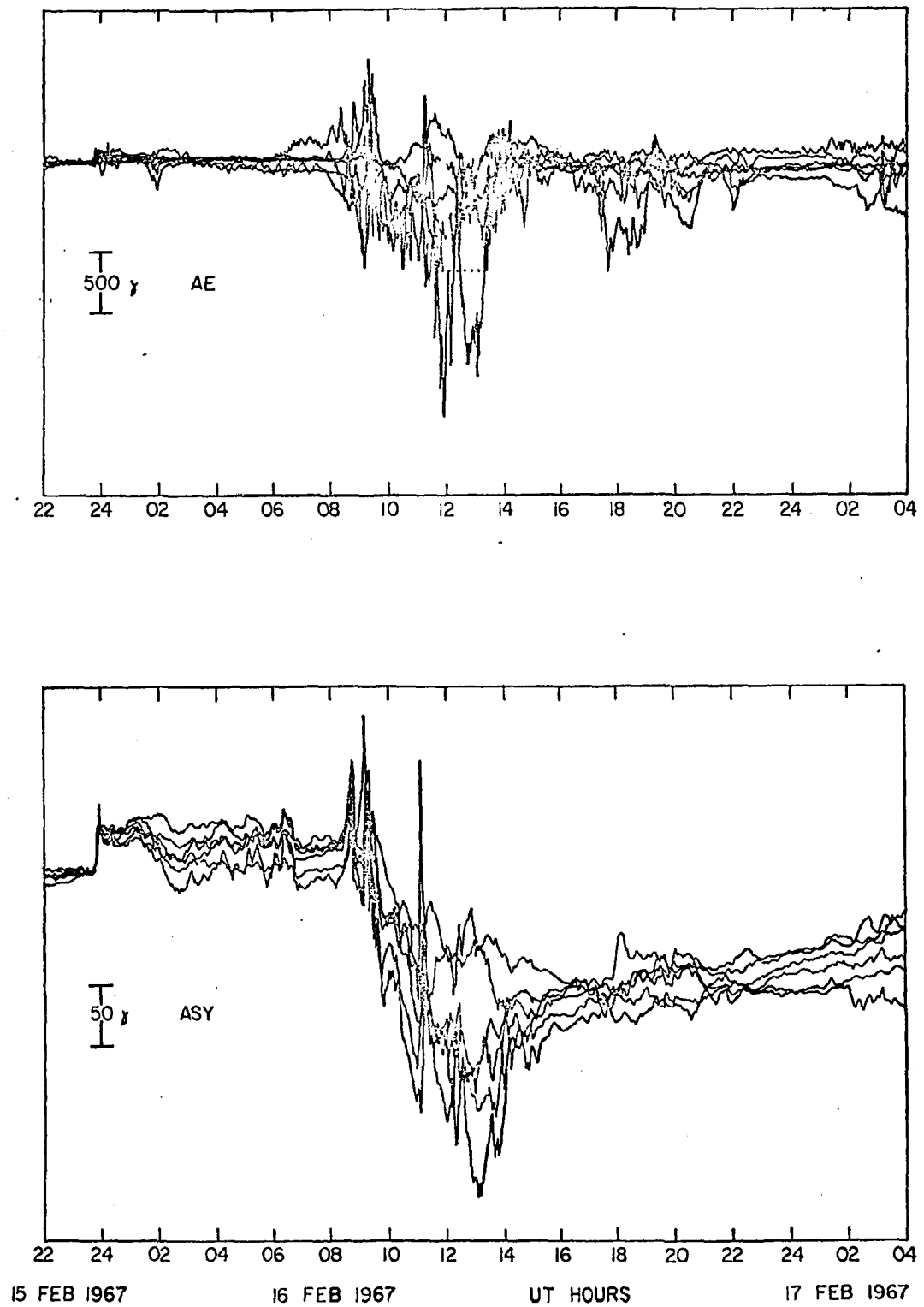

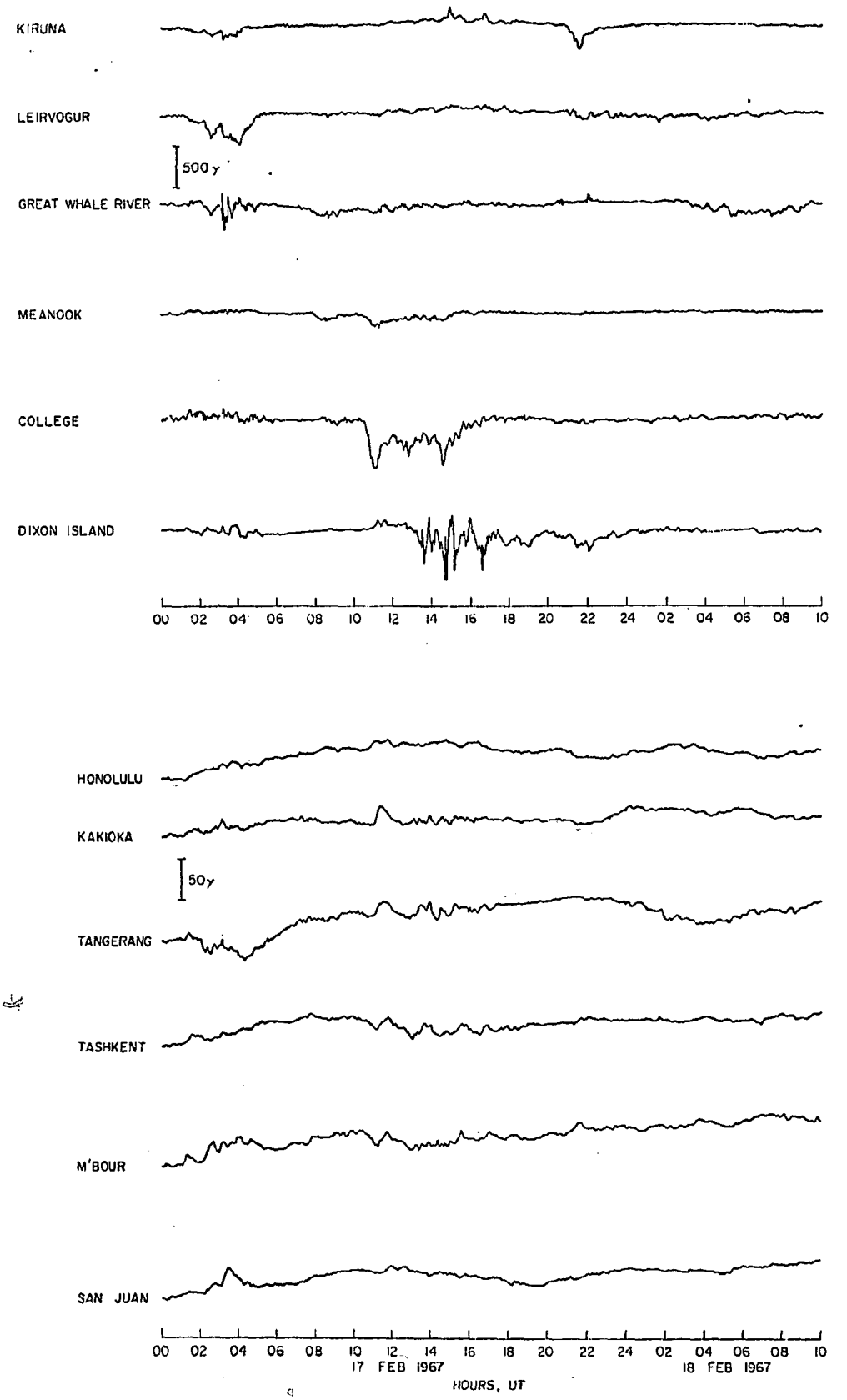

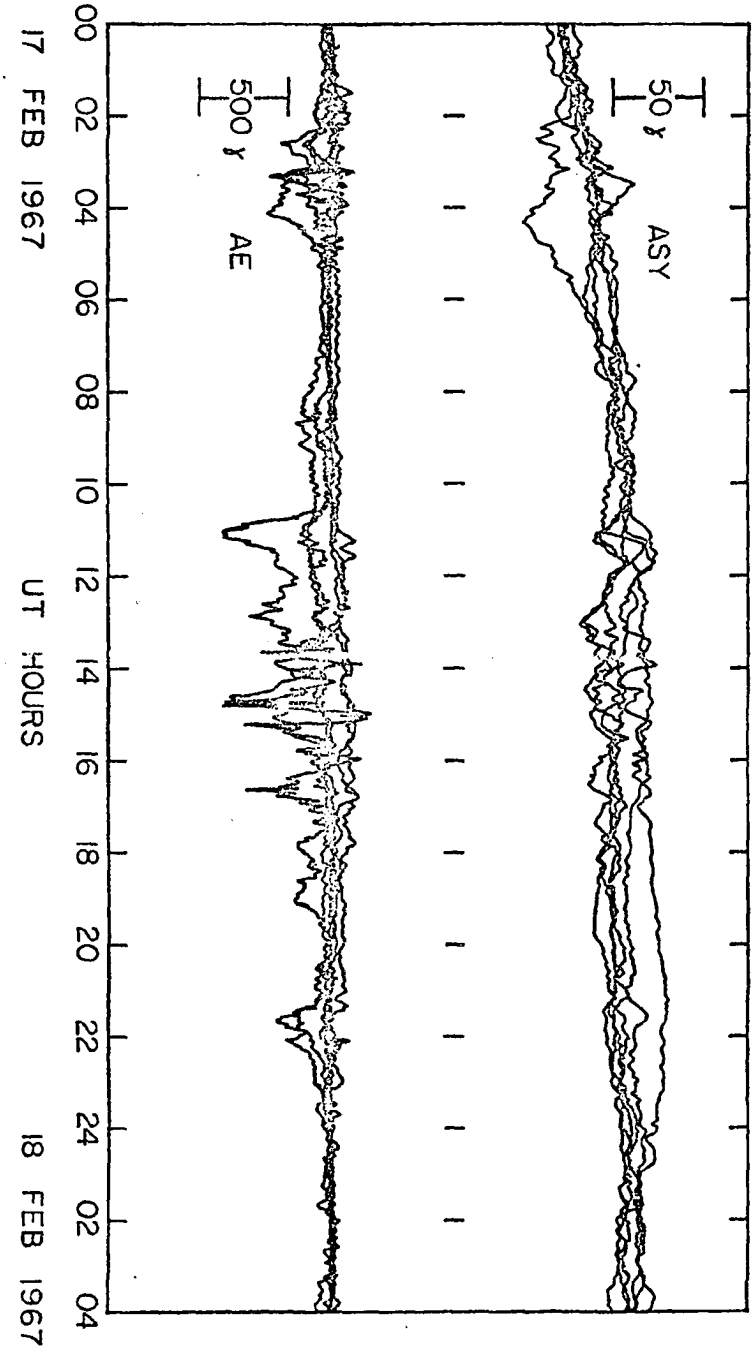

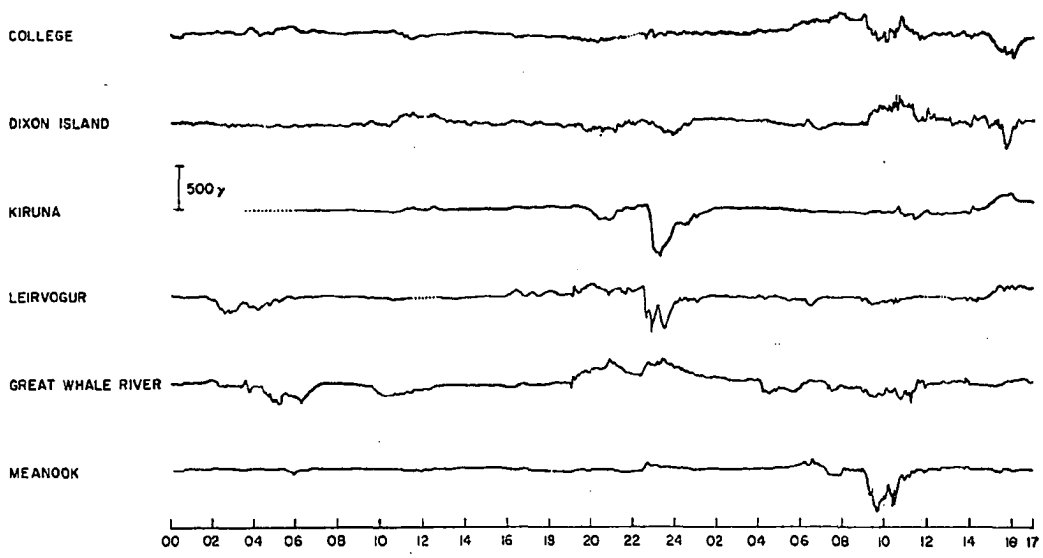

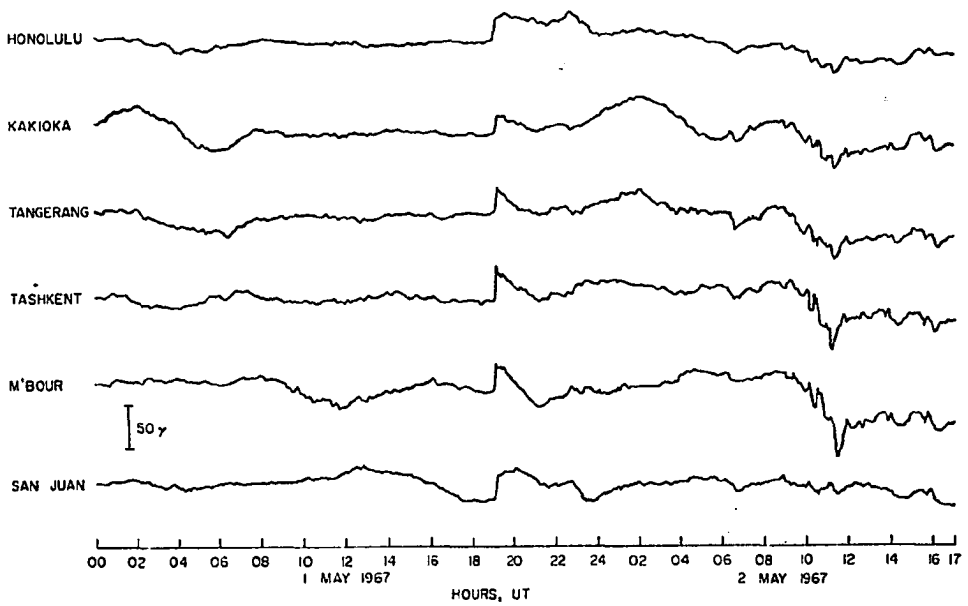

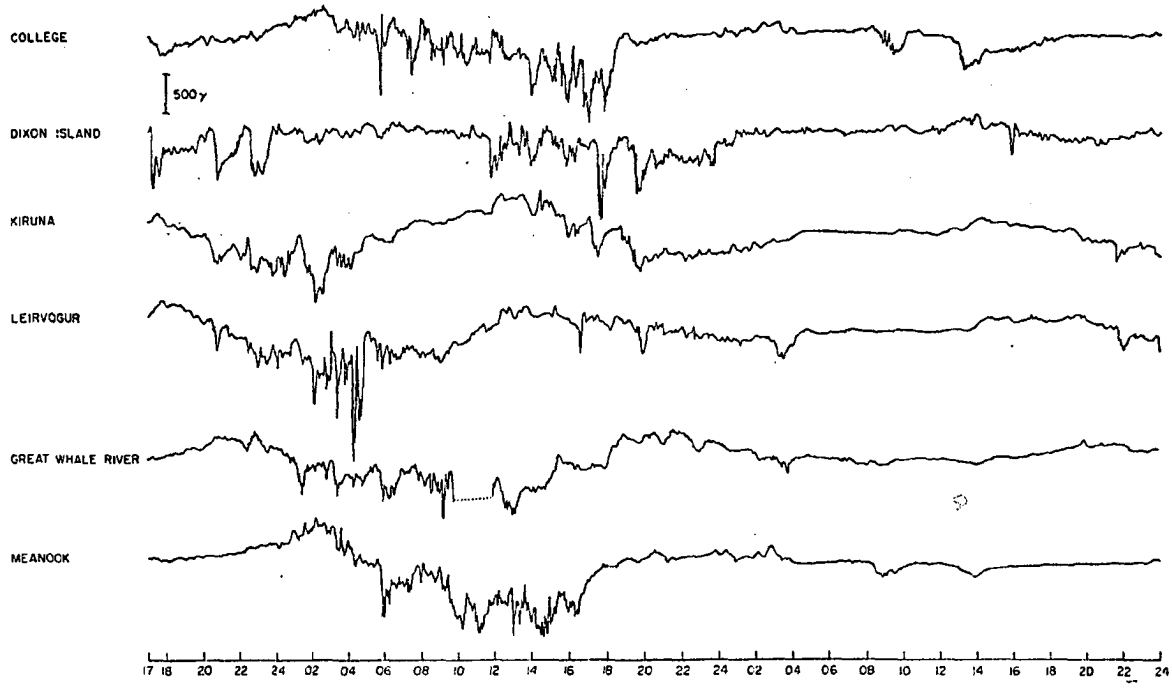

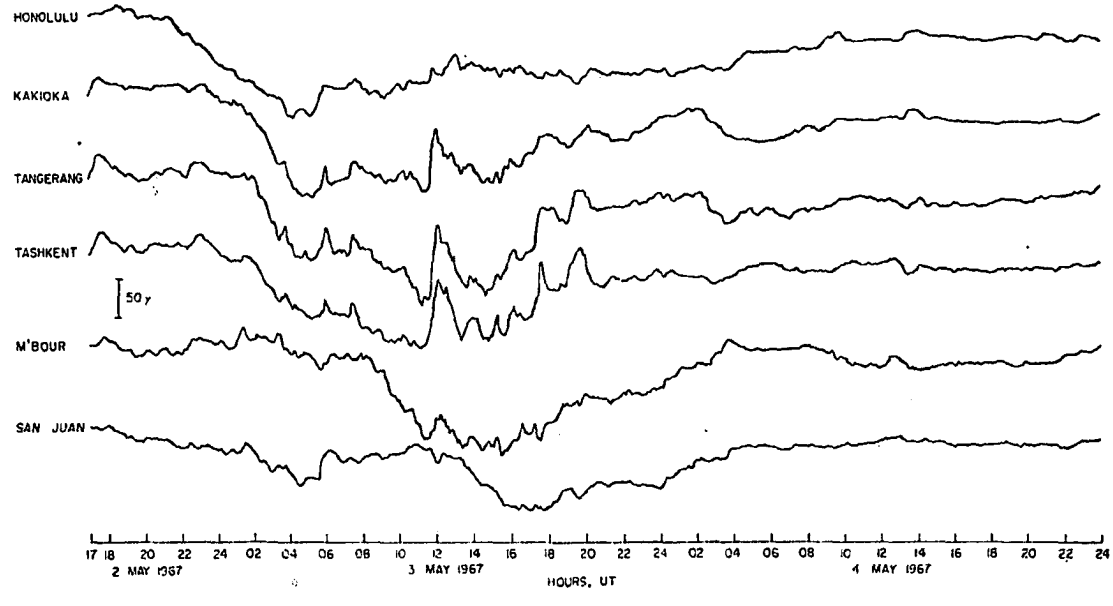

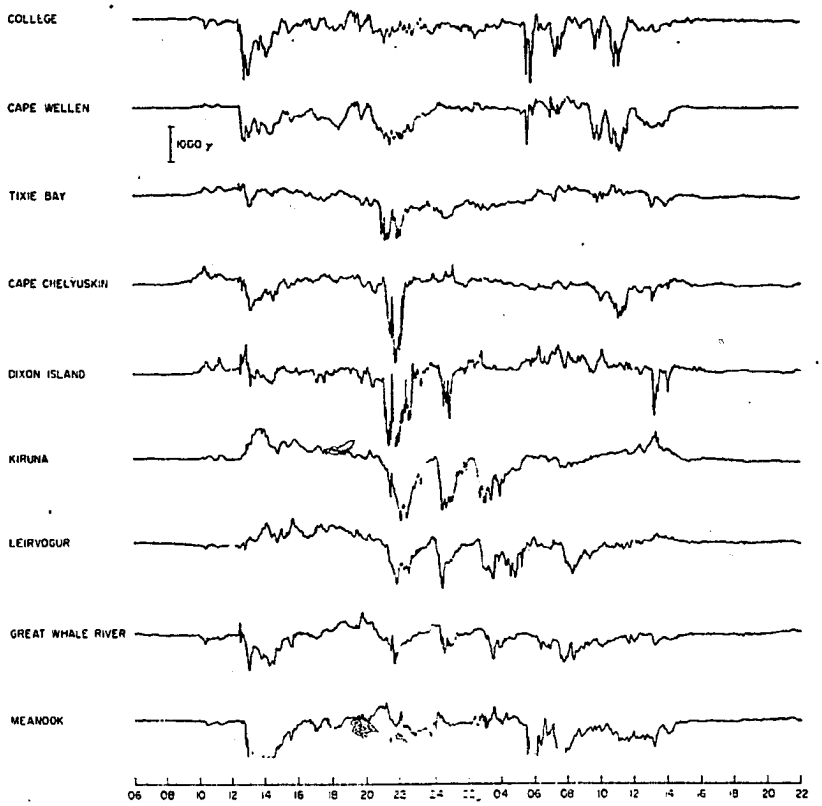

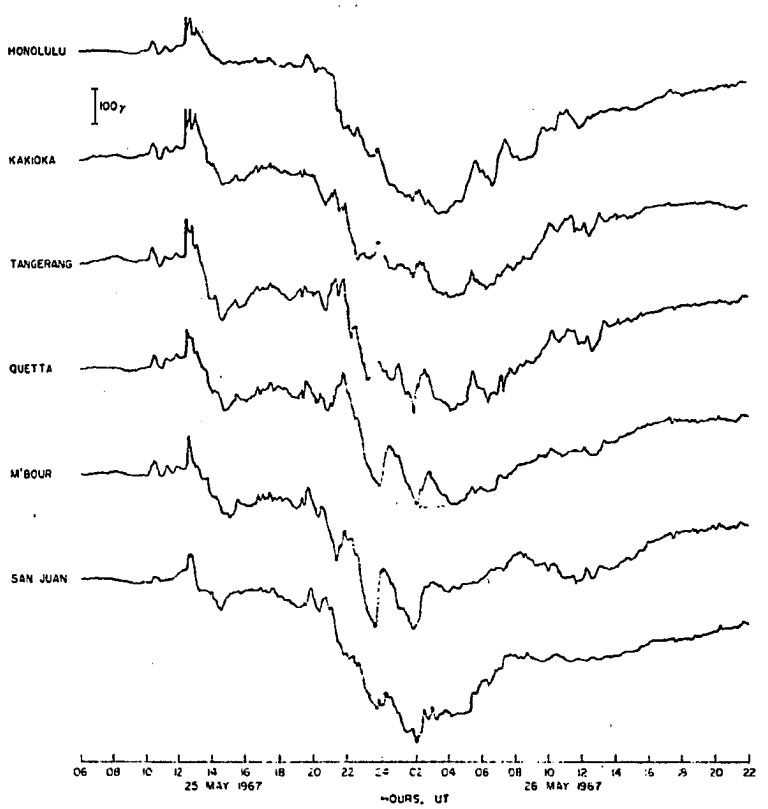

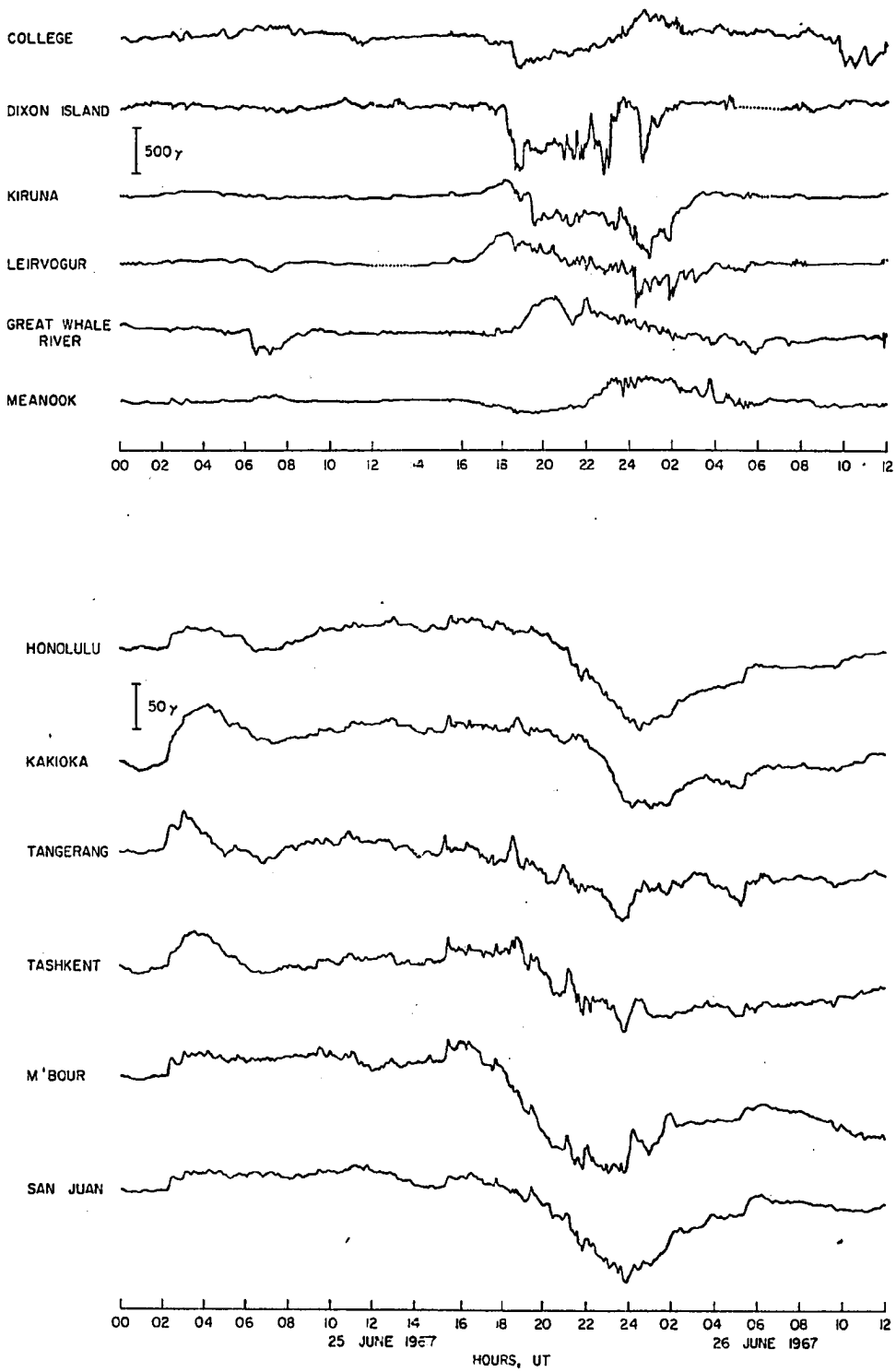

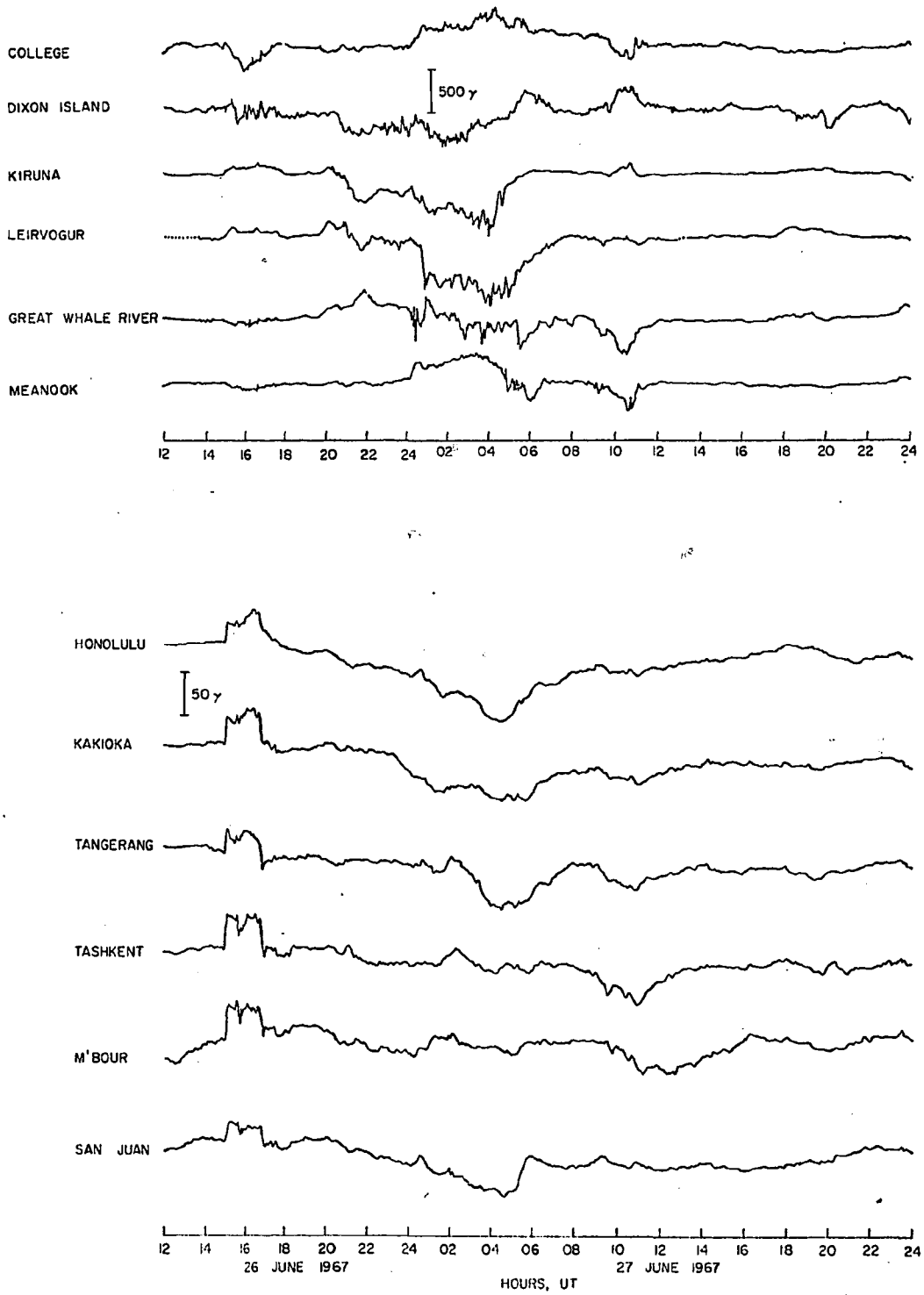

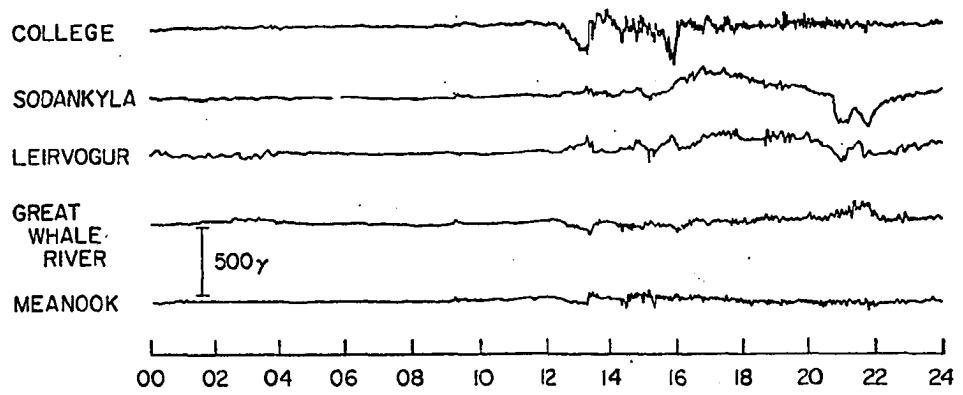

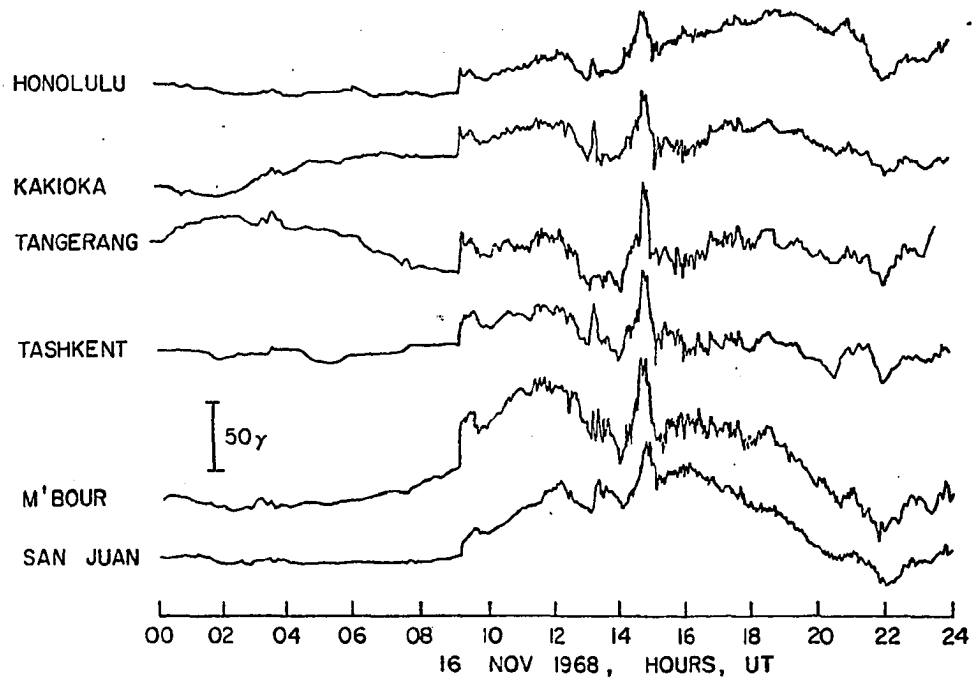

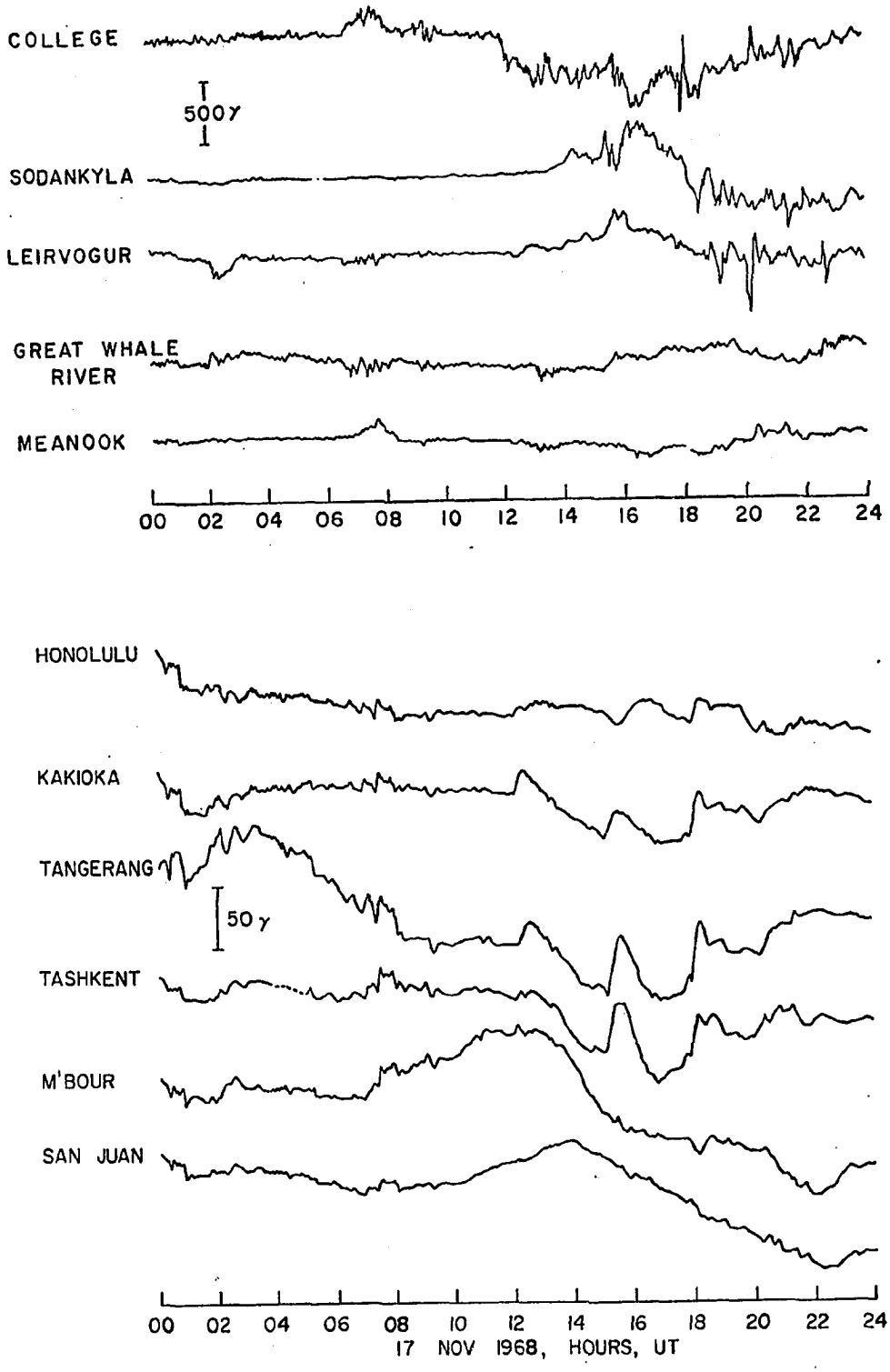

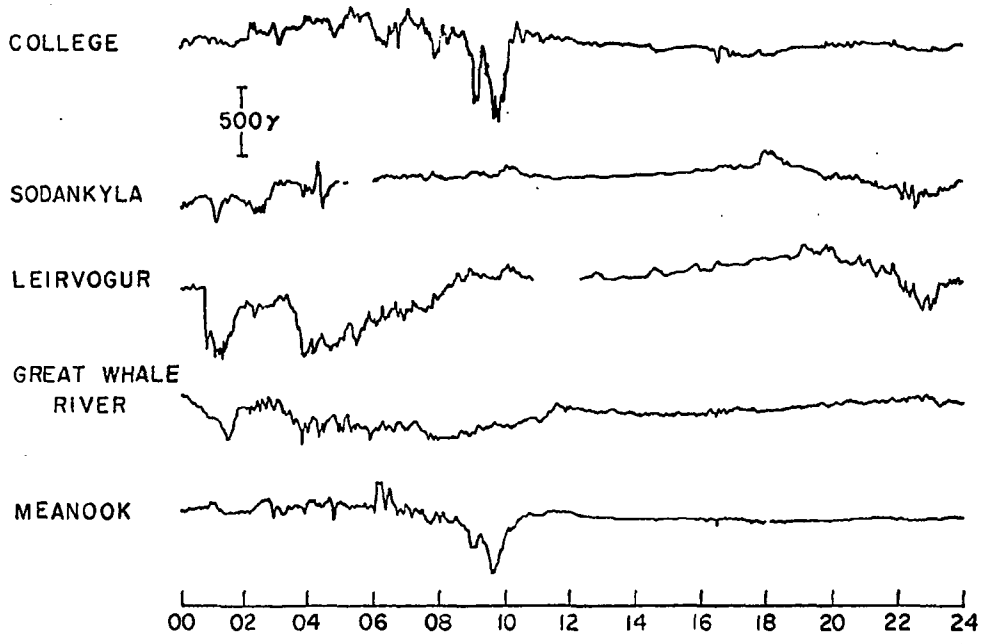

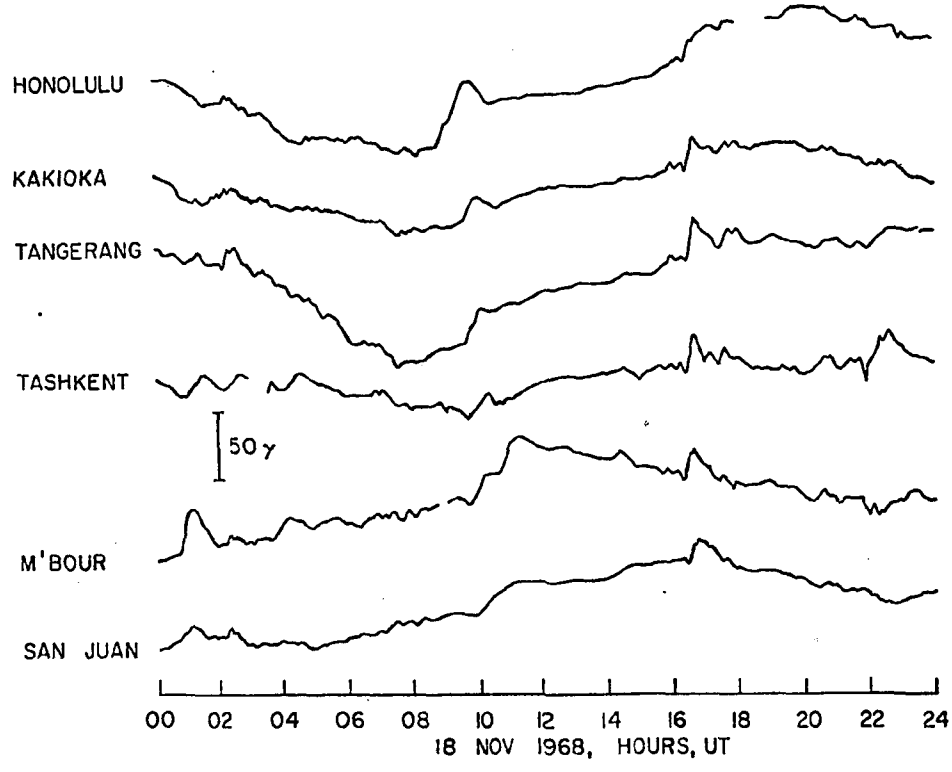

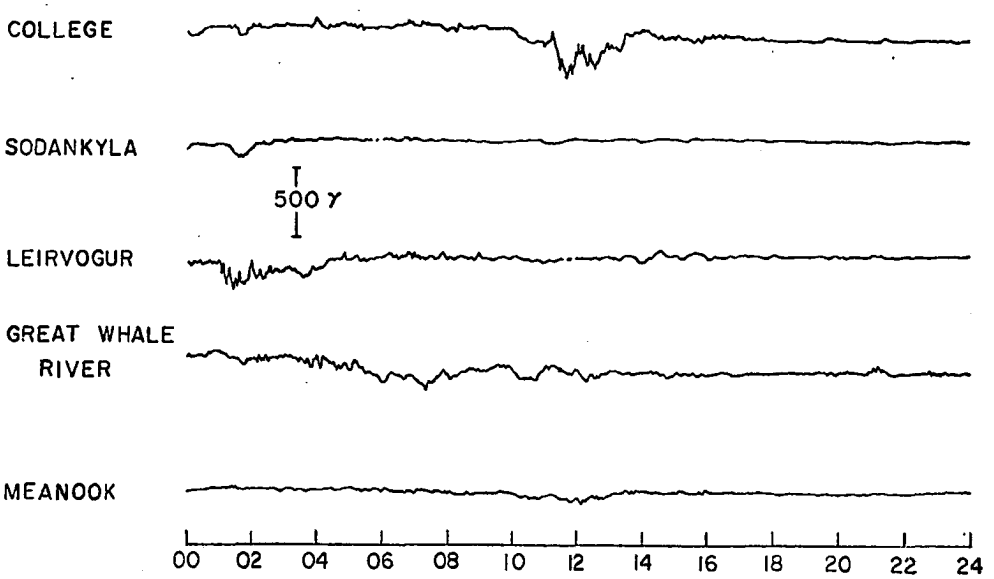

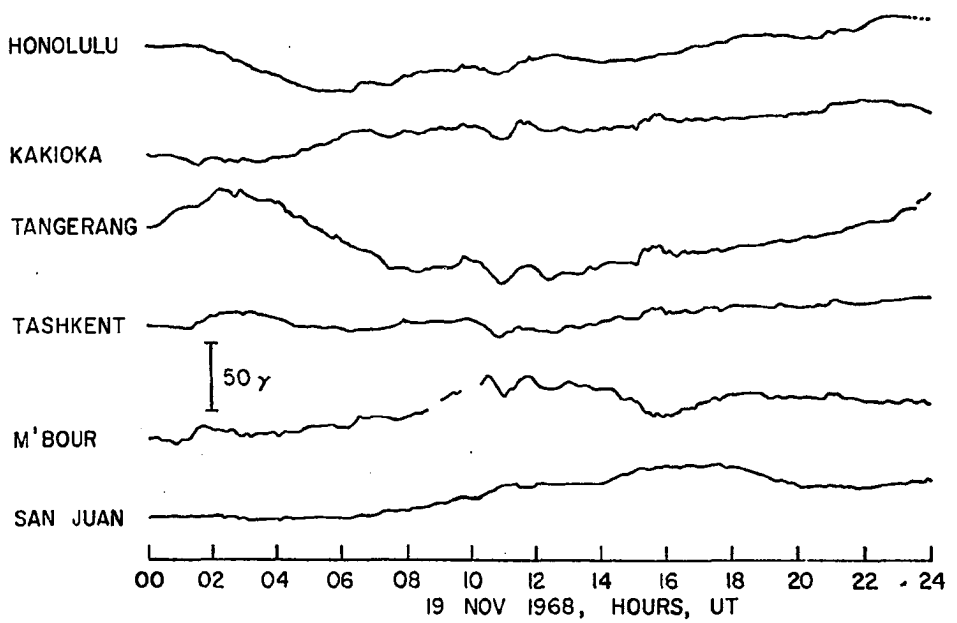

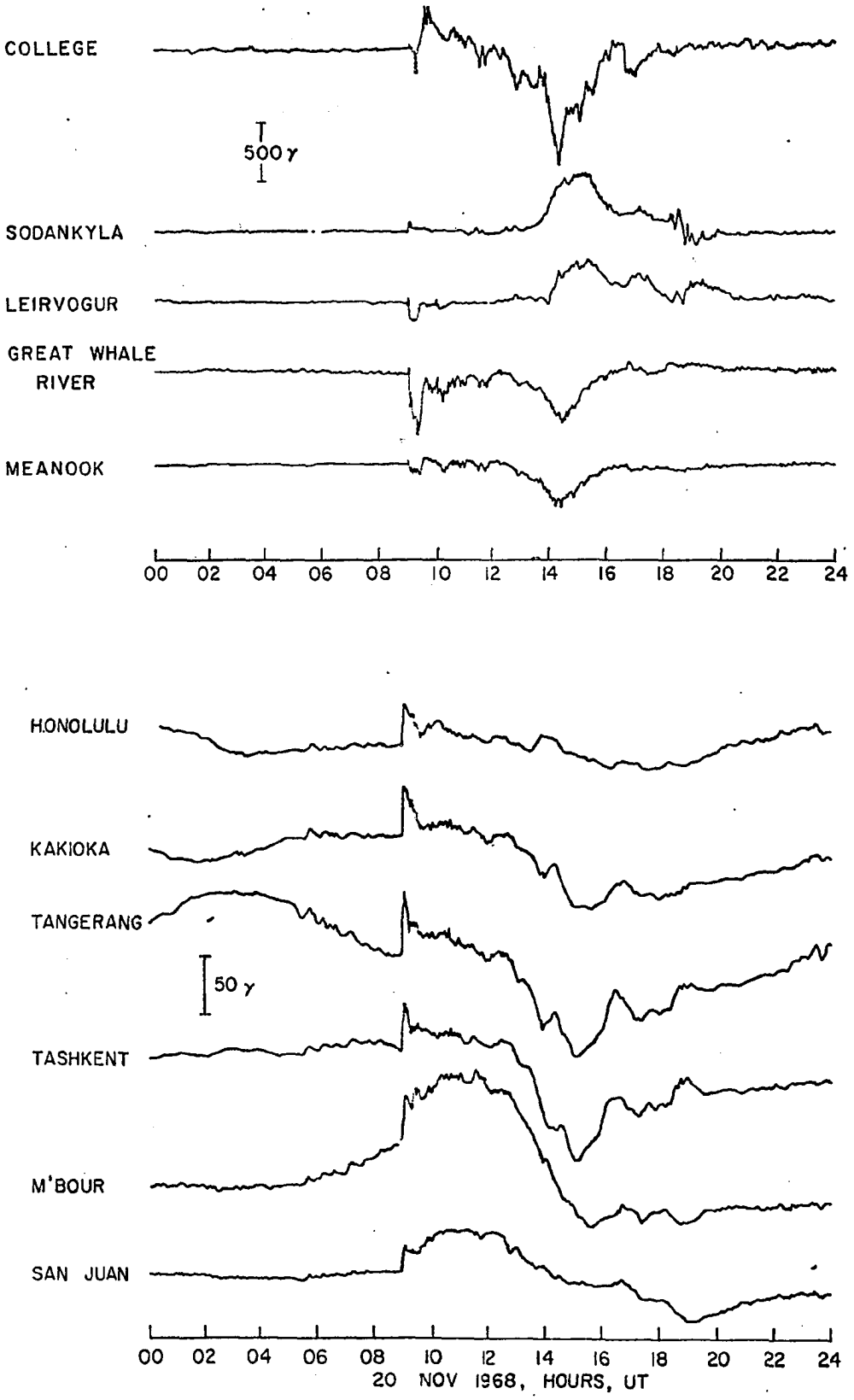

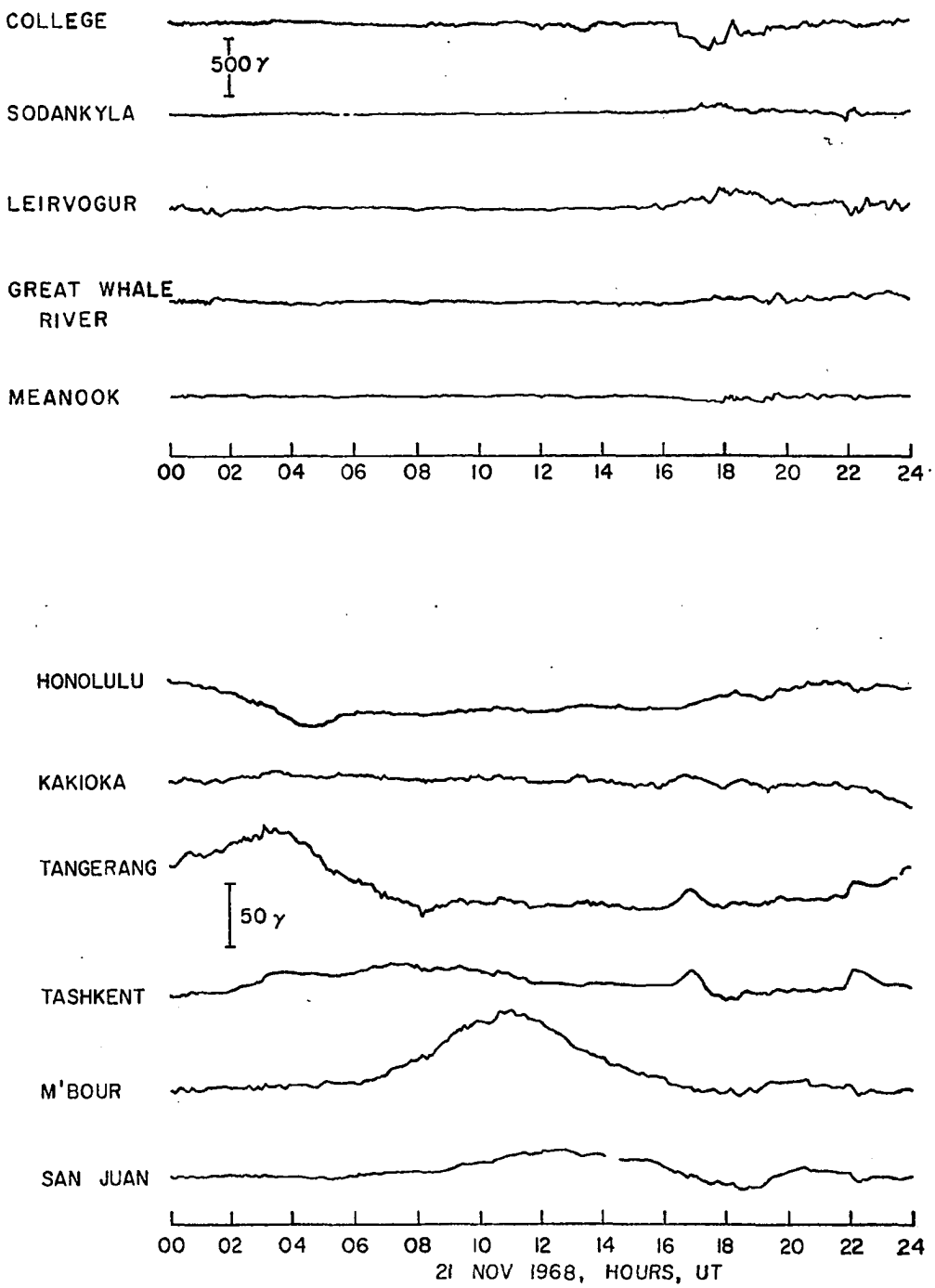

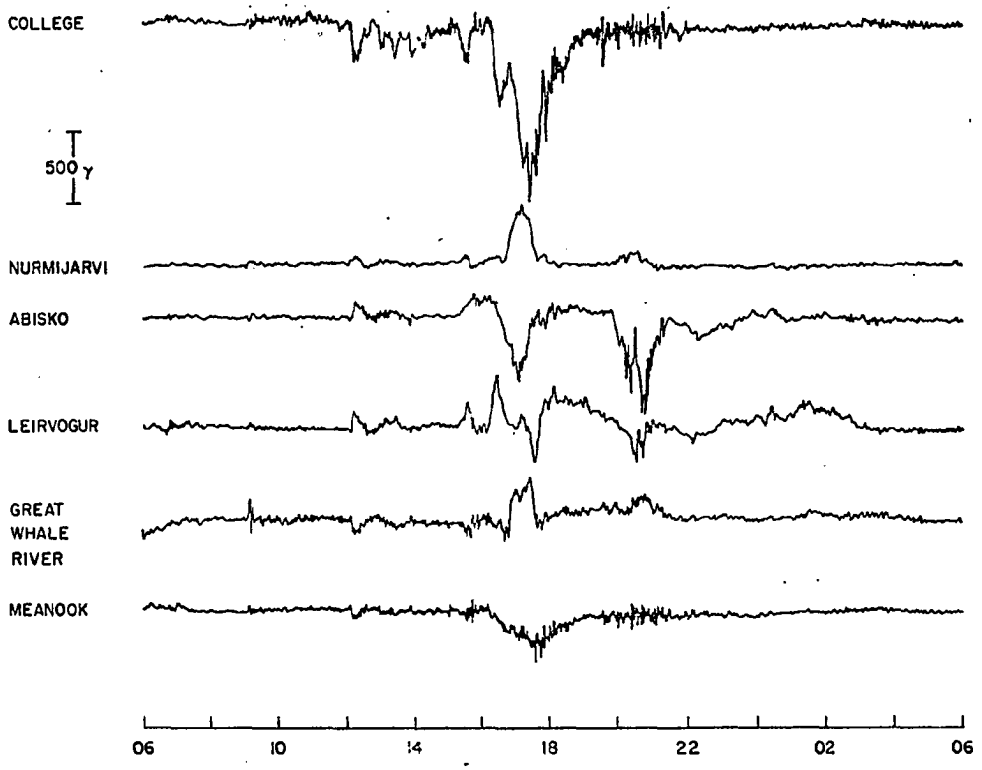

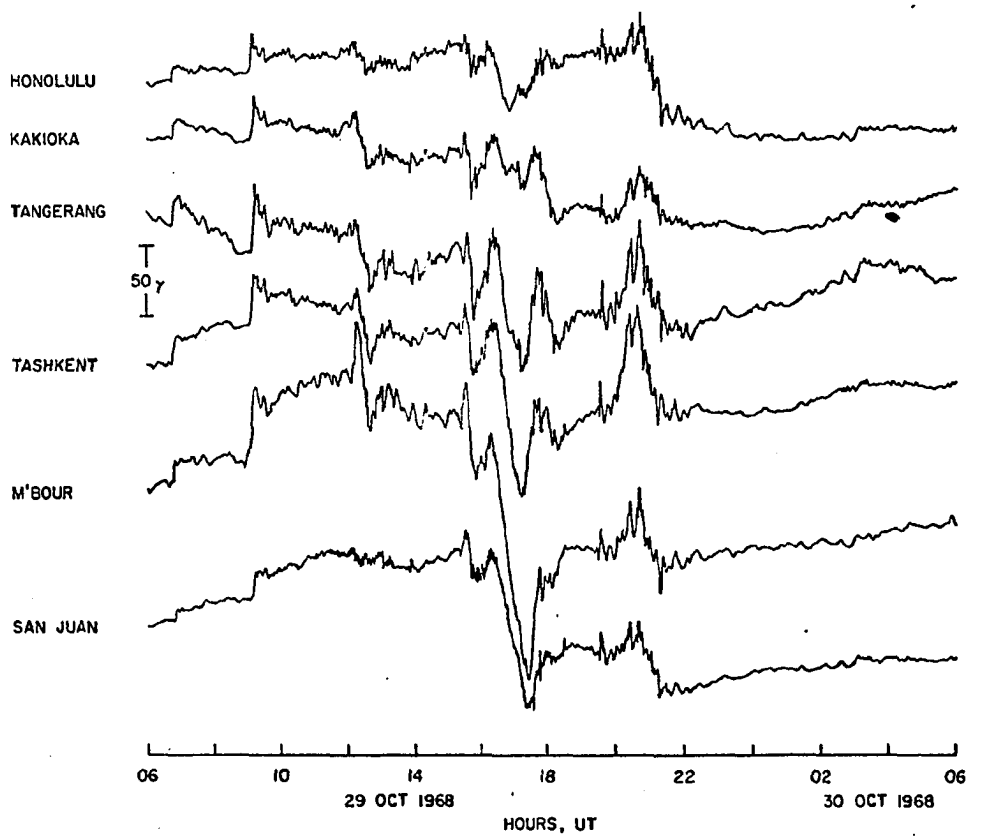

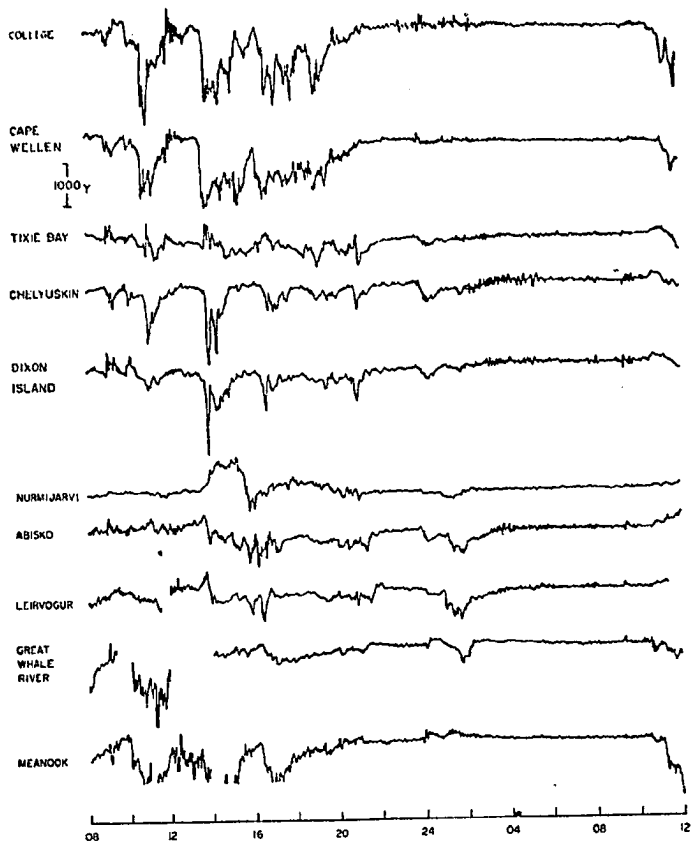

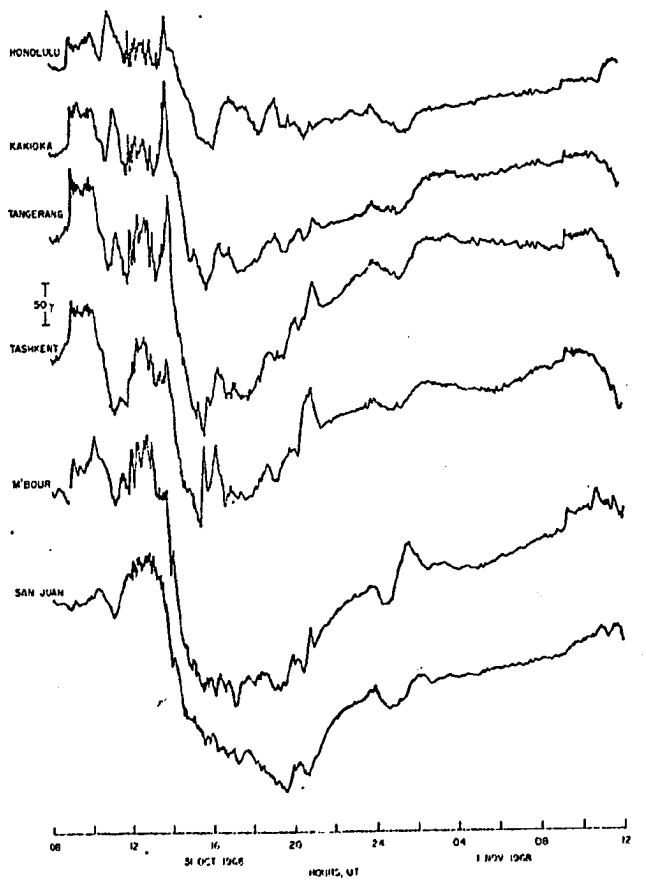

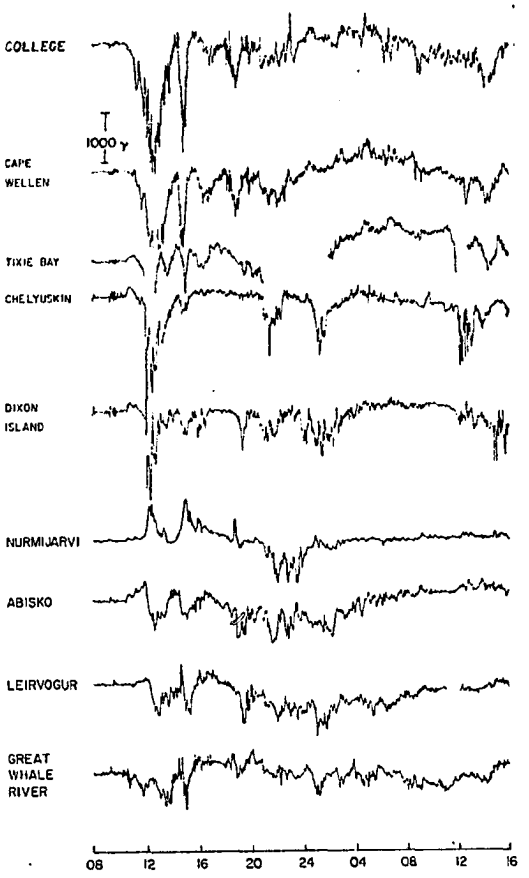

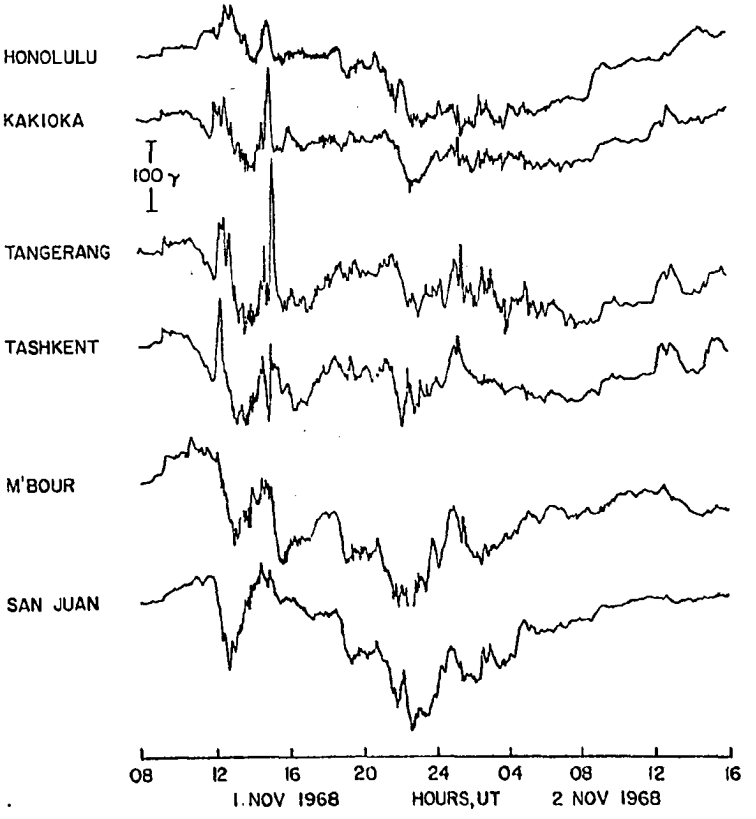

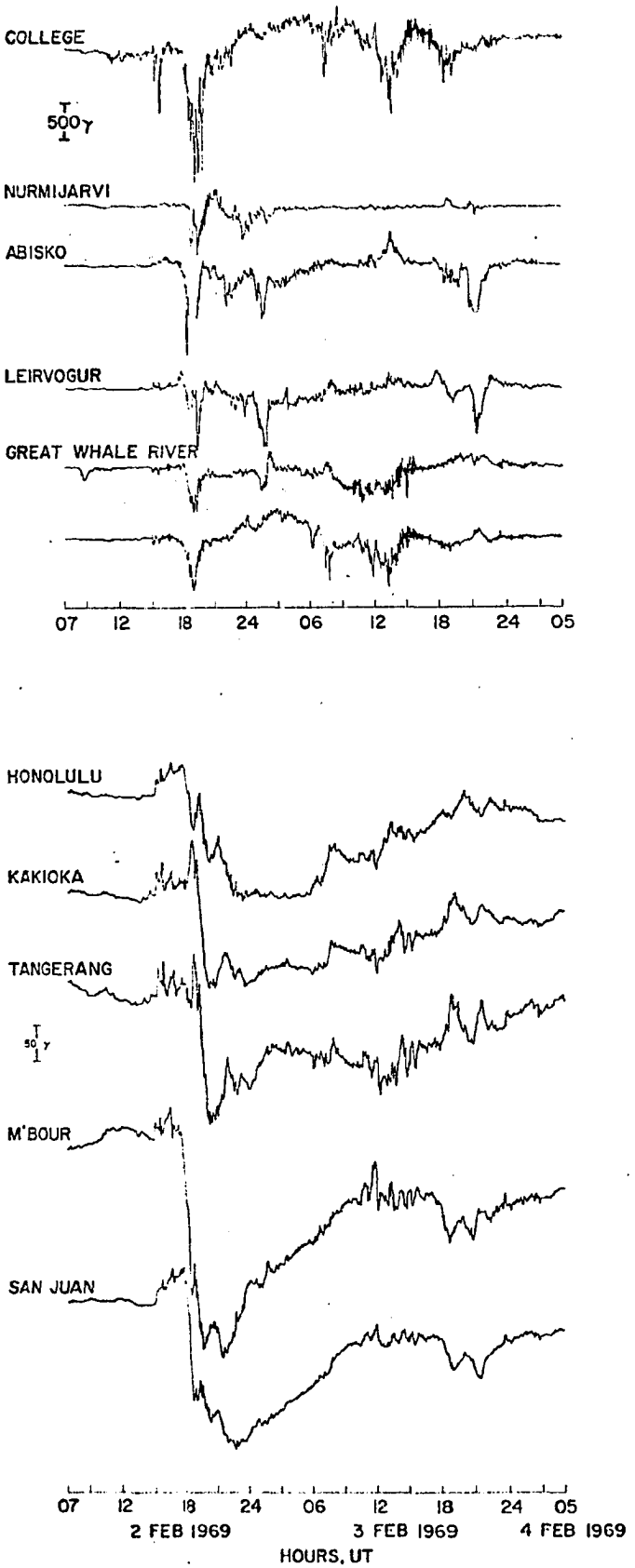

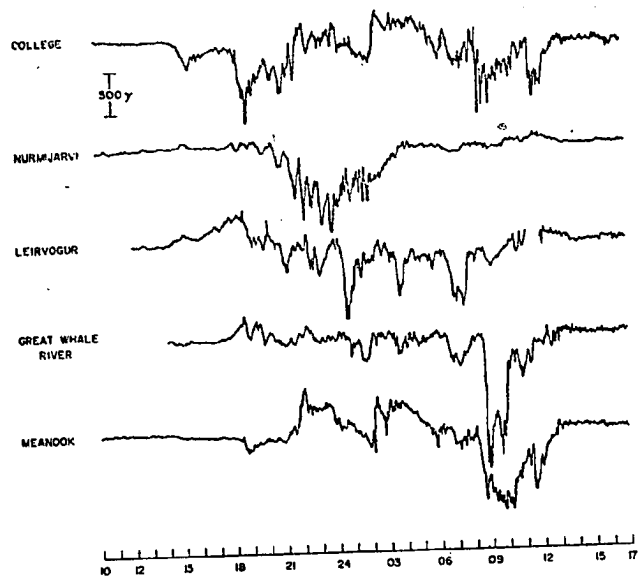

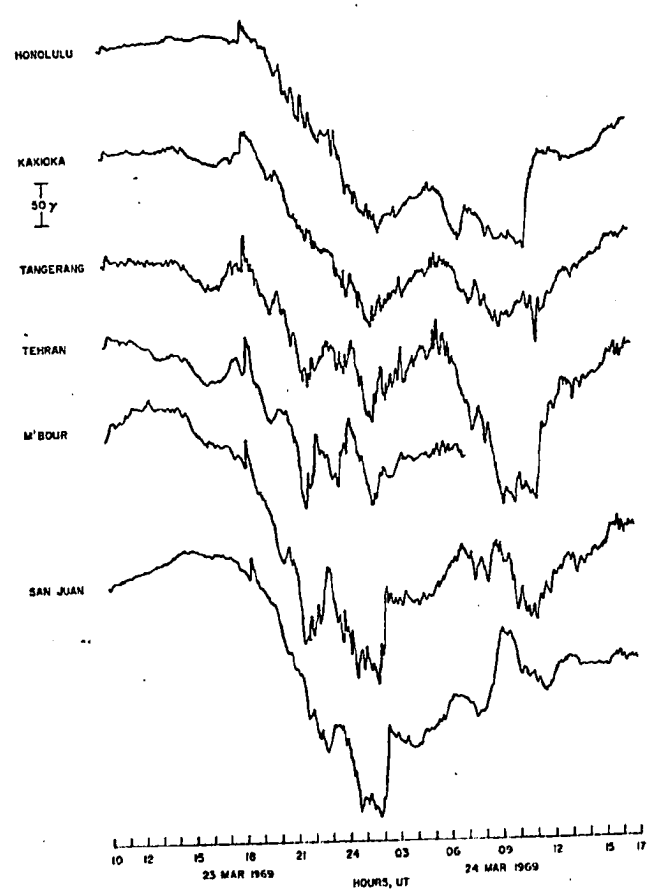

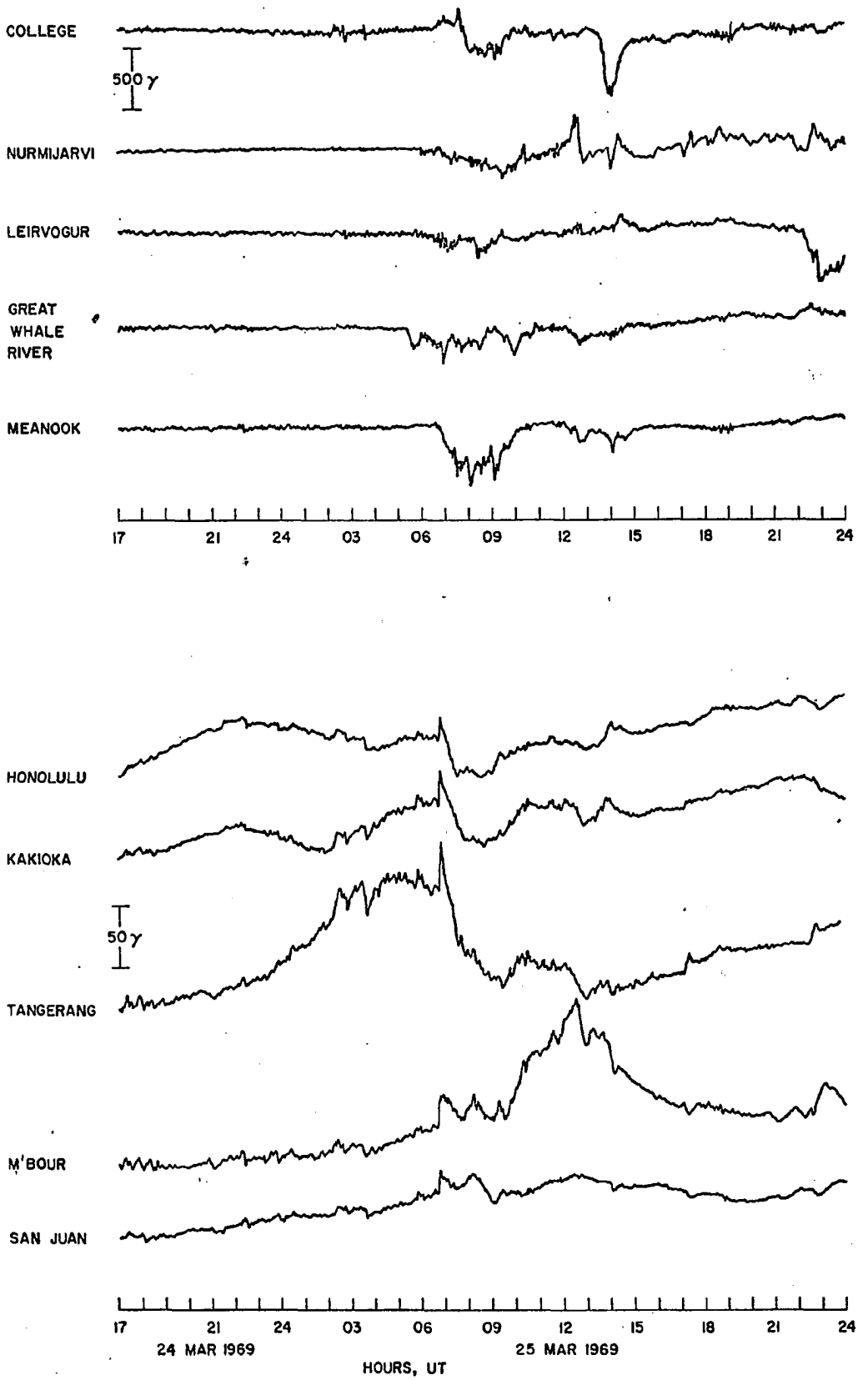

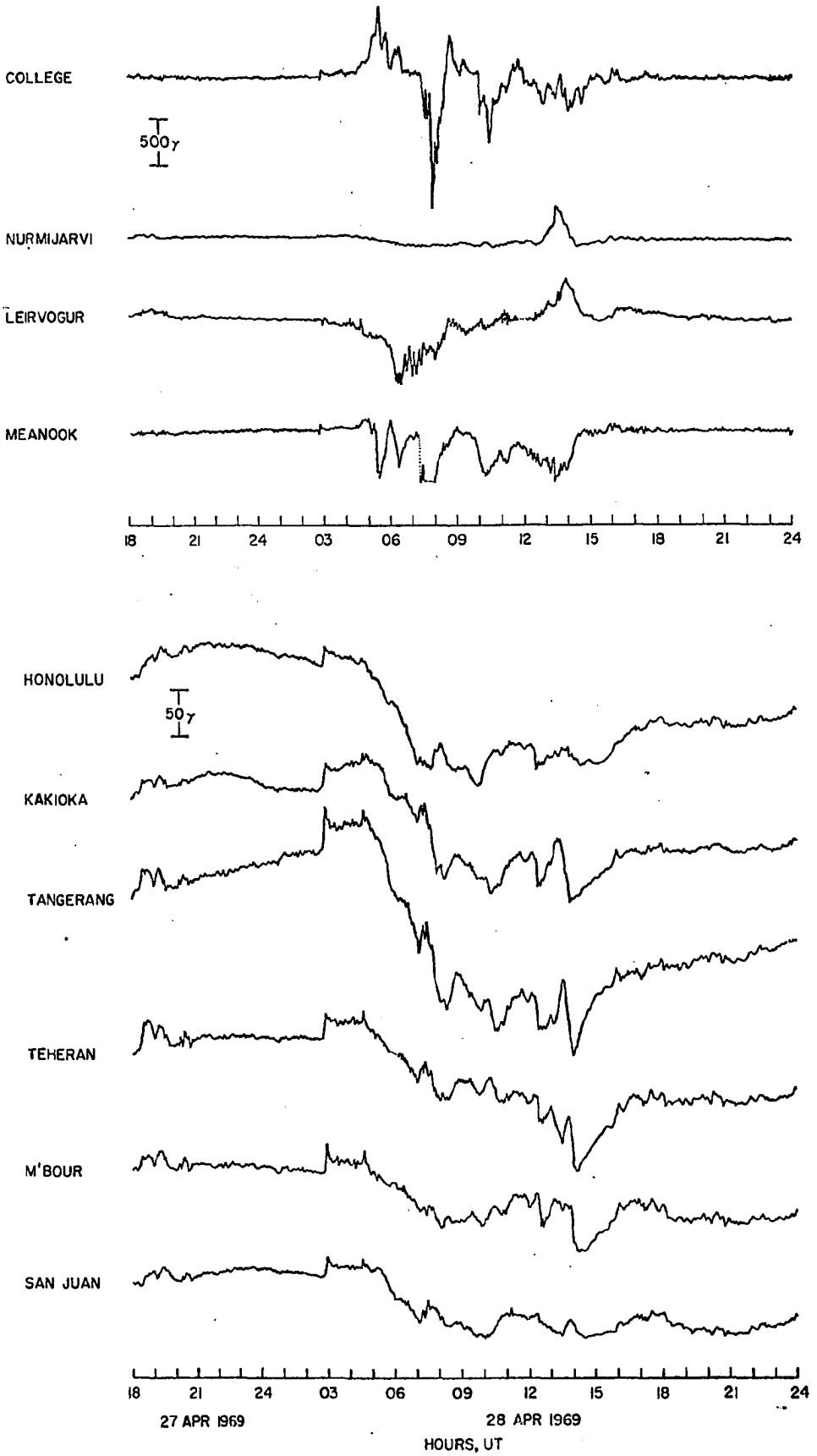

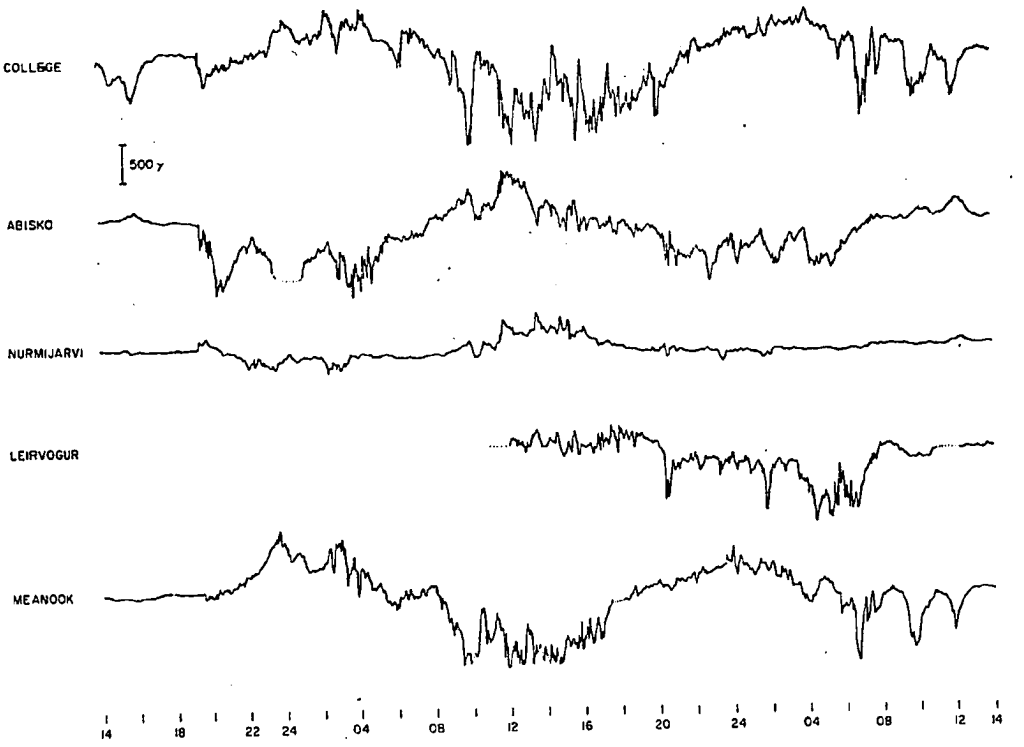

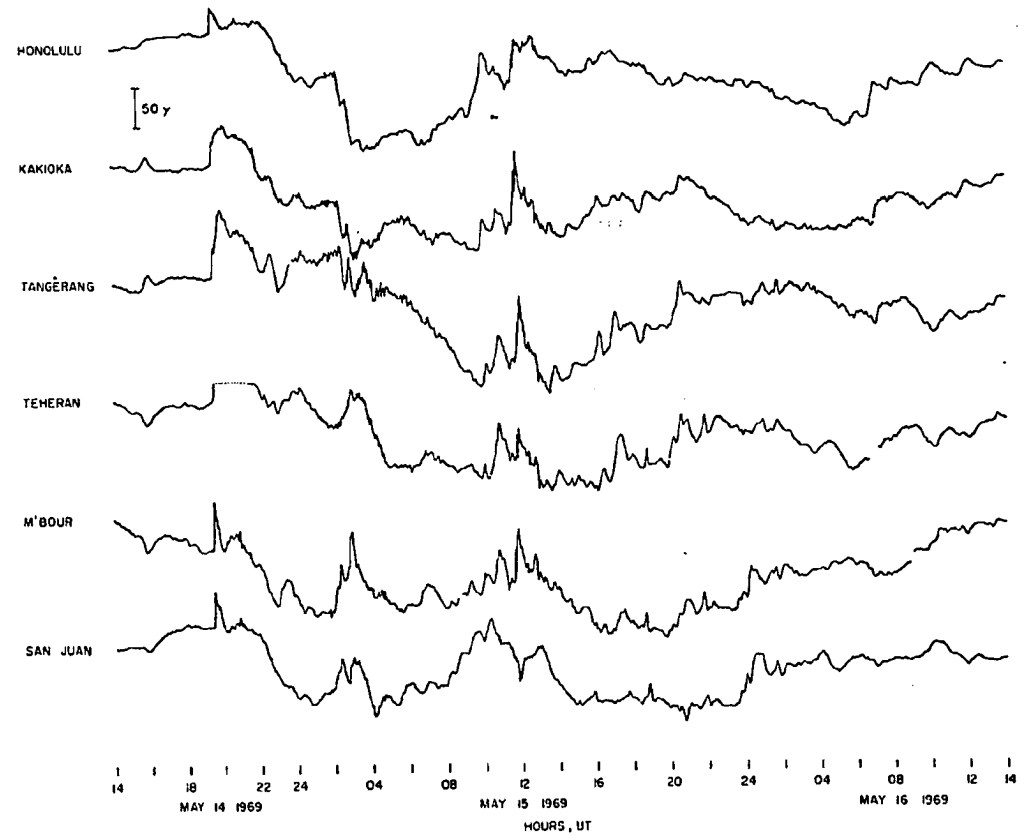

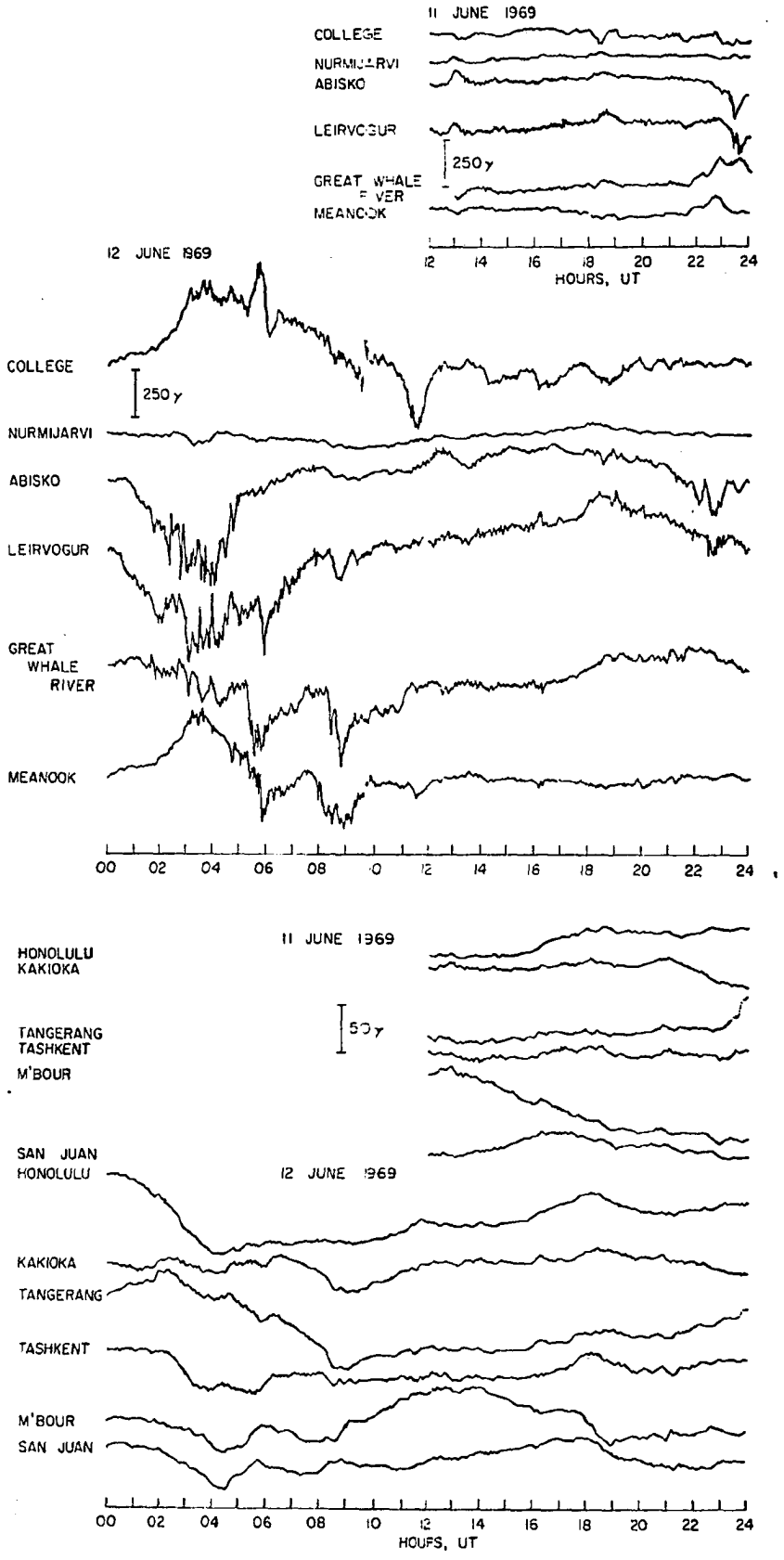

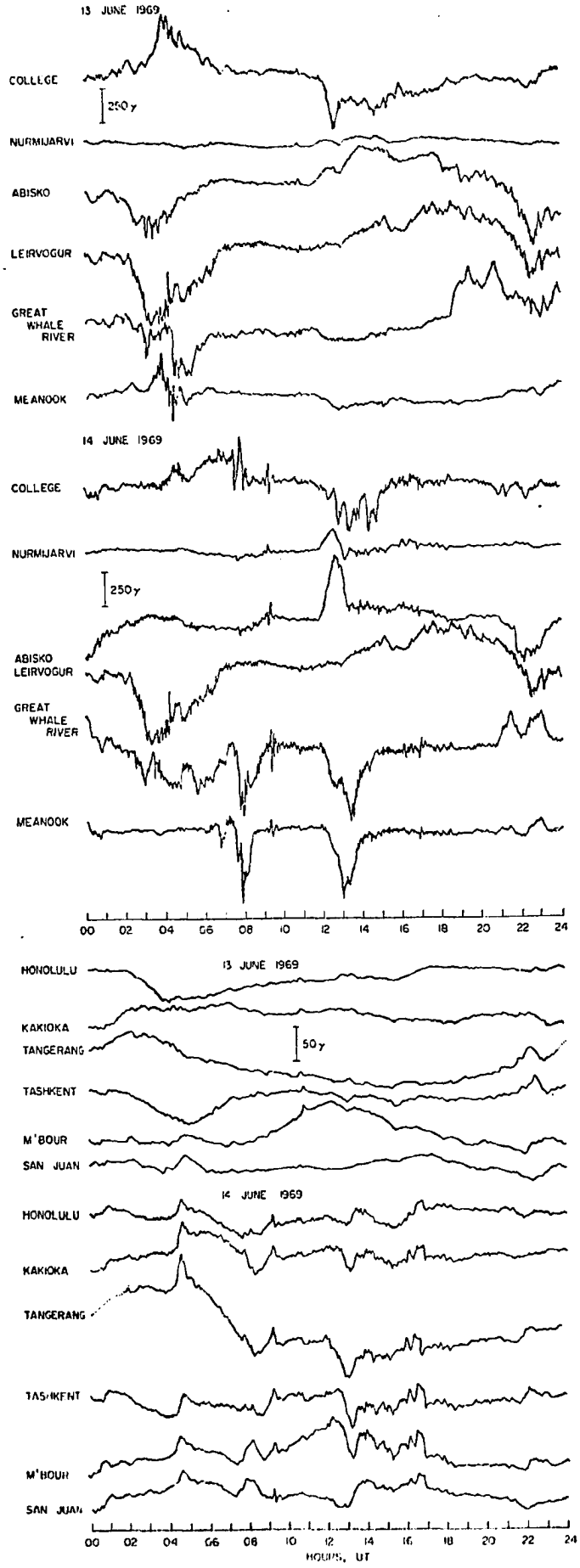

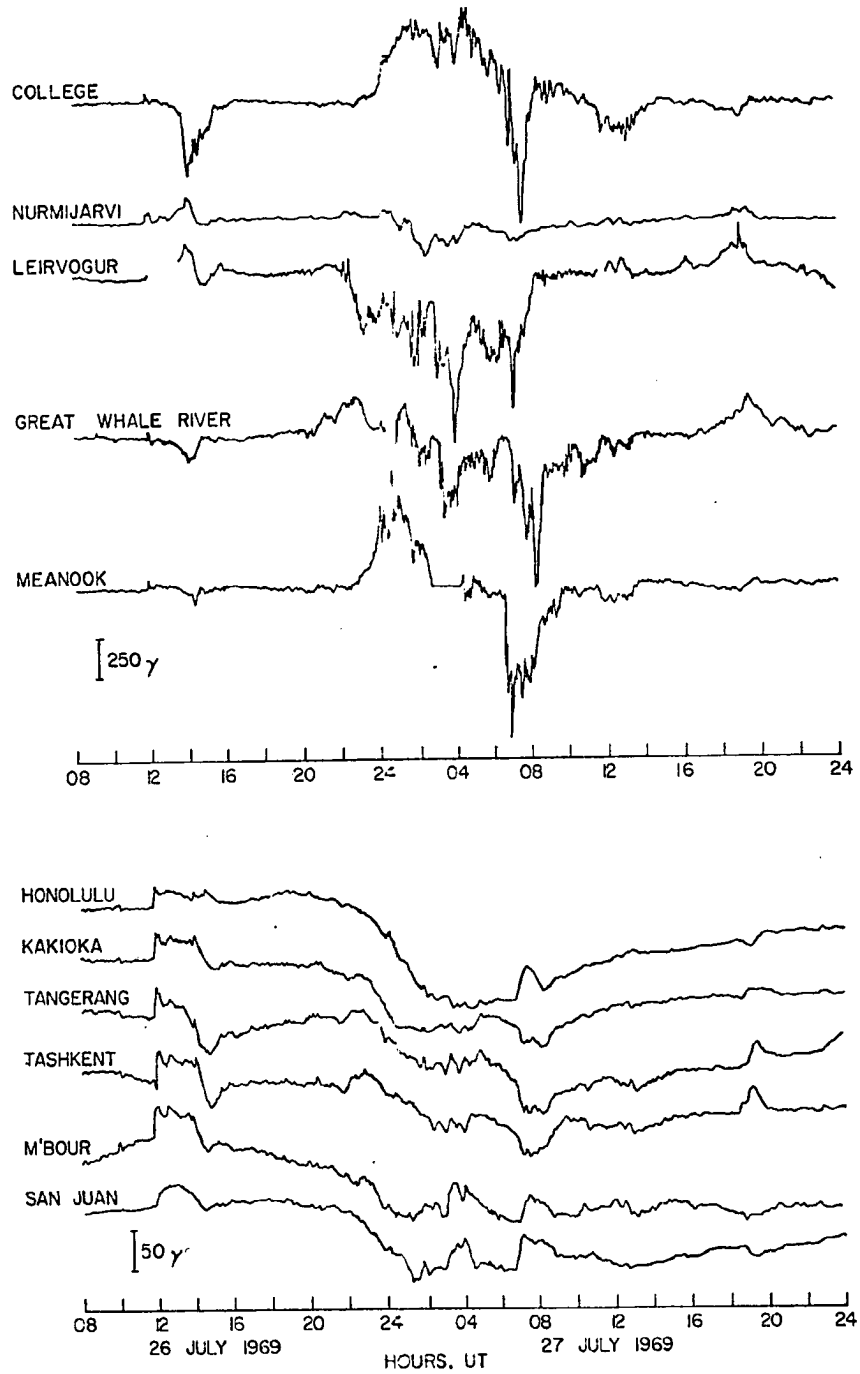

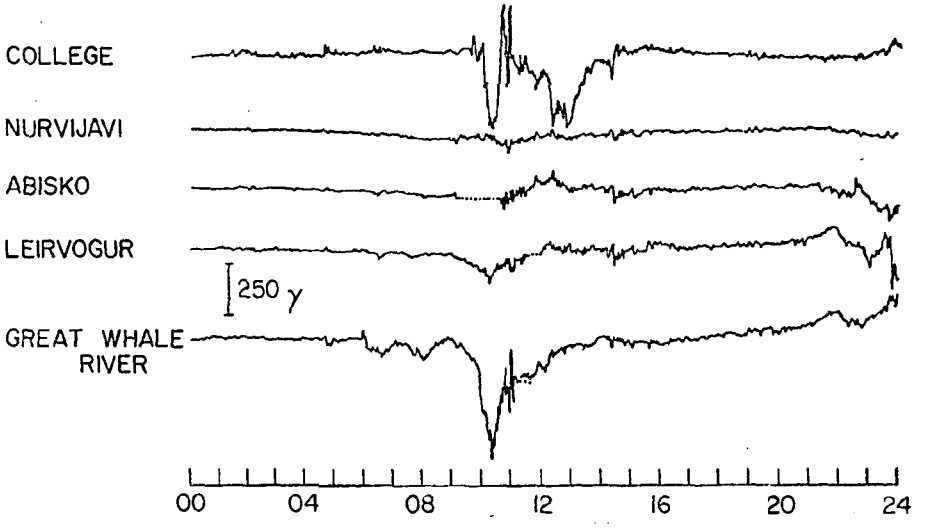

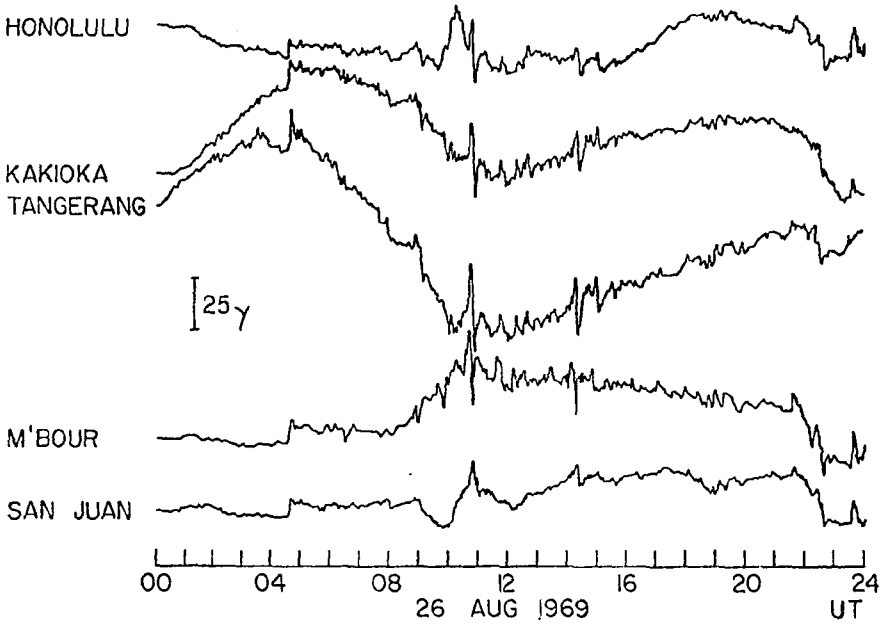

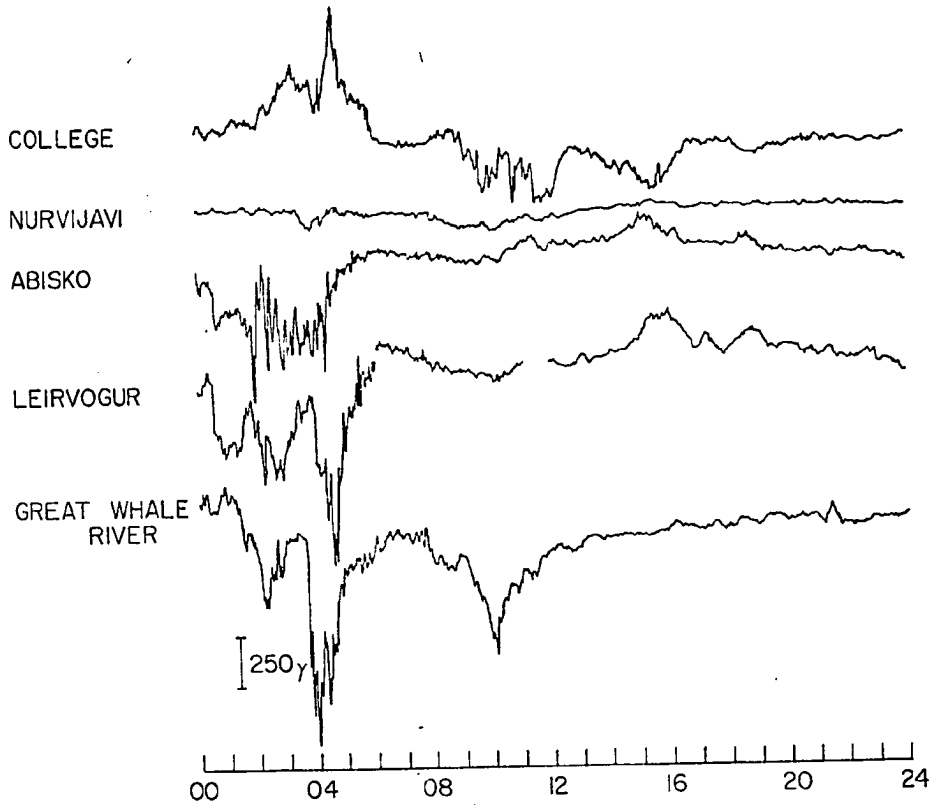

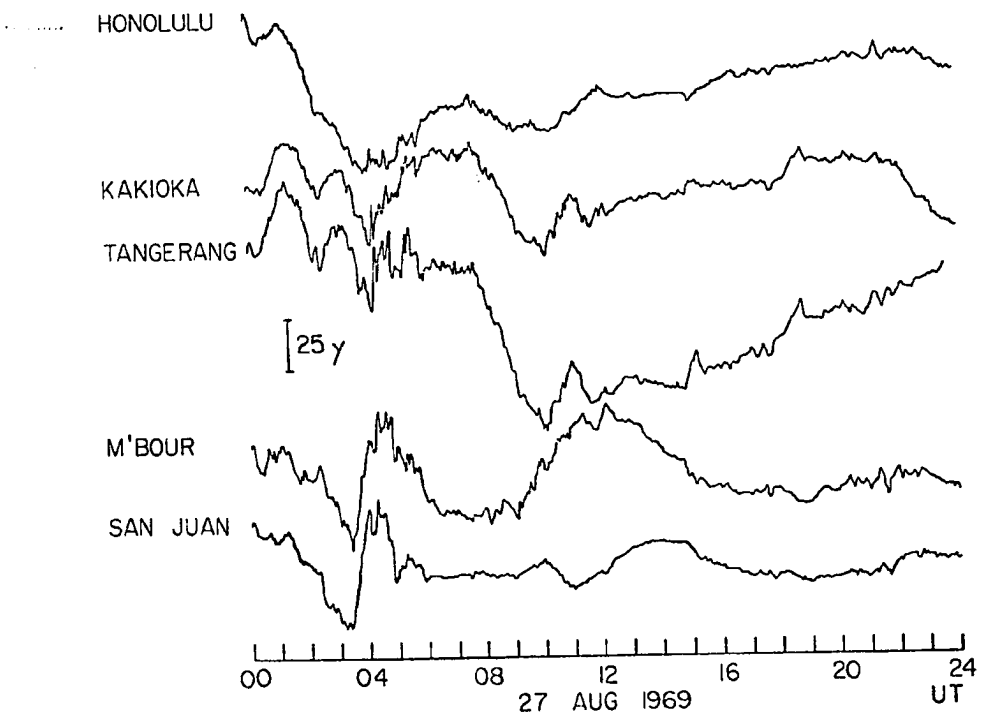

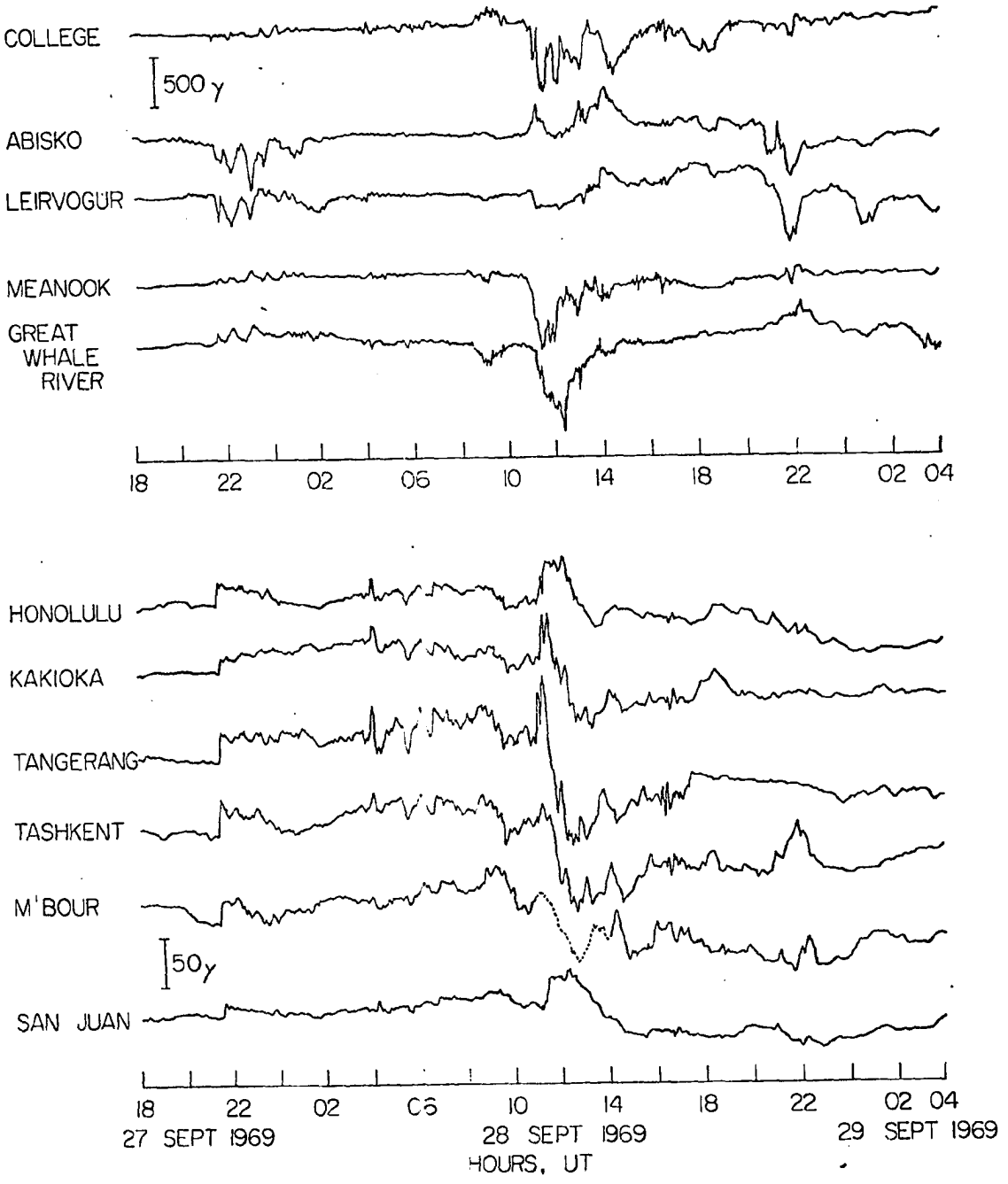

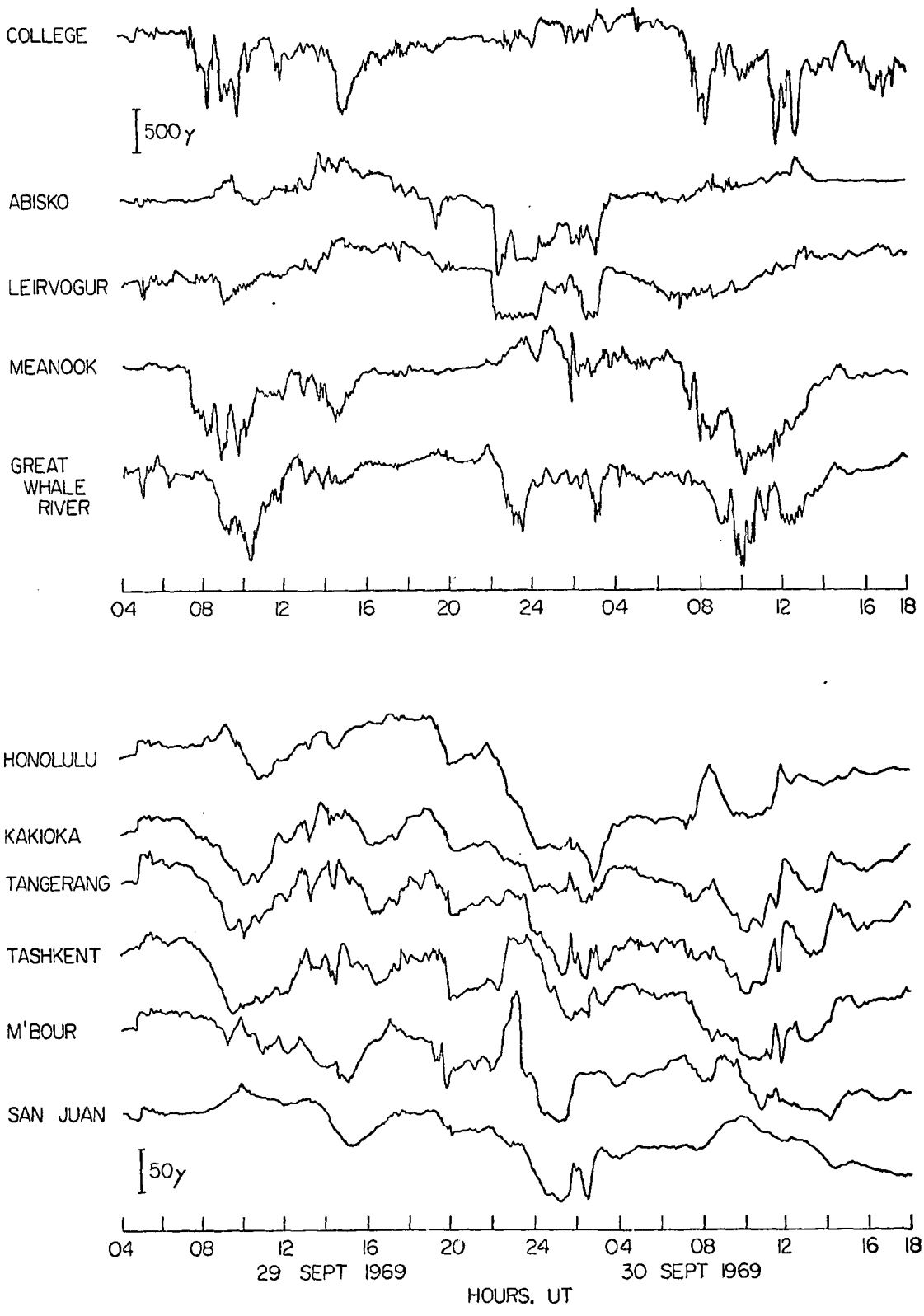

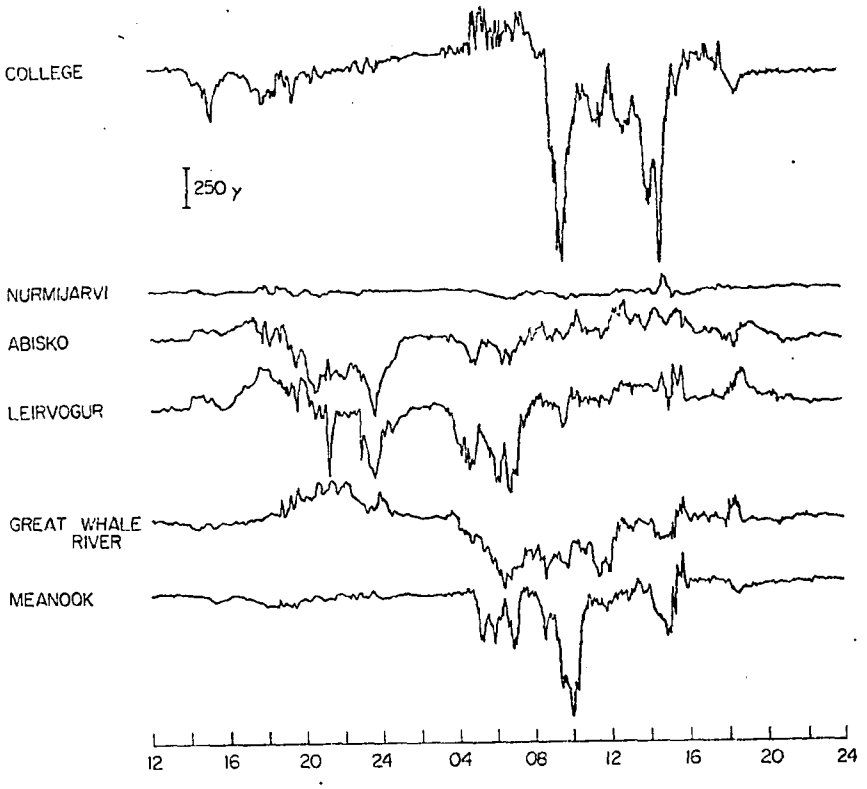

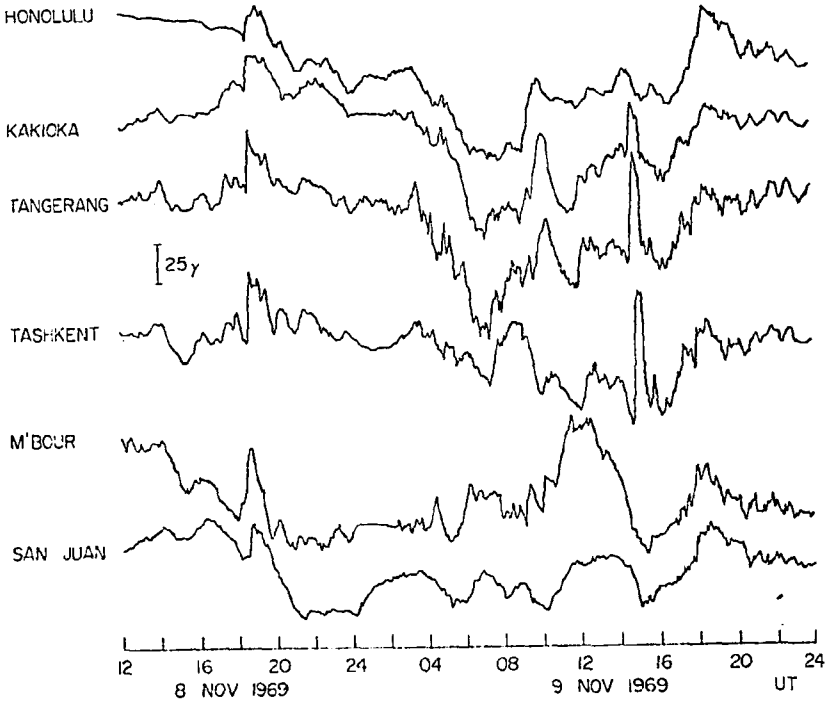

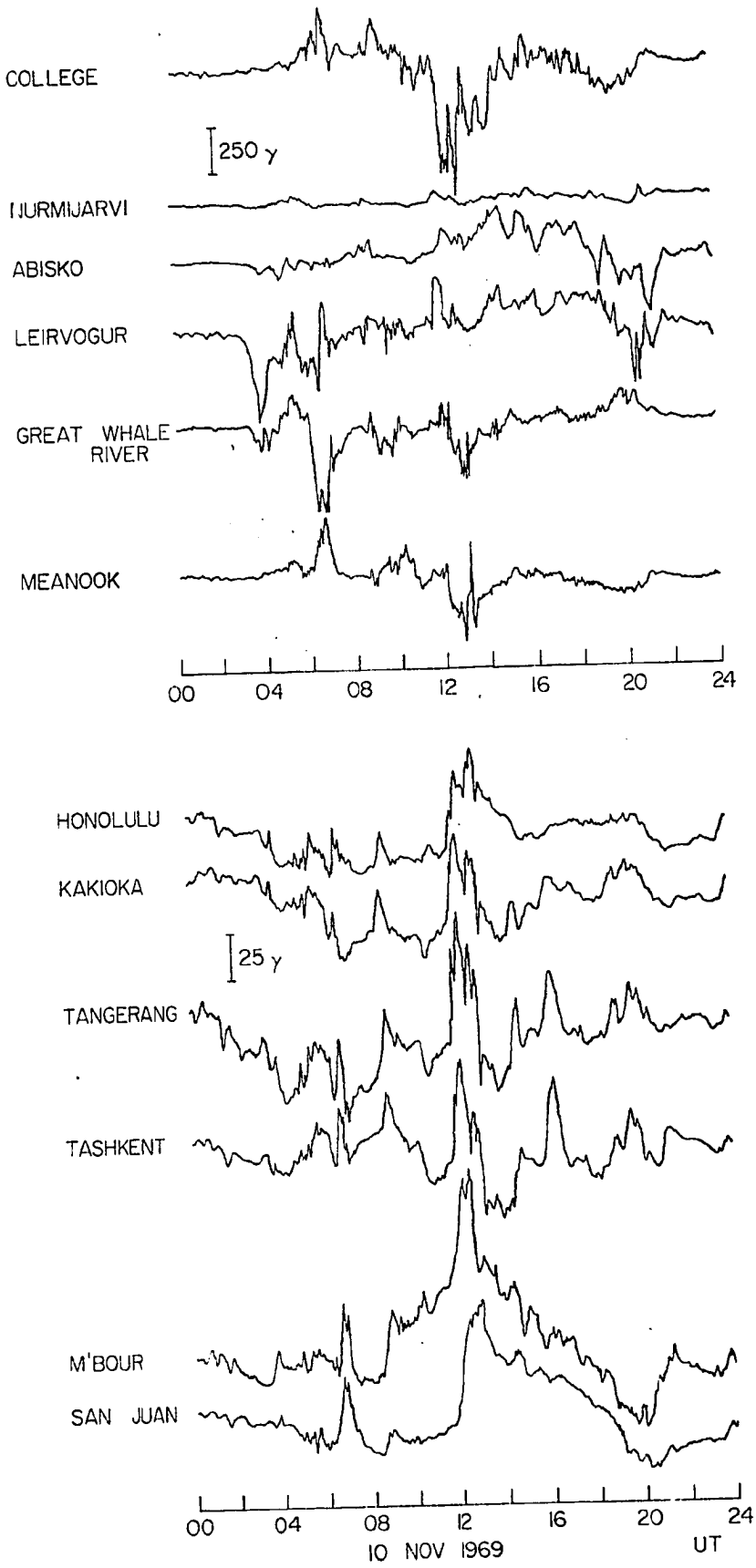

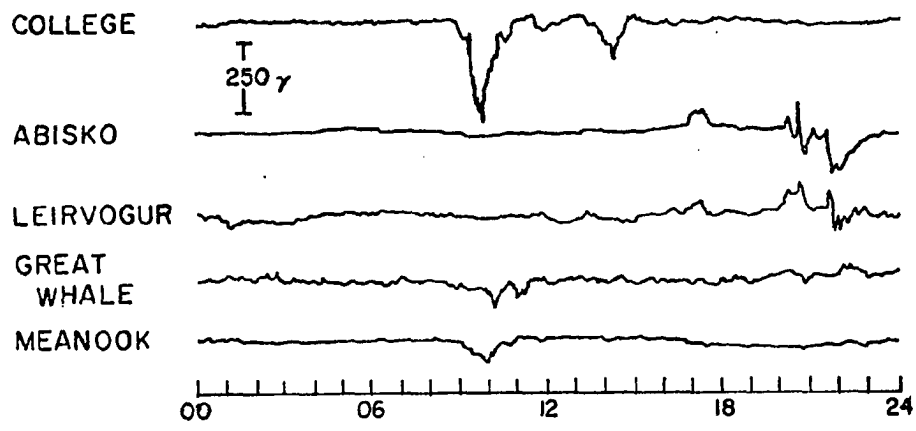

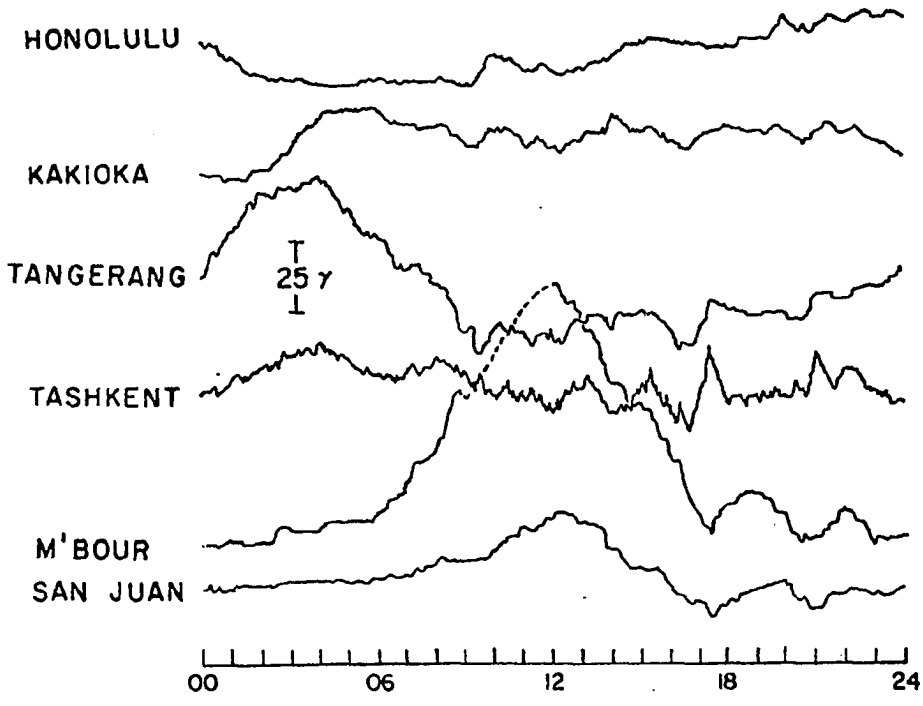

24 NOV 1969 HOURS, UT

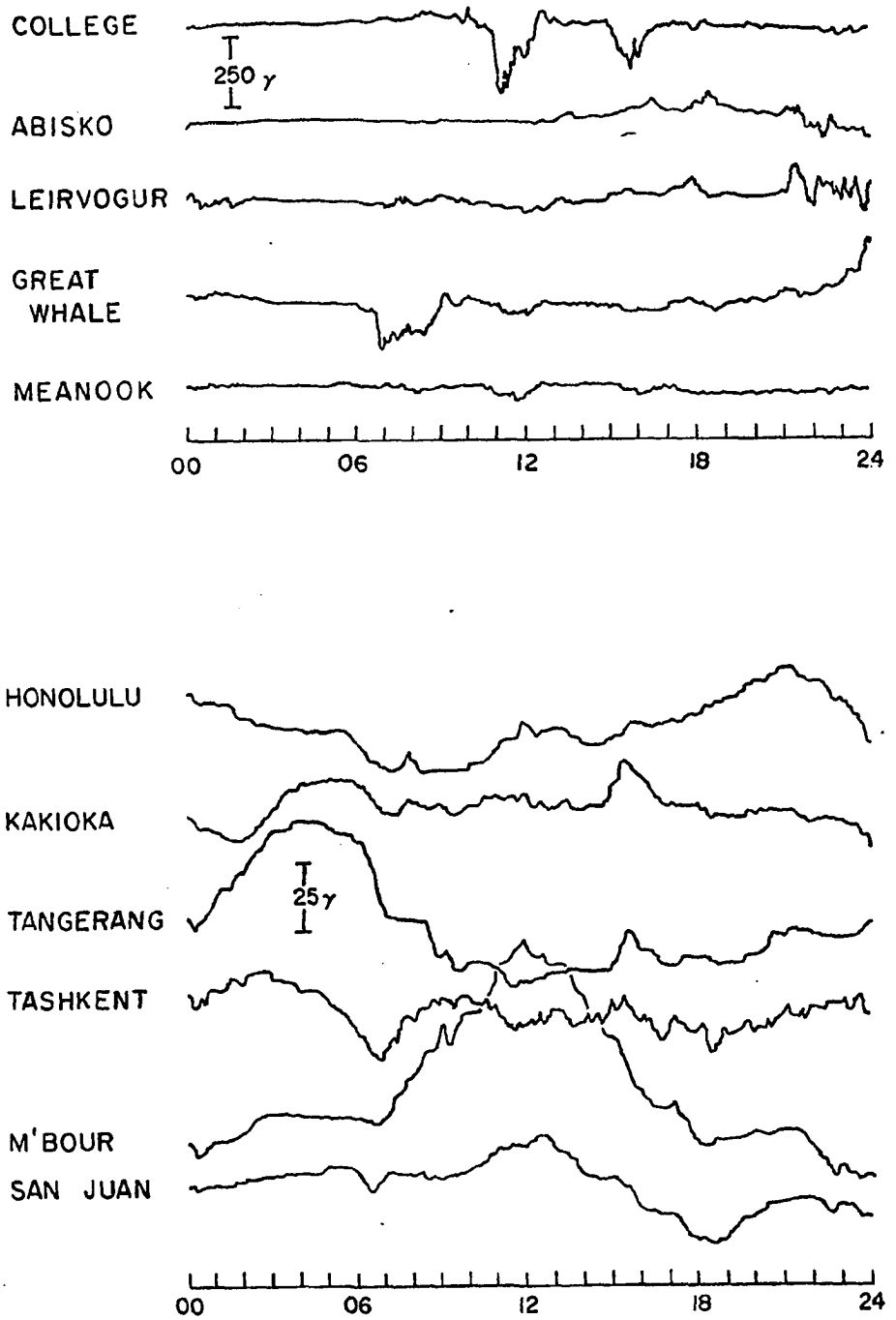

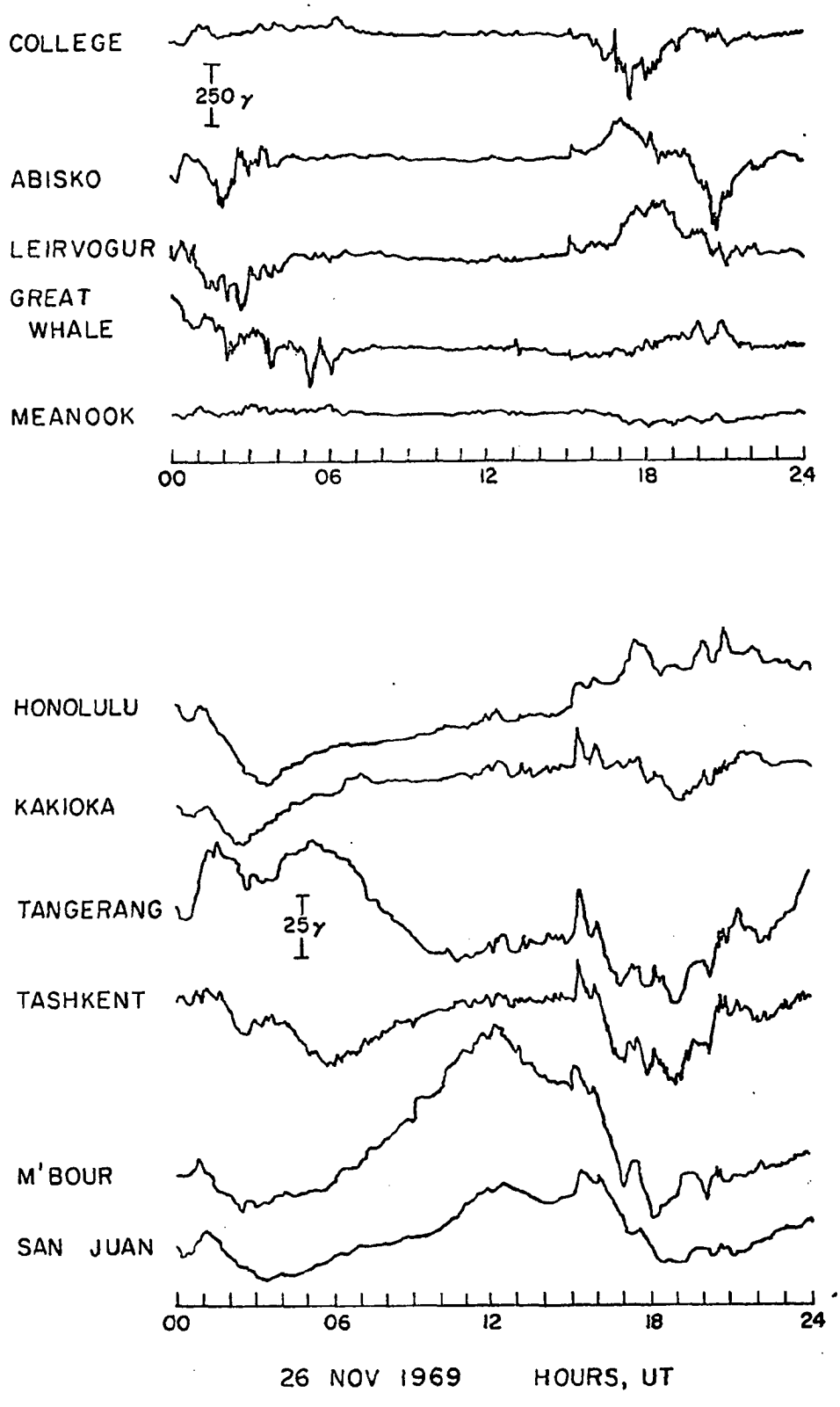

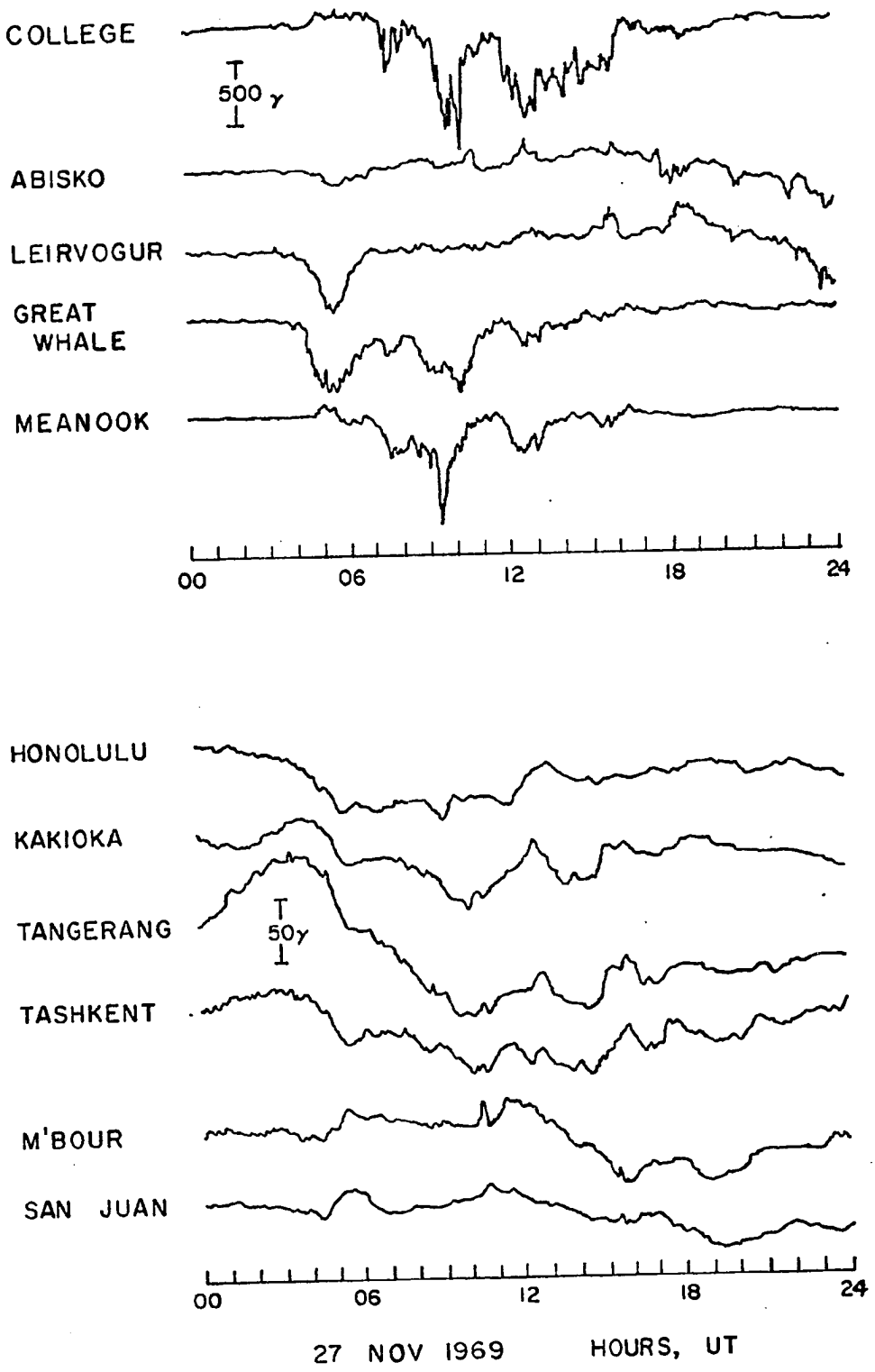

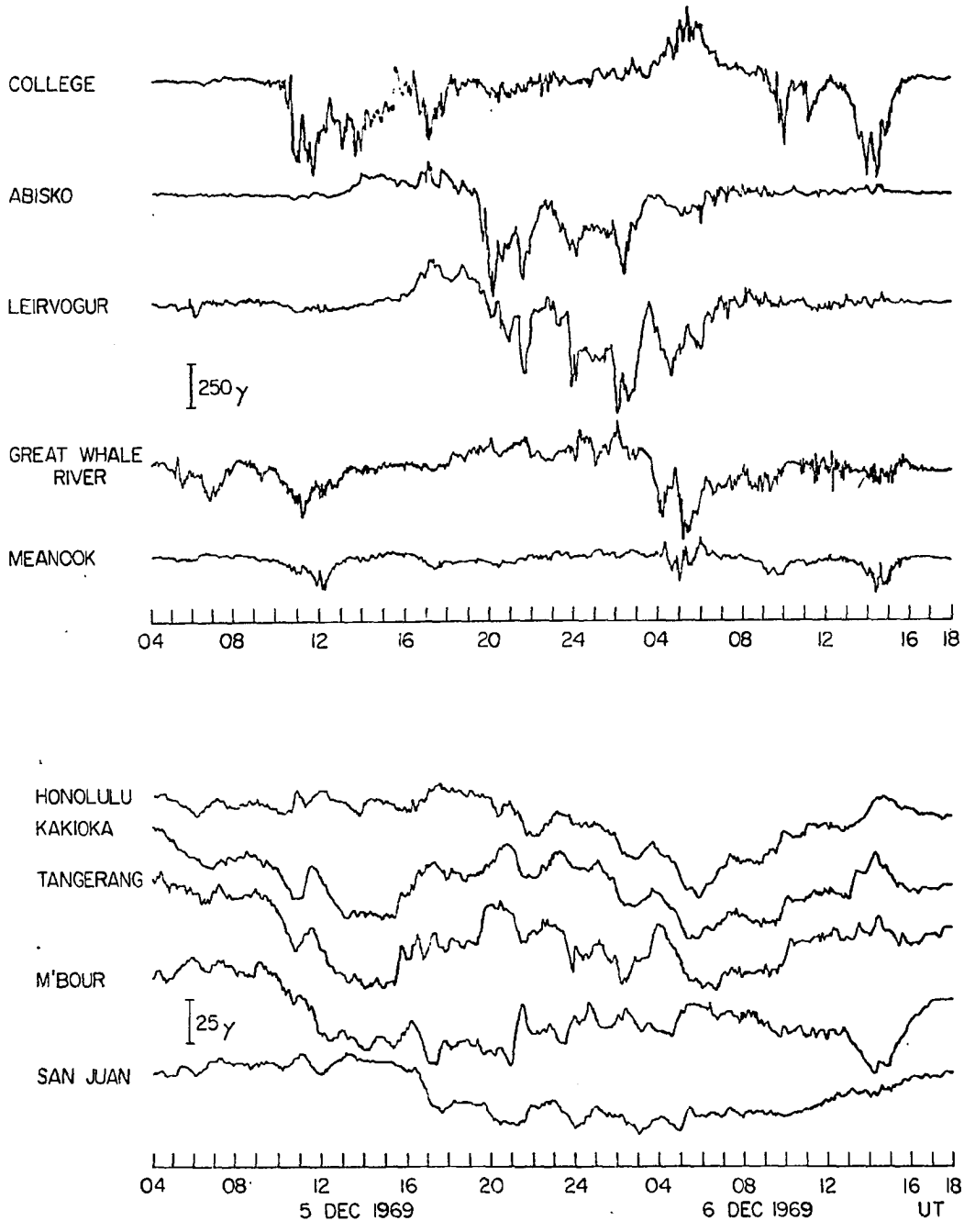

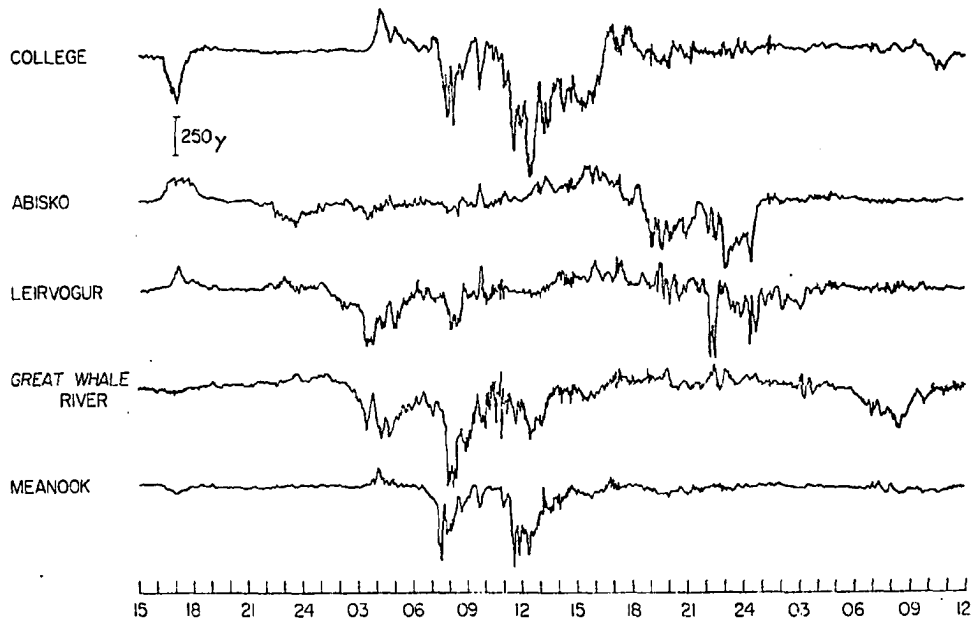

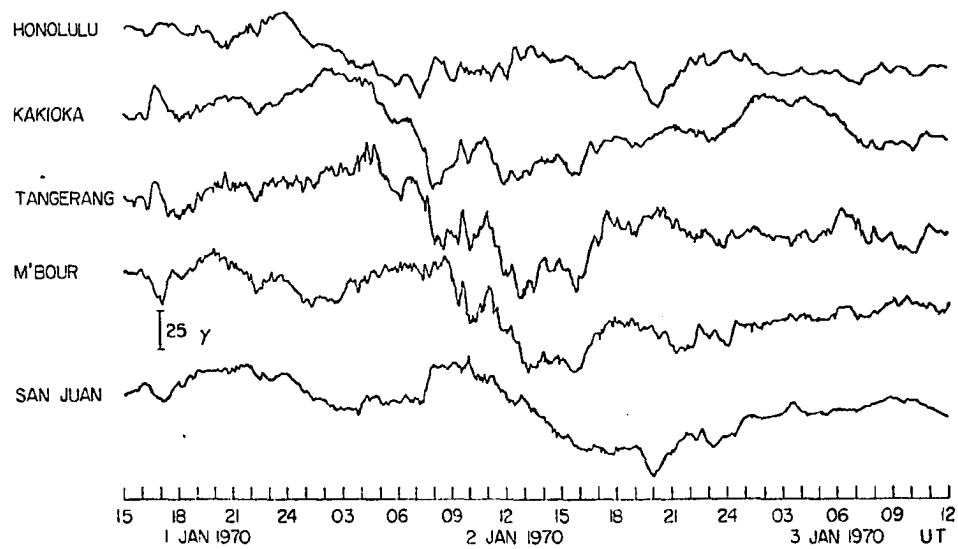

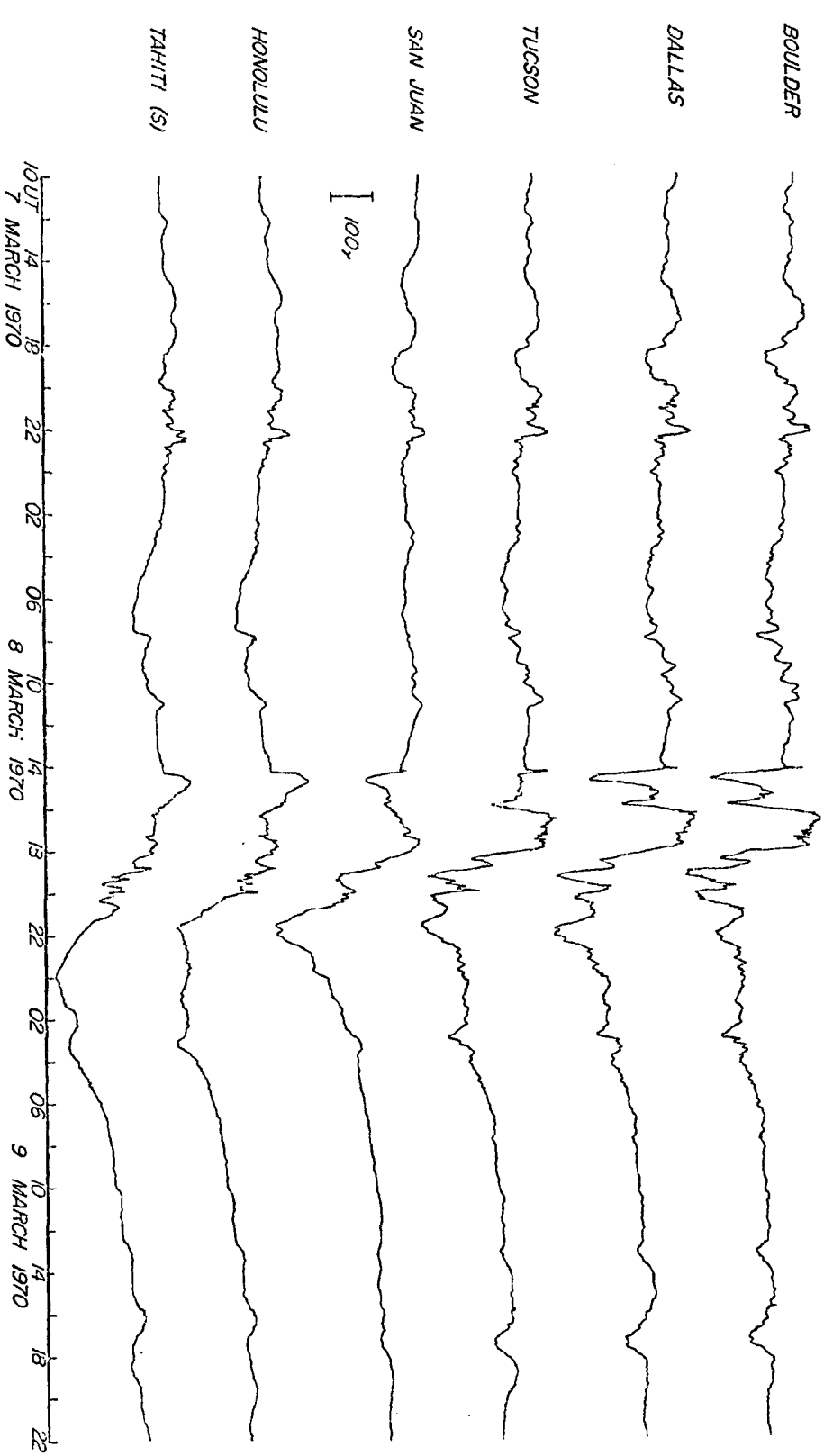

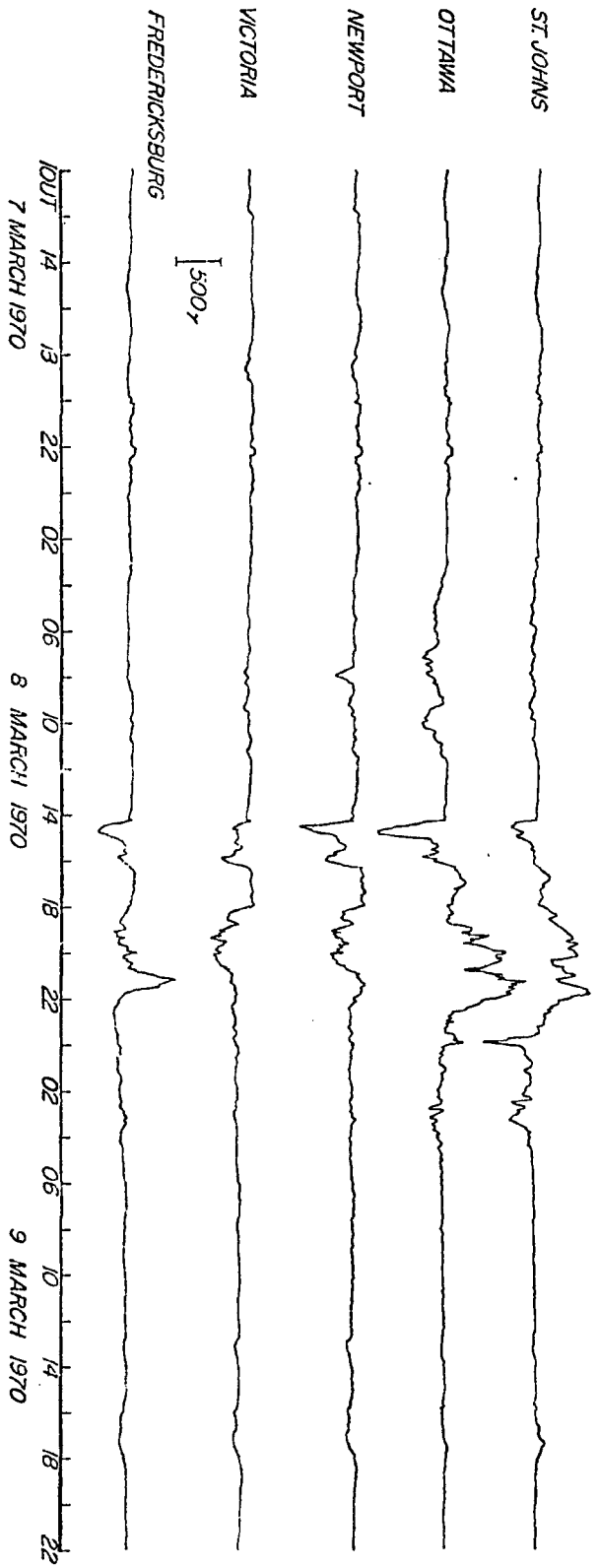

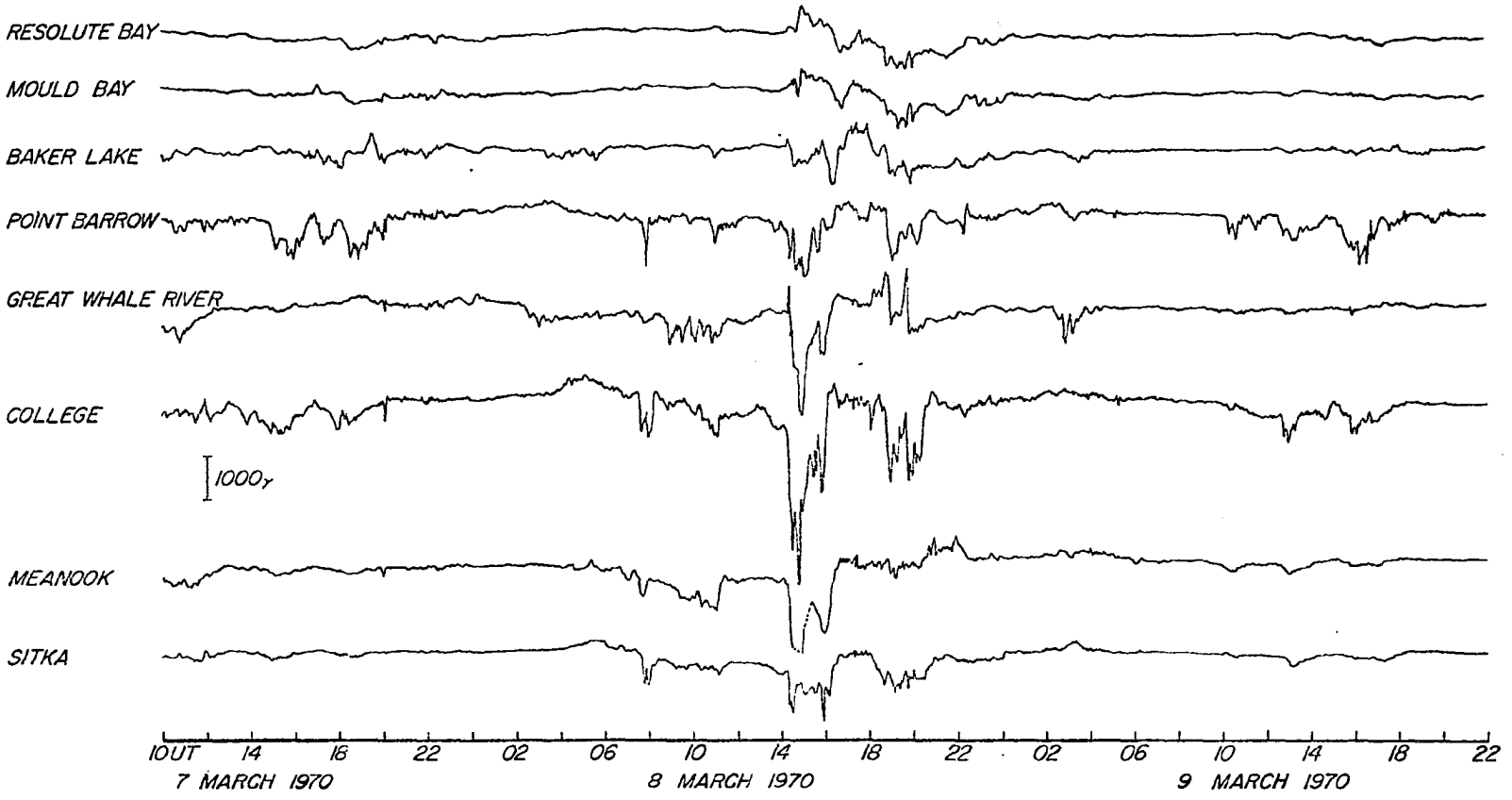

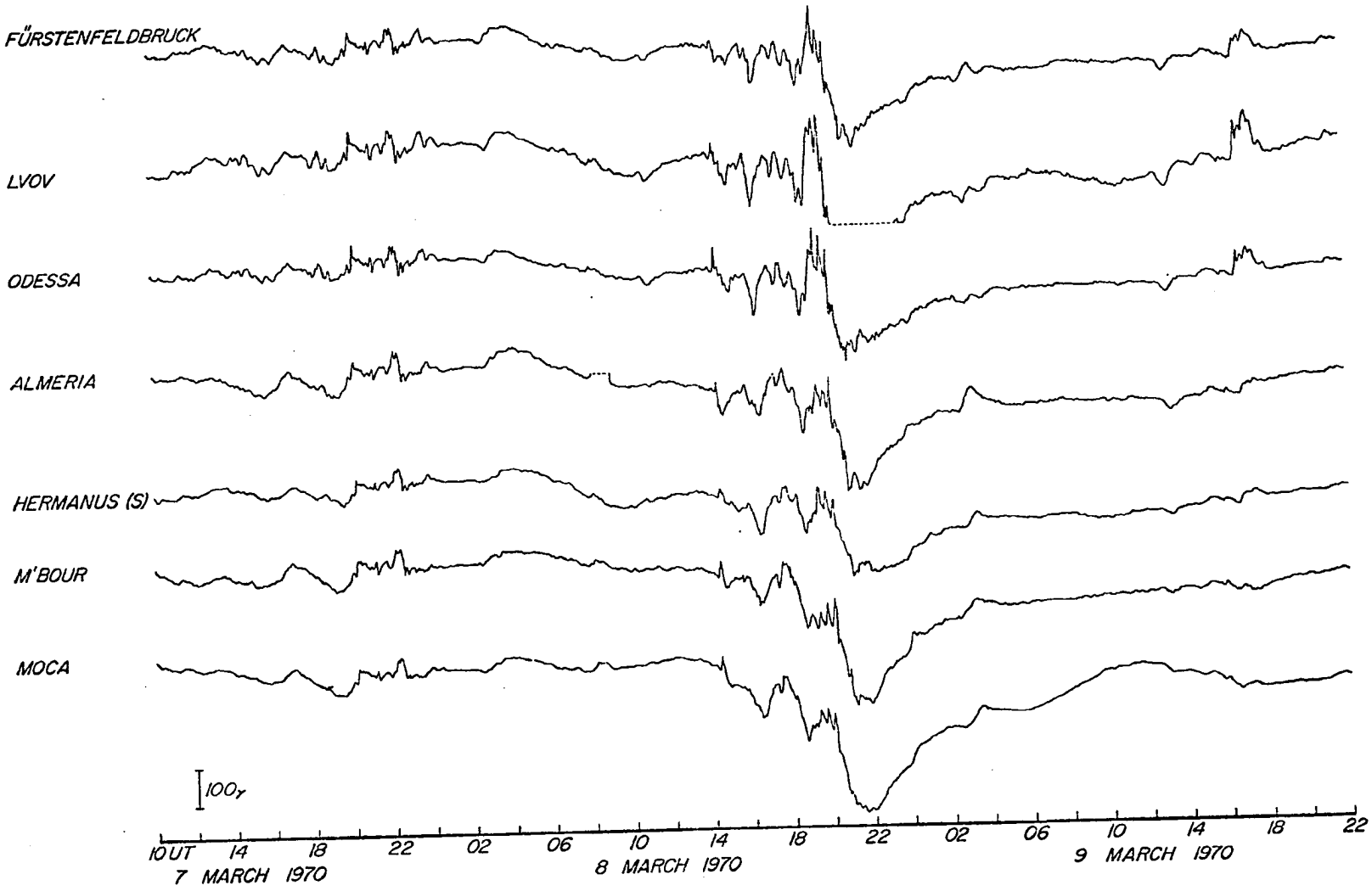

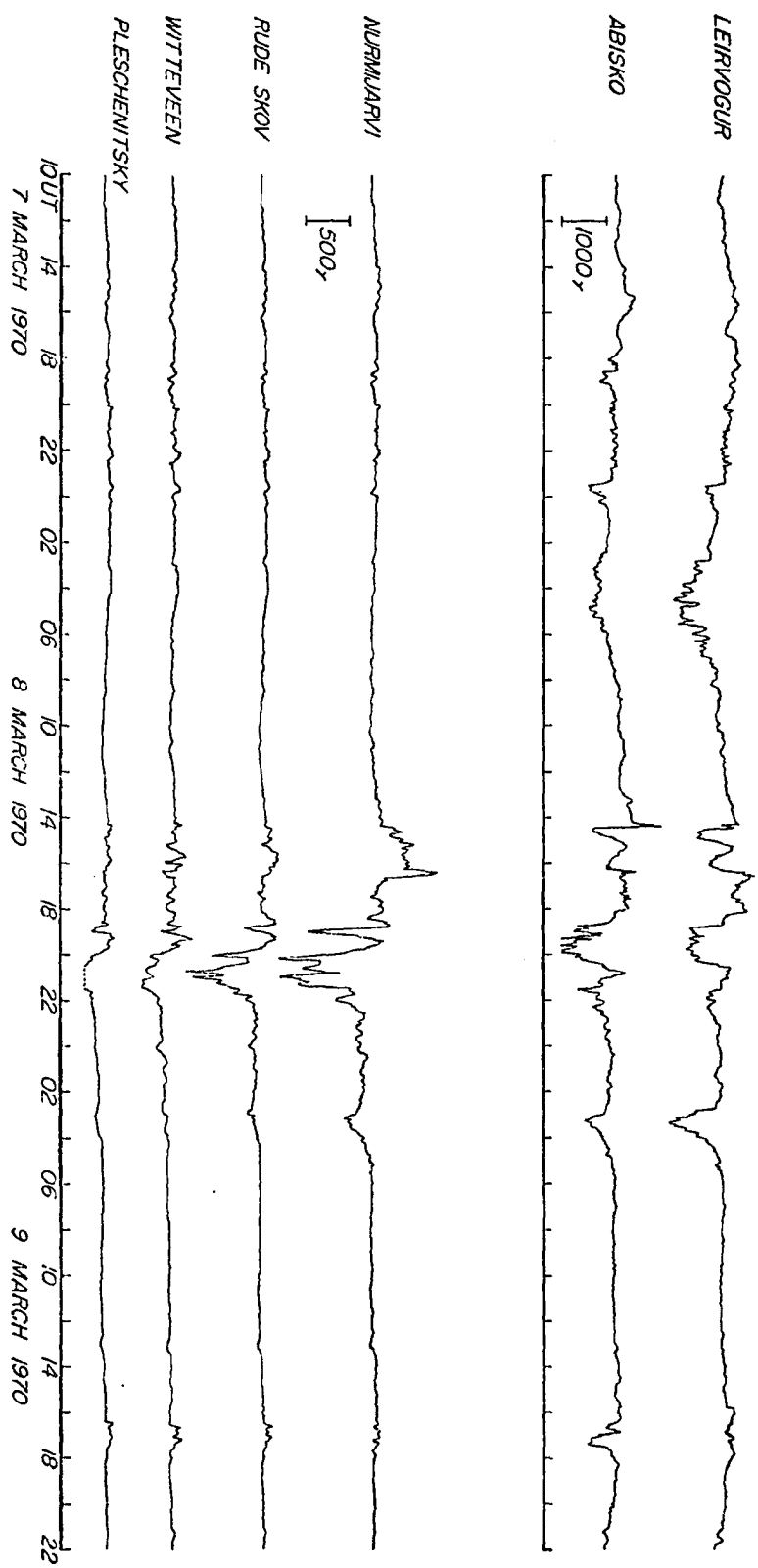

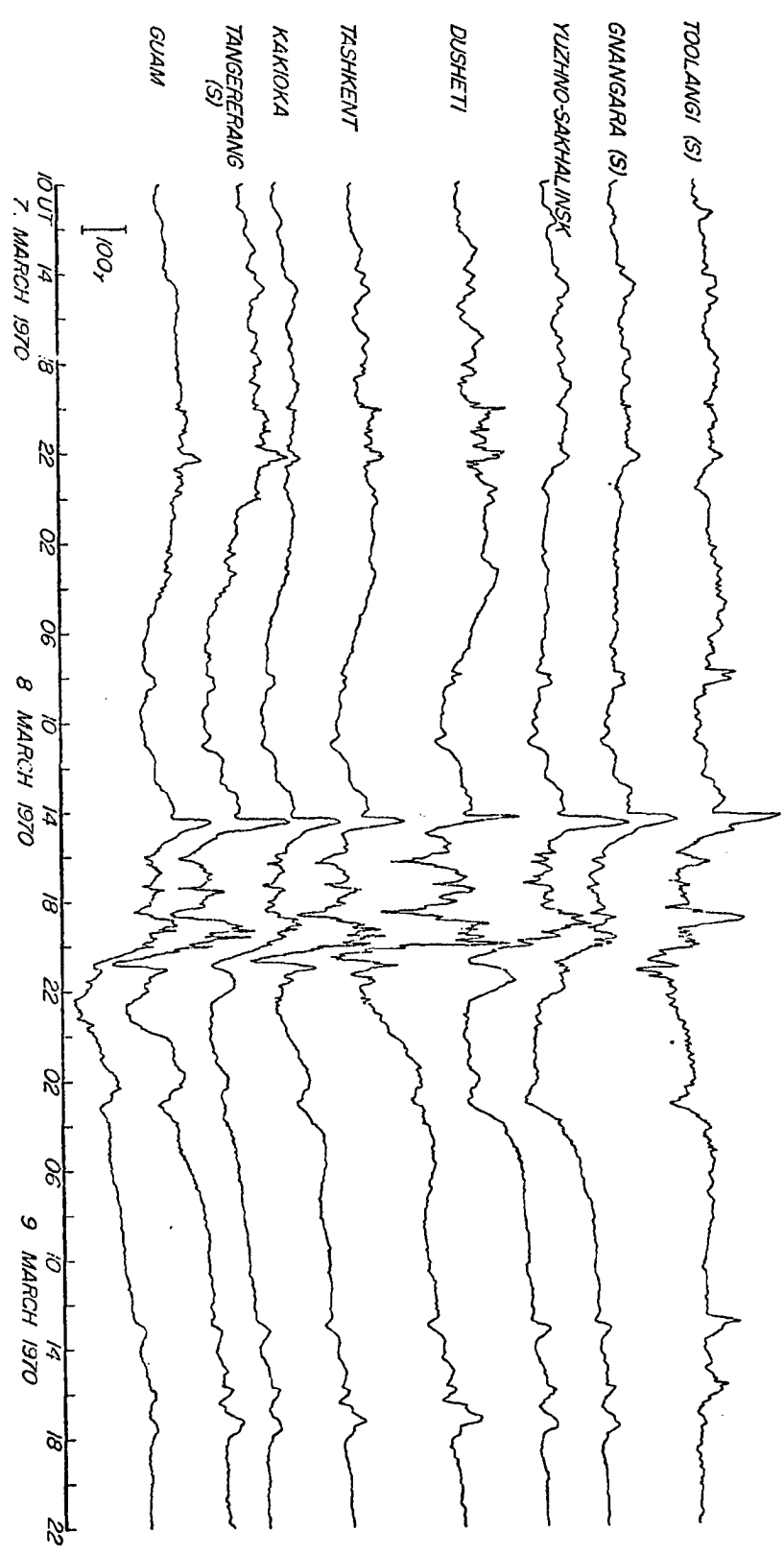

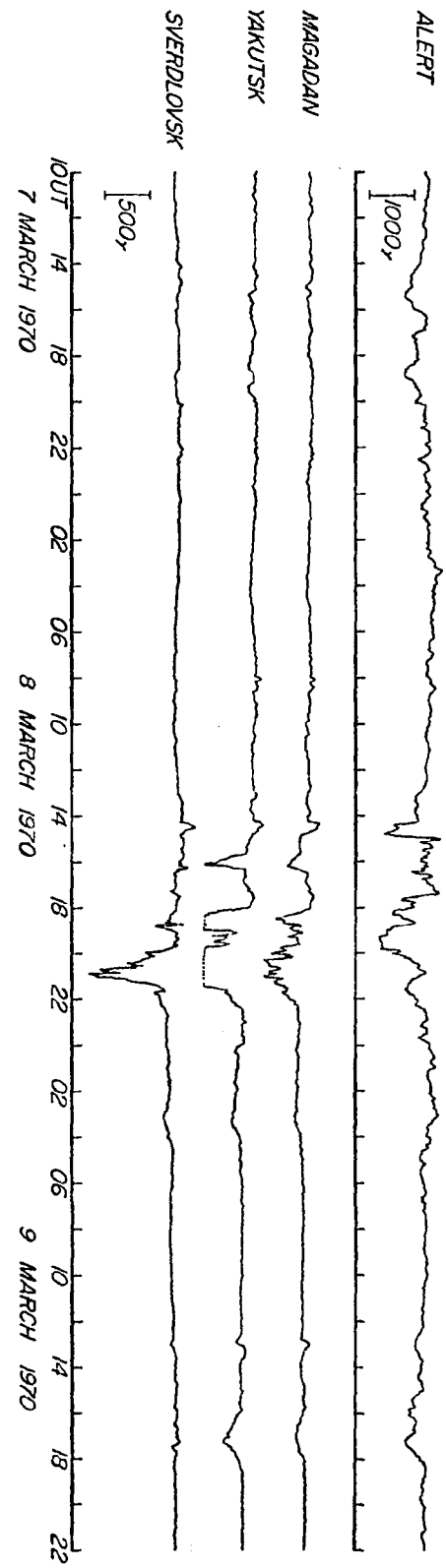

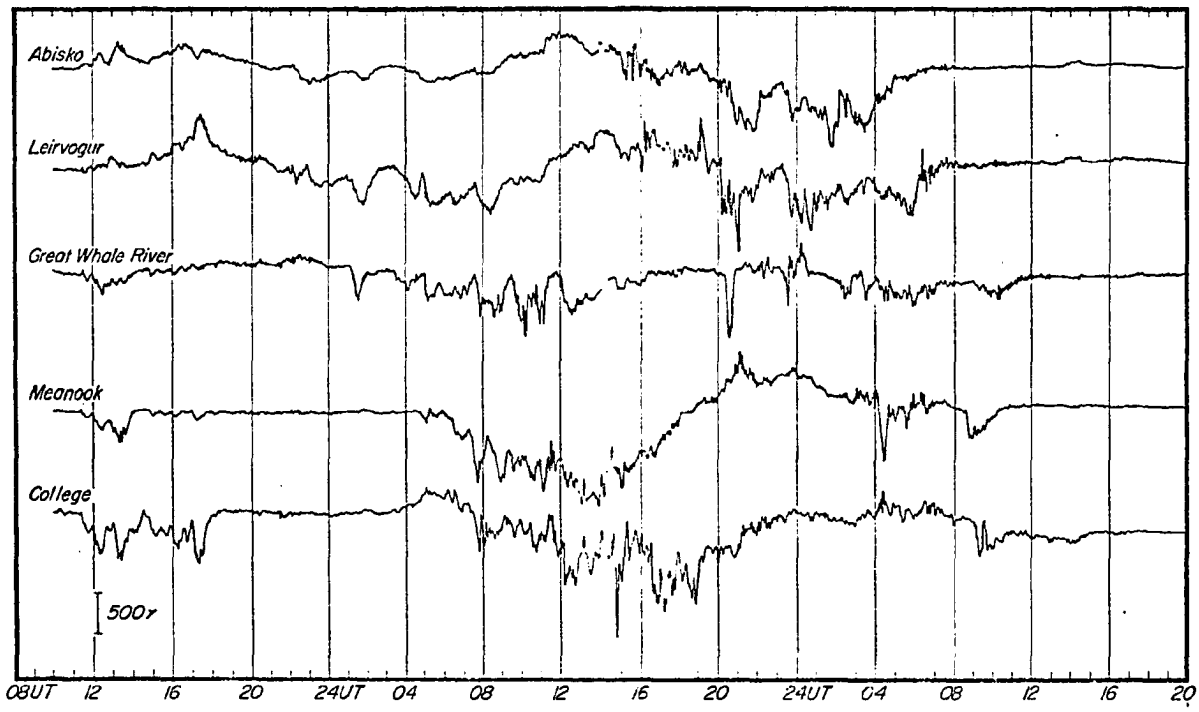

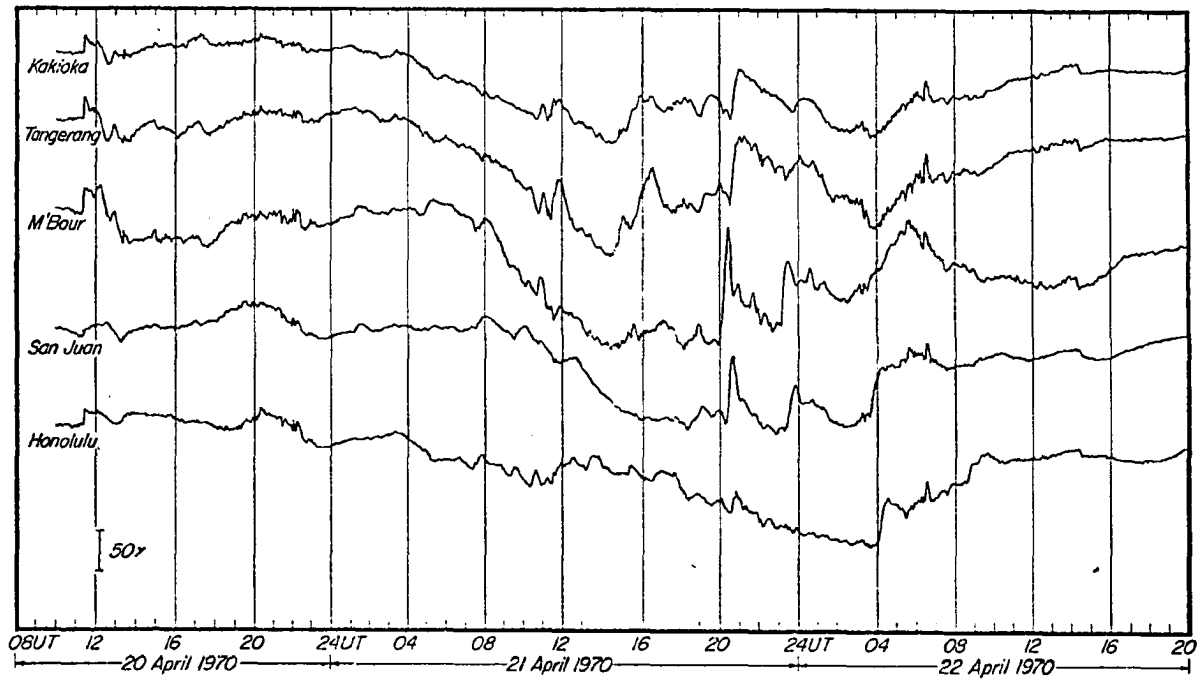

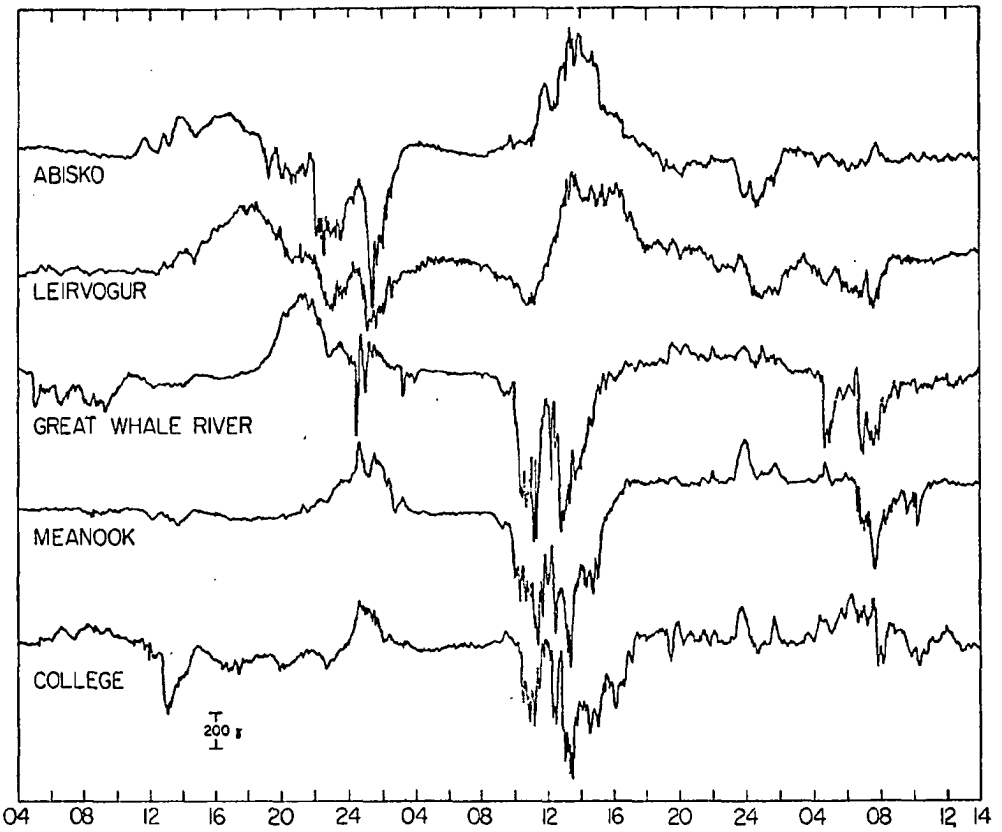

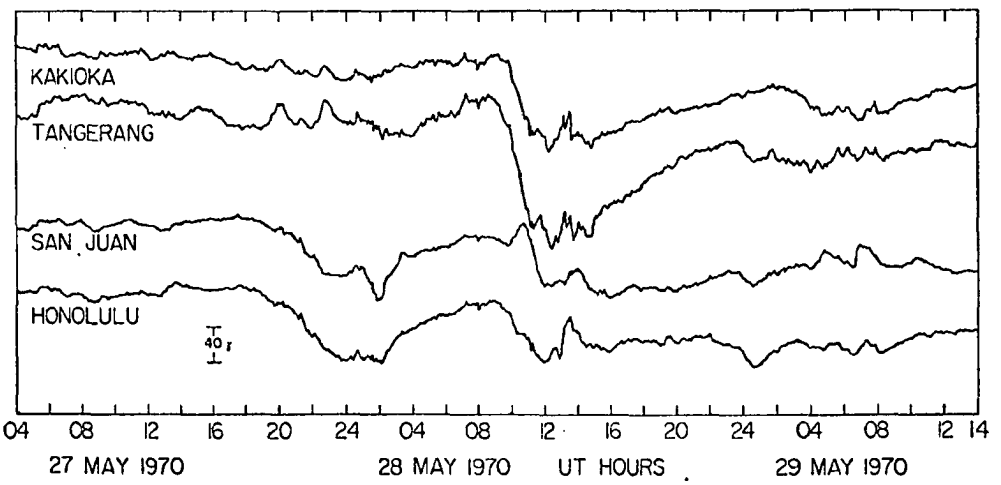

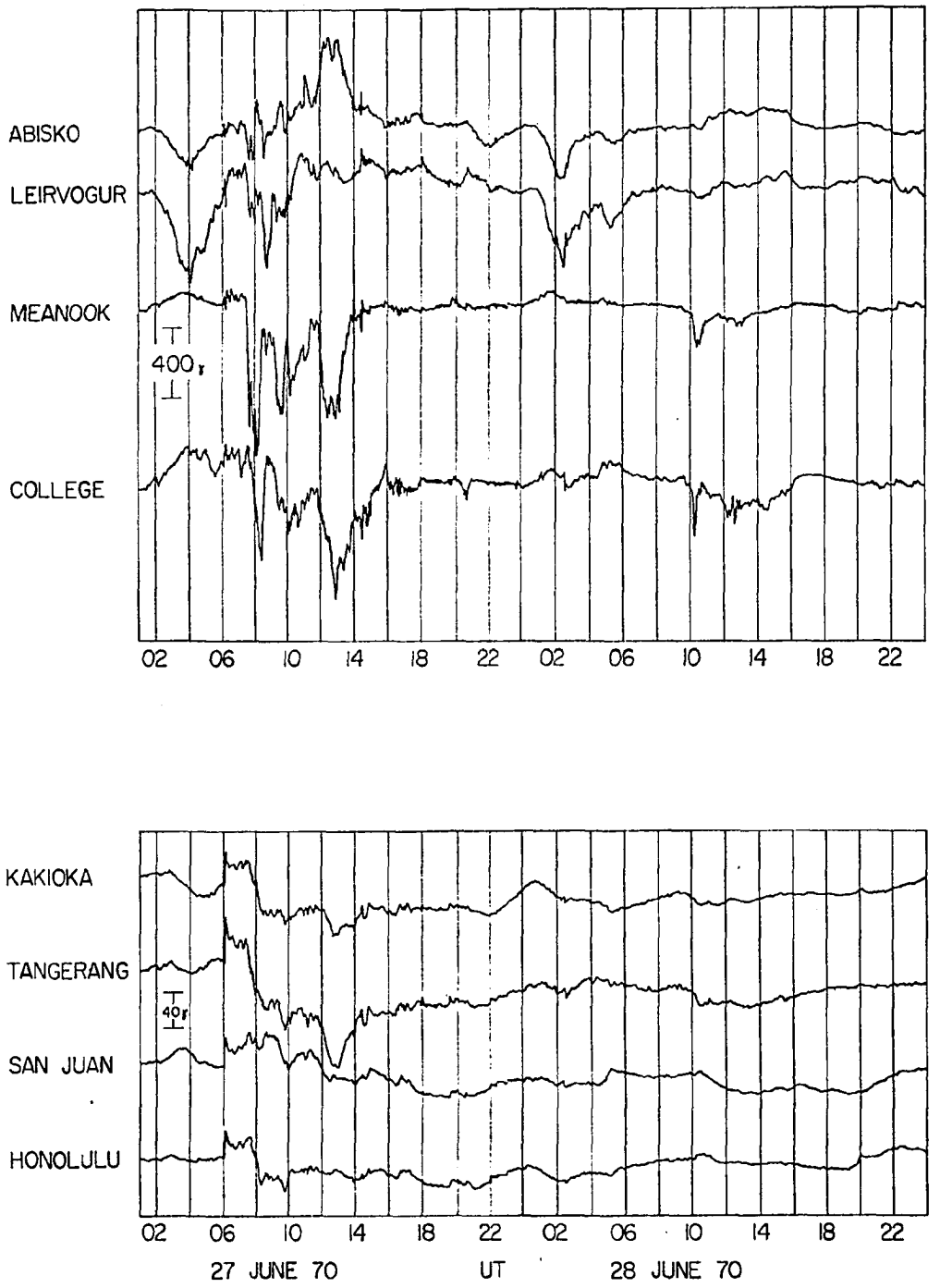

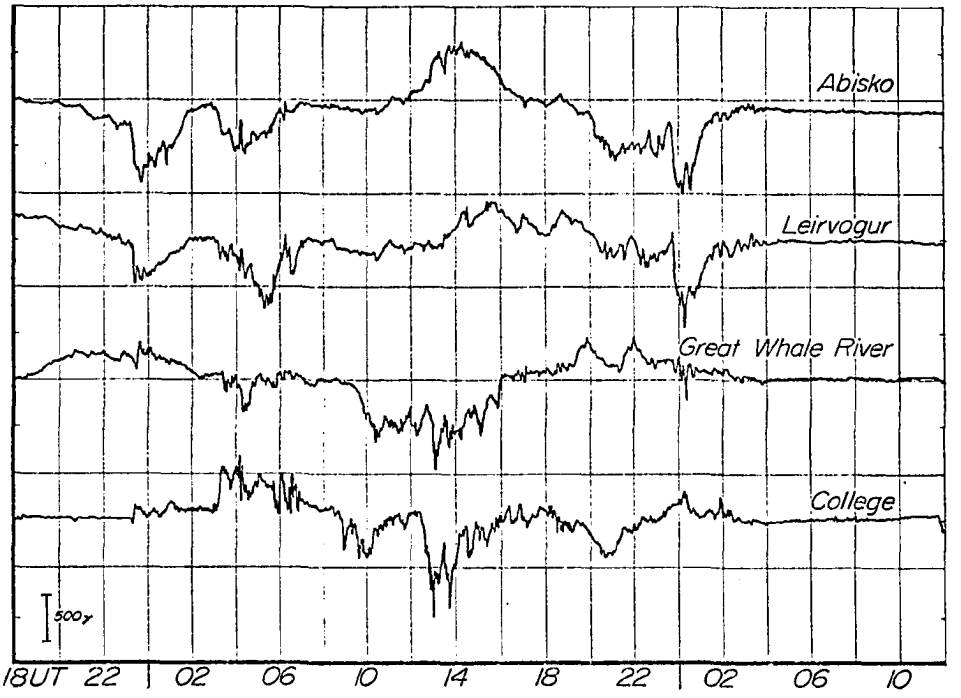

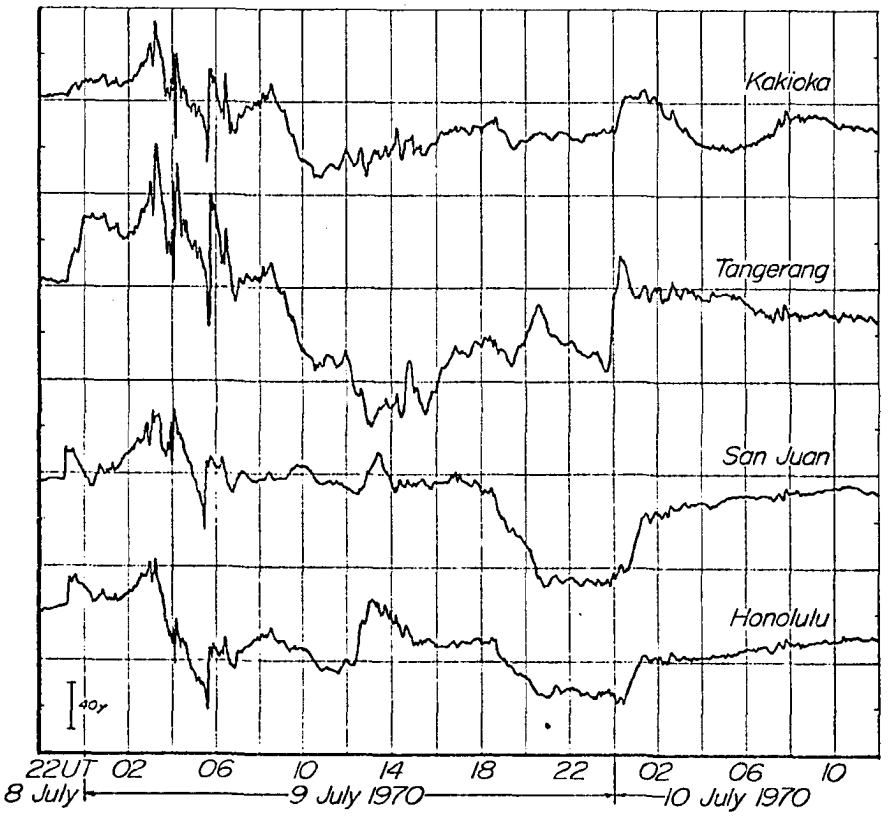

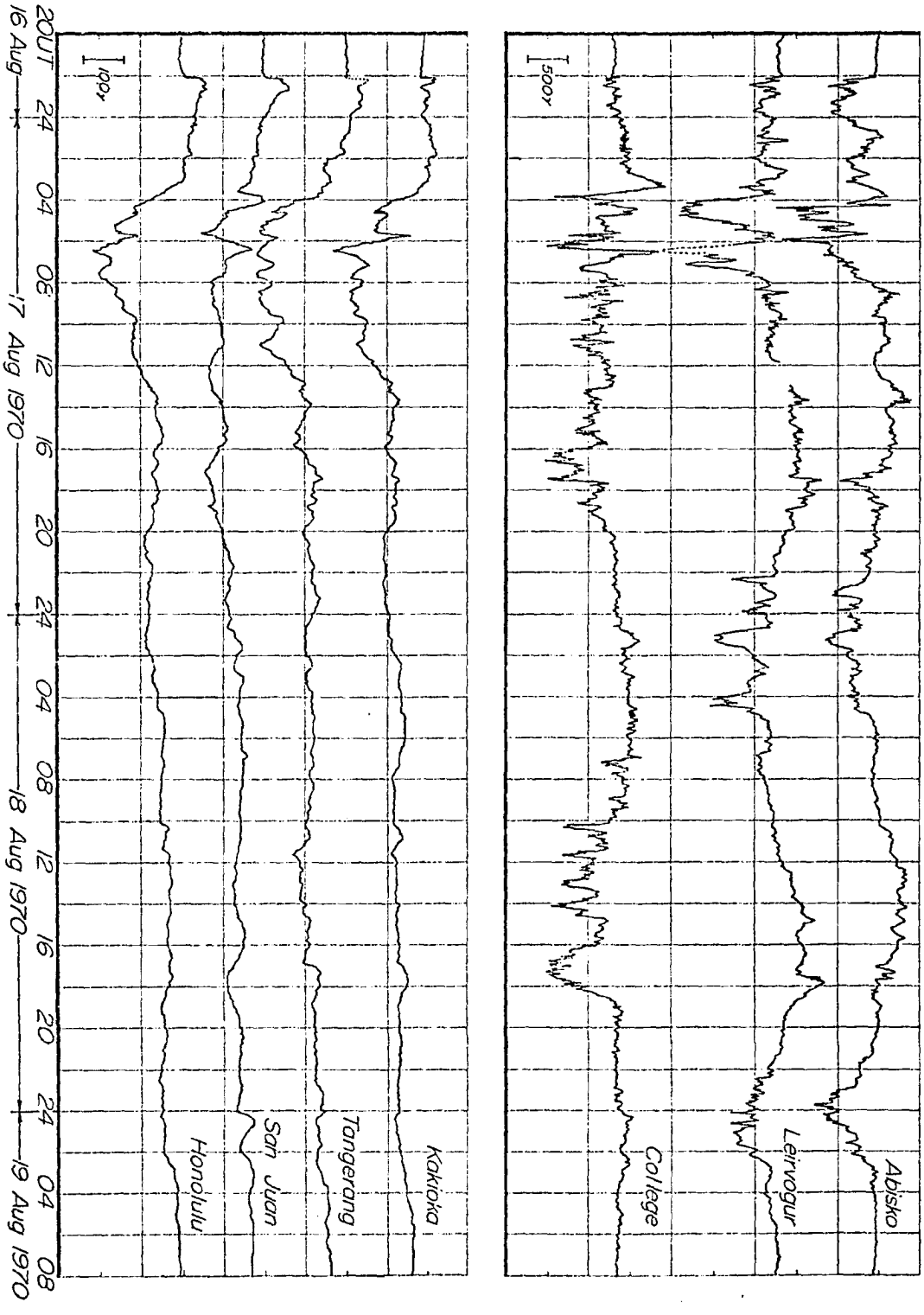

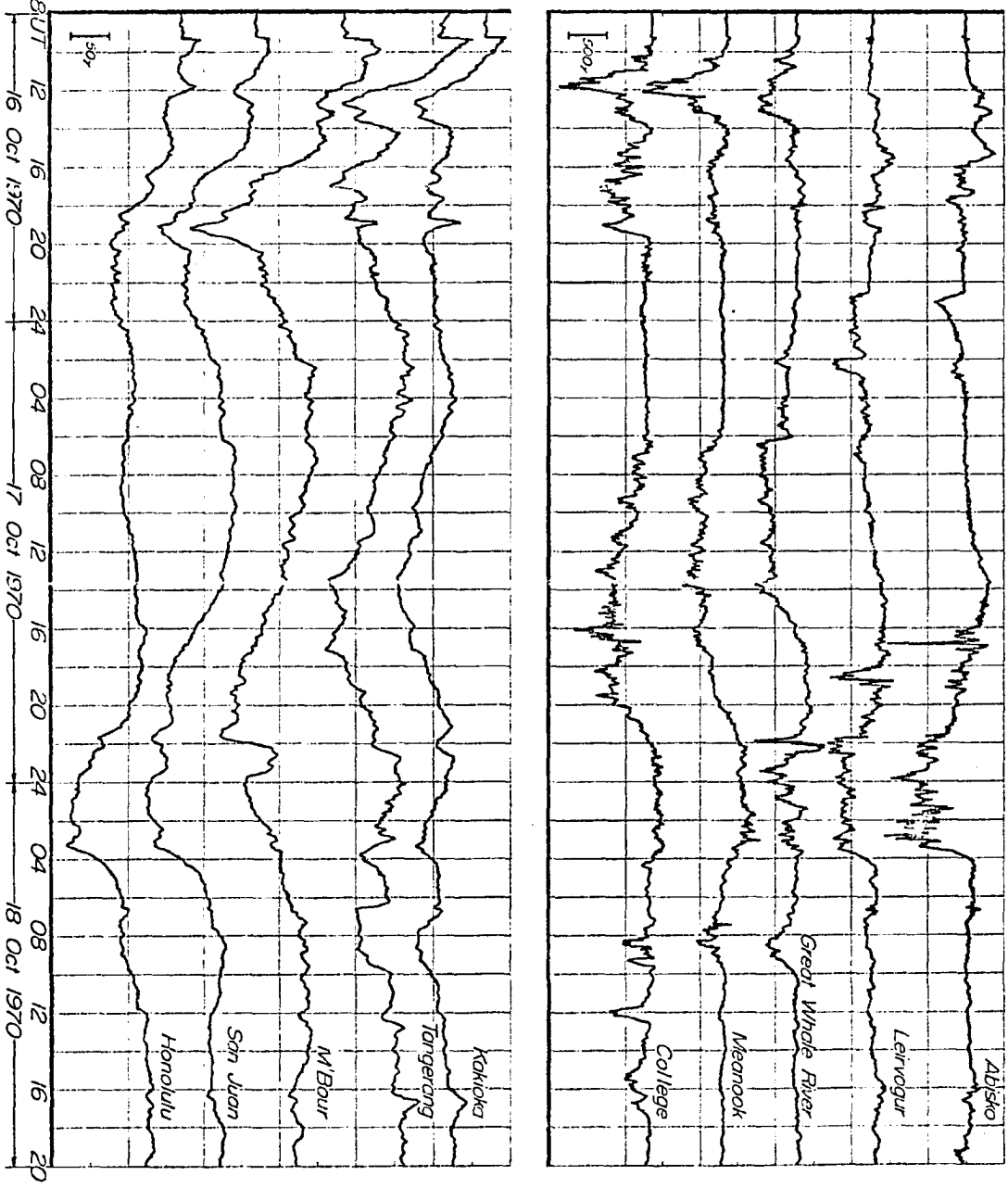

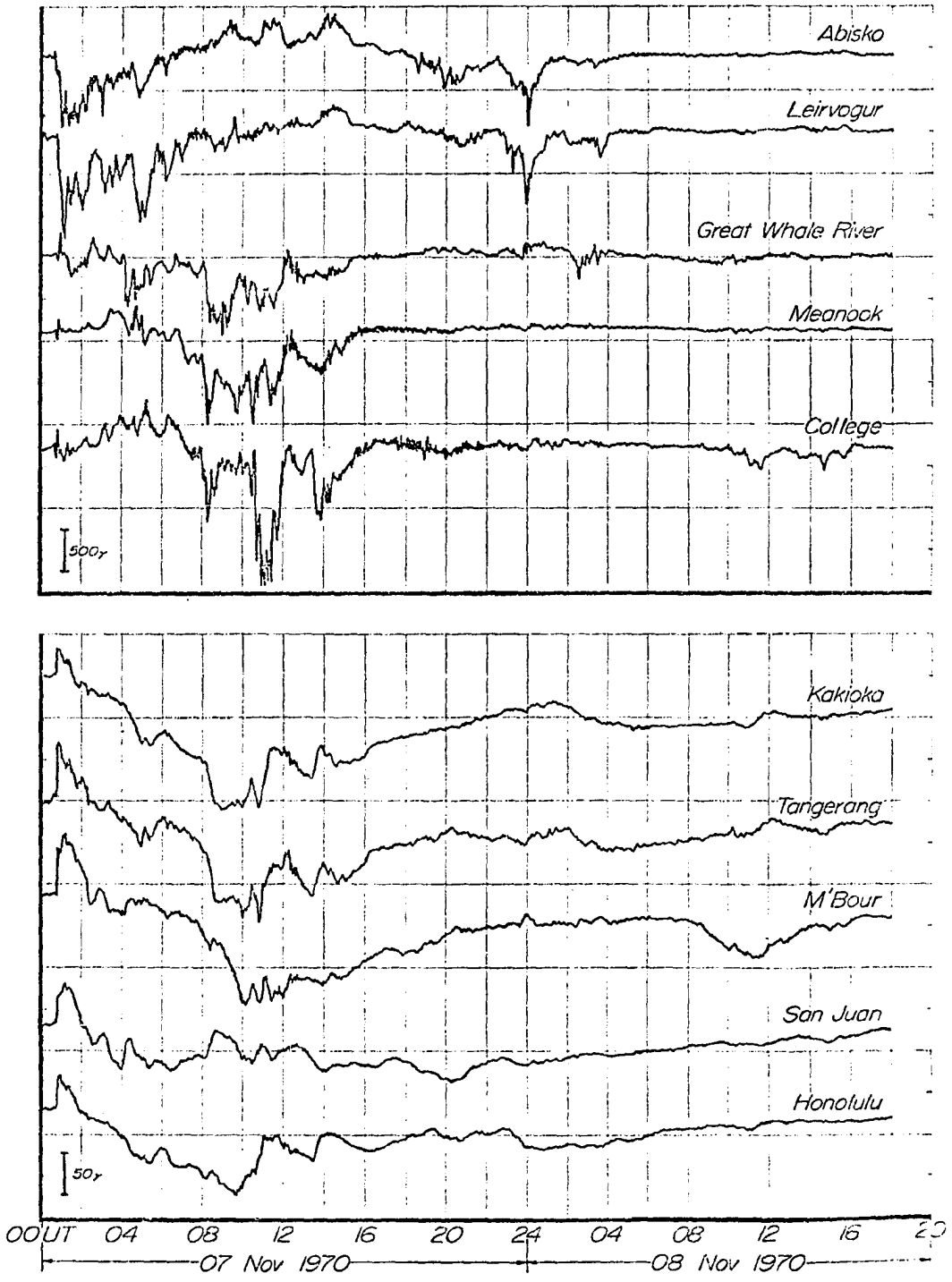

APPENDIX II

The computer program for the models in Section 6.2 is listed here. The program is the same one as used by Akasofu (1970) except for modifications of the current functions as described in Section 6.2.

The main routine is labeled "MAINPGM". The subroutines for computing ring current and north and south auroral electrojet current fields are labeled 'EQUATR', and 'AURORN' and 'AURORS', respectively. The subroutine for integrating the field aligned current contribution is labeled 'FDLINE' and 'FLDINT'. The current functions are computed in the multiple entry function subprogram 'CURR' with entries: 'ARNCUR', 'ARSCUR', 'FLDCUR', and 'EQTCUR'.

Specifically, the program is for model B of Section 6.2, which differs from model A by the addition of the eastward ring current I_o.

```
DOS FORTRAN IV 360N-FO-479 3-1          MAINPGM          DATE   04/23/70     TIME    17.27.40      PAGE 0001

                C     FOR DR. AKASOFU BY B. MORTON, GEOPHYSICAL INSTITUTE, U. OF ALASKA
                C     REFERENCE.. ON CURRENT SYSTEMS PROPOSED FOR SD IN THE THEORY OF
                C     MAGNETIC STORMS BY C. B. KIRKPATRICK, JOURNAL OF GEOPHYSICAL
                C     MAGNETIC FIELD GENERATED BY MODEL CURRENTS AROUND THE EARTH.
                C     RESEARCH, DEC 1952, PGS 511-526
                C
                C     THE MAGNETIC FIELD AT A POINT IS COMPUTED AS GENERATED BY THE
                C     FOLLOWING CURRENTS.
                C     1. A LINE CURRENT FLOWING IN THE EQUATORIAL CIRCLE OF RADIUS K.
                C     2. A SHEET CURRENT FLOWING ALONG THE LINES OF FORCE FROM THE
                C        AURORAL CIRCLES INTO THE EQUATORIAL CIRCLES.
                C     3. A LINE CURRENT FLOWING IN THE AURORAL CIRCLES.
                C
                C     ARRAYS OF AZIMUTH INTEGRATION LIMITS.
0001                  REAL AL1(5),AL2(5)
0002                  REAL K,KSQ,IO
0003                  INTEGER PUNCH/2/
0004                  COMMON K,IO,PHI1,PHI2,PO,ZO,PHIO,A,B,EL,KSQ
0005                  DEG=.0174533
                C
                C   COPY TITLE AND SCALE CARDS FOR PLOT DECK
                C              (NOD 6 APRIL 1970)
                C
0006                  READ(1,111)
0007                  WRITE(PUNCH,111)
0008                  READ(1,111)
0009                  WRITE(PUNCH,111)
0010             111  FORMAT(80H
                     1                    )
                C     READ AND PRINT LINE PARAMETERS FOR ONE GROUP OF POSITIONS.
0011                1 READ(1,2,END=49)K,IO,AL1(1),AL2(1),CLATN1,CLATN2,CLATS1,CLATS2,
                     1        NUMBER                                                    APR 9
0012             2    FORMAT(8F8.0,I16)                                                 APR 6
0013                4 FORMAT(10F8.0)
                C     K,IO                MODEL CURRENT PARAMETERS.
                C     CLATN1,CLATN2       INTEGRATION LIMITS ON NORTH FIELD LINE CURRENT.
                C     CLATS1,CLATS2       INTEGRATION LIMITS ON SOUTH FIELD LINE CURRENT.
                C     AL1       ARRAY OF LOWER AZIMUTH LIMITS FOR INTEGRALS.
                C     AL2       ARRAY OF UPPER AZIMUTH LIMITS FOR INTEGRALS.
0014                  KSQ=K*K
0015                  THETA1=CLATN1*DEG
0016                  THETA2=CLATN2*DEG
0017                  THETS1=CLATS1*DEG
0018                  THETS2=CLATS2*DEG
                C     PRINT PAGE HEADING AND SET LINE COUNTER.
0019                  WRITE(3,3) K,IO,        CLATN1,CLATN2,CLATS1,CLATS2,NUMBER
0020               30 FORMAT('1',30X,'MODEL CURRENT PARAMETERS'/' K=',F5.2,'  IO=',F9.0,
                     1                        '  COLAT-N1=',F6.2,'  COLAT-N2=',
                     2F6.2,'  COLAT-S1=',F6.2,'  COLAT-S2=',F6.2,'   GROUP',I4)
0021                  LINES=2
                C     READ POSITION CARD. TEST FOR /* CARD AT END OF GROUP.
0022               10 READ(1,11,END=1)CLATO,RO,AZO
0023               11 FORMAT(3F6.2)
0024               12 THETAO=CLATO*DEG
```

```
0025            PO=RC*SIN(THETAO)
0026            ZO=RC*COS(THETAO)
0027            PHIO=AZO*DEG
0028            A=PO/K
0029            B=ZO/K
0030            EL=RC/K
              C     TURN PAGE AND REPEAT HEADING IF NECESSARY.
0031            IF(LINES-27)14,13,13
0032         13 WRITE(3,3)K,IO,        CLATN1,CLATN2,CLATS1,CLATS2,NUMBER
0033            LINES=2
0034         14 LINES=LINES+30
              C     PRINT POSITION AND HEADING.
0035            WRITE(3,15)CLATO,RO,AZO,PO,ZO
0036         15OFORMAT('OPOSITION  COLAT.=',F6.2,'  DIST.=',F7.4,'  AZ.=',F6.2,
               1'  RHO=',F7.4,'  Z=',F8.4//    41X,'FIELD COMPONENTS'/' CURRENT
               2          AZ. LIMITS          H-RHO       H-PHI        H-Z
               3 H          Z          E')
0037            KP=1
0038            WRITE(PUNCH,16)K,IO,CLATN1,CLATN2,CLATS1,CLATS2,NUMBER,KP          APR 6
0039         16 FORMAT(F6.3,F8.0,4F8.4,T75,I4,I2)
0040            KP=2
0041            WRITE(PUNCH,17)CLATO,RO,AZO,PO,ZO,NUMBER,KP                        APR 6
0042         17 FORMAT(5F8.4,T75,I4,I2)
              C     ZERO OUT SUMS OF COMPONENTS.
0043            HPT=0.
0044            HOT=0.
0045            HZT=0.
0046            HT=0.
0047            ZT=0.
0048            ET=0.
              C     COMPUTE PRINT AND PUNCH NORTH FIELD LINE INTEGRALS.
0049            I=1                                                                APR 6
0050            PHI1=AL1(I)*DEG
0051            PHI2=AL2(I)*DEG
0052            CALL FDLINE(THETN1,THETN2,THETAO,HP,HO,HZ,H,Z,E)
              C     PRINT AND ADD TO SUMS.
0053            WRITE(3,18)AL1(I),AL2(I),HP,HO,HZ,H,Z,E
0054         18 FORMAT(' NORTH FIELD LINE  ',2F7.2,3X,1P6E12.4)
0055         19 FORMAT(1P6E12.4,T75,I4,I2)
0056            HPT=HPT+HP
0057            HOT=HOT+HO
0058            HZT=HZT+HZ
0059            HT=HT+H
0060            ZT=ZT+Z
0061         40 ET=ET+E
              C     COMPUTE, PRINT AND ADD FIELD FROM SOUTH FIELD LINE CURRENT.
0062            PHI1=AL1(I)*DEG
0063            PHI2=AL2(I)*DEG
0064            CALL FDLINE(THETS1,THETS2,THETAO,HP,HO,HZ,H,Z,E)
0065            WRITE(3,20)AL1(I),AL2(I),HP,HO,HZ,H,Z,E
0066         20 FORMAT(' SOUTH FIELD LINE  ',2F7.2,3X,1P6E12.4)
0067            HPT=HPT+HP
0068            HOT=HOT+HO
0069            HZT=HZT+HZ
```

```
0070              HT=HT+H
0071              ZT=ZT+Z
0072           42 ET=ET+E
                C     COMPUTE, PRINT AND ADD FIELD FROM EQUATORIAL CURRENT.
0073              PHI1=AL1(I)*DEG
0074              PHI2=AL2(I)*DEG
0075              CALL EQUATR(HP,HO,HZ,H,Z,E)
0076              WRITE(3,22)AL1(I),AL2(I),HP,HO,HZ,H,Z,E
0077           22 FORMAT(' EQUATORIAL LINE   ',2F7.2,3X,1P6E12.4)
0078              HPT=HPT+HP
0079              HOT=HOT+HO
0080              HZT=HZT+HZ
0081              HT=HT+H
0082              ZT=ZT+Z
0083           44 ET=ET+E
                C     COMPUTE, PRINT AND ADD FIELD FROM NORTH AURORA CURRENT.
0084              PHI1=AL1(I)*DEG
0085              PHI2=AL2(I)*DEG
0086              CALL AURORN(HP,HO,HZ,H,Z,E)
0087              WRITE(3,24)AL1(I),AL2(I),HP,HO,HZ,H,Z,E
0088           24 FORMAT(' NORTH AURORAL LINE',2F7.2,3X,1P6E12.4)
0089              HPT=HPT+HP
0090              HOT=HOT+HO
0091              HZT=HZT+HZ
0092              HT=HT+H
0093              ZT=ZT+Z
0094           46 ET=ET+E
                C     COMPUTE, PRINT AND ADD FIELD FROM SOUTH AURORA CURRENT.
0095              PHI1=AL1(I)*DEG
0096              PHI2=AL2(I)*DEG
0097              CALL AURORS(HP,HO,HZ,H,Z,E)
0098              WRITE(3,26)AL1(I),AL2(I),HP,HO,HZ,H,Z,E
0099           26 FORMAT(' SOUTH AURORAL LINE',2F7.2,3X,1P6E12.4)
0100              HPT=HPT+HP
0101              HOT=HOT+HO
0102              HZT=HZT+HZ
0103              HT=HT+H
0104              ZT=ZT+Z
0105           48 ET=ET+E
                C     PRINT TOTAL FIELD.
0106              WRITE(3,28)HPT,HOT,HZT,HT,ZT,ET
0107           28 FORMAT(' TOTAL',30X,1P6E12.4)
0108              KP=3
0109              WRITE(PUNCH,19)HPT,HOT,HZT,HT,ZT,ET,NUMBER,KP                    APR 6
                C     GO READ NEXT CARD.
0110              GO TO 10
0111           49 CALL EXIT                                                       APR 9
0112              END
```

```
OS FORTRAN IV 360N-FO-479 3-1          FOLINE            DATE   03/31/70      TIME    13.05.34      PAGE 0001

0001            SUBROUTINE FOLINE(THETA1,THETA2,THETA0,HP,H0,HZ,H,Z,EE).
          C     COMPUTE FIELD DUE TO CURRENT ALONG FIELD LINES.
0002            REAL KAY,KSQ,IO
0003            COMMON KAY,IC,PHI1,PHI2,P0,Z0,PHI0,A,B,EL,KSQ
          C     INTEGRATE BY TRAPEZOIDAL RULE WITH VARIABLE STEP SIZE.
0004            THETA=THETA1
0005            H1=0.
0006            H2=0.
0007            H3=0.
0008            STEPA=0.
0009          5 THETA=THETA+STEPA
0010            U=COS(THETA)
0011            V=1.-U*U
0012            C=KSQ*V*V*(1.-3.*U*U/V)
0013            B=KSQ*SQRT(V)*A*(2.-3.*V)
0014            F=3.*KSQ*V*A*U
          C     COMPUTE B1(THETA), B2(THETA), B3(THETA)
0015            CALL FLDINT(THETA,B1,B2,B3)
0016            RMN=SQRT(KSQ*V**3*P0*P0+KSQ*U*U*V*V-2.*Z0*KAY*U*V+Z0*Z0
           $-2.*P0*KAY*SQRT(V)**3)
0017            STEPB=SIGN(AMIN1(.00139*5.24*RMN*RMN,.020+.139*RMN,.131,
           $ABS(THETA2-THETA)),THETA2-THETA)
0018            STPS=.5*(STEPA+STEPB)
0019            H1=H1-C*B1*STPS
0020            H2=H2+(C*B2+C*B3)*STPS
0021            H3=H3-E*B1*STPS
0022            IF(ABS(STEPB)-.0001745)10,10,7
0023          7 STEPA=STEPB
0024            GO TO 5
0025         10 HP=H1*1.5679E-5
0026            H0=H2*1.5679E-5
0027            HZ=H3*1.5679E-5
0028            H=(A*HZ-B*HP)/EL
0029            Z=-(A*HP+B*HZ)/EL
0030            EE=HC
0031            RETURN
0032            END
```

```
DOS FORTRAN IV 360N-FO-479 3-1          FLDINT              DATE    05/31/70      TIME     13.06.26       PAGE 0001

0001                SUBROUTINE FLDINT(THETA,BE1,BE2,BE3)
                C   INTEGRATE FOR EFFECT OF CURRENT ALONG FIELD LINES.
0002                REAL KAY,KSQ,IO
0003                COMMON KAY,IO,PHI1,PHI2,PO,ZO,PHIO,A,B,EL,KSQ
                C   R IS DIST. FROM THE FIELD POINT. COMPUTE PART OF R WHICH IS A
                C   FUNCTION OF THETA ONLY.
0004                U=COS(THETA)
0005                USQ=U*U
0006                SSQ=1.-USQ
0007                RU=KSQ*SSQ**3+PO**2+KSQ*USQ*SSQ**2-2.*ZO*KAY*U*SSQ+ZO**2
                C   COMPUTE FACTOR FOR PART OF R WHICH IS FUNC. OF PSI AND THETA.
0008                RF=-2.*PO*KAY*(SQRT(SSQ))**3
                C   INTEGRATE BY TRAPEZOIDAL RULE WITH VARIABLE STEP SIZE.
0009                PHI=PHI1
0010                B1=0.
0011                B2=0.
0012                B3=0.
0013                STEPA=0.
0014              5 PHI=PHI+STEPA
0015                PSI=PHI-PHIO
0016                CPSI=COS(PSI)
0017                R=SQRT(RU+RF*CPSI)
0018                STEPB=AMIN1(.00139+5.24*R*R,.020+.139*R,.262,PHI2-PHI)
0019                FUNC=FLOCOR(PHI,IO)/(R*R*R)
0020                STPS=.5*(STEPA+STEPB)
0021                B1=B1+FUNC*SIN(PSI)*STPS
0022                B2=B2+FUNC*CPSI*STPS
0023                B3=B3+FUNC*STPS
0024                IF(STEPB-.000174S)10,10,7
0025              7 STEPA=STEPB
0026                GO TO 5
0027             10 CONTINUE
0028                BE1=B1
0029                BE2=B2
0030                BE3=B3
0031                RETURN
0032                END
```

```
OOS FORTRAN IV 360N-FO-479 3-1          EQUATR          DATE   03/31/70     TIME    13.07.20      PAGE 0001

0001                SUBROUTINE EQUATR(HP,HO,HZ,H,Z,E)
                C   INTEGRATE FOR EFFECT OF EQUATORIAL CURRENT.
0002                REAL KAY,KSQ,IO
0003                COMMON KAY,IO,PHI1,PHI2,PO,ZO,PHIO,A,B,EL,KSQ
                C   R IS DIST. FROM THE FIELD POINT. COMPUTE PART OF R WHICH IS A
                C   FUNCTION OF THETA ONLY. THETA=PI/2. U=COS(THETA)
0004                RU=KSQ+PO*PO+ZO*ZO
                C   COMPUTE FACTOR FOR PART OF R WHICH IS FUNC. OF PSI AND THETA.
0005                RF=-2.*KAY*PO
                C   INTEGRATE BY TRAPEZOIDAL RULE WITH VARIABLE STEP SIZE.
0006                PHI=PHI1
0007                B1=0.
0008                B2=0.
0009                B3=0.
0010                STEPA=0.
0011              5 PHI=PHI+STEPA
0012                PSI=PHI-PHIO
0013                CPSI=COS(PSI)
0014                R=SQRT(RU+RF*CPSI)
0015                STEPB=AMIN1(.00139+5.24*R*R,.020+.139*R,.262,PHI2-PHI)
0016                FUNC=ECTCUR(PHI,IO)/(R*R*R)
0017                STPS=.5*(STEPA+STEPB)
0018                B1=B1+FUNC*SIN(PSI)*STPS
0019                B2=B2+FUNC*CPSI*STPS
0020                B3=B3+FUNC*STPS
0021                IF(STEPB-.0001745)10,10,7
0022              7 STEPA=STEPB
0023                GO TO 5
0024             10 CONTINUE
0025                HP=KAY*ZO*B2*1.5679E-5
0026                HO=KAY*ZO*B1*1.5679E-5
0027                HZ=KAY*(KAY*B3-PO*B2)*1.5679E-5
0028                H=(A*HZ-B*HP)/EL
0029                Z=-(A*HP+B*HZ)/EL
0030                E=HO
0031                RETURN
0032                END
```

```
OOS FORTRAN IV 360N-FO-479 3-1          AURORN          DATE   04/31/70     TIME     13.00.14      PAGE 0001

0001                  SUBROUTINE AURORN(HP,HO,HZ,H,Z,E)
                C     INTEGRATE FOR EFFECT OF NORTH AURORAL CURRENT.
0002                  REAL KAY,KSQ,IO
0003                  COMMON KAY,IC,PHI1,PHI2,PO,ZO,PHIO,A,B,EL,KSQ
                C     R IS DIST. FROM THE FIELD POINT. COMPUTE PART OF R WHICH IS A
0004                  U=COS(.0047709)
0005                  USQ=U*U
0006                  SSQ=1.-USQ
0007                  RU=.159984*PC*PO*(.93363-ZO)**2
                C     COMPUTE FACTOR FOR PART OF R WHICH IS FUNC. OF PSI AND THETA.
0008                  RF=-2.*.39998*PC
                C     INTEGRATE BY TRAPEZOIDAL RULE WITH VARIABLE STEP SIZE.
0009                  PHI=PHI1
0010                  B1=0.
0011                  B2=0.
0012                  B3=0.
0013                  STEPA=0.
0014                5 PHI=PHI+STEPA
0015                  PSI=PHI-PHIO
0016                  CPSI=COS(PSI)
0017                  R=SQRT(RU+RF*CPSI)
0018                  STEPB=AMIN1(.00139+5.24*R*R,.020+.139*R,.262,PHI2-PHI)
0019                  FUNC=ARACOS(PHI,IO)/(R*R*R)
0020                  STPS=.5*(STEPA+STEPB)
0021                  B1=B1+FUNC*SIN(PSI)*STPS
0022                  B2=B2+FUNC*CPSI*STPS
0023                  B3=B3+FUNC*STPS
0024                  IF(STEPB-.COC1745)10,10,7
0025                7 STEPA=STEPB
0026                  GO TO 5
0027               10 CONTINUE
0028                  HP=.39998*(ZO-.93363)*B2*1.5679E-5
0029                  HO=.39998*(ZO-.93363)*B1*1.5679E-5
0030                  HZ=.39998*(.39998*B3-PO*B2)*1.5679E-5
0031                  H=(A*HZ-B*HP)/EL
0032                  Z=-(A*HP+B*HZ)/EL
0033                  E=HO
0034                  RETURN
0035                  END
```

```
OOS FORTRAN IV 360N-FO-479 3-1          AURORS          DATE   03/31/70     TIME    13.09.08      PAGE 0001

0001            SUBROUTINE AURORS(HP,HO,HZ,H,Z,E)
                C       INTEGRATE FOR EFFECT OF SOUTH AURORAL CURRENT.
0002            REAL KAY,KSQ,IO
0003            COMMON KAY,IC,PHI1,PHI2,PO,ZO,PHIO,A,B,EL,KSQ
                C       R IS DIST. FROM THE FIELD POINT. COMPUTE PART OF R WHICH IS A
                C       FUNCTION OF THETA ONLY. THETA=156.9053DEG=2.736822RAD.
0004            D=COS(2.736822)
0005            USQ=U*U
0006            SSQ=1.-USQ
0007            RO=.159984*PO*PO*(-.93363-ZO)**2
                C       COMPUTE FACTOR FOR PART OF R WHICH IS FUNC. OF PSI AND THETA.
0008            RF=-2.*.39998*PO
                C       INTEGRATE BY TRAPEZOIDAL RULE WITH VARIABLE STEP SIZE.
0009            PHI=PHI1
0010            B1=0.
0011            B2=0.
0012            B3=0.
0013            STEPA=0.
0014          5 PHI=PHI+STEPA
0015            PSI=PHI-PHIO
0016            CPSI=COS(PSI)
0017            R=SQRT(RO+RF*CPSI)
0018            STEPB=AMIN1(.00139+5.24*R*R,.020+.139*R,.262,PHI2-PHI)
0019            FUNC=ARSCUR(PHI,IO)/(R*R*R)
0020            STPS=.5*(STEPA+STEPB)
0021            B1=B1+FUNC*SIN(PSI)*STPS
0022            B2=B2+FUNC*CPSI*STPS
0023            B3=B3+FUNC*STPS
0024            IF(STEPB-.00C1745)10,10,7
0025          7 STEPA=STEPB
0026            GO TO 5
0027         10 CONTINUE
0028            HP=.39998*(ZO+.93363)*B2*1.5679E-5
0029            HO=.39998*(ZO+.93363)*B1*1.5679E-5
0030            HZ=.39998*(.39998*B3-PO*B2)*1.5679E-5
0031            H=(A*HZ-B*HP)/EL
0032            Z=-(A*HP+B*HZ)/EL
0033            E=HO
0034            RETURN
0035            END
```

```
DOS FORTRAN IV 360V-F0-479 3-1          CURR                DATE   04/28/70      TIME    17.20.01      PAGE 0001

0001                FUNCTION CURR(PHI,IO)
                C EVALUATE CURRENT VALUES FROM 4 SOURCES
                C FOR AKASOFU MAGNETIC FIELD MODELS          MODEL = B
                C
                C       S.GELLER FOR K.KAWASAKI      31 MARCH 1970
                C
0002                REAL IO,PI/3.1415927/,TWOPI/6.283185/
0003                INTEGER TYPE,QUAD
                C
                C GENERAL ENTRY, EVALUATE QUADRANTS, ADJUST ANGLE, SELECT TYPE
                C
0004             10 P= AMOD(PHI+TWOPI, TWOPI)
0005                QUAD=12
0006                IF(P .GT. PI) QUAD=34
0007                GO TO TYPE,(1,2,3,4)
                C
                C
                C ENTRY POINTS, WHICH IDENTIFY TYPE OF CURRENT DESIRED
                C       (NOTE THAT CURR IS NEVER CALLED ITSELF)
                C
                C NORTH AURORAL JET
0008                ENTRY ARNCUR(PHI,IO)
0009                ASSIGN 1 TO TYPE
0010                GO TO 10
                C SOUTH AURORAL JET
0011                ENTRY ARSCUR(PHI,IO)
0012                ASSIGN 2 TO TYPE
0013                GO TO 10
                C FIELD-ALIGNED SHEET CURRENT
0014                ENTRY FLDCUR(PHI,IO)
0015                ASSIGN 3 TO TYPE
0016                GO TO 10
                C EQUATORIAL RING CURRENT
0017                ENTRY EQTCUR(PHI,IO)
0018                ASSIGN 4 TO TYPE
0019                GO TO 10
                C
                C
                C PROCESSING ROUTINES
                C
                C NORTH AURORAL JET CURRENT
0020             1      IF(QUAD .EQ. 12) CURR=0.
0021                    IF(QUAD .EQ. 34) CURR= - IO * SIN(P)**2
0022                    RETURN
                C
                C SOUTH AURORAL JET CURRENT
0023             2      GO TO 1
                C
                C SHEET CURRENT (FIELD ALIGNED)
0024             3      IF(QUAD .EQ. 12) CURR= 0.0
0025                    IF(QUAD .EQ. 34) CURR= IO * SIN(2.*P)
0026                    RETURN
                C
                C EQUATORIAL RING CURRENT
```

```
IBM OS FORTRAN IV 360N-FC-472 3-1          CURR              DATE   04/28/70     TIME     17.20.01      PAGE 0002

0027          4     IF(IOLAD .EQ. 12) CURR= -2. * IO *IO
0028                IF(IOLAD .EQ. 34) CURR= - 2. * IO * COS(PI**2 *IO
0029                RETURN
0030                END
```

APPENDIX III

This Appendix is a listing of the computer program used to calculate the fields of the ring and magnetotail currents and the earth's dipole-image dipole (simulating boundary currents) for the midnight magnetic meridian plane as described in Section 6.3. These programs plot field direction grids and field lines in the midnight magnetic meridian plane.

The original sub-routines of Akasofu (1966) are used to calculate the ring current field. These are labeled 'CURSE' and 'RING'. 'FCENT', 'G1', 'G2', 'ALPHA' correspond to r_{eo}, g_1, g_2, and p of Section 6.3 respectively. A grid of ring current values for $r \leq 10\ R_e$ calculated by Akasofu is extended by interpolation to in-between points. 'RTAB' calculates values for points $\geq 10\ R_e$; 'FJ' corresponds to $n_o\varepsilon$ of Section 6.3.

A grid of field line directions may be obtained from the program labeled 'KKGRID' and tracings of field lines by the program 'KKFIELD'. The Z-component (positive in the antisolar direction in the equatorial plane) and the X-component (positive northward from the equatorial plane) of the earth's dipole image dipole and the tail current are calculated by the sub-programs 'ZCOMP' and 'PCOMP', respectively. 'J_o/c', 'RHO PR', 'D' and 'N' correspond to B_{so}, ρ', d and n of Section 6.3, respectively.

A sub-routine to determine the proper step-size in the field line tracing program is labeled 'KSTEP'. The sub-routine 'EDGE' determines the ring current field in the equatorial plane and the edges of the tail current, where the tail current field is non-analytic.

```
OOS FORTRAN IV 360N-FO-479 3-1        RTAB              DATE   01/14/71     TIME    13.30.13      PAGE 0001

            C RING CURRENT CALCULATIONS
0001              DIMENSION    CUR  (25,100), FJ(4), CON(4)
0002              COMMON CUR, A, W, X
0003              DATA  CON / 4*0.0 /
0004              W = 6.990E-6
0005          100 READ(1,1100,END=999)FCENT,G1, G2, ALPHA, (FJ(I),I=1,4)
0006         1100 FORMAT ( 8F10.0 )
0007              IF(FCENT.NE.CON(1)) GO TO 110
0008              IF(G1.NE.CON(2)) GO TO 110
0009              IF(G2.NE.CON(3)) GO TO 110
0010              IF(ALPHA.NE.CON(4)) GO TO 110
0011              GO TO 120
0012          110 CALL CURSE (FCENT,G1,G2,ALPHA)
0013              CON(1) = FCENT
0014              CON(2) = G1
0015              CON(3) = G2
0016              CON(4) = ALPHA
0017          120 NFJ = 0
0018          121 NFJ = NFJ + 1
0019              TEST = 0.
0020              IF(NFJ.GT.4) GO TO 100
0021              IF ( FJ(NFJ) .GT. 0. ) GO TO 125
0022              IF ( FJ(NFJ) .EQ. 0. ) GO TO 100
0023              TEST = 1.
0024              FJ(NFJ) = ABS(FJ(NFJ))
0025          125 WRITE (3,3301) FCENT, G1, G2, ALPHA, FJ(NFJ)
0026         3301 FORMAT ('1', 10X,'FCENT = ',F6.2, 5X,'G1 =  ', F6.3,5X,'G2 = ',
                1        F6.3,5X,'ALPHA = ',F6.2,5X,'FJ = ',F8.1,// )
0027              IF ( TEST .EQ. 0. ) GO TO 130
0028          127 READ(1,1500) XT, YT, IZ8, IP8
0029         1500 FORMAT ( 2F10.0, 2I5 )
0030              IF ( XT .EQ. 0. ) GO TO 121
0031              PHIR = ATAN (YT/XT )
0032              PHI = PHIR*57.2957795
0033              COSP = COS(PHIR)
0034              COS2P = COSP * COSP
0035              R = SQRT ( XT*XT + YT*YT )
0036              F = R/COS2P
0037              CALL RING ( F, PHI, GP, GZ, GH )
0038                 KP = GP * FJ(NFJ)
0039              KZ = GZ * FJ(NFJ)
0040              WRITE (3,4000) KP, IP8, KZ, IZ8
0041         4000 FORMAT (' ', '   KP CALCULATED AS ', I6, '  SHOULD HAVE VALUE OF',
                1        I6,// '   KZ CALCULATED AS ',I6, '  SHOULD HAVE VALUE OF',
                2        I6,//)
0042              GO TO 127
0043          130 WRITE(3,3302)
0044         3302 FORMAT (' ','       P          Z       BGHP       BGHZ  ', //)
0045              DO 180 JP = 12, 20, 4
0046              X = JP
0047              DO  170 JZ = 1, 9, 4
0048              Y = JZ
0049              PHIR = ATAN(Y/X)
0050              PHI  = PHIR * 57.2957795
```

```
0051                COSP = COS(PHIR)
0052                COS2P = COSP*COSP
0053                R = SQRT(X*X + Y*Y)
0054                F = R / COS2P
0055                CALL RING ( F, PHI, HPI, HZ, H )
0056                IP = HPI * FJ(NFJ)
0057                IZ = HZ  * FJ(NFJ)
0058                WRITE (3,3303) JP,JZ,IP,IZ
0059             3303 FORMAT(' ', 4I10 , / )
0060              170 CONTINUE
0061              180 CONTINUE
0062                  GO TO 121
0063              999 WRITE(3,3304)
0064             3304 FORMAT(' END OF JOB' )
0065                  CALL EXIT
0066                  END
```

```
DOS FORTRAN IV 360N-FO-479 3-1        CURSE          DATE   01/07/71    TIME   07.04.13    PAGE 0001

0001              SUBROUTINE CURSE(FCENT,G1,G2,ALPHA)
0002              DIMENSION CUR( 25,100)
0003              COMMON CUR,A,W,X
0004              BALPHA=(ALPHA+2.)/(4.*(ALPHA+3.))
0005              X=3.*FCENT*FCENT*(1.-6.*BALPHA)
0006              A=-X*W
0007              DO 33 I=1,25
0008              PR=(2.*I-1.)/57.29578
0009              SINP=SIN(PR)
0010              SIN2P=SINP*SINP
0011              COSP=COS(PR)
0012              OD=3.*(1.-6.*BALPHA)*(1.+SIN2P)*COSP**(5.+3.*ALPHA)/
                  1(1.+3.*SIN2P)**(2.+ALPHA/4.)
0013              ODPK=6.*ALPHA*BALPHA*SIN2P*(3.+5.*SIN2P)*COSP**(3.*ALPHA+3.)/
                  1(1.+3.*SIN2P)**(4.+ALPHA/2.)
0014              E=2.*BALPHA*COSP**(3.*ALPHA+3.)/(1.+3.*SIN2P)**(ALPHA/4.)
0015              DO 44 J=1,100
0016              Z=1.+.1*J-FCENT
0017              Z2=Z*Z
0018              F2=Z+FCENT
0019              A2=F2*F2
0020              A3=A2*F2
0021              IF(Z)55,66,66
0022           55 G=G1
0023              GO TO 77
0024           66 G=G2
0025           77 B=EXP(-G*G*Z2)
0026              E=2.*G*G*Z*A3*B
0027              C=A2*B
0028           44 CUR(I,J)=(C*(D+DPK)+E*F)/X
0029           33 CONTINUE
0030              RETURN
0031              END
```

```
DOS FORTRAN IV 360N-FO-479 3-1        RING        DATE  01/07/71   TIME  07.04.50   PAGE 0001

0001                SUBROUTINE RING(F,PHI,HPI,HZ,H)
0002                COMMON CUR(25,100),A,W,X
0003                PHIR=PHI/57.29578
0004                COSP=COS(PHIR)
0005                COS2P=COSP*COSP
0006                COS3P=COSP*COS2P
0007                FTM=F*COS2P*SIN(PHIR)
0008                FL=F*COS3P
0009                FL2=FL*FL
0010                HPI=0.
0011                HZ=0.
                C   SET INITIAL VALUE OF P.
0012                P=-1.
                C   LOOP THRU VALUES OF P. COMPUTE FUNCTIONS OF P ONLY.
0013                DO 22 I=1,25
0014                P=P+2.
0015                PR=P/57.29578
0016                CSP=COS(PR)
0017                CS2P=CSP*CSP
0018                CS3P=CSP*CS2P
0019                C2S1P=CS2P*SIN(PR)
                C   LOOP ON F2 VALUES FROM 1.2 THRU 11.1.
0020                F2=1.1
0021                DO 20 J=1,100
0022                F2=F2+.1
                C   COMPUTE EVEN FUNCTIONS OF F2 AND P.
0023                FN=F2*CS3P
0024                FN2=FN*FN
0025                G=FN*CSP
0026                CURAG=CUR(I,J)*A*G
                C   CALCULATE FOR POSITIVE P.
0027                IF(ABS(F-F2)-.0512,3,3
0028              2 IF(ABS(PHI-PI-1.)8,3,3
0029              3 FM=FTM-F2*C2S1P
0030                FM2=FM*FM
0031                FMFL2=FL2+FM2
0032                D1=(FN+FL)**2+FM2
0033                D2=(FN-FL)**2+FM2
0034                FA=SQRT(4.*FN*FL/D1)
0035                IF(FA)16,4,4
0036              4 IF(FA-1.)6,5,5
0037              5 FK=6.50
0038                FE=1.00
0039                GO TO 7
0040             16 FK=1.570796
0041                FE=1.570796
0042                GO TO 7
0043              6 ETA=1.-FA*FA
0044                BE=-ALOG(ETA)
0045                ETA2=ETA*ETA
0046               OFK=1.386294+.1119723*ETA+.0725296*ETA2
                   1+(.5+.1213478*ETA+.0288729*ETA2)*BE
0047               OFE=1.+.4630151*ETA+.1077812*ETA2+(.2452727*ETA
                   1+.0412496*ETA2)*BE
```

```
0048            7 CURDG=CURAG/SQRT(D1)
0049              B=FE/D2
0050              HPI=HPI+CURDG/FL*FM*(-FK+(FN2+FMFL2)*B)
0051              HZ=HZ+CURDG*(FK+(FN2-FMFL2)*B)
                C     CALCULATE FOR -P. SIN(P) IS ONLY ODD FUNCTION.
0052            8 IF(ABS(F-F2)-.05)9,10,10
0053            9 IF(ABS(PHI+PI)-1.)20,10,10
0054           10 FM=FTM+F2*C2SIP
0055              FM2=FM*FM
0056              FMFL2=FL2+FM2
0057              D1=(FN+FL)**2+FM2
0058              D2=(FN-FL)**2+FM2
0059              FA=SQRT(4.*FN*FL/D1)
0060              IF(FA)15,11,11
0061           11 IF(FA-1.)13,12,12
0062           12 FK=6.50
0063              FE=1.00
0064              GO TO 14
0065           15 FK=1.570796
0066              FE=1.570796
0067              GO TO 14
0068           13 ETA=1.-FA*FA
0069              BE=-ALOG(ETA)
0070              ETA2=ETA*ETA
0071             OFK=1.386294+.1119723*ETA+.0725296*ETA2
                 1+(.5+.1213478*ETA+.0288729*ETA2)*BE
0072             OFE=1.+.4630151*ETA+.1077812*ETA2+(.2452727*ETA
                 1+.0412496*ETA2)*BE
0073           14 CURDG=CURAG/SQRT(D1)
0074              B=FE/D2
0075              HPI=HPI+CURDG/FL*FM*(-FK+(FN2+FMFL2)*B)
0076              HZ=HZ+CURDG*(FK+(FN2-FMFL2)*B)
0077           20 CONTINUE
0078           22 CONTINUE
0079              H=SQRT(HPI**2+HZ**2)
0080              RETURN
0081              END
```

```
005 FORTRAN IV 360V-F0-479 3-1        KKGRID          DATE   02/05/71     TIME    09.42.36      PAGE 0001

                C
                C ROUTINE TO MAP MAGNETIC FIELD AS A GRID RATHER THAN INDIVIDUAL
                C FIELD LINES
                C
0001                  DIMENSION PARM(7)
0002                  DIMENSION    RZ(20,10), RP(20,10)
0003                  DIMENSION    RZ(20,10),RP(20,10)
0004                  EQUIVALENCE      (PARM(1),RJ0),  (PARM(2),RP1),  (PARM(3),D),
                     2 (PARM(4),Z1),   (PARM(5),Z2),   (PARM(6),EM),   (PARM(7),EN)
0005                  COMMON /FIELD/ PARM
                C
                C
                C
0006                  DTR = 3.141593 / 180.0
0007                  IO = 0
                C
                C ZERO OUTPRING CURRENT ARRAYS AND FIELD ARRAYS
                C
0008                  DO 4 I = 1, 20
0009                  DO 3 J = 1, 10
0010                  RZ(I,J) = 0.0
0011                  RP(I,J) = 0.0
0012                  BZ(I,J) = 0.0
0013                  BP(I,J) = 0.0
0014                3 CONTINUE
0015                4 CONTINUE
                C
                C INITIALIZE PLOTTER ROUTINES
                C
0016                  CALL PLOTST
                C
                C READ SPECIAL INPUT PARAMETERS
                C
                C
                C USE OF NOP1 AND NOP2
                C NOP1 CONCERNS WHAT TO DO WITH RING CURRENT
                C        NOP1 =  0 NO RING CURRENT CONSIDERED
                C        NOP1 = +1 GRID OF RING CURRENT ADDED TO FIELD COMPONENTS
                C        NOP1 = -1 GRID OF RING CURRENT ALONE
                C
                C NOP2 CONCERNS HOW TO GET FIELD COMPONENTS
                C        NOP2 = -1 READ FIELD COMPONENTS FROM CARDS
                C        NOP2 =  0 INTEGRATE TO GET FIELD COMPONENTS - NO DECK PUNCHED
                C        NOP2 = +1 INTEGRATE TO GET FIELD COMPONENTS - PUNCH DECK
                C
0017                1 READ(1,1000,END=999) JO, RP, D, Z1, Z2, EM, EN, EJ, NOP1, NOP2
0018             1000 FORMAT ( I5, 7F10.0 , 2I2 )
0019                  RJO = JO * 1.0E-6
0020                  IF ( NOP1 .EQ. 0 ) GO TO 9
                C
                C READ ARRAYS OF RING CURRENT COEFFICIENTS
                C
0021                  DO 5 I = 1, 20
0022                  READ ( 1, 1010 ) IC, (RZ(IC,J1,J=1,10)
```

```
OOS FORTRAN IV 360N-F0-479 3-1        KKGRID          DATE   02/06/71     TIME   00.42.36     PAGE 0002

0023          1010 FORMAT ( I2, 1X, 10F7.0 )
0024             5 CONTINUE
0025               DO 6 I = 1, 20
0026               READ ( 1,1010) IC,(RP(IC,J),J=1,10)
0027             6 CONTINUE
0028               DO 8 I = 1, 20
0029               DO 7 J = 1, 10
0030               RZ(I,J) = RZ(I,J) * 1.0E-05 * ( EJ / 4500. )
0031               RP(I,J) = RP(I,J) * 1.0E-05 * ( EJ / 4500. )
0032             7 CONTINUE
0033             8 CONTINUE
0034               WRITE(3,3000)
0035          3000 FORMAT('1', T40, 'FIELD LINE TRACE PROGRAM - KOJI KAWASAKI MODEL',
                     1       ///,'  INPUT PARAMETERS      J0/C     RHO PR          D     ',
                     2       '    Z1        Z2          M          N          EJ' )
0036               WRITE(3,3002) (PARM(I),I=1,7), EJ
0037          3002 FORMAT(' ', 20X, 7E10.5, ' ', E10.5 )
                  C
                  C READ ARRAY OF FIELD COEFFICIENTS
                  C
0038               IF ( NP22 .GE. 0 ) GO TO 109
0039               DO 105 I = 1,20
0040               READ ( 1,2010)  IC, ( RZ(IC,J),J=1,10)
0041          2010 FORMAT ( I2, 1X, 10F7.5 )
0042           105 CONTINUE
0043               DO 106 I = 1,20
0044               READ(1,2010) IC, (RP(IC,J),J=1,10)
0045           106 CONTINUE
                  C
                  C DRAW AND LABEL SEMI-EARTH FIGURE AT LEFT SIDE OF PLOT
                  C
0046           109 ANG = 3.141593 / 30.0
0047               ANG2 = ANG
0048               CALL SYMBOL (0.0, 4.25, .14, 'S', 0.0, 1 )
0049               CALL PLOT ( 0.0, 4.5, 3)
0050               CALL PLOT ( 0.0, 5.5, 2)
0051               CALL SYMBOL (0.0, 5.60, .14, 'N', 0.0, 1 )
0052               CALL PLOT ( 0.0, 5.5, 3)
0053               DO 10 I = 1, 30
0054               X = .5 * SIN(ANG)
0055               Y = 5. + .5*COS(ANG)
0056               CALL PLOT( X, Y, 2 )
0057            10 ANG = ANG + ANG2
                  C
                  C DRAW AND LABEL EQUATORIAL AXIS TO RIGHT OF EARTH FIGURE  -  SCALE
                  C USED IS 2 EARTH RADII PER INCH
                  C
0058               CALL PLOT ( 0.0, 5.0, 3 )
0059               DO 15 I = 1,22
0060               X = I*.5
0061               CALL SYMBOL ( X, 5.0, .07, 13, 0.0, -1 )
0062            15 CONTINUE
0063               CALL PLOT ( 0.0, 5.0, 2 )
0064               DO 16 I = 5,20,5
```

```
OOS FORTRAN IV 360N-FO-479 3-1        XXGRID          DATE   12/06/71     TIME   00.42.26     PAGE 0003

0065                X = I *.5 - .25
0066                XFP = I
0067                CALL PLOT ( X, 4.80, 3)
0068                CALL NUMBER ( X, 4.80, .14, XFP, 0.0, 1)
0069             16 CONTINUE
0070                CALL PLOT ( 10.3, 4.80, 3 )
0071                CALL SYMBOL ( 10.3, 4.80, .14, 'EARTH RADII', 0.0, 11 )
0072                CALL PLOT ( 8.0, 4.0, 3 )
0073                CALL SYMBOL ( 8.0, 4.0, 0.21, 'FIELD LINE TRACE', 0.0,16 )
0074                CALL PLOT ( 8.5, 3.6, 3 )
0075                CALL SYMBOL ( 8.5, 3.6, 0.14, 'K. KAWASAKI  MODEL', 0.0, 17 )
0076                X = 10.5
0077                DO 30 I = 1,7
0078                Y = 1.0 - 0.2*I
0079                CALL PLOT ( X, Y, 3 )
0080                GO TO (21, 22, 23, 24, 25, 26, 27 ), I
0081             21 CALL SYMBOL ( X, Y, .14, 'J0/C = ', 0.0, 7)
0082                CALL NUMBER (-0.0,-0.0,-0.0, PARM(I), 0.0, 4 )
0083                GO TO 30
0084             22 CALL SYMBOL ( X, Y, 0.14, 'PHO PR = ', 0.0, 9 )
0085                GO TO 28
0086             23 CALL SYMBOL ( X, Y, 0.14, 'D = ', 0.0, 4 )
0087                GO TO 28
0088             24 CALL SYMBOL ( X, Y, 0.14, 'Z1 = ', 0.0, 5 )
0089                GO TO 28
0090             25 CALL SYMBOL ( X, Y, 0.14, 'Z2 = ', 0.0, 5 )
0091                GO TO 28
0092             26 CALL SYMBOL ( X, Y, 0.14, 'M = ', 0.0, 4 )
0093                GO TO 28
0094             27 Y = 0.2
0095                CALL SYMBOL ( X, Y, 0.14, 'N = ', 0.0, 4 )
0096             28 CALL NUMBER(-0.0,-0.0,-0.0, PARM(I), 0.0, 2 )
0097             30 CONTINUE
                 C
                 C
                 C
0098                IF ( NOP1. EQ. 0 ) GO TO 36
0099                Y = 0.0
0100                CALL SYMBOL ( X, Y, 0.14, 'FJ = ', 0.0, 5 )
0101                CALL NUMBER ( -0.0, -0.0, -0.0, FJ, 0.0, 2 )
0102             36 WRITE (3,3023)
0103           3023 FORMAT ('1',7X,'Z',14X,'P',13X,'BZ',13X,'BP',14X,'B', // )
0104                N = 0
0105                IDD = 1
0106                IF ( NOP2 .EQ. -1 ) IDD = 2
0107                B = 1.0
0108                DO 50 I = 1,20
0109                DO 40 J = 1,10
0110                X = I
0111                Y = J
0112                GO TO (37,38), IDD
0113             37 CALL ZCOMP ( X, Y, BZ(I,J), IO, FJ )
0114                CALL PCOMP ( X, Y, BP(I,J), IO, FJ )
0115             38 BZ(I,J) = BZ(I,J) + BZ(I,J)
```

```
0116                BP(I,J) = BP(I,J) + RP(I,J)
0117                R = SQRT( RZ(I,J)*RZ(I,J) + BP(I,J)*BP(I,J) )
0118                WRITE(3,3004)X, Y, RZ(I,J), BP(I,J), R
0119             3004 FORMAT (' ', 5 ( 1X, E12.5, 2X ) )
0120                DX = .3 * RZ(I,J) / R
0121                DY = .3 * BP(I,J) / R
0122                XP = (X+DX)*.5
0123                YP = (Y+DY)*.5 + 5.
0124                CALL PLOT ( XP,YP,3)
0125                XP = (X-DX)*.5
0126                YP = (Y- DY)*.5 + 5.
0127                CALL PLOT (XP,YP,2)
0128                RZ(I,J) = RZ(I,J) - RZ(I,J)
0129                BP(I,J) = BP(I,J) - BP(I,J)
0130                N = N + 1
0131                IF ( N .LT.55 ) GO TO 35
0132                N = 0
0133                WRITE(3,3023)
0134             35 CONTINUE
0135             40 CONTINUE
                 C
                 C PUNCH DECK IF OPTION REQUIRES
                 C
0136                IF ( NOP2 .NE. 1 ) GO TO 50
0137                WRITE(2,2000) I, (RZ(I,K),K=1,10)
0138             2000 FORMAT ( I2, ' ', 10E7.5, '  Z' )
0139                WRITE(2,2001) I, ( BP(I,K),K=1,10)
0140             2001 FORMAT ( I2, ' ', 10E7.5, '  P' )
0141               50 CONTINUE
0142              999 CALL PLOT (0.0, 0.0, 100 )
0143                WRITE(3,3006)
0144             3006 FORMAT('0  END OF JOB ' )
0145                CALL EXIT
0146                END
```

```
      C
      C FIELD LINE TRACE PROGRAM  -  KOJI KAWASAKI MODEL
      C
0001        DIMENSION       XP(300),        YP(300),        BZ(300),
           1 BP(300),        PARM(7)
0002        DIMENSION    BOZ(20,10), BOP(20,10),  BDZ(20,10),  BDP(20,10)
0003        EQUIVALENCE      (PARM(1),RJ0),   (PARM(2),RP1),   (PARM(3),D),
           2 (PARM(4),Z1),    (PARM(5),Z2),    (PARM(6),EM),    (PARM(7),EN)
0004        COMMON /FIELD/ PARM
0005        COMMON / INTERP / BOZ, BOP, BDZ, BDP
      C
      C
0006        DTR = 3.141593 / 180.0
      C
      C INITIALIZE PLOTTER ROUTINES
      C
0007        CALL PLOTST
      C
      C READ SPECIAL INPUT PARAMETERS
      C
      C
      C USES OF FJ, INT, NOP1, AND NOP2
      C  FJ NE 0 MEANS RING CURRENT IS INCLUDED AND READ A DECK OF RING
      C       CURRENT COEFFICIENTS
      C  INT NE 0 MEANS READ A DECK OF FIELD COEFFICIENTS AND INTERPOLATE
      C  INT EQ 0 MEANS INTEGRATE TO GET FIELD COMPONENTS
      C
      C  NOP1 = 0 -- START ON EARTH - READ A CARD SPECIFYING LATITUDE
      C                    IN DEGREES --- READ A 2A CARD
      C  NOP1 = 1 -- START AT POINT (Z0,P0) - READ A 2A CARD
      C  NOP2 = +1 TRACE TOWARD EARTH
      C  NOP2 = -1 TRACE AWAY FROM EARTH
      C
      C  PROGRAM WILL NOT LET YOU START ON EARTH AND TRACE TOWARDS IT--
      C  DEFAULTS WILL BE SUPPLIED AND YOU WILL TRACE AWAY FROM EARTH TO
      C A DISTANCE OF 20 EARTH RADII
      C
0008         1 READ(1,1000,END=999) J0, RPR, D, Z1, Z2, EM, EN, FJ, NOP1, NOP2,
            1                       INT
0009       1000 FORMAT ( I5, 7F10.0, 2I2, I1 )
0010        RJ0 = J0 * 1.0E-5
0011        WRITE(3,3000)
0012       3000 FORMAT('1', 140, 'FIELD LINE TRACE PROGRAM - KOJI KAWASAKI MODEL',
           1      /// ' INPUT PARAMETERS      J0/C      RHO PR        D     ',
           2      '      Z1          Z2          M           N          FJ' )
0013        WRITE(3,3002) (PARM(I),I=1,7), FJ
0014       3002 FORMAT(' ', 20X, 7F10.5, ' ', F10.5 )
0015        IF ( FJ .EQ. 0. ) GO TO 6
      C
      C READ RING CURRENT COEFFICIENTS
      C
0016        DO 2 I = 1,20
0017        READ ( 1,1100) IC, (BOZ(IC,J),J=1,10)
0018       1100 FORMAT(I2, I4, 10F7.0)
```

```
DOS FORTRAN IV 360N-FO-479 3-1        KREFIELD        DATE   02/07/71    TIME    17.57.29      PAGE 0002

0019            2 CONTINUE
0020              DO 3 I = 1,20
0021              READ(1,1100) IC, (RDP(IC,J),J=1,10)
0022            3 CONTINUE
                C
                C ADJUST COEFFICIENTS FROM GAMMAS TO GAUSS AND FOR EJ NE 4500
0023              DO 5 I = 1,20
0024              DO 4 J = 1,10
0025              RDZ(I,J) = RDZ(I,J) * 1.0E-5 * (EJ/4500.)
0026              RDP(I,J) = RDP(I,J) * 1.0E-5 * (EJ/4500.)
0027            4 CONTINUE
0028            5 CONTINUE
0029              IF ( INT .EQ. 0) GO TO 9
                C
                C READ DECK OF FIELD COEFFICIENTS
                C
0030              DO 7 I = 1,20
0031              READ(1,1110) IC, (RDZ(IC,J),J=1,10),
0032           1110 FORMAT(I2, 1X, 10F7.5 )
0033            7 CONTINUE
0034              DO 8 I = 1,20
0035              READ(1,1110) IC, (RDP(IC,J),J=1,10)
0036            8 CONTINUE
                C
                C DRAW AND LABEL SEMI-EARTH FIGURE AT LEFT SIDE OF PLOT
                C
0037            9 ANG = 3.141593 / 30.0
0038              ANG2 = ANG
0039              CALL SYMBOL (0.0, 4.25, .14, 'S', 0.0, 1 )
0040              CALL PLOT ( 0.0, 4.5, 3)
0041              CALL PLOT ( 0.0, 5.5, 2)
0042              CALL SYMBOL (0.0, 5.60, .14, 'N', 0.0, 1 )
0043              CALL PLOT ( 0.0, 5.5, 3)
0044              DO 10 I = 1, 30
0045              X = .5 * SIN(ANG)
0046              Y = 5. + .5*COS(ANG)
0047              CALL PLOT( X, Y, 2 )
0048           10 ANG = ANG + ANG2
                C
                C DRAW AND LABEL EQUATORIAL AXIS TO RIGHT OF EARTH FIGURE  -  SCALE
                C USED IS 2 EARTH RADII PER INCH
                C
0049              CALL PLOT ( 0.0, 5.0, 3 )
0050              DO 15 I = 1,22
0051              X = I*.5
0052              CALL SYMBOL ( X, 5.0, .07, 13, 0.0, -1 )
0053           15 CONTINUE
0054              CALL PLOT ( 0.0, 5.0, 2 )
0055              DO 16 I = 5,20,5
0056              X = I *.5 - .25
0057              XFP = I
0058              CALL PLOT ( X, 4.80, 3)
0059              CALL NUMBER ( X, 4.80, .14, XFP, 0.0, 1)
0060           16 CONTINUE
```

```
0041              CALL PLOT ( 10.3, 5.10, 3 )
0042              CALL SYMBOL ( 10.3, 5.10, .14, 'EARTH RADII', 0.0, 11 )
0043              CALL PLOT ( 8.0, 9.0, 3 )
0044              CALL SYMBOL ( 8.0, 9.0, 0.21, 'FIELD LINE TRACE', 0.0,16 )
0045              CALL PLOT ( 8.5, 4.6, 3 )
0046              CALL SYMBOL ( 8.5, 8.6, 0.14, 'K. KAWASAKI MODEL', 0.0, 17 )
0047              X = 10.5
0048              DO 40 I = 1,7
0049              Y = 1.6 - 0.2*I
0050              CALL PLOT ( X, Y, 3 )
0051              GO TO (21, 22, 23, 24, 25, 26, 27 ), I
0052           21 CALL SYMBOL ( X, Y, .14, 'J0/C = ', 0.0, 7)
0053              CALL NUMBER (-0.0,-0.0,-0.0, PARM(I), 0.0, 5 )
0054              GO TO 30
0055           22 CALL SYMBOL ( X, Y, 0.14, 'J00 P2 = ', 0.0, 9 )
0056              GO TO 28
0057           23 CALL SYMBOL ( X, Y, 0.14, 'D = ', 0.0, 4 )
0058              GO TO 28
0059           24 CALL SYMBOL ( X, Y, 0.14, 'Z1 = ', 0.0, 5 )
0060              GO TO 28
0061           25 CALL SYMBOL ( X, Y, 0.14, 'Z2 = ', 0.0, 5 )
0062              GO TO 28
0063           26 CALL SYMBOL ( X, Y, 0.14, 'H = ', 0.0, 4 )
0064              GO TO 28
0065           27 Y = 0.2
0066              CALL SYMBOL ( X, Y, 0.14, 'N = ', 0.0, 4 )
0067           28 CALL NUMBER(-0.0,-0.0,-0.0, PARM(I), 0.0, 2 )
0068           30 CONTINUE
0069              Y = 0.0
0070              CALL SYMBOL ( X, Y, 0.14, 'EJ = ',0.0, 5)
0071              CALL NUMBER ( -0.0, -0.0, -0.0, EJ, 0.0, 2)
                  C
                  C COMBINE RING AND FIELD COMPONENTS
                  C
0072              IF ( INT.EQ.0.0 .OR. EJ.EQ.0.  ) GO TO 43
0073              DO 38 I = 1,20
0074              DO 36 J = 1,10
0075              BOZ(I,J) = BOZ(I,J) + ROZ(I,J)
0076              BOR(I,J) = BOR(I,J) + ROR(I,J)
0077           36 CONTINUE
0078           38 CONTINUE
0079           40 IF ( SOR1 .NE. 0 ) GO TO 45
                  C
                  C WHEN SOR1 EQUALS 0 STARTING LOCATION OF FIELD LINE TO BE TRACED
                  C IS READ IN AS LATITUDE IN DEGREES PHI0 AND CHANGED TO RADIANS  - THE
                  C INITIAL Z0 AND R0 ARE THEN CALCULATED
                  C
0080              READ ( 1,1001) PHI0, ZERO, STEP, IRET, IHALF, IOBL
0081           1001 FORMAT( F10.3, 10X, F10.0, F10.0, 30X, 3I1 )
0082              IF ( PHI0.NE.0.0 ) GO TO 42
                  C
                  C END CURRENT PLOT RECORD SINCE BLANK CARD SIGNALS END OF FIELD LINES TO
                  C BE PLOTTED ON THIS PARTICULAR PLOT
                  C
```

```
0103          41 CALL PLOT ( 15.0, 0.0, -3 )
0104             GO TO 1
0105          42 WRITE(3,3003) PHID
0106        3003 FORMAT('0', 10X, ' TRACE OF FIELD LINE ',F4.0,' DEGREES FROM JF',
                1       ' AXIS' )
0107             PHIR = PHID * DTR
0108             IF ( ZEND .EQ. 0.0 ) ZEND = 20.0
0109             IF ( NOP2 .EQ. +1 ) NOP2 = -1
0110             Z0 = COS(PHIR)
0111             P0 = SIN(PHIR)
0112             GO TO 48
                 C
                 C WHEN NOP1 EQUALS 1 STARTING LOCATION OF FIELD LINE TO BE TRACED
                 C IS READ IN AS THE INITIAL Z0 AND P0
                 C
0113          45 READ (1,1011) Z0, P0, ZEND, STEP, IRET, IHALF, IDBL
0114        1011 FORMAT ( 4F10.0, 30X, 3I1 )
0115             IF ( Z0 .EQ. 0.0 ) GO TO 41
0116             IF ( NOP2 .EQ. +1 .AND. ZEND .EQ. 0.0 ) ZEND = 1.0
0117             IF ( NOP2 .EQ. -1 .AND. ZEND .EQ. 0.0 ) ZEND = 20.0
0118             WRITE (3,3014) Z0, P0, ZEND
0119        3014 FORMAT ( '0', 10X, ' TRACE OF FIELD LINE STARTING AT POINT Z0 ='
                1       , F9.6, ' AND P0 = ', F9.4, ' ENDING ', F9.4,
                2       ' EARTH RADII FROM ORIGIN' )
                 C
                 C J IS INDEX INTO ARRAY OF POINTS TO BE PLOTTED
                 C STEP IS SET INITIALLY TO .125 OR 1/8 EARTH RADII IF UNSPECIFIED
                 C AND THEN ADJUSTED BY IHALF AND IDBL
                 C
0120          48 IF ( STEP .EQ. 0.0 ) STEP = 0.125
0121             IF ( IHALF .NE. 0 ) STEP = STEP / 2.**IHALF
0122             IF ( IDBL .NE. 0 ) STEP = STEP * 2.**IDBL
0123             J = 1
0124             XP(J) = Z0
0125             YP(J) = P0
0126             DIR = NOP2
                 C
                 C POSITION PLOTTER AT START OF THE FIELD LINE BEING TRACED
                 C
0127          49 X = XP(J)* 0.5
0128             Y = YP(J)* 0.5 + 5.0
0129             IF ( IRET .EQ. 2 ) Y = 5. - YP(J)*0.5
0130             CALL PLOT ( X, Y, 3 )
0131             WRITE (3,3023)
0132        3023 FORMAT ('0',7X,'Z',14X,'P',13X,'BZ',13X,'BP',14X,'B', // )
0133             ICHK = 0
                 C
                 C COMPUTE COMPONENTS OF MAGNETIC FIELD AT XP(J),YP(J) USING ROUTINES
                 C PCOMP AND ZCOMP
                 C
0134          50 CALL PCOMP ( XP(J), YP(J), BP(J), INT, FJ )
0135             CALL ZCOMP ( XP(J), YP(J), BZ(J), INT, FJ )
0136             IF ( J .LT. 3 ) GO TO 55
0137             IF ( ICHK .NE. 0 ) GO TO 55
```

```
0138                J3 = J - 2
                    C
                    C PLOT THE THIRD POINT BACK SINCE IT WILL BE KEPT AS A VALID POINT
                    C
0139                X = XP(J3) * 0.5
0140                Y = YP(J3) * 0.5 + 5.0
0141                IF ( Y .GT. 10. ) Y = 10.
0142                IF ( IRET .EQ. 2 ) Y = 5. - YP(J3)*0.5
0143                CALL PLOT ( X, Y, 2 )
0144                B = SQRT ( BZ(J3) * BZ(J3) + BP(J3) * BP(J3) )
0145                WRITE (3,3004) XP(J3), YP(J3), BZ(J3), BP(J3), B
0146           3004 FORMAT (' ', 5 ( 1X, F12.5, 2X ) )
0147             55 IF ( J .EQ. 300 ) GO TO 90
0148                IF ( ICHK .EQ. J ) GO TO 95
0149                CALL KSTEP ( STEP,DIR,IDBL,IHALF,ICHK,XP,YP,BZ,BP,ZEND,J )
0150                GO TO 50
                    C
                    C MORE THAN 300 POINTS ARE NEEDED TO DEFINE THE FIELD LINE - PRINT A
                    C MESSAGE AND PLOT WHAT IS AVAILABLE
                    C
0151                90 WRITE (3,3005)
0152           3005 FORMAT(' ','MORE THAN 300 POINTS REQUIRED TO PLOT FIELD LINE' )
                    C
                    C PLOT THE LAST TWO POINTS OF THE FIELD LINE IN THE NORTHERN
                    C HEMISPHERE AND PRINT THE CORRESPONDING FIELD VALUES
                    C
0153                95 CONTINUE
0154                K = J - 1
0155                X = XP(K) * 0.5
0156                Y = YP(K) * 0.5 + 5.0
0157                IF ( IRET .EQ. 2 ) Y = 5. - YP( K)*0.5
0158                CALL PLOT ( X, Y, 2 )
0159                B = SQRT ( BZ(K)*BZ(K) + BP(K)*BP(K) )
0160                WRITE(3,3004) XP(K),YP(K),BZ(K),BP(K),B
0161                X = XP(J) * 0.5
0162                Y = YP(J) * 0.5 + 5.0
0163                IF ( IRET .EQ. 2 ) Y = 5. - YP( J)*0.5
0164                CALL PLOT ( X, Y, 2 )
0165                B = SQRT ( BZ(J)*BZ(J) + BP(J)*BP(J) )
0166                WRITE(3,3004) XP(J), YP(J), BZ(J), BP(J), B
0167                IF ( IRET .EQ. 2 ) GO TO 40
0168                IF ( IRET .EQ. 0 ) GO TO 98
0169                XP(1) = XP(J)
0170                YP(1) = YP(J)
0171                DIR = -1. * DIR
0172                ZEND = 20
0173                J = 1
0174                WRITE (3,3007)
0175           3007 FORMAT (10', 29 ('**'), ' RETURN TRACE ', 29 ('**'), // )
0176                IRET = 2
0177                GO TO 49
                    C
                    C PLOT SOUTHERN HEMISPHERE AS A REFLECTION OF THE NORTHERN IF RETURN
                    C TRACE IS NOT REQUIRED
```

```
                C
     0178         98 X = XP(I) * 0.5
     0179            Y = 5.0 - 0.5*YP(I)
     0180            CALL PLOT ( X, Y, 3)
     0181            I = J
     0182            DO 110 J = 1,I
     0183            X = XP(J) * 0.5
     0184            Y = 5.0 - 0.5 * YP(J)
     0185            IF ( Y .LT. -10. ) Y = -10.
     0186            CALL PLOT (X, Y, 2)
     0187        110 CONTINUE
                C
                C GO CHECK IF ANOTHER FIELD LINE IS TO BE INCLUDED IN THIS PLOT
                C
     0188            GO TO 40
                C
                C END OF JOB - END FILE PLOT TAPE AND WRITE MESSAGE
                C
     0189        999 CALL PLOT (0.0, 0.0, 100 )
     0190            WRITE(3,3006)
     0191       3006 FORMAT('0  END OF JOB ' )
     0192            CALL EXIT
     0193            END
```

```
OOS FORTRAN IV 360N-FO-479 3-1          PCOMP              DATE   07/19/71      TIME     14.08.30      PAGE 0001

0001                SUBROUTINE PCOMP ( ZO, PO, BPO, INT, FJ, ILT )
                    C
                    C ROUTINE COMPUTES THE P-COMPONENT OF THE MAGNETIC FIELD AT INPUT
                    C COORDINATES ( ZO,PO ). - USES K.KAWASAKI'S MODEL
                    C
0002                     DIMENSION        PARM(7),          T(4),          S(4),
                    1 F(4)
0003                     DIMENSION ILT (3)
0004                     DIMENSION    BPZ(20,10), BPP(20,10),  BPZ(20,10),  BPP(20,10)
0005                     COMMON /FIELDZ/PARM
0006                     COMMON / INTERP / BPZ, BPP, BPZ, BPP
0007                     EQUIVALENCE      (PARM(1),BJO),   (PARM(2),RPR),  (PARM(3),O),
                    1 (PARM(4),Z1),  (PARM(5),Z2),  (PARM(6),FM),  (PARM(7),FN)
0008                     EQUIVALENCE      (T(1),TO),       (T(2),T13),     (T(3),T12),
                    1 (T(4),TN),     (S(1),SO),       (S(2),S13),     (S(3),S12),
                    2 (S(4),SN),     (F(1),FO),       (F(2),F13),     (F(3),F12),
                    3 (F(4),FN)
0009                     IF ( INT .EQ. 0 ) GO TO 100
                    C
                    C INTEGRATION SECTION
                    C
                    C
                    C SET UP CONSTANTS FOR THIS PARTICULAR RUN
                    C
0010                1 SQPO = PO * PO
0011                     SQPR = RPR * RPR
0012                     Z02  = (ZO - Z2) * (ZO - Z2)
0013                     Z01  = (ZO - Z1) * (ZO - Z1)
0014                     RRP  = RPR * PO * 2.0
0015                     SQO  = O * O
0016                     SQZO = ZO * ZO
0017                     VAL1 = 0.
0018                     IF ( PO.EQ.0. .AND. ILT(1).EQ.0 ) GO TO 70
                    C
                    C FIRST EVALUATE INTEGRAL AS THETA GOES FROM 0 TO PI / 2.0 RADIANS.
                    C START WITH STEPSIZE OF  1/20 OR ABOUT 9 DEGREES AND ADJUST AS NEEDED
                    C ALLOWABLE ERROR IS SET AT 0.0001.  INITIAL CONDITIONS ARE THETA = 0.0
                    C AND F = 0.0
                    C
0019                     ERR = 0.0001
0020                     TO = 0.0
0021                     FO = 0.0
0022                     YO = 0.0
0023                     W = 3.141593 / 20.0
0024                     TLIM = 3.141593 / 2.0
                    C
                    C COMPUTE FUNCTION VALUES AT TO, TO + W/3, TO + W/2, AND TO + W.
                    C FIRST CHECK IF STEP WILL TAKE US BEYOND END - IF SO ADJUST W
                    C
0025                10 IF ( TO+W .GT. TLIM ) W = TLIM - TO
0026                15 T13 = TO + W/3.0
0027                     T12 = TO + W/2.0
0028                     TN  = TO + W
0029                     SO  = SIN (TO)
```

```
0030              S13 = SIN (TI3)
0031              S12 = SIN (TI2)
0032              SN  = SIN (TN)
0033              TERM = SQRO * SQR8
0034              DO 25 I = 1, 4
0035              01 = SQRT (TERM - RRP*S(I) + Z02 )
0036              02 = SQRT (TERM + RRP*S(I) + Z02 )
0037              03 = SQRT (TERM - RRP*S(I) + Z01 )
0038              04 = SQRT (TERM + RRP*S(I) + Z01 )
0039              F(I) = RR3 * S(I) * .5 *( 1.0 /01 + 1.0/02 - 1.0/03 - 1.0/04 )
0040           25 CONTINUE
                C
                C CALCULATE CONSTANTS FOR VERSONS VERSION OF THE RUNGE KUTTA INTEGRATION
                C SEE R.A. BUCKINGHAM'S NUMERICAL METHODS PG 242 FOR DETAILS OF METHOD
                C ADVANTAGE OF THIS METHOD IS THAT ESTIMATE OF ERROR IS AVAILABLE
                C
0041              CONST = W / 3.0
0042              RK1  = CONST * F1
0043              RK2  = CONST * F13
0044              RK3  = CONST * F12
0045              RK4  = CONST * F12
0046              RK5  = CONST * F1
0047              Y = 0.5 * ( RK1 + 4.*RK4 + RK5 ) + YO
                C
                C GET ESTIMATE OF ERROR AND ADJUST W IF NECESSARY
                C
0048              ERR =ABS ( 2.0*RK1 - 9.0*RK3 + 8.0*RK4 - RK5 ) / 10.0
0049              IF (ERR .GT. .10*EPK) GO TO 30
0050              IF (ERR.LT. EPK/32.) GO TO 35
0051              GO TO 36
                C HALVE THE STEP SIZE AND RECOMPUTE NEW POINT
                C
0052           30 W = W / 2.0
0053              GO TO 15
                C
                C DOUBLE STEP SIZE FOR FUTURE POINTS KEEPING POINT JUST CALCULATED
                C
0054           35 W = W * 2.0
0055           36 TO = TN
0056              YO = Y
0057              IF ( TN .NE. TLIM ) GO TO 10
                C
                C WE ARE FINISHED WITH THE INTEGRAL  -  EVALUATE OTHER TERMS
                C
                C
                C DOUBLE VALUE OF THE INTEGRAL FROM 0 TO PI/2 TO GET VALUE FROM
                C 0 TO PI
                C
0058              VALI = Y * 2.0
                C
0059           75 VALL = 0.
0060              IF ( PO.EQ.0..AND. ILT(2).EQ.0 ) GO TO 85
                C
                C EVALUATE LOGARITHMIC TERM
```

```
OS FORTRAN IV 360N-FO-476 3-1          PCOMP              DATE   07/19/71     TIME    14.08.30      PAGE 0003

                C
0061                 F(1) = SQRT ( SQPO + SQPR + ZO2 ) + RPR
0062                 F(2) = SQRT ( SQPO + SQPR + ZO1 ) - RPR
0063                 F(3) = SQRT ( SQPO + SQPR + ZO1 ) + RPR
0064                 F(4) = SQRT ( SQPO + SQPR + ZO2 ) - RPR
0065                 VALL = ALOG ( (F(1)*F(2)) / (F(3)*F(4)) )
                C
0066              85 VALO = 0.
0067                 IF ( PO.EQ.0. .AND. ILT(3).EQ.0 ) GO TO 90
                C
                C EVALUATE FINAL TERM FOR SHEET FIELD
                C
0068                 TERM1 = (SQZO - 2.0*SQPO) / (SQPO * SQZO)**2.5
0069                 SUM1  = SQZO * (SQO- SQPO + SQZO + 2.0*ZO*PO )
0070                 SUM2  = SQPO * ( -2.0*SQPO + 2.0*PO*ZO + SQO )
0071                 TNUM  = SUM1 * ( SUM1 + SUM2 )
0072                 TDEN  = (SQPO + SQZO)*(SQO + SQPO + SQZO + 2.0*PO*ZO)**2.5
0073                 TERM2 = TNUM / TDEN
0074                 VALO  = EM *(TERM1 + TERM2)
                C
                C COMBINE ALL VALUES TO GET FIELD COMPONENT
                C
0075              90 BPO =  -1.0 * BJO * (VALI - VALL) + VALO
0076                 IF ( INT .NE. 0 ) GO TO 150
0077                 GO TO 200
                C
                C INTERPOLATE - FIRST FIND THE 4 POINTS AROUND THE GIVEN PT (ZO,PO)
0078              100 I1 = ZO
0079                 I2 = I1 + 1
0080                 J1 = PO
0081                 J2 = J1 + 1
                C
                C CHECK IF WITHIN 1 F.R. OF AXIS - IF SO GO CALL EDGE TO INTERPOLATE
                C RING CURRENT VALUES THEN INTEGRATE FOR THE REST OF THE FIELD AND
                C COMBINE
                C
0082                 IF ( I1.EQ.0 .OR. J1.EQ.0 ) GO TO 1
                C
                C INTERPOLATE FIELD NOT ON EDGE - FORCE J2 TO BE LT 10 F.R.
                C BL = BOTTOM LEFT, TL = TOP LEFT, ETC - FIELD VALUES AT CORNORS
                C
0083                 IF ( J2 .GT. 10 )  J2 = 10
0084                 BL = BOP(I1,J1)
0085                 TL = BOP(I1,J2)
0086                 BR = BOP ( I2,J1)
0087                 TR = BOP(I2,J2)
0088                 TT = (ZO - I1) * (TR - TL) + TL
0089                 BB = (ZO - I1) * (BR - BL) + BL
0090                 BPO = ( PO - J1 ) * ( TT - BB ) + BB
0091                 GO TO 200
0092              150 CALL EDGE ( I1, I2, J1, J2, FJ, FP, I, PO, ZO)
0093                 BPO = BPO + FP
0094              200 RETURN
0095                 END
```

```
DOS FORTRAN IV 360N-FO-479 3-1          ZCOMP              DATE    02/19/71      TIME     14.07.21      PAGE 0001

0001                SUBROUTINE ZCOMP ( ZO, PO, BZO, JNT, FJ, ILT )
                    C
                    C ROUTINE COMPUTES THE Z-COMPONENT OF THE MAGNETIC FIELD AT INPUT
                    C COORDINATES (ZO,PO). - USES K. KAWASAKI'S MODEL
                    C ADDITIONAL INFORMATION ABOUT METHODS CAN BE FOUND IN PCOMP SINCE
                    C SAME GENERAL FORM WAS USED IN BOTH AND NOT ALL COMMENTS REPEATED
                    C
0002                      DIMENSION        PARM(7),        T(4),           S(4),
                        1 F(4),            VALI(2),        VALT(2)
0003                      DIMENSION ILT(3)
0004                      DIMENSION  BOZ(20,10), BOP(20,10),  BOZ(20,10),  BOP(20,10)
0005                      COMMON /FIELDZ/ PARM
0006                      COMMON / INTERP / BOZ, BOP, BOZ, BOP
0007                      EQUIVALENCE      (PARM(1),RJO),  (PARM(2),RPR),  (PARM(3),O),
                        1 (PARM(4),Z1),    (PARM(5),Z2),   (PARM(6),EM),   (PARM(7),EN),
                        3 (T(1),TO),       (T(2),T13),     (T(3),T12),     (T(4),TN),
                        4 (S(1),SO),       (S(2),S13),     (S(3),S12),     (S(4),SN),
                        5 (F(1),FO),       (F(2),F13),     (F(3),F12),     (F(4),FN)
0008                      IF ( JNT .NE. 0 ) GO TO 100
                    C
                    C INTEGRATION SECTION
                    C
                    C
                    C SET UP CONSTANTS
                    C
0009                  1 SOPO = PO * PO
0010                    SOPR = RPR * RPR
0011                    ZO2 = (ZO - Z2) * (ZO - Z2)
0012                    ZO1 = (ZO - Z1) * (ZO - Z1)
0013                    RRP = RPR * PO * 2.0
0014                    SOO = O * O
0015                    SOZO = ZO * ZO
                    C
0016                    VALT(1) = 0.
0017                    VALI(2) = 0.
0018                    IF ( PO.EQ.0. .AND. ILT(1).EQ.0 ) GO TO 70
                    C EVALUATE THE FIRST INTEGRAL AS THETA GOES FROM 0 TO PI      RADIANS
                    C START WITH STEP OF 18 DEGREES, ALLOWABLE ERROR OF 0.0001. INITIAL
                    C CONDITIONS ARE THETA = 0.0  AND  F = 0.0
                    C
0019                      JNT = 1
                    C
                    C INT SPECIFIES WHICH INTEGRAL IS BEING EVALUATED
                    C
0020                      ERR = 0.0001
0021                      TO  = 0.0
0022                      FO  = 0.0
0023                      YO = 0.0
0024                      ILIM = 3.141593
0025                      W = 3.141593 / 10.0
                    C
                    C COMPUTE FUNCTION VALUES AT TO, TO + W/3, TO + W/2, AND  TO + W.
                    C FIRST CHECK IF STEP WILL TAKE US BEYOND END - IF SO ADJUST
0026                  10 IF ( TO + W .GT. ILIM ) W = ILIM - TO
```

```
0027          15 T13 = T0 + W/3.0
0028             T12 = T0 + W/2.0
0029             TN  = T0 + W
0030             DO 17 I = 1,4
0031          17 S(I) = SIN(T(I))
0032             DO 25 I = 1,4
0033             Q1 = RP2 * (RPK - P0*S(I))
0034             Q2 = Z0 - Z1
0035             Q3 = Z0 - Z2
0036             Q4 = (S)P0 + SQPR - 3RP* S(I) ) * 2.0
0037             Q5 = SQRT ( SQP0 + SQPR - RRP*S(I) + Z01 )
0038             Q6 = SQRT ( SQP0 + SQPR - RRP*S(I) + Z02 )
0039             F(I) = (Q1/Q4) * ( Q2/Q5 - Q3/Q6 )
0040          25 CONTINUE
               C
               C CALCULATE CONSTANTS FOR JEFSONS VERSION OF KUTTA INTEGRATION AS IN
               C ROUTINE RCOMP
               C
0041             2a CON = W /3.0
0042             RK1 = CON * F0
0043             RK2 = CON * F13
0044             RK3 = CON * F13
0045             RK4 = CON * F12
0046             RK5 = CON * FN
0047             Y = 0.5 * ( RK1 + 4.*RK4 + RK5 ) + Y0
               C
               C ESTIMATE ERROR
               C
0048             ERR =ABS (2.0 *RK1 - 9.0*RK3 + 8.0*RK4 - RK5) / 10.0
0049             IF (ERR.GT. 10.* EOK ) GO TO 30
0050             IF (ERR.LT. EOK/32. ) GO TO 35
0051             GO TO 36
               C
               C HALVE STEP SIZE
               C
0052          30 W = W / 2.0
0053             GO TO (15,55), INT
               C
               C DOUBLE STEP SIZE
               C
0054          35 W = W * 2.0
0055          36 T0 = TN
0056             Y0 = Y
0057             IF ( TN .EQ. TLIM ) GO TO 37
0058             GO TO (10,50),INT
0059          37 VAL(INT) = Y
0060             GO TO (40,70), INT
               C
               C EVALUATE THE SECOND INTEGRAL - SAME LIMITS ETC AS FIRST INTEGRAL
               C
0061          40 INT = 2
0062             T0 = 0.0
0063             Y0 = 0.0
0064             TLIM = 3.141593
```

```
005 FORTRAN IV 360N-FO-479 3-1      ZCOMP              DATE   02/19/71     TIME    14.07.21      PAGE 0003

0065              W = 3.141593 / 10.0
0066           50 IF ( TO + W .GT. TLIM ) W = TLIM - TO
0067           55 T13 = TO + W/3.0
0068              T12 = TO + W/2.0
0069              TN = TO + W
0070              DO 57 I = 1,4
0071           57 S(I) = SIN(T(I))
0072              DO 65 I = 1,4
0073              D1 = RPR * ( RPR + PO*S(I))
0074              D2 = ZO - Z2
0075              D3 = ZO - Z1
0076              D4 = (SQPO + SQPR + RRP* S(I) ) * 2.0
0077              D5 = SQRT ( SQPO + SQPR + RRP*S(I) + Z02 )
0078              D6 = SQRT ( SQPO + SQPR + RRP*S(I) + Z01 )
0079              F(I) = (D1/D4) * ( D2/D5 - D3/D6 )
0080           65 CONTINUE
0081              GO TO 26
0082           70 VALT(1) = 0.
0083              VALT(2) = 0.
0084              IF ( PO.EQ.0. .AND. ELT(2).EQ.0 ) GO TO 85
                C
                C EVALUATE TRIGONOMETRIC EXPRESSIONS
                C
0085              F(1) = RPR * (ZO - Z2 )
0086              F(2) = SQRT ( SQPO + SQPR + Z02 )
0087              VALT(1) = ATAN ( F(1) / (PO * F(2) ) )
0088              F(1) = RPR * (ZO - Z1 )
0089              F(2) = SQRT ( SQPO + SQPR + Z01 )
0090              VALT(2) = ATAN ( F(1) / ( PO * F(2) ) )
                C
                C FORCE VALUES TO BE BETWEEN -PI/2 AND +PI/2 RADIANS
                C
0091              RTD = 180.0 / 3.141593
0092              DTR = 1.0 / RTD
0093              DO 80 I = 1,2
0094              VALT(I) = VALT(I) * RTD
0095              IF ( VALT(I) .GT. 90. ) VALT(I) = VALT(I) - 180.
0096              VALT(I) = VALT(I) * DTR
0097           80 CONTINUE
0098           85 VAL0 = 0.
0099              IF ( PO.EQ.0. .AND. ELT(3).EQ.0 ) GO TO 90
                C
                C EVALUATE SHEET CURRENT TERM
                C
0100              TERM1 = ZO / ( SQPO +  SQZ01**2.5
0101              TERM2 = EN * (ZO + 3) / ( S00 + SQZ0 + SQPO + 2.0*D*ZO1**2.5
0102              VAL0 = 3.0 * EM * PO * ( TERM1 + TERM2 )
                C
                C COMBINE ALL
                C
0103           90 SUM = VALT(1) + VALT(2) - 2. * VALT(1) + 2. * VALT(2)
0104              PJO = -1.0 * PJO* SUM - VAL0
0105              IF ( JNT .NE. 0 ) GO TO 150
0106              GO TO 290
```

```
                C
                C INTERPOLATE - FIRST FIND THE 4 POINTS AROUND THE GIVEN PT (ZO,PO)
0107              100 II = ZO
0108                  I2 = II + 1
0109                  J1 = PO
0110                  J2 = J1 + 1
                C
                C CHECK IF WITHIN 1 E.R. OF AXIS - IF SO,GO CALL EDGE TO INTERPOLATE
                C RING CURRENT VALUES THEN INTEGRATE FOR THE REST OF THE FIELD AND
                C COMBINE
                C
0111                  IF ( II.EQ.0 .OR. J1.EQ.0 ) GO TO 1
                C
                C INTERPOLATE FIELD NOT ON EDGE - FORCE J2 TO BE LT 10 E.R.
                C BL = BOTTOM LEFT, TL = TOP LEFT, ETC - FIELD VALUES AT CORNERS
                C
0112                  IF ( J2 .GT. 10 )  J2 = 10
0113                  BL = BOZ(I1,J1)
0114                  TL = BOZ(I1,J2)
0115                  BR = BOZ ( I2,J1)
0116                  TR = BOZ(I2,J2)
0117                  TT = (ZO - II) * (TR - TL) + TL
0118                  BB = (ZO - II) * (BR - BL) + BL
0119                  BZO = ( PO - J1 ) * ( TT - BB ) + BB
0120                  GO TO 200
0121              150 CALL EDGE ( I1, I2, J1, J2, EJ, EZ, Z, PO, ZO)
0122                  BZO = BZO + EZ
0123              200 RETURN
0124                  END
```

```
DOS FORTRAN IV 360N-FO-479 3-1        KSTEP          DATE   02/11/71     TIME    18.35.56      PAGE 0001

0001            SUBROUTINE KSTEP ( STEP,DIR,IDBL,IHALF,LAST,XP,YP,BZ,BP,ZEND,J )
                C
                C ROUTINE EXAMINES LATEST TWO OR THREE POINTS AND ADJUSTS THE STEPSIZE
                C ACCORDING TO THE RATE OF CHANGE OF EITHER THE INTENSITY OR DIRECTION
                C OF THE MAGNETIC FIELD - INPUT PARAMETERS ARE
                C      STEP   -  CURRENT VALUE OF STEP TAKEN ALONG FIELD LINE
                C      DIR    -  DIRECTION OF TRACE  -1 AWAY FROM EARTH, +1 TOWARDS EARTH
                C      IDBL   -  NUMBER OF TIMES STEP HAS BEEN DOUBLED - MAX IS 3
                C      IHALF  -  NUMBER OF TIMES STEP HAS BEEN HALVED - MAX IS 3
                C      LAST   -  IF NOT 0 ON INPUT JUST TAKE A STEP AND DO NOT CHECK
                C                THE STEP SIZES
                C     XP,YP   -  THE ARRAY OF INPUT COORDINATES
                C     BZ,BP   -  COMPONENTS OF THE FIELD AT XP,YP
                C     ZEND    -  FINAL VALUE OF THE Z-COMPONENT
                C     J       -  CURRENTLY CALCULATED POINT
                C
                C                          OUTPUT PARAMETERS ARE
                C      LAST   -  SET HIGH IF THE POINT TO BE CALCULATED IS THE LAST ONE
                C                OF THE TRACE  OR THE 300TH POINT
                C     J       -  NEXT POINT TO BE CALCULATED
                C
0002            DIMENSION       XP(300),        YP(300),        BZ(300),
               1 BP(300)
                C
0003            NEW = 0
0004           1 J1 = J
0005            J2 = J - 1
0006            INEG = 0
0007            ID = 0
0008            B1 = SQRT ( BZ(J1)*BZ(J1) + BP(J1)*BP(J1) )
                C
                C IF THIS IS THE VERY FIRST POINT JUST INCREMENT AND RETURN - OR IF
                C THIS IS A RECOMPUTED POINT
                C
0009            IF ( LAST.NE.0 ) GO TO 70
0010            IF ( J.EQ. 0 ) GO TO 70
0011            IFIX = 0
0012            B2 = SQRT ( BZ(J2)*BZ(J2) + BP(J2)*BP(J2) )
0013            DB = ABS ( B1 - B2 )
                C
                C DB IS CHANGE IN FIELD INTENSITY IN GAUSS - IF DB IS .1 OR GREATER WE
                C WANT THE STEP SIZE TO BE NO LARGER THAN .5 THE BASIC STEP SIZE IN
                C EARTH RADII SO STEP IS HALVED TILL IHALF IS 1.  IF DB IS BETWEEN .01
                C AND .099 WE WANT THESTEP SIZE TO BE NO LARGER THAN THE BASIC STEP
                C SIZE SO STEP IS HALVED TILL IDBL IS 0.  IN BOTH CASES IFIX IS SET
                C EQUAL TO 1 SO WHEN CHECK IS MADE ON CHANGE OF DIRECTION THE STEP WILL
                C NOT BE INCREASED.  IF DB IS LESS THAN .01 THE STEP SIZE ID ADJUSTED
                C BY CHANGE IN DIRECTION ONLY
                C
0014            IF ( DB .LT. 0.01 ) GO TO 40
0015            IF ( IDBL .EQ. 0 ) GO TO 12
0016            ASSIGN 10 TO IRET
0017            GO TO 100
0018           10 IF ( IDBL .NE. 0 ) GO TO 100
```

```
0019          12 IF ( DB .LT. 0.1 ) GO TO 20
0020             IF ( IHALF .GE. 2 ) GO TO 20
0021             ASSIGN 20 TO IRET
0022             GO TO 100
0023          20 IFIX = 1
0024             GO TO 50
0025          40 IF ( IDBL .GE. 1 ) GO TO 50
0026             ID = 1
0027             GO TO 150
                 C
                 C ADJUST STEP CONSIDERING CHANGE OF DIRECTION IF THREE POINTS ARE
                 C AVAILABLE
                 C
0028          50 ID = 0
0029             J3 = J - 2
0030             IF ( J3 .EQ. 0 ) GO TO 70
0031             S12 = ( YP(J2) - YP(J1) )/( XP(J2) - XP(J1) )
0032             S23 = ( YP(J3) - YP(J2) )/( XP(J3) - XP(J2) )
0033             DS = ABS ( S23 - S12 )
                 C
                 C DS IS CHANGE IN DIRECTION OF FIELD - IF THE ADJUSTED DS IS LESS THAN
                 C .25 DOUBLE STEP SINCE DIRECTION IS ALMOST A STRAIGHT LINE. IF DS IS
                 C BETWEEN .25 AND .75 LEAVE STEP SIZE AS IS SINCE CHANGE IS MODERATE.
                 C IF DS IS BETWEEN .75 AND 1.50 HALVE STEP ONCE, IF BETWEEN 1.50 AND 3.0
                 C HALVE IT TWICE, IF GREATER THAN 3.00 THREE TIMES SINCE VERY ABRUPT
                 C CHANGE HAS OCCURRED IN DIRECTION
                 C
0034             ADJ = IDBL + 1
0035             ADJ = .25*ADJ*ADJ - .50*ADJ + 1.25
0036             DS = DS*ADJ
0037             IF ( DS .LE. 0.25 ) GO TO 150
0038          55 IF ( DS .LT. 0.75 ) GO TO 70
0039             ASSIGN 60 TO IRET
0040             GO TO 100
0041          60 IF ( DS .LT. 1.50 ) GO TO 70
0042             ASSIGN 65 TO IRET
0043             GO TO 100
0044          65 IF ( DS .LT. 3.00 ) GO TO 70
0045             ASSIGN 70 TO IRET
0046             GO TO 100
                 C
                 C NEW STEPSIZE HAS BEEN COMPUTED - CONVERT THIS TO X & Y STEPS,
                 C INCREMENT J, COMPUTE NEW XP, YP, AND SET LAST
                 C
0047          70 IF ( ID .EQ. 1 ) GO TO 40
0048             LAST = NEW
0049             IF (NEW .LE. 0 ) GO TO 75
0050             J = J2
0051             NEW = -1
0052             GO TO 1
0053          75 XSTEP = DIR * ( BZ(J1)*STEP/B1 )
0054             YSTEP = DIR * ( BP(J1)*STEP/B1 )
0055             J = J + 1
0056          80 XP(J) = XP(J1) + XSTEP
```

```
0057            YP(J) = YP(J1) + YSTEP
                C
                C CHECK IF NEW POINT IS IN RANGE  - IF TRACING AWAY FROM EARTH ZEND IS
                C MAX ALLOWABLE EARTH RADII OUT.  - IF TRACING TOWARD THE EARTH ZEND IS
                C MIN ALLOWABLE EARTH RADII OUT - DEFAULT IS 1 FOR TOWARD AND 20 AWAY
                C
0058            IF ( DIR .EQ. +1 ) GO TO 90
0059            IF ( XP(J) .LT. ZEND ) GO TO 200
0060            FAC = ( ZEND - XP(J1) )/(XP(J)- XP(J1))
0061            XP(J) = ZEND
0062            YP(J) = FAC*YSTEP + YP(J1)
0063            LAST = J
0064            GO TO 200
0065          90 RAD = SQRT (XP(J)*XP(J) + YP(J)*YP(J))
0066            IF ( RAD .GT. ZEND ) GO TO 200
0067            DIS = SQRT (XP(J1)*XP(J1) + YP(J1)*YP(J1) )
0068            FAC = (DIS - ZEND)/(DIS - RAD)
0069            XP(J) = XP(J1) + FAC*XSTEP
0070            YP(J) = YP(J1) + FAC*YSTEP
0071            LAST = J
                C
                C CHECK IF THE NEW YP IS POSITIVE - IF IT GOES BELOW 0 HALVE XSTEP AND
                C YSTEP AND RECOMPUTE XP AND YP TIL POSITIVE THEN SET LAST POINT
                C INDICATOR BEFORE LEAVING SUBROUTINE
                C
0072          200 IF ( YP(J) .GT. 0.0 ) GO TO 300
0073            INEG = 1
0074            YSTEP = YSTEP / 2.
0075            XSTEP = XSTEP / 2.
0076            GO TO 80
                C
                C STEP SIZE TOO LARGE TO BE ACCURATE - HALVE THE STEP SIZE THEN SET J
                C BACK TWO POINTS AND RECALCULATE THEM USING NEW STEP SIZE. HALVING IS
                C ALLOWED TO OCCURE THREE TIMES WITH MINIMUM STEP BEING .016 EARTH RADII
                C
0077          100 IHALF = IHALF + 1
0078            IF ( IHALF .GT. 3 ) GO TO 115
0079            STEP = STEP /2.0
0080            IF (IDBL .EQ. 0 ) GO TO 120
0081            IDBL = IDBL - 1
0082            IHALF = IHALF - 1
0083            GO TO 120
0084          115 IHALF = 3
0085          120 NEW = 1
0086            GO TO IRET,( 10, 20, 60, 65, 70 )
                C
                C STEP SIZE SMALLER THAN REQUIRED - DOUBLE IT FOR NEXT CALCULATIONS
                C KEEPING CURRENT POINTS.  DOUBLING IS ALLOWED TO OCCURE 3 TIMES WITH
                C A MAXIMUM STEP SIZE OF 1 EARTH RADII
                C
0087          150 IF ( IFIX .NE. 0 ) GO TO 70
0088            IDBL = IDBL + 1
0089            IF ( IDBL .GT. 3 ) GO TO 155
0090            STEP = STEP * 2.0
```

```
0091              IF ( IHALF .EQ. 0 ) GO TO 70
0092              IHALF = IHALF - 1
0093              IDBL = IDBL - 1
0094              GO TO 70
0095          155 IDBL = 3
0096              GO TO 70
0097          300 IF ( INEG .EQ. 1 ) LAST = J
0098              RETURN
0099              END
```

```
0001            SUBROUTINE EDGE ( I1, I2, J1, J2, FJ, B, ICD , PO, ZO )
                C
                C ROUTINE INTERPOLATES THE RING CURRENT IN AN AREA 1 EARTH RADII FROM
                C EITHER THE Z OR P AXIS.  IF ICD = 1 - FIND P COMPONENT OF RING
                C CURRENT, IF ICD = 2 - FIND Z COMPONENT
                C
0002            DIMENSION    XP (20),  YP(10),  XZ(20),  YZ(10),  P(4),  Z(4)
0003            DIMENSION    BDZ(20,10),  BDP(20,10),  RDZ(20,10), RDP(20,10)
0004            COMMON  /INTERP /  BDZ, BDP, RDZ, RDP
                C
0005            DATA XZ / 20 * 0.0 /
0006            DATA  XP / -.00323,  -.00317,  -.00692,  -.00486,  +.00127,
                1          +.00193,  +.00095,  +.00055,  +.00035,  +.00024,
                2          +.00018,  +.00014,  +.00011,  +.00008,  +.00007,
                3          +.00006,  +.00005,  +.00004,  +.00003,  +.00002  /
0007            DATA  YP / -.00324,  -.00284,  -.00224,  -.00150,  -.00125,
                1          -.00096,  -.00060,  -.00045,  -.00035,  -.00030  /
0008            DATA  YZ / -.00030,  -.00004,  -.00013,  -.00016,  -.00019,
                1          -.00017,  -.00012,  -.00011,  -.00009,  -.00008  /
0009            DATA   Z / -.00000,  -.00000,  -.00001,  -.00002 /
0010            DATA   P / -.00323,  -.00324,  -.00325,  -.00326 /
0011            DATA  FJ / 0.0 /
                C
                C ADJUST FOR FJ OTHER THAN 4500.
                C
0012            IF ( FJ .EQ. FJ ) GO TO 20
0013            FJ0 = 4500.
0014            IF ( FJ .NE. 0. ) FJ0 = FJ
0015            FAC = FJ / FJ0
0016            FJ = FJ
0017            DO 10 K = 1,10
0018            KK = 10 + K
0019            XP(K) = XP(K) * FAC
0020            YP(K) = YP(K) * FAC
0021            XZ(K) = XZ(K) * FAC
0022            YZ(K) = YZ(K) * FAC
0023            XP(KK) = XP(KK) * FAC
0024            XZ(KK) = XZ(KK) * FAC
0025         10 CONTINUE
                C
                C FIND POSITION OF SQUARE - IN CORNER OR ON X OR Y AXIS
                C
0026         20 IF (I1 .NE. J1 ) GO TO 100
                C
                C IN CORNER - FIND DISTANCE OF POINT FROM ORIGIN
                C
0027            D = SQRT (ZO*ZO + PO*PO)
0028            I = 10*D -10
0029            IF ( I .EQ. 0 ) I = 1
0030            IF ( I .GT. 4 ) I = 4
0031            B = P(I)
0032            IF ( ICD .EQ. 2) B = Z(I)
0033            GO TO 300
0034        100 IF ( I1 .EQ. 0) GO TO 150
```

```
DOS FORTRAN IV 360N-FO-479 3-1        EDGE                DATE   02/23/71    TIME    11.29.50      PAGE 0002

                C
                C ON Z AXIS - FIND FIELD IN CORNERS
                C
0035                 IF ( ICO .EQ. 2 ) GO TO 125
                C
                C SET UP FOR P COMP
                C
0036                 BL = XP(I1)
0037                 BR = XP(I2)
0038                 TL = ROP(I1,1)
0039                 TR = ROP(I2,1)
0040                 GO TO 200
                C
                C SET UP Z COMP
                C
0041            125  BL = XZ(I1)
0042                 BR = XZ(I2)
0043                 TL = ROZ(I1,1)
0044                 TR = ROZ(I2,1)
0045                 GO TO 200
                C
                C ON P AXIS
                C
0046            150  IF ( ICO .EQ. 2 ) GO TO 175
                C
                C SET UP P COMP
                C
0047                 BL = YP(J1)
0048                 BR = ROP(1,J1)
0049                 TL = YP(J2)
0050                 TR = ROP(1,J2)
0051                 GO TO 200
                C
                C SET UP Z COMP
                C
0052            175  BL = YZ(J1)
0053                 BR = ROZ(1,J1)
0054                 TL = YZ(J2)
0055                 TR = ROZ(1,J2)
                C
                C INTERPOLATE
                C
0056            200  TO= ( Z0 - I1) * (TR - TL) + TL
0057                 BO= ( Z0 - I1) * (BR - BL) + BL
0058                 B = ( P0 - J1) * (TO - BO) + BO
                C
0059            300  RETURN
                C
0060                 END
```

REFERENCES

Chapter I

Armstrong, J. C. and A. J. Zmuda, Field-aligned current at 1100 km in the auroral region measured by satellite, J. Geophys. Res., 75, 7122-7127, 1970.

Bame, S. J., J. R. Asbridge, H. E. Felthauser, R. A. Olson, and I. B. Strong, Electrons in the plasma sheet of the earth's magnetic tail, Phys. Rev. Letters, 16, 138-140, 1966.

Behannon, K. W. and N. F. Ness, Magnetic storms in the earth's magnetic tail, J. Geophys. Res., 71, 2327-2351, 1966.

Biermann, L., Kometenschweife und solare korpuskularstrahlung, Zeit. Astrophys., 29, 274-286, 1951.

Birkeland, K., Expédition Norvégienne de 1899-1900, Resultats Magnetiques, Vidersk. Skrifter, I. Mat. Natarv. Kl. 1901, 1-80, 1901.

Birkeland, K., The Norwegian Aurora Polaris Expedition 1902-1903, First and Second Section, On the cause of magnetic storms and the origin of terrestrial magnetism, H. Aschehoug & Co., Christiana, 1908.

Birkeland, K., Phenomenes celestes et analogies experimentales, Comptes Rendus, Acad. Sci. Paris, 153, 938-940, 1911.

Cahill, L. J., Jr., The geomagnetic field, Space Physics, pp. 301-349, ed. by D. P. Le Galley and A. Rosen, John Wiley & Sons, Inc., New York, 1964.

Cahill, L. J., Jr., Inflation of the inner magnetosphere during a magnetic storm, J. Geophys. Res., 71, 4505-4519, 1966.

Cahill, L. J., Jr., Magnetosphere inflation during four magnetic storms in 1965, J. Geophys. Res., 75, 3778-3788, 1970.

Cahill, L. J. and P. G. Amazeen, The boundary of the geomagnetic field, J. Geophys. Res., 68, 1835-1843, 1963.

Cain, J. C., I. R. Shapiro, J. D. Stolarik, and J. P. Heppner, Vanguard 3 magnetic-field observations, J. Geophys. Res., 67, 5055-5069, 1962.

Chapman, S., An outline of a theory of magnetic storms, Proc. Roy. Soc. London, A95, 61-83, 1918.

Chapman, S. and V. C. A. Ferraro, A new theory of magnetic storms, Nature, 126, 129-130, 1930; Terr. Magn., 36, 77-97 and 171-186, 1931; Terr. Magn., 37, 147-156, 1932.

Cloutier, P. A., H. R. Anderson, R. J. Park, R. R. Vondrak, R. J. Spiger, and B. R. Sandel, Detection of geomagnetically aligned currents associated with an auroral arc, J. Geophys. Res., 75, 2595-2600, 1970.

Coleman, P. J., Jr., Geomagnetic storms at ATS I, Intercorrelated Satellite Observations Related to Solar Events, pp. 251-279, ed. by V. Manno and D. E. Page, D. Reidel Publishing Co., Dordrecht, Holland, 1970.

Coleman, P. J., Jr., and W. D. Cummings, Simultaneous magnetic field variations at the earth's surface and at synchronous equatorial distance. Part II. Magnetic storms, Radio Science, 3, 762-765, 1968.

Coleman, P. J., Jr., and W. D. Cummings, Stormtime disturbance fields at ATS I, J. Geophys. Res., 76, 51-62, 1971.

Cummings, W. D., J. N. Barfield, and P. J. Coleman, Jr., Magnetospheric substorms observed at synchronous orbit, J. Geophys. Res., 73, 6687-6698, 1968.

Cummings, W. D. and P. J. Coleman, Jr., Simultaneous magnetic field variations at the earth's surface and at synchronous equatorial distance. Part I. Bay-associated events, Radio Science, 3, 758-761, 1968a.

Cummings, W. D. and P. J. Coleman, Jr., Magnetic fields in the magnetopause and vicinity at synchronous altitude, J. Geophys. Res., 73, 5699-5718, 1968b.

Dolginov, S. Sh., E. G. Eroshenko, L. N. Zhukov, and L. O. Tyurmina, Measuring the magnetic fields of the earth and moon by means of Sputnik III and Space Rockets I and II, pp. 863-868, Proc. First Intern. Space Sci. Symp., H. K. Kallman-Bigl, ed. North Holland, Amsterdam, 1960.

Fairfield, D. H. and N. F. Ness, Configuration of the geomagnetic tail during substorms, J. Geophys. Res., 75, 7032-7047, 1970.

Frank, L. A., On the extraterrestrial ring current during geomagnetic storms, J. Geophys. Res., 72, 3753-3767, 1967.

Frank, L. A., Direct detection of asymmetric increases of extraterrestrial 'ring current' proton intensities in the outer radiation zone, J. Geophys. Res., 75, 1263-1268, 1970.

Laird, M. J., Structure of the neutral sheet in the geomagnetic tail, J. Geophys. Res., 74, 133-136, 1969.

Moos, N. A. F., Colaba Magnetic Data, 1846 to 1905, Bombay, 1910.

Needham, J., Science and Civilization in China, Vol. 4, Part 1, Cambridge University Press, London, 1962.

Ness, N. F., The earth's magnetic tail, J. Geophys. Res., 70, 2989-3005, 1965.

Ness, N. F., C. S. Scearce and S. C. Cantarano, Probable observations of the geomagnetic tail at 10^3 earth radii by Pioneer 7, J. Geophys. Res., 72, 3769-3776, 1967.

Schmidt, A., Erdmagnetismus, Enzyklopädie der Mathematischen Wissenschaften, Band VI, Leipzig, 1917.

Speiser, T. W., and N. F. Ness, The neutral sheet in the geomagnetic tail: its motion, equivalent currents, and field line connection through it, J. Geophys. Res., 72, 131-141, 1967.

Sonett, C. P., E. J. Smith, D. L. Judge and P. J. Coleman, Jr., Current systems in the vestigial geomagnetic field: Explorer VI, Phys. Rev. Letters, 4, 161-163, 1960.

Störmer, C., Sur les trajectories des corpuscles electrises dans l'space sons l'action du magnetisme terrestre avec application aux aurores boreales, Arch. Sci. Phys. Nat. Geneve, 32, 117-123, 1911.

Wolfe, J. H., R. W. Silva, D. D. McKibbin, and R. H. Mason, Preliminary observations of a geomagnetospheric wake at 1000 earth radii, J. Geophys. Res., 72, 4577-4581, 1967.

REFERENCES

Chapter 2

Akasofu, S.-I., Electrodynamics of the magnetosphere: Geomagnetic storms, Space Sci. Rev., 6, 21-143, 1966.

Akasofu, S.-I., Magnetosphere and magnetospheric substorm, Ann. de Geophys., 24, 1-6, 1968.

Ashour, A. A., The evaluation of the field of the currents induced in the earth by an external field whose distribution is known numerically, Radio Science, 6, 171-173, 1971

Ashour, A. A. and A. T. Price, Night-time earth currents associated with the daily magnetic variations, Geophys. J., 10, 1-15, 1965-66.

Axford, W. I. and C. O Hines, A unified theory of high-latitude geophysical phenomena and geomagnetic storms, Can. J. Phys., 39, 1433-1464, 1961.

Axford, W. I., The interaction between the solar wind and the earth's magnetosphere, J. Geophys. Res., 67, 3791-3796, 1962.

Axford, W. I., Viscous interaction between the solar wind and the earth's magnetosphere, Planet. Space Sci., 12, 45-53, 1964.

Baker, W. G. and D. F. Martyn, Electric currents in the ionosphere, I. The conductivity, Phil. Trans. Roy. Soc. A., 246, 281-294, 1953.

Boström, R., A model of the auroral electrojets, J. Geophys. Res., 69, 4983-4999, 1964.

Butler, S. T. and K. A. Small, The excitation of atmospheric oscillations, Proc. Roy. Soc. London (A), 274, 91-121, 1963.

Chapman, S., The solar and lunar diurnal variation of the earth's magnetism, Phil. Trans. Roy. Soc. London, A, 218, 1-118, 1919.

Chapman, S. and J. Bartels, Geomagnetism, Oxford Univ. Press, 1940.

Chapman, S. and V. C. A. Ferraro, A new theory of magnetic storms, Terr. Magn. Atmosph. Elec., 36, 77-97, 1931; ibid, 171-186, 1931.

Cummings, W. D., P. J. Coleman, Jr. and G. L. Siscoe, Quiet day magnetic field at ATS-1, J. Geophys. Res., 76, 926-932, 1971.

Fejer, J. A., Semi-diurnal currents and electron drifts in the ionosphere, J. Atmosph. Terr. Phys., 4, 184-203, 1953.

Fejer, J. A., Theory of the geomagnetic daily disturbance variations, J. Geophys. Res., 69, 123-137, 1964.

Feldstein, Ya. I. and A. N. Zaytsev, Magnetic field variations at high latitudes on quiet days in summer during the IGY, Geomagnetism Aeronomy, 7, 160-162, 1967.

Ferraro, V. C. A., On the theory of the first phase of a geomagnetic storm, J. Geophys. Res., 57, 14-49, 1952.

Föppl, H., G. Haerendel, L. Haser, R. Lüst, F. Melzner, B. Meyer, H. Neuss, H.-H. Rabben, E. Rieger, J. Stöcker, Preliminary results of electric field measurements in the auroral zone, J. Geophys. Res., 73, 21-26, 1968.

Frank, L. A., Plasma in the earth's polar magnetosphere, University of Iowa Report 70-55, November, 1970.

Hasegawa, M., Provisional report of the statistical study on the diurnal variations of terrestrial magnetism in the north polar regions, Transactions of Washington Meeting, Sept. 4-15, 1939, I.U.G.G. - A.T.M.E., Bull. No. 11, 311-318, A. H. R. Goldie, ed., Edinburgh, 1940.

Heppner, J. P., J. D. Stolarik and E. M. Wescott, Electric field measurements and identification of currents causing magnetic disturbances in the polar cap, Goddard Space Flight Center NASA preprint, X-645-71-50, October, 1970.

Kawasaki, K. and S.-I. Akasofu, Polar solar daily geomagnetic variations on exceptionally quiet days, J. Geophys. Res., 72, 5363-5671, 1967.

Maeda, H., On the residual part of the geomagnetic Sq field in the middle and lower latitudes during the International Polar Year, 1932-1933, J. Geomagnet. Geoelec., 5, 39-51, 1953.

Matsushita, S., Lunar geomagnetic variations, J. Geomagnet. Geoelec., 18, 163-172, 1966.

Matsushita, S., Solar quiet and lunar daily variation fields, Physics of Geomagnetic Phenomena, I, 301-424, ed. by S. Matsushita and W. H. Campbell, Academic Press, New York, 1967.

Matsushita, S., Lunar tides in the ionosphere, Handbuch der Physik, XLIX, Geophysik II/2, 547-602, Springer Verlag, Heidelberg, 1969.

Matsushita, S. and H. Maeda, On the geomagnetic solar quiet daily variation field during the I.G.Y., J. Geophys. Res., 70, 2535-2558, 1965a.

Matsushita, S. and H. Maeda, On the geomagnetic lunar daily variation field, J. Geophys. Res., 70, 2559-2570, 1965b.

Mead, G. D., Deformation of the geomagnetic field by the solar wind, J. Geophys. Res., 69, 1181-1195, 1964.

Nagata, T. and S. Kokubun, An additional geomagnetic daily variation in field (S_q^p-field) in the polar region on geomagnetically quiet days, Rept. Ionosphere Space Res. Japan, 16, 256-274, 1962.

Nishida, A., S. Kokubun and N. Iwasaki, Annual variation in the magnetospheric configuration and its influence on the polar magnetic field, Rept. Ionosphere Space Res. Japan, 20, 73-78, 1966.

Olson, W. P., Contribution of nonionospheric currents to the quiet daily magnetic variations at the earth's surface, J. Geophys. Res., 75, 7244-7249, 1970.

Piddington, J. H., Geomagnetic storm theory, J. Geophys. Res., 65, 93-106, 1960.

Piddington, J. H., A hydromagnetic theory of geomagnetic storms and auroras, Planet. Space Sci., 9, 947-960, 1962.

Piddington, J. H., Geomagnetic storms, auroras and associated effects, Space Sci. Rev., 3, 724-780, 1964.

Piddington, J. H., The magnetosphere and its environs, Planet. Space Sci., 13, 363-367, 1965.

Schuster, A., The diurnal variation of terrestrial magnetism, Phil. Trans. Roy. Soc. London, A, 180, 467-518, 1889.

Siebert, M., Atmospheric tides, Advances in Geophysics, Vol. 7, 105-187, ed. by H. E. Landsberg and J. Van Mieghem, Academic Press, London, 1961.

Siscoe, G. L., A unified treatment of magnetospheric dynamics, Planet. Space Sci., 14, 947-967, 1966.

REFERENCES

Chapter 3

Akasofu, S.-I. and S. Chapman, On the asymmetric development of magnetic storm fields in low and middle latitudes, Planet. Space Sci., 12, 607-626, 1964.

Akasofu, S.-I. and C.-I. Meng, Non-uniform growth of the ring current belt, Planet. Space Sci., 17, 707-714, 1969.

Akasofu, S.-I., P. D. Perreault and S. Yoshida, The geomagnetic and cosmic ray storm of May 25/26, 1967, Solar Phys., 8, 464-476, 1969.

Beard, D. B., M. Bird and Y. H. Huang, Self consistent theory of the magnetotail, Planet. Space Sci., 18, 1349-1355, 1970.

Cahill, L. J., Jr., Inflation of the inner magnetosphere during a magnetic storm, J. Geophys. Res., 71, 4505-4519, 1966.

Chapman, S., An outline of a theory of magnetic storms, Proc. Roy. Soc., London, A, 95, 61-83, 1918.

Chapman, S., The electric current systems of magnetic storms, Terr. Mag., 40, 349-370, 1935.

Coleman, P. J., Jr., Geomagnetic storms at ATS-I, Intercorrelated Satellite Observations Related to Solar Events, V, Manno and D. E. Page, eds., D. Reidel Pub. Co., 251-279, 1970.

Coleman, P. J., Jr. and W. D. Cummings, Storm-time disturbance fields at ATS-I, J. Geophys. Res., 76, 51-62, 1971.

Crooker, N. U. and G. L. Siscoe, A study of the geomagnetic disturbance field asymmetry, Proceedings of Upper Atmospheric Currents and Electric Fields Symposium, Boulder, Colorado, September 1970, pp. 156-162, ESSA Tech. Memo. ERLTM-ESL12, 1970.

Cummings, W. D. and P. J. Coleman, Jr., Simultaneous magnetic field variations at the earth's surface and at synchronous, equatorial distance, Part I: Bay associated events, Radio Science, 3, 758-761, 1968.

Cummings, W. D., J. N. Barfield and P. J. Coleman, Jr., Magnetospheric substorms observed at the synchronous orbit, J. Geophys. Res., 73, 6687-6698, 1968.

Davis, T. N. and M. Sugiura, Auroral electrojet activity index AE and its universal time variation, J. Geophys. Res., 71, 785-801, 1966.

DeForest, S. E. and C. E. McIlwain, Plasma clouds in the magnetosphere, Univ. Cal. San Diego, UCSD-SP-70-04, September 1970.

Fairfield, D. H. and N. F. Ness, Configuration of geomagnetic tail during substorms, J. Geophys. Res., 75, 7032-7047, 1970.

Hones, E. W. Jr., J. R. Asbridge and S. J. Bame, Time variations of the magnetotail plasma sheet at 18 R_e determined from concurrent observations by a pair of Vela satellites, submitted to J. Geophys. Res., November 1970.

Meng, C.-I. and S.-I. Akasofu, The geomagnetic storm of April 17/18, 1965, J. Geophys. Res., 72, 4905-4916, 1967.

Nikolsky, A. P., Dual laws of the course of magnetic disturbances and the nature of mean regular variations, Terr. Mag. and Atmos. Elec., 52, 147-173, 1947.

REFERENCES

Chapter 4

Akasofu, S.-I., Model ring current belts, University of Iowa Report 66-28, 1966.

Akasofu, S.-I. and S. Chapman, The ring current, geomagnetic disturbance, and the Van Allen radiation belts, J. Geophys. Res., 66, 1321-1350, 1961.

Behannon, K. W., Mapping of the earth's bow shock and magnetic tail by Explorer 33, J. Geophys. Res., 73, 907-930, 1968.

Behannon, K. W. and N. F. Ness, Magnetic storms in the earth's magnetic tail, J. Geophys. Res., 71, 2327-2351, 1966.

Cahill, L. J. Jr., Inflation of the inner magnetosphere during a magnetic storm, J. Geophys. Res., 71, 4505-4519, 1966.

Coleman, P. J., Jr., Geomagnetic storms at ATS-1, Inter-correlated satellite observations related to solar events, 251-279. Proceedings of the Third ESLAB/ESRIN Symposium, Noordwijk, The Netherlands, Sept. 16-19, 1969, ed. by V. Manno and D. E. Page, D. Reidel Publishing Co., Dordrecht, Holland, 1970.

Coleman, P. J. Jr., and W. D. Cummings, Storm-time disturbance fields at ATS-1, J. Geophys. Res., 76, 51-62, 1971.

Frank, L. A., On the extraterrestrial ring current during geomagnetic storms, J. Geophys. Res., 72, 3753-3767, 1967.

Frank, L. A., On the relationship of the plasma sheet, ring current, trapping boundary and plasmapause near the magnetic equator and local midnight, U. of Iowa Rept. 70-33, 1970.

Hoffman, R. A. and L. J. Cahill, Jr., Ring current particle distributions derived from ring current magnetic field measurements, J. Geophys. Res., 73, 6711-6723, 1968.

Ness, N. F., The earth's magnetic tail, J. Geophys. Res., 70, 2989-3005, 1965.

Sozou, C. and D. W. Windle, A self consistent ring current in the earth's dipole field, Planet. Space Sci., 17, 375-387, 1969.

Williams, D. J. and G. D. Mead, Nightside magnetosphere configuration as obtained from trapped electrons at 1100 kilometers, J. Geophys. Res., 70, 3017-3029, 1965.

REFERENCES

Chapter 5

Akasofu, S.-I., Large-scale auroral motions and polar magnetic disturbances -II: The changing distribution of the aurora during large magnetic storms, J. Atmos. Terr. Phys., 24, 723, 1962.

Ballif, J. R. and D. E. Jones, The magnetic morphology of solar streams and its relation to geomagnetic storms, J. Geophys. Res., 72, 5173-5184, 1967.

Burlaga, L. F., Discontinuities and shock waves in the interplanetary medium and their interaction with the magnetosphere, NASA, Goddard Space Flight Center preprint, X-692-70-154, 1970.

Burlaga, L. F. and N. F. Ness, Macro- and micro-structure of the interplanetary magnetic field, Canadian J. Phys., 46, S962, 1968.

Burlaga, L. F. and N. F. Ness, Tangential discontinuities in the solar wind, Solar Physics, 9, 467-477, 1969.

Dungey, J. W., Interplanetary magnetic field and the auroral zones, Phys. Rev. Letters, 6, 47-48, 1961.

Dungey, J. W., Interactions of solar plasma with the geomagnetic field, Planet. Space Sci., 10, 233-237, 1963.

Fairfield, D. H., Polar magnetic disturbances and the interplanetary magnetic field, Goddard Space Flight Center Publ. X-612-67-338, Greenbelt, Maryland, July, 1967.

Fairfield, D. H. and L. J. Cahill, Jr., Transition region magnetic field and polar magnetic disturbances, J. Geophys. Res., 71, 155-169, 1966.

Rostoker, G. and C.-G. Fälthammar, Relationship between changes in the interplanetary magnetic field and variations in the magnetic field at the earth's surface, J. Geophys. Res., 72, 5853-5863, 1967.

Rostoker, G., Relationship between the onset of a geomagnetic bay and the configuration of the interplanetary magnetic field, J. Geophys. Res., 73, 4382-4387, 1968.

Schatten, K. H. and J. M. Wilcox, Response of the geomagnetic activity index Kp to the interplanetary magnetic field, J. Geophys. Res., 72, 5185-5191, 1967.

Schieldge, J. P. and G. L. Siscoe, A correlation of the occurrence of simultaneous sudden magnetospheric compressions and geomagnetic bay onsets with selected geophysical indices, J. Atmos. Terr. Phys., 32, 1819-1830, 1970.

Siscoe, G. L., L. Davis, Jr., P. J. Coleman, Jr., E. J. Smith and D. E. Jones, Power spectra and discontinuities of the interplanetary magnetic field: Mariner 4, J. Geophys. Res., 73, 61-82, 1968.

Snyder, C. W., M. Neugebauer and U. R. Rao, The solar wind velocity and its correlation with cosmic-ray variations and geomagnetic activity, J. Geophys. Res., 68, 6361-6370, 1963.

Taylor, H. E., Sudden commencement associated discontinuities in the interplanetary magnetic field observed by IMP 3, Solar Phys., 6, 320-334, 1969.

Wilcox, J. M., K. E. Schatten and N. F. Ness, Influence of interplanetary magnetic field and plasma on geomagnetic activity during quiet-sun conditions, J. Geophys. Res., 72, 19-26, 1967.

Wilson, C. R. and M. Sugiura, Hydromagnetic interpretation of sudden commencements of magnetic storms, J. Geophys. Res., 66, 4097-4111, 1961.

REFERENCES

Chapter 6

Akasofu, S.-I., Model ring current belts, University of Iowa Report 66-28, 1966.

Akasofu, S.-I., Magnetospheric substorm as a discharge process, Nature, 221, No. 5185, 1020-1022, 1969.

Akasofu, S.-I., A model current system for the magnetospheric substorm, pp. 34-45, Particles and Fields in the Magnetosphere, ed. by B. M. McCormac, D. Reidel Publishing Company, Dordrecht, Holland, 1970.

Akasofu, S.-I., and S. Chapman, The ring current, geomagnetic disturbance, and the Van Allen radiation belts, J. Geophys. Res., 66, 1321-1350, 1961.

Akasofu, S.-I., and C.-I. Meng, A study of polar magnetic substorms, J. Geophys. Res., 74, 293-313, 1969.

Antonova, A. Ye., and V. P. Shabanskiy, Structure of the geomagnetic field at great distances from the earth, Geomagnetism and Aeronomy, 8, 639-647, 1968.

Armstrong, J. C., and A. J. Zmuda, Field-aligned current at 1100km in the auroral region measured by satellite, J. Geophys. Res., 75, 7122-7127, 1970.

Ashour, A. A., The evaluation of the field of the currents induced in the earth by an external field whose distribution is known numerically, Radio Science, 6, 171-173, 1971.

Beard, D. B., M. Bird, and Y. I. Huang, Self-consistent theory of the magnetotail, Planet. Space Sci., 18, 1349-1355, 1970.

Bonnevier, B., R. Boström, and G. Rostoker, A three-dimensional model current system for polar magnetic substorms, J. Geophys. Res., 75, 107-122, 1970.

Cloutier, P. A., H. R. Anderson, R. J. Park, R. R. Vondrak, R. J. Spiger, and B. R. Sandel, Detection of geomagnetically aligned currents associated with an auroral arc, J. Geophys. Res., 75, 2595-2600, 1970.

Cummings, W. D., J. N. Barfield and P. J. Coleman, Jr., Magnetospheric substorms observed at the synchronous orbit, J. Geophys. Res., 73, 6687-6698, 1968.

Hones, E. W., Jr., Motions of charged particles trapped in the earth's magnetosphere, J. Geophys. Res., 68, 1209-1219, 1963.

Kawasaki, K. and S.-I. Akasofu, The computed distribution of geomagnetic disturbance vectors for model three-dimensional current system, Planet. Space Sci., submitted October 1970.

Kirkpatrick, C. B., On current systems proposed for SD in the theory of magnetic storms, J. Geophys. Res., 57, 511-526, 1952.

Meng, C.-I., and S.-I. Akasofu, A study of polar magnetic substorms, 2. Three dimensional current system, J. Geophys. Res., 74, 4035-4053, 1969.

Parker, E. N., Newtonian development of the hydromagnetic properties of ionized gases of low density, Phys. Rev., 107, 924-933, 1957.

Silsbee, H. C. and E. H. Vestine, Geomagnetic bays, their frequency, and current systems, Terr. Magn. Atmos. Elect., 47, 195-208, 1942.

Williams, D. J. and G. D. Mead, Nightside magnetosphere configuration as obtained from trapped electrons at 1100 kilometers, J. Geophys. Res., 70, 3017-3029, 1965.

Zmuda, A. J., J. C. Armstrong, and F. T. Heuring, Characteristics of transverse magnetic disturbances observed at 1100 kilometers in the auroral oval, J. Geophys. Res., 75, 4757-4762, 1970.

Zmuda, A. J., F. T. Heuring, and J. H. Martin, Dayside magnetic disturbances at 1100 kilometers in the auroral oval, J. Geophys. Res., 72, 1115-1117, 1967.

Zmuda, A. J., J. H. Martin, and F. T. Heuring, Transverse magnetic disturbances at 1100 kilometers in the auroral region, J. Geophys. Res., 71, 5033-5045, 1966.

REFERENCES

Chapter 7

Akasofu, S.-I. and S. Yoshida, The structure of the solar plasma flow generated by solar flares, Planet. Space Sci., 15, 39-47, 1967.

Armstrong, J. C. and A. J. Zmuda, Field-aligned current at 1100km in the auroral region measured by satellite, J. Geophys. Res., 75, 7122-7127, 1970.

Ashour, A. A., The evaluation of the field of the currents induced in the earth by an external field whose distribution is known numerically, Radio Science, 6, 171-173, 1971.

Cahill, L. J. and P. G. Amazeen, The boundary of the geomagnetic field, J. Geophys. Res., 68, 1835-1843, 1963.

Coleman, P. J., Jr., Geomagnetic storms at ATS I, Intercorrelated Satellite Observations Related to Solar Events, pp. 251-279, ed. by V. Manno and D. E. Page, D. Reidel Publishing Co., Dordrecht, Holland, 1970.

Coleman, P. J., Jr., and W. D. Cummings, Simultaneous magnetic field variations at the earth's surface and at synchronous equatorial distance. Part II. Magnetic storms, Radio Science, 3, 762-765, 1968.

Feldstein, Ya. I. and A. N. Zaytsev, Magnetic field variations at high latitudes on quiet days in summer during the IGY, Geomagnetism Aeronomy, 7, 160-162, 1967.

Frank, L. A., On the extraterrestrial ring current during geomagnetic storms, J. Geophys. Res., 72, 3753-3767, 1967.

Frank, L. A., Direct detection of asymmetric increases of extra-terrestrial 'ring current' proton intensities in the outer radiation zone, J. Geophys. Res., 75, 1263-1268, 1970.

Frank, L. A. and D. A. Gurnett, On the distributions of plasmas and electric fields over the auroral zones and polar caps, U. of Iowa Report 71-5, February, 1971.

Heppner, J. P., J. D. Stolarik and E. M. Wescott, Electric field measurements and identification of currents causing magnetic disturbances in the polar cap, Goddard Space Flight Center NASA preprint, Z-645-71-50, October, 1970.

Hones, E. W., Jr., J. R. Asbridge and S. J. Bame, Time variations of the magnetotail plasma sheet at 18 R_e determined from concurrent observations by a pair of Vela satellites, submitted to J. Geophys. Res., November 1970.

Kawasaki, K. and S.-I. Akasofu, Polar solar daily geomagnetic variations on exceptionally quiet days, J. Geophys. Res., 72, 5363-5671, 1967.

O'Brien, B. J., Direct observations of dumping of electrons at 1000-kilometer altitude and high latitudes, J. Geophys. Res., 67, 1227-1233, 1962.

Piddington, J. H., Geomagnetic storms, auroras and associated effects, Space Sci. Rev., 3, 724-780, 1964.

Schieldge, J. P. and G. L. Siscoe, A correlation of the occurrence of simultaneous sudden magnetospheric compressions and geomagnetic bay onsets with selected geophysical indices, J. Atmos. Terr. Phys., 32, 1819-1830, 1970.